NEW FORMULAE FOR THE INITIAL DESIGN IN THE OPTIMIZATION OF T-JUNCTION MANIFOLD MULTIPLEXERS

A. Morini, T. Rozzi, M. Morelli
Dipartimento di Elettronica ed Automatica
Università di Ancona, I-60131 Ancona, Italy.

ABSTRACT

We present an effective criterium for the choice of the starting point in the optimization of T-manifold multiplexers. Given N separately designed channel filters, the method provides the expressions for their locations with respect to the manifold as well as the spacings between the junctions forming the manifold itself.
By inspection of the results it is seen that the proposed formulae perform considerably better than the standard ones based on stub models. In fact, in the non-contiguous case, the design is almost complete when the junctions forming the manifold have certain characteristics.
In the contiguous case, a further optimization is required but the initial choice is very close to the final solution.

INTRODUCTION

Nowadays, the most common method for the design of microwave multiplexers is based on optimization [1], [2]. The entire configuration, i.e. manifold and filters, is determined by minimizing a proper objective function, that often depends on hundreds of variables.
It is evident that the choice of the starting point, i.e. the initial multiplexer configuration, is crucial in view of reducing the optimization time and avoiding local minima traps, which frequently occur in minimizations over a number of variables.
On the other hand, the criteria appeared in literature are either extremely intuitive, as those based on the assumption that a filter in its outband can be taken as a stub [1], or quite sophisticated, as those where the filter prototypes are modified in order to account for the interaction with other channels [3], [4]. In both cases, however, the junctions forming the manifold are treated as ideal, at the initial step.
In this contribution, we propose quite a general criterium for the choice of the starting point of an optimization-based design approach. The method takes advantage from the knowledge of both the actual response of the filters and of the specific junctions forming the manifold, as they are simulated by full-wave analyses.
The resulting formulae are expressed in closed form in terms of the scattering parameters of the filters and junctions. They do not take into account of the interaction via higher order modes possibly occurring between junctions and filters. At the first step of the design, however, such an interaction can be neglected, as it will be taken into account in the further optimization of the functional deriving from the full-wave analysis of the whole device.
We will specialize our design method to the significant case of a T-junction manifold multiplexer.

This work was partially supported by MURST.

DIPLEXER DESIGN

Let us consider a three-port junction **J** of scattering matrix **S**. It can be proved that, at a given frequency f, it is always possible to minimize the reflectivity of the two-port junction obtained by closing an arm of a reciprocal and lossless three-port junction, say port 2, on a reactive load jX, provided that the load is positioned at the distance:

$$l(f) = \frac{\psi - \phi}{2\beta} \qquad (1)$$

where $e^{j\psi}$ is the reflection of the reactive load, β the propagation constant of the feed waveguides

WE 4A

0-7803-3814-6/97/$5.00 © IEEE

and

$$\phi = 2\tan^{-1}\frac{-b+\sqrt{a^2+b^2-c^2}}{c-a} \qquad (2)$$

The real quantities a, b and c depend on the scattering parameters of the junction and assume the following expressions:

$$\begin{aligned} a &= \frac{a_{33}}{a_{11}}(1+a_{22}^2)\sin(\phi_s-\phi_{11}-\phi_{33}) - \\ &\quad a_{22}(1+(\tfrac{a_{33}}{a_{11}})^2)\sin\phi_{22} \\ b &= \frac{a_{33}}{a_{11}}(1+a_{22}^2)\cos(\phi_s-\phi_{11}-\phi_{33}) - \\ &\quad a_{22}(1+(\tfrac{a_{33}}{a_{11}})^2)\cos\phi_{22} \\ c &= 2\frac{a_{33}}{a_{11}}a_{22}\sin(\phi_{11}+\phi_{22}+\phi_{33}-\phi_s) \end{aligned} \qquad (3)$$

where $S_{ii} = a_{ii}e^{j\phi_{ii}}$ are the scattering matrix diagonal parameters and $e^{j\phi_s}$ is the determinant of the scattering matrix of the three-port junction computed at the frequency f.

The corresponding value of the minimum reflectivity is given by:

$$\rho_{min} = a_{11}\left|\frac{1-\frac{a_{33}}{a_{11}}e^{j(\phi+\phi_s-\phi_{11}-\phi_{33})}}{1-a_{22}e^{j(\phi+\phi 22}}\right| \qquad (4)$$

Note that $\rho_{min} = 0$ only if $a_{11} = a_{33}$. Now, we want to realize a diplexer using such a junction and two given filters F_1 and F_2.

Noting that a filter in its out-band is an almost reactive load, formula (1) gives the criterium we are looking for. This is to connect the filters to ports 1 and 2 of the junction at the distances l_1 and l_2, respectively, in such a way that the two-port obtained by closing arm 1 of the junction on filter 1 has minimum reflection at the midband frequency of the second filter (f_2) and vice versa. Note that ψ appearing in (1) must be chosen as $\angle S_{11}^{F_1}(f_2)$ and $\angle S_{11}^{F_2}(f_1)$ respectively.

It is also worth noting that this approach is quite general, as it applies to junctions realized by any technology, its derivation being based only on the reciprocity and losslessness of the junction.

Of course, the perfomance of the diplexer will depend on the specific junction employed. In this regard, the Y-junction seems to be the best solution, because $S_{11} = S_{22} = S_{33}$ and its response is almost flat on the whole band, as discussed in a previous paper [5].

For a T-junction (Fig. 1) at a given frequency, the minimum reflection of the two-port obtained by closing port 1 on F_1 at the distance given by (1) is still zero, since $S_{33} = S_{22}$ at any frequency, provided that F_1 is in its outband. Conversely, when F_2 is placed at port 2, we can just reach a minimum of reflectivity, but not zero, since $a_{11} \neq a_{33}$. Therefore the resulting diplexer performace will be perfect at the midband frequency of the filter loading port 2, while it will deteriorate somewhat at the midband frequency of the filter loading port 1, being still acceptable in many practical cases.

MULTIPLEXER DESIGN

The above idea can easily be extended to the design of a multiplexer, as indicated in the case of Y-junction manifolds [6]. N filters F_i of scattering matrices $\mathbf{S}^{F_i}$, ordered in such a way that $f_i < f_{i+1}$, where f_i is the midband frequency of F_i, are connected to N identical T-junctions of scattering matrix S_T as indicated in Fig. 2. The distances l_k and ls_k are calculated as follows:

i) l_k is calculated so as to obtain a matched two-port between ports 3 and 2 of the $k-th$ junction at frequency f^* (where f^* is the arithmetic mean of f_1, f_2,...,f_{k-1}), when port 1 is closed on F_k; in this case $e^{j\psi} = S_{11}^{F_k}(f^*)$;

ii) ls_k is the distance between port 3 of the $k-th$ junction and the reactive load jX that minimizes the reflection of the resulting two-port at the frequency f_k; for $k > 1$, jX is the input impedance seen to the right of port 2 of the $(k-1)-th$ junction calculated at the frequency f_k; for $k = 1$, $jX = 0$, being the input impedance of a short-circuit.

Formula ii) is valid provided that filters F_1, F_2, ..., F_{k-1} appear as reactive loads at the frequency f_k, as always occurs in practice.

RESULTS

Formula 1 was validated by considering several three-port junctions both in rectangular waveguide and in microstrip technology. Regarding the T -junction, we considered the E-plane case and calculated the optimum distances at which a

short must be placed in order to obtain the maximum return loss at port 3, at 10 GHz, when the short loads either port 2 (T_2) or port 1 (T_1). The scattering parameters employed in expression 1 were computed by full-wave analysis. By means of 1, the theoretical optimum positions are: $l_1 = 38.222\,mm$ and $l_2 = 35.498\,mm$. The experiment, performed by means of a commercial E-plane T-junction in WR90 waveguide, was carried out by moving the short until minimum reflection was found. We measured the optimum distances $l_{e1} = 38.38mm$ and $l_{e2} = 35.62mm$. The slight deviation is probably due to the mechanical tolerances of the T-junction ($\pm 0.050mm$). The input reflection of the junction loaded as above is shown in Fig.3.

Regarding the multiplexer, we can show at the moment just theoretical results concerning the simulation of an E-plane T-manifold multiplexer employing E-plane septate filters. Although the simulations of both filters and junctions, separately considered, are very accurate [7], the model does not take into account the interaction between junction and filters via higher order modes. On the other hand, the single mode assumption was validated by an inspection of the final dimensions of the sections, always longer than $\lambda_g/4$, and, besides, the results obtained are to be taken just as starting point for a full-wave multiaccessible mode optimization. Moreover there is great practical effectiveness in simple formulae, a fact that depends strongly on the above single mode assumption. In order to appreciate the usefulness of formula (1), we compared the initial responses of many multiplexers designed as illustrated above with those designed according to the existing formulae (3.5.8-12) of [1]. The latter give the initial lengths usually employed as starting design of T-junction manifold multiplexers. Of course, in both cases final design requires an optimization step, but the comparison is very interesting in order to evaluate how close the initial design comes to the final solution. As a first example, we considered a 9-channel non contiguous multiplexer, employing Tchebysheff 7-poles 50 MHz bandwidth E-plane filters and E-plane T-junctions; the spacing between channels is 60 MHz. As can be seen, the reflection keeps lower than -12 dB for all channels (Fig. 4). In the contiguous case, results deteriorate a little. As an example, Fig. 5 shows the response of a 6-channel contiguous multiplexer employing Tchebysheff 7-poles 50 MHz bandwidth E-plane filters and E-plane T-junctions. Channels are separated by 5 MHz. Even in this case, the advantage of the proposed solution with respect to the standard one is evident.

CONCLUSIONS

An analytical and simple criterium for the choice of the initial guess in the optimization of T-junction manifold multiplexers has been presented. It provides closed form expressions giving the positions at which filters have to be placed and the distances separating the junctions in the manifold. The approach is quite general, being based on the analysis of the scattering matrices of the three-port blocks forming the manifold.

REFERENCES

[1] J. Uher, J. Bornemann, U. Rosenberg, ' Waveguide Components for Antenna Feed Systems', *Artech House*, 1993;

[2] M. Guglielmi, ' Simple CAD procedure for microwave filters and multiplexer', *IEEE Trans on MTT*, vol.42, no 7, July 1994, pp. 1347-1352;

[3] J.D. Rhodes and R. Levy, 'A generalized multiplexer theory', *IEEE Trans on MTT*, vol.27, no 2, Feb. 1979, pp. 99-111;

[4] J.D. Rhodes and R. Levy, ' Design of general manifold multiplexers ',*IEEE Trans on MTT* , vol.27, no 2, Feb. 1979, pp. 111-122;

[5] A. Morini and T.Rozzi, ' Constraints to the optimum performances and bandwidth limitations of diplexers employing symmetric three-port junctions', *IEEE Trans on MTT* , vol.44, no 2, Feb. 1996, pp. 242-248;

[6] A. Morini, "Design of multiplexers employing interconnected Y-junction manifolds", to appear on *International Journal of Microwave and Millimeter-Wave Computer-Aided Engineering* , Special Issue on Passive and Active Filters and Multiplexers;

[7] T. Rozzi, F. Moglie, A. Morini, W. Gulloch and M. Politi, ' Accurate full-band equivalent circuits of inductive posts in rectangular waveguide', *IEEE Trans on MTT*, vol.40, no 5, May. 1992, pp. 1000-1009;

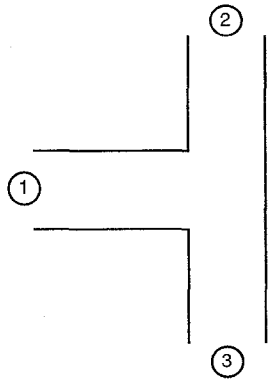

Fig. 1. Transverse section of a T-junction

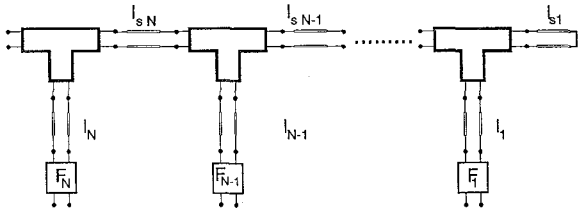

Fig. 2. Layout of the T-manifold multiplexer

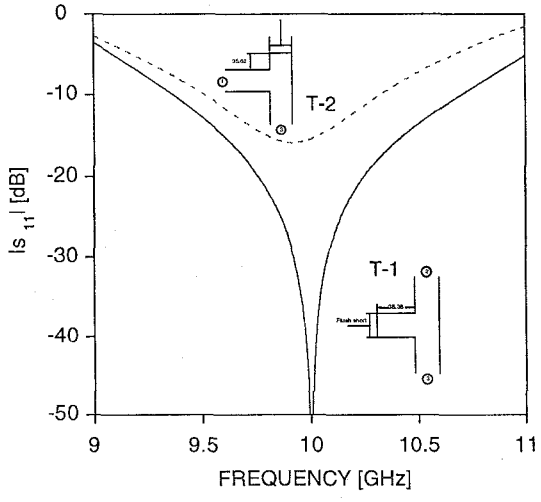

Fig. 3. Reflection at the port 3 of the T-junction, when T-1) a short loads port 1; T-2) a short loads port 2. Shorts are placed at the distances which minimize the input reflection at 10 GHz

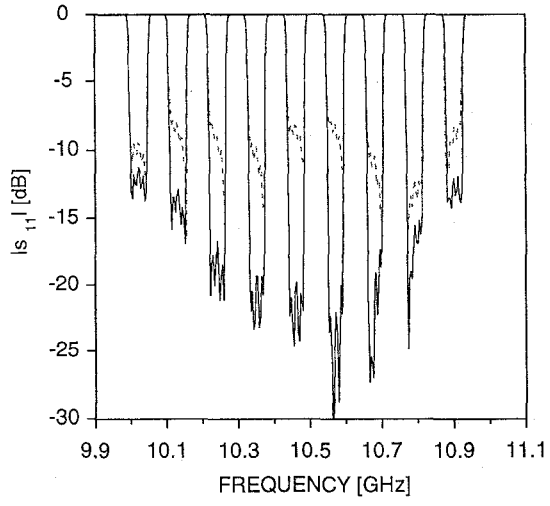

Fig. 4. Reflection at the common port of a un-optimized 9-channel not contiguous multiplexer, employing septate E-plane filters and an E-plane T-junction manifold. The dashed line is obtained by spacing junctions and channel filters according to formulae (3.5.8-12) of [1]; The continuous line refers to our method

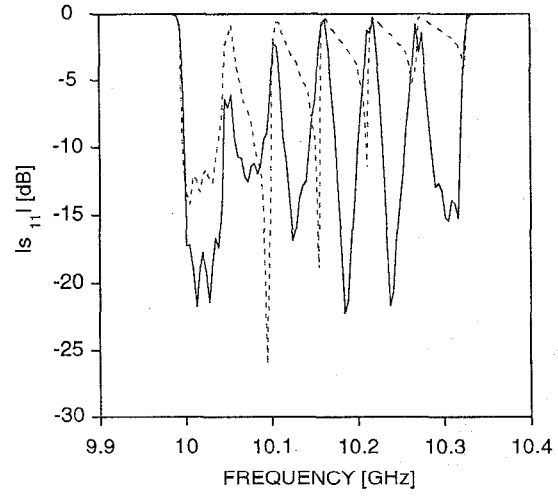

Fig. 5. Reflection at the common port of a un-optimized 6-channel contiguous multiplexer, employing septate E-plane filters and an E-plane T-junction manifold. The dashed line is obtained by spacing junctions and channel filters according to formulae (3.5.8-12) of [1]; The continuous line refers to our method

Waveguide Diplexer and Multiplexer Design

A. A. Kirilenko, S. L. Senkevich, V. I. Tkachenko, and B. G. Tysik

***Abstract*—A new computer-aided procedure of designing waveguide manifold multiplexers, which combines a rigorous numerical analysis of electromagnetic characteristics of the key elements of the structure and a simple circuit engineering design technique, is proposed. This procedure enables one to obtain the required multiplexer characteristics without any experimental corrections at the minimum computer time expense. Typical design results are given to demonstrate the efficiency of the method.**

I. Introduction

THE problems of the millimeter wave radio signal dividing and combining have a certain number of specific points consisting first of all in the increase of requirements to the key-elements [1]–[4].

This paper presents a new approach to the design of manifold multiplexers, which is remarkable for its simplicity and rigorous electromagnetic treatment and enables one to avoid an approximate lumped circuit description of T-junctions [2]. As concrete examples of its implementation, two modifications of multiplexer and diplexer structures based on the bandpass filters (BPF) with all-metal inserts and the E and H-plane T-junctions are considered. In the first modification the multiplexer channels are placed in the side arms of a rectangular shorted waveguide (see Fig. 1(a)), which serves as a manifold. In the second modification the diplexer channels are placed in the T-junction through arms (see Fig. 1(c) and (d)). Algorithms of rigorous computation of insertion loss characteristics (ILC) of the designed structures were formed by combining the multimode scattering matrices of key discontinuities, namely waveguide bifurcations and T-junctions.

The proposed multiplexer design procedure has two features. Firstly, in channel filters design the structure of the "strip and T-junction with a shorted through arm" type is chosen as the first K-invertor, rather than a single strip as in the case of filters in regular waveguides. Secondly, this approach enables one to reduce the design of a multiplexer to the step-by-step application of the known BPF designing procedure. In this step-by-step procedure of channel filter designing, the characteristics of the earlier designed part of the structure are rigorously incorporated, which allows to immediately take into account the main part of the crosstalk between channels.

II. Electromagnetic Model

Rigorous analysis of the considered structures is based on the preliminary obtaining S-matrices of waveguide bifurcations and T-junctions. The algorithms of their computation are based on the well known Galerkin procedures [5], [6]. The waveguide bifurcation S-matrix was calculated by using of the set of orthogonal polynomials with the weight, that take account of edge behavior of the field [5]. It allows to eliminate low frequency shift of design results which took place in the case of the set of trigonometric functions. Characteristics of the composite structure are easily obtained by means of generalized S-matrix technique [7]. The ohmic loss in the designed structure was taken account of by using the perturbation method [8].

Let us define $L^{(q)} = -20Lg|T_q|$ dB as the insertion loss for the q-th channel of a multiplexer. Here T_q is the transmission coefficient of the incident H_{10} mode of the manifold into the same mode of the q-th channel. The design and analysis were carried out in terms of the relative values $\chi = a/\lambda$ where l is the free-space wavelength, a is the waveguide width. In estimating the ohmic loss the actual value of the frequency f and real geometrical parameters of a waveguide were taken into account. Multiplexer arms are numbered in the order of the increasing distance from the shorted end of the manifold.

III. Multiplexers with a Successive Arrangement of Channels

The input task for the multiplexer design is formed on the basis of the requirements to the insertion loss characteristics in each channel. For each channel the following set is determined: the kind of the insertion loss characteristics (Chebyshev or Batterworth), the insertion loss level in the passband $L_R^{(q)}$; values characterizing passband and edge steepness: $L_A^{(q)}$, $L_B^{(q)}$, $\chi_A^{(q)}$, $\chi_B^{(q)}$, $\chi_1^{(q)}$, $\chi_2^{(q)}$, (Fig. 1(b)). Besides, let us define the value

$$GW_q = 2(\chi_1^{(q+1)} - \chi_2^{(q)})/(\chi_2^{(q)} + \chi_2^{(q+1)} - \chi_1^{(q)} - \chi_1^{(q+1)})$$

and call it the guardband width between the q-th and the $(q+1)$-th multiplexer channels. This value characterizes the frequency shift between channels and will be used below.

First of all let us note that the "straightforward" approach, which is based on placing filters, designed for a regular waveguide, into the output arms of a multiplexer, does not produce good results, because the T-junction with shorted through arm proper cannot be matched satisfactorily . In this case the best SWR is not less than 1.7 at $0.55 \leq \chi \leq 0.85$ and significantly increases as χ tends to 1.0. It holds true both for the E and to H-plane T-junctions. The first strip and resonator lengths of the channel filters have to be corrected in the appropriate manner to compensate the input channel irregularity. That is why, the blocks of the "strip and T-

Manuscript received August 4, 1993; revised January 7, 1994.

The authors are with the Institute of Radiophysics and Electronics, Kharkov, 310085, Ukraine.

IEEE Log Number 9402420.

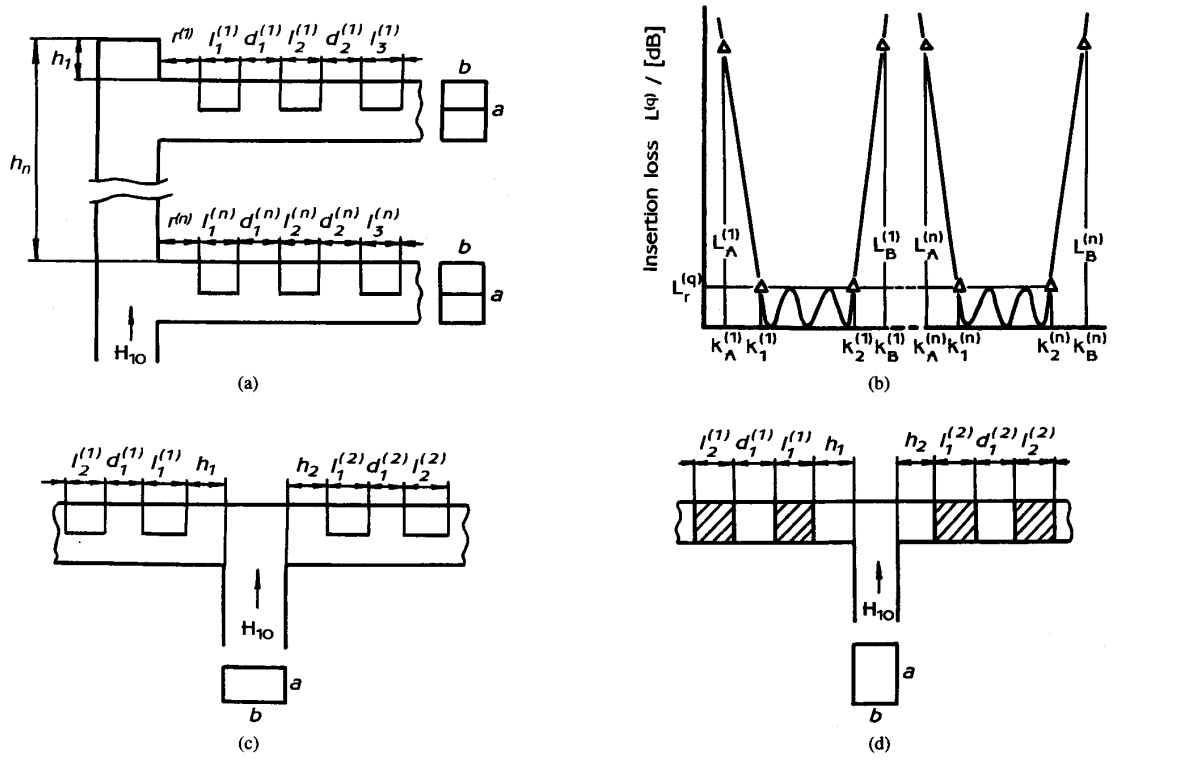

Fig. 1 Structures of multiplexer with successive arrangement of channels (a) and diplexer formed by H-plane (c) and E-plane (d) T-junctions. Input request for designing (b).

junction with a shorted through arm" type are chosen as the first channel filters K-invertors [9].

The second main idea of the proposed design procedure lies in placing the first strips of the channel filters into the "mouths" of the side arms ($r^{(q)} = 0$ in Fig. 1(a)). It reduces to the minimum the crosstalk of channels and provides the maximum separation of parasitic resonances from operating frequency band. Characteristics of T-junction with the filter placed in the above-mentioned manner are presented in Fig. 2.

Calculations show that $|T_{31}|^2 \leq 10^{-4}$ (the insertion loss is more than 40 dB) and $|R_{11}|^2 \leq 0.03$ (the return loss exceeds 15 dB) even at the tuning-off from the channel central frequency by the value of the BPF's passband. Therefore, we can conclude that at guardband widths $GW_{j-1,j} \geq 1$ in the passband of the j-th channel the rest of the channels are "locked" and the multiplexer design problem is reduced to the step-by-step designing of the channel filters, the first K-invertors of which are blocks of the "T-junction with a strip in the side arm and a shorted through arm" type. The insertion loss in the low-frequency region is higher than one in the high-frequency region. From this point of view one has to design at first turn multiplexer channels with higher central frequencies and to place them in the side arms, which are more distant from the common input.

For further improvement of the procedure of multiplexer design the distances h_q are obtained from the condition of the best matching of T-junction with the designed part of multiplexer structure in the through arm. After that the first strip length $l_1^{(q)}$ and the resonator length $d_1^{(q)}$ are found by varying the strip length of the structure of the "T-junction with a designed part of multiplexer structure in the through arm and a strip in the side one" type. It allows to rigorously take into

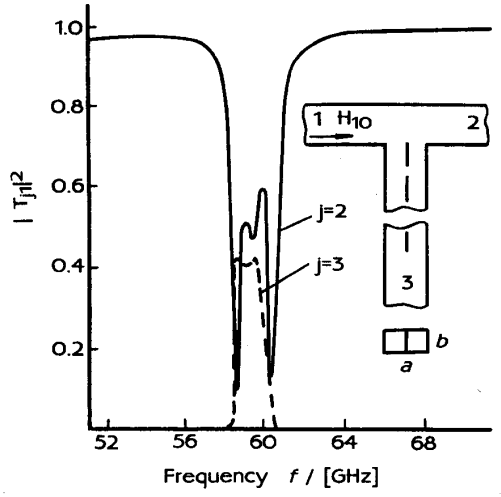

Fig. 2. Power transmission coefficients of H-plane T-junction with a filter in the side arm for through (solid line) and side (dashed line) ones.

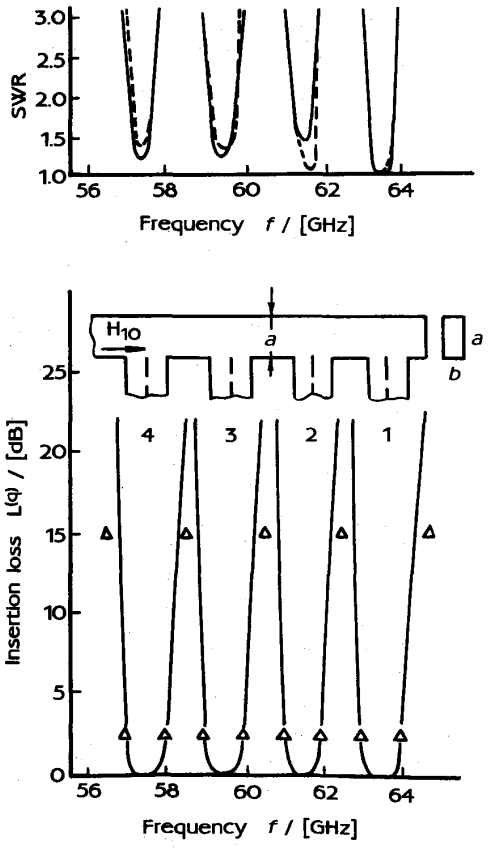

Fig. 3. Characteristics of four-channel multiplexer with five resonator channel filters at the direct and reverse arrangement of channels (solid and dashed lines, respectively).

account the electromagnetic properties of the already designed part of the multiplexer in the design of each next channel.

Let us consider the results of the design of the four-channel multiplexer formed by the 3.6mm × 1.8mm waveguides and having narrow band frequency channels $(2(\chi_2^{(q)} - \chi_1^{(q)})/(\chi_2^{(q)} + \chi_1^{(q)}) = 1\%–3\%)$. The strip diaphragms thickness was 50 μm. Five-resonator BPF's with the Batterworth characteristics have been chosen as channel filters. SWR in the through arm and channel ILC's are presented in Fig. 3. The input task is shown by triangles. In the first case the multiplexer channels are arranged from the shorted end of manifold in the order of decreasing of central frequencies (direct arrangement). As it is seen from the figure, the characteristics of the designed structure satisfy the input task completely.

The rearrangement of channels in the order of the increase of their central frequencies (reverse arrangement) leads to somewhat different distances $h^{(q)}$ and to the same strip lengths. As it is seen from Fig. 3 such an arrangement does not effect the characteristics of the highest-frequency channel but seriously disturbs the SWR of the others.

Note that the proposed designing procedure may be easily extended to the cases when the first channel filter is placed in the through arm of the manifold and any side arm is located at the opposite side of the manifold. In the first case the first BPF is designed as a filter in a regular waveguide and the farthest from the common input T-junction is matched preliminary by displacement of this BPF as the whole.

The typical cpu time for designing a four-channel multiplexer with five-resonator BPF's is about half an hour for the IBM PC 386.

IV. Diplexers Formed by T-Junctions. Iterative Design Procedure

Consider a diplexer formed by the T-junction which is excited from the side arm (see Fig. 1(c) and (d)) and its channel filters are located in the through arms. Significant difference of this structure from the preceding ones lies in the fact that when designing the channel BPF's, one should take into account the channel crosstalk. Here the first strips of both BPF's cannot be placed in the arm "mouths" ($h_{1,2} = 0$) as there arises a problem of the T-junction matching at two different channel frequencies. As it was obtained by means of numerical experiments, the first strip lengths often become equal to zero even when the simplest tasks for ILC are realized, if additional fine-tuning elements are not used.

In this diplexer structure we applied waveguide sections of the lengths $h_{1,2} \neq 0$ as tuning elements. That is why the importance of exact accounting of channel crosstalk increased. The impossibility of using step-by-step design has led to the development of an iterative procedure. Its essence consists in the optimization of the location of the filter at designing the opposite one, in the exact calculation of electromagnetic characteristics of "T-junction with the filter in one arm and the strip in other one" at the synthesis of first K-invertors and in iterative revision of the filter dimensions by means of their resynthesis.

At such an approach only the lengths of the first strips and resonators in both channels vary. The reason of iterative process termination is the achievement of the situation when the resonators and strips lengths corrections become lower than possible technology tolerances. It is worth noting that as a rule there is no necessity to use more than five or six steps of the iterative procedure for realizing conventional tasks for the ILCs in the range of $0.5 < \chi < 0.8$.

As an example, Fig. 4(a) presents the dependences of the insertion loss for both channels of the diplexer formed by an H-plane T-junction designed according to the procedure discussed above. The results of one and five iteration design are considered here. It is seen that at one iteration design the characteristics of diplexer channels do not satisfy the input task with regard to the bandpass and loss. In the second case these requirements are fulfilled completely.

Characteristics of the diplexer formed by an E-plane T-junction designed according to the same input task are shown in Fig. 4(b). The iterative procedure, as in the case of the H-plane T-junction, has enabled us to improve the device's characteristics considerably. When comparing the plots in Fig. 4 one can see that the characteristics of both the diplexers practically coincide. However the values of minimum SWR are less and the high-frequency edge steepness is higher in the E-case than ones in the H-case.

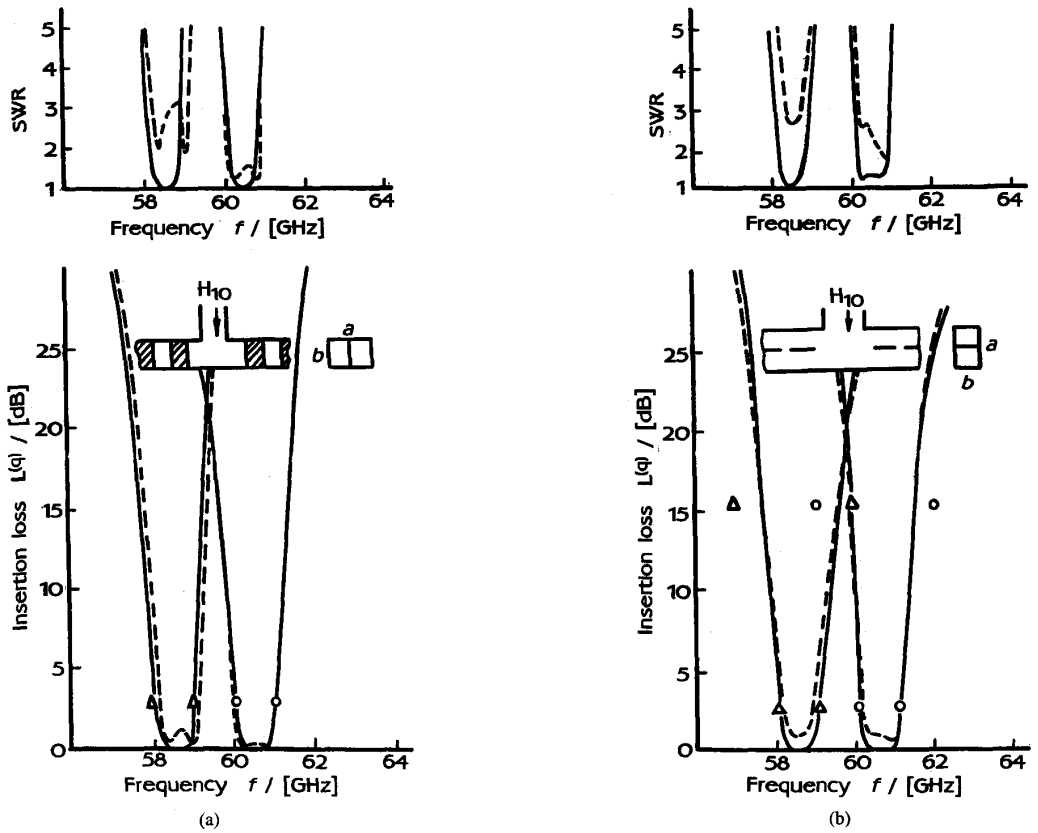

Fig. 4. Characteristics of diplexers formed by E-plane (a) and H-plane (b) T-junction (dashed lines one iteration, solid ones five iteration).

The cpu time for designing a diplexer formed by a T-junction with five-resonator channel BPF's is 24 min for the IBM PC 386.

V. Conclusion

Examples presented above demonstrate that considered microwave waveguide multiplexer structures and their design procedures are very simple and effective in the wide range of input tasks. Difficulties arise when guardband width tends to zero or when the central frequency of a channel is near the cutoff point of a higher order mode. In the first case one should use some iterative or numerical optimization procedures in order to account for the crosstalk of the channels. Then the time of computation increases greatly. In the second case we can, for example, place channel filters into one H-plane step-narrowed waveguide section in order to decrease the value of χ at the same frequency. Another way is to modify the circuit designing technique itself, namely to account for the dispersion of the K-invertor characteristics.

References

[1] A. A. Ishuk and L. M. Martinov, "Principles of constructing frequency dividing/combining microwave systems, *Zarubezhnaya Radioelektronika,* no 7, pp. 34-50, 1986.

[2] J. D. Rodes and R. Lewy, "Design of general manifold multiplexers," *IEEE Trans. Microwave Theory Tech.,* vol. MTT-27, pp. 111-123, 1979.

[3] J. Dittloff, F. Arndt, "Rigorous field theory design of millimeter-wave E-plane integrated circuit multiplexers", *IEEE Trans. Microwave Theory Tech,* vol. 37, pp. 340-3350, Feb. 1989.

[4] C. Nguen and K. Chang, "Design and performance of a W-band broad band finline diplexer with over 20 GHz bandwidth, *IEEE MTT-S Microwave Symp. Dig.,* pp. 349-352, St Louis, MO, June 1985.

[5] V. P. Lyapin, V. S. Mikhalevsky, and G. P. Sinyavsky, "Solution of difraction problem by plane resonant discontinuities in rectangular waveguide with accounting of edge singularity," Izvestiya vuzov. *Radioelectronica,* vol. 25, no. 1, pp. 13-26, 1984.

[6] L. A. Rud', "Wave diffraction from T-junctions of rectangular waveguides," *Radiotekhnika i Elektronika,* vol. 29, no 9, pp. 1711-1719, 1984.

[7] R. Mittra and S. W. Lee, *Analytical Techniques in the Theory of Guided Waves.* New York: Macmillan, 1971.

[8] A. S. Ilynsky and G. Y. Slepyan, and A. Y. Slepian, *Propagation, Scattering and Dissipation of Electromagnetic Waves,* New York: IEEE Press, 1993.

[9] D. L. Mattey, L. Young, and E. M. T. Jones, *Microwave Filters, Impedance-Matching Networks and Coupling Structures.* New-York: McGraw-Hill, 1964.

A. A. Kirilenko, for a photograph and biography, see page 1392 of this issue.

S. L. Senkevich, for a photograph and biography, see page 1392 of this issue.

V. I. Tkachenko, photograph and biography, not available at time of publication.

B. G. Tysik, photograph and biography, not available at time of publication.

Design and Performance of a Ku-band 8 Channel Contiguous OMUX for Satellite Applications

G G Connor and M J Perren

1. Introduction

Output Multiplexers (OMUXes) for satellite communications have, over the past few years, been increasing in complexity and performance. Systems are continually packing more channels within the allocated bands whilst maintaining stringent loss and pass band requirements. The contiguous nature of such requirements, however, tend to degrade the pass band performance so that larger variations of group delay and loss are produced, especially near the useable band edge. This paper describes a method of minimising this problem at Ku-band.

2. Multiplexing Techniques

Two major options are available for multiplexion. Starting from doubly terminated prototypes gives eventual contiguous channel responses having increased rejection characteristics but with higher insertion loss and group delay variations within the pass band. Alternatively, we may start from a singly terminated prototype. Here, the desired filter response is achieved only after multiplexion and so no increased rejection or pass band variations are evident. The choice will usually be based on the precise requirements of a given application. Since we are aiming to produce a low insertion loss and group delay variation, the singly terminated prototype was selected.

3. Channel Filter Prototype

The general requirements for the channel filters are shown in Table 1. Preliminary analyses showed the pseudo-elliptic function filter of degree 4 to have around 40 nS group delay variation (inclusive of temperature variation effects and adequate set-up margins/mechanical effects. An alternative function, derived from the maximally flat amplitude response (Butterworth), was investigated. This type of channel response showed a remarkable improvement in group delay variation (17nS) after multiplexion. Since the design emphasis was placed on low insertion loss and group delay variations, Butterworth channel filters were selected.

4. Multiplexing Technique

The configuration of the multiplexer is shown in Figure 1. The channel filters are connected to a waveguide manifold via E-plane T-junctions. The equivalent circuit of this configuration is shown in Figure 2. To begin the design process, the singly terminated prototypes were initially synthesised as coupling matrices and the input couplings amended to allow for the impedance transformation inherent in a rectangular waveguide E-plane T-junction. The series reactances of each channel's T-junction model were combined to form a single reactance at the termination of the manifold. This reactance could then be combined with a simple reactance nulling network derived via [1]. The channels were separated along the manifold by approximately half wavelengths.

The performance of this initial design is shown in Figures 3 and 4.

G G Connor, M J Perren, British Aerospace plc

The second phase of the design process relied on computer based optimisation of manifold lengths, branch guide lengths and those elements of the filters closest to the manifold. The optimisation resulted in the performance shown in Figures 5 to 7.

5. Multiplexer Performance

The channel filters cavities and irises were manufactured and assembled for individual tuning. A Hewlett-Packard HP8510 analyser was used, allowing each filter to be tuned for both phase and amplitude. After tuning, the filters were attached to the manifold and the complete multiplexer fine tuned. The resulting multiplexer performance is given in Figures 8 to 10. It is apparent that the desired group delay performance has been achieved. The loss of the channel filters varied between 0.7dB and 0.8dB at band centre, dependent mostly upon the position of the channel with respect to the reactance nulling network which is tuned to the centre of the multiplexer band. It is worth noting that this variation in return loss will effectively be removed by a broad band transmit filter which would generally be required, either to clean up any spurious responses from the stop band or in the diplexer as part of a combined receive/transmit antenna feed.

6. Conclusions

It has been shown that it is possible to reduce the group delay variation across the useable band in contiguous multiplexer channels by the use of singly terminated Butterworth prototype channel filters. The singly terminated prototype resulted in a simple and speedy design route, the performance of the multiplexer being almost obtained without the need for optimisation. The effectiveness of the design relies heavily on accurate models for both channel filters and E-plane T-junctions. The overall effectiveness of reducing the group delay variation may be compromised by the associated reduction in rejection between channels, producing increased variations due to multipath effects. Analyses at BAe suggest an overall advantage to the Butterworth configuration as the increased variations due to multipath are insufficient to attain the 40nS values from a typical high rejection solution.

7. References

[1] Microwave Filters, Impedance-Matching Networks and Coupling Structures. G Matthaei, L Young, E M T Jones, Artech House.

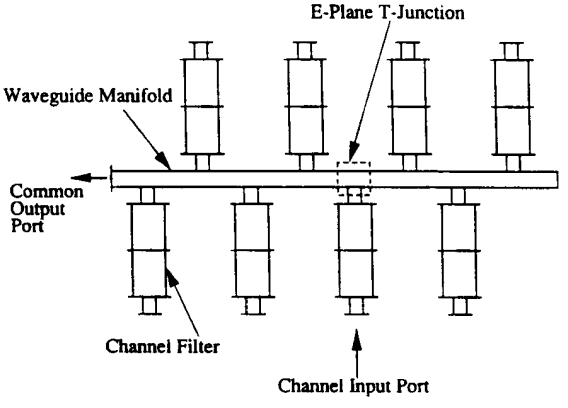

Figure 1 Configuration of Output Multiplexer

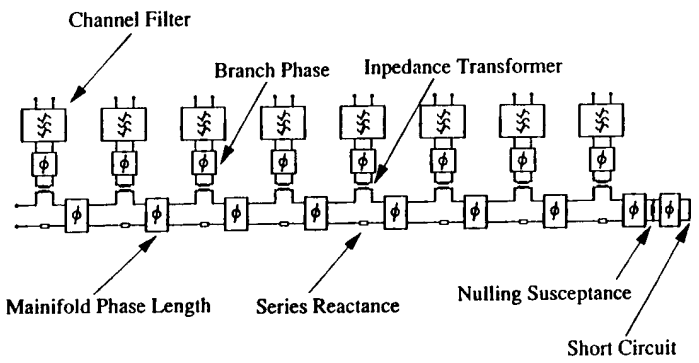

Figure 2 Multiplexer Equivalent Circuit

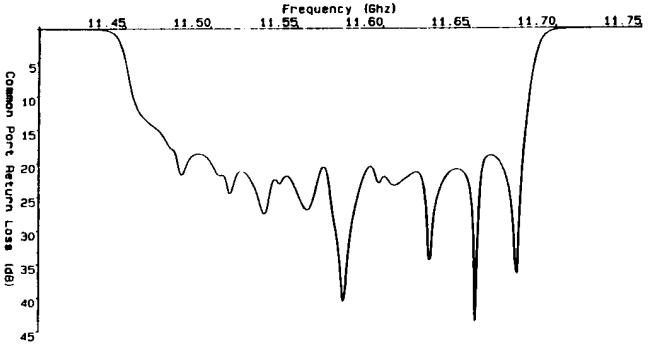

Figure 3 Designed Return Loss

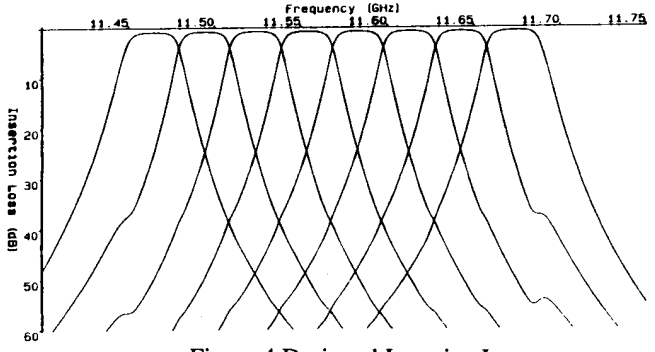

Figure 4 Designed Insertion Losses

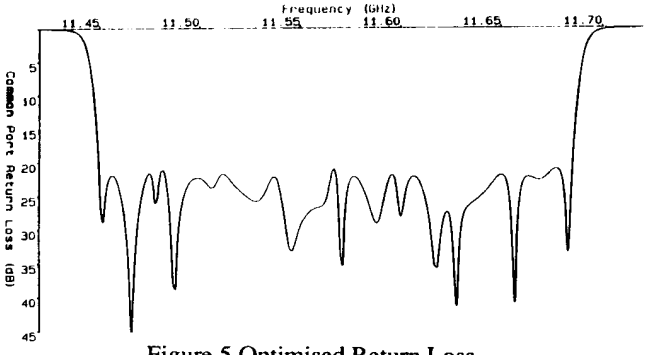

Figure 5 Optimised Return Loss

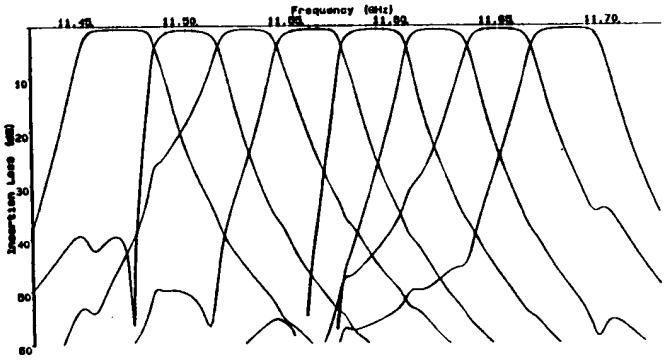

Figure 6 Optimised Insertion Losses

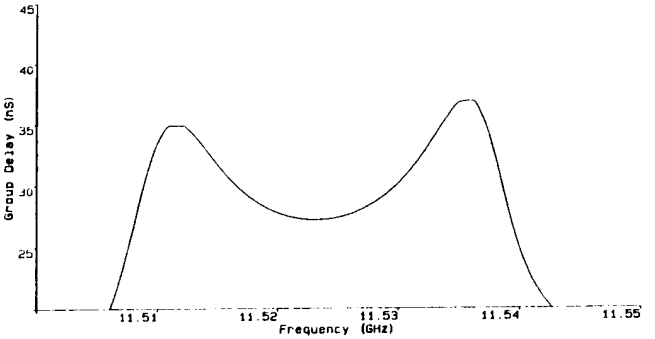

Figure 7 Optimised Channel Group Delay

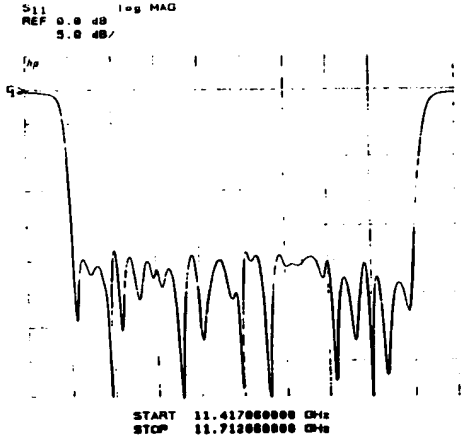

Figure 8 Measured Return Loss

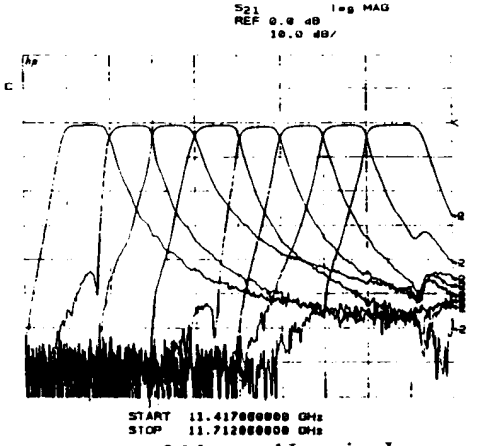

Figure 9 Measured Insertion Loss

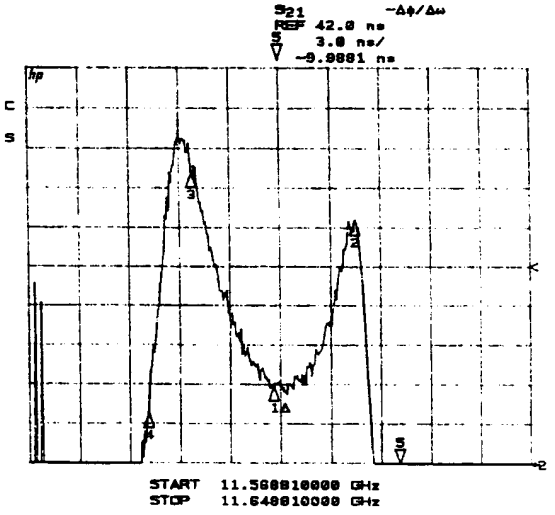

Figure 10 Measured Channel Group Delay

Parameter		Specification
Channel Centre Frequencies		11.46425GHz 11.49375GHz 11.52325GHz 11.55275GHz 11.58225GHz 11.61175GHz 11.64125GHz 11.67075GHz
Mid Band Insertion Loss		0.9dB max
Insertion Loss Variation		
	FO ±6MHz	0.2dB p-p max
	FO ±8MHz	0.4dB p-p max
	FO ±10MHz	0.8dB p-p max
	FO ±12MHz	1.6dB p-p max
	FO ±13MHz	3.0dB p-p max
Insertion Loss Slope		
	FO ±6MHz	0.08dB/MHz max
	FO ±8MHz	0.14dB/MHz max
	FO ±10MHz	0.25dB/MHz max
	FO ±12MHz	0.5dB/MHz max
	FO ±13MHz	1.0dB/MHz max
Out of Band Rejection		
	FO ±20MHz	7dB min
	FO ±30MHz	25dB min
Group Delay Variation		
	FO ±6MHz	6.0ns p-p max
	FO ±8MHz	5.5ns p-p max
	FO ±10MHz	8.0ns p-p max
	FO ±13MHz	18.ns p-p max
Power Handling		8 carriers simultaneously @ 58W per carrier
Thermal		
	Non-operating	-30 to +80°C
	Qualification	+20 to +80°C
	Acceptance	+25 to +75°C
	Operating	+30 to +70°C
Input/Output Return Loss		20dB

Table 1 OMUX Specification

Ridge Waveguide Divider Junctions for Wide-Band Multiplexer Applications

Yunchi Zhang, Jorge A. Ruiz-Cruz, and Kawthar A. Zaki

Department of Electrical and Computer Engineering, University of Maryland, College Park, MD 20742, USA (ychzhang@umd.edu)

Abstract — **Ridge waveguide divider junctions are introduced and applied to wide-band multiplexer applications. A rigorous analysis and optimization process by Mode Matching Method (MMM) is employed to design the junctions that yield low reflection coefficient in common port and almost equal transmission coefficients in the other two ports over a wide frequency band. Two design examples of wide-band diplexer and triplexer using such junctions are presented. All the components involved in the diplexer/triplexer designs are rigorously modeled and cascaded by MMM. Optimization procedures by MMM are also applied in these two designs to improve the performance. Multiplexers using such junctions can be built in either metallic form or low-temperature co-fired ceramic (LTCC) technology.**

Index Terms — **Multiplexer, junction, diplexer, triplexer, mode matching method, ridge waveguide, LTCC.**

I. Introduction

The development of millimeter-wave communications and transceiver technology has created the need for compact, wide-band, high-performance diplexers and multiplexers. Usually waveguide-type multiplexers are the most suitable choices to achieve these requirements. Previous waveguide-type multiplexer designs consist of 1) E and H-plane manifold multiplexers, 2) E and H-plane T-junction-type multiplexers, 3) E and H-plane divider-type multiplexers [1], 4) Ridge waveguide T-junction-type multiplexers [2], etc. Rectangular waveguide junctions are usually employed in 1) – 3), which are not applicable for wide-band multiplexer design due to the limited mono-mode frequency range of rectangular waveguides. Ridge waveguides have much wider mono-mode frequency range than rectangular waveguides, which makes them a good choice for wide-band multiplexer design. In [2], a wide-band diplexer using ridge waveguide T-junction has been presented. The disadvantage of ridge waveguide T-junction-type multiplexers is that the physical size, especially the cross section, is large and the physical layout makes it very difficult to integrate them inside a system.

Ridge waveguide divider junctions as in Fig. 1 are presented in this paper. Such junctions have small cross sections and can still achieve wide-band match of the common port. Multiplexers using these junctions can have not only very wide fractional bandwidth, but also very compact size, which makes them easily be integrated into a system. Analysis and design of the junctions by mode matching method (MMM) are discussed.

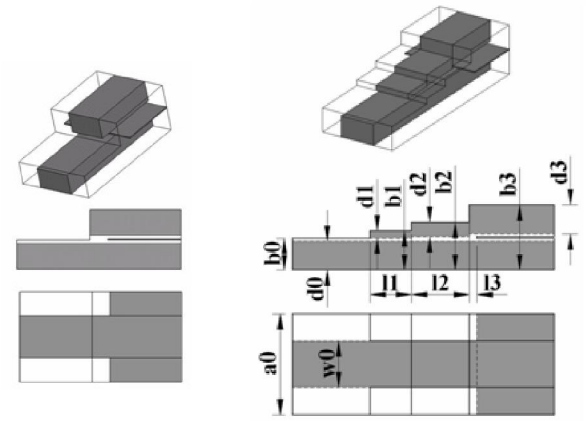

(a) (b)

Fig. 1. (a) Structure of a simple ridge waveguide divider junction; (b) Structure of a transformer-embedded divider junction.

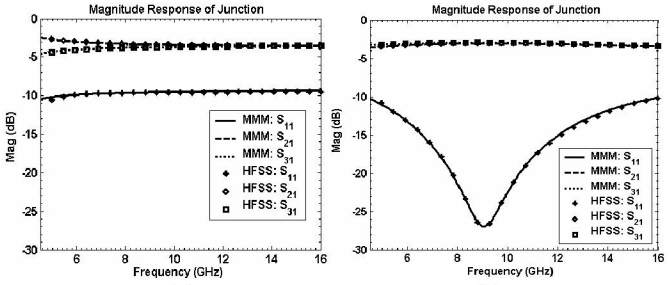

(a) (b)

Fig. 2. (a) Magnitude response of Fig. 1(a) by MMM and HFSS; (b) Magnitude response of Fig. 1(b) by MMM and HFSS. Both junctions are designed for LTCC application. Dimensions of Fig. 1(b) are: *a0*=260mil, *w0*=120mil, *b0*=82.28mil, *b1*=100.98mil, *b2*=123.42mil, *b3*=168.3mil, *d0*=74.8mil, *d1*=18.7mil, *d2*=37.4mil, *d3*=74.8mil, *l1*=108mil, *l2*=149mil, *l3*=9mil.

Two design examples, one diplexer and one triplexer, using ridge waveguide divider junctions are given in this paper. Both designs have very wide fractional bandwidth, 95% for diplexer and 50% for triplexer. Ridge waveguide evanescent mode bandpass filters are employed for all the channel filters. The diplexer/triplexer is designed to be built in LTCC technology. Multiplexer designs in metallic form using the presented junctions are also possible.

II. Ridge Waveguide Divider Junctions

Waveguide junctions are very important components in many microwave applications, especially in multiplexer

0-7803-9542-5/06/$20.00 ©2006 IEEE

designs. These junctions are usually lossless reciprocal three ports and all three ports can not be matched simultaneously. However, in multiplexer applications, it is often desirable to have the junction with one of its ports well matched over a wide frequency band [2]. Fig. 1(a) shows a simple ridge waveguide divider junction. A common port of single ridge waveguide is connected to a double ridge waveguide, and then to two separated output ports of single ridge waveguides. Many modes are excited in the double ridge waveguide by the common port waveguide, and then excite the fundamental mode of the two output waveguides. The performance of this simple junction (as in Fig. 2(a)) is not very good and is mainly limited by the discontinuity between the common port and the double ridge waveguide. To improve the performance, a matched transformer can be introduced between the common port and the double ridge waveguide. Fig. 1(b) shows the improved junction configuration. For both structures, usually the shorter the double ridge waveguide, the better the performance. This length can be set as the achievable minimum length of the employed manufacture technology.

To design such junction as in Fig. 1(b), an analysis and optimization procedure by MMM is applied. The eigen-modes and eigen-field distributions of each ridge waveguide cross section are found first by the same method as in [3]. The discontinuities between waveguides are then characterized as the generalized scattering matrix (GSM) by MMM. Finally all the GSMs are cascaded together to have the frequency response of the whole junction. In the analysis, the three port junction can be represented as a generalized two port network, which is very convenient to cascade the junction with other channel filters for the analysis of multiplexer. The optimization goal of the junction is to have low reflection coefficient from the common port and almost equal transmission coefficients to the two output ports. Shown in Fig. 2(b) is the optimized junction response, which shows a very good wide-band performance. Response by Ansoft HFSS is also given in Fig. 2 to show the agreement with MMM.

III. Multiplexer Design Examples

To show the feasibility of applying ridge waveguide divider junctions to wide-band multiplexer applications, two design examples are presented.

A. Diplexer Design and Modeling

The requirements of a wide-band diplexer are: 1) Pass bands of channel filter 1 and channel filter 2: 4.5 – 6.15 GHz and 9.0 – 12.5 GHz; 2) Minimum passband return loss: 18 dB; 3) Maximum passband insertion loss: 2.5 dB; 4) Minimum stopband attenuation at the other channel: 60 dB. The relative bandwidth of the whole diplexer is about 95%. Channel filter 1 has relative bandwidth of about 31% and channel filter 2 has about 33%. The diplexer is designed based on LTCC technology. The relative permittivity of dielectric material is

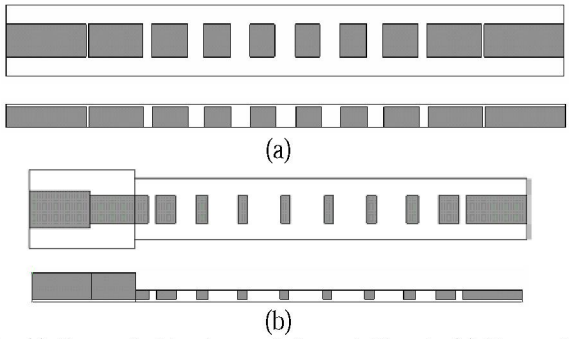

Fig. 3. (a) Top and side views of channel filter 1; (b) Top and side views of channel filter 2 including transformer in-front.

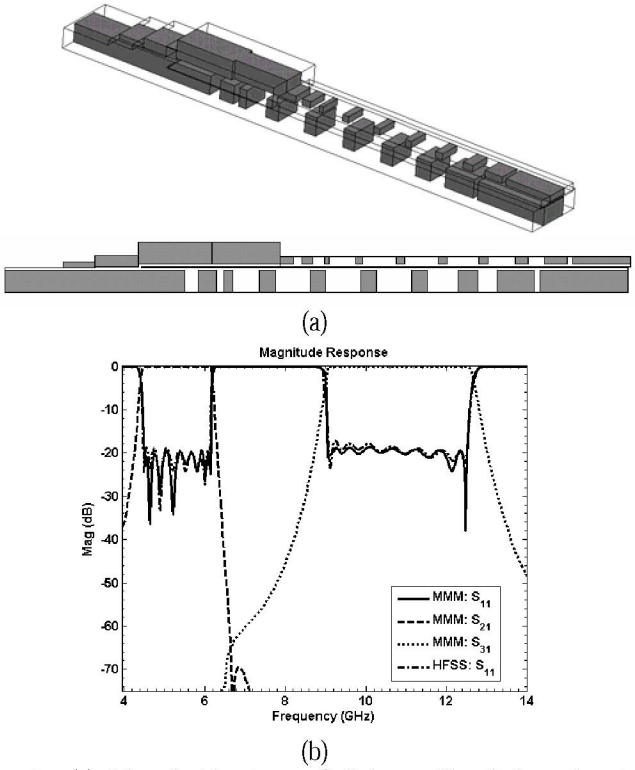

Fig. 4. (a) 3d and side views of diplexer. The diplexer housing dimensions are a=260 mil, b=168.3 mil (45 layers), l=2130 mil. The gap of filter ridge waveguide is 7.48mil (2 layers). (b) Magnitude response of diplexer by MMM and HFSS.

5.9. The thickness of each dielectric layer is 3.74mil and the thickness of metallization is 0.4mil. The diplexer height must be multiples of dielectric layers.

The junction as in Fig. 1(b) is employed for this diplexer design. Its response as in Fig. 2(b) shows very good performance through the whole diplexer band.

Channel filter 1 and channel filter 2 are ridge waveguide evanescent mode bandpass filters. Shown in Fig. 3(a) and Fig. 3(b) are the top and side views of filter 1 and filter 2, respectively. The cross sections of the ridge waveguides employed by these two filters are different due to the difference of the filter center frequencies. Filter 1 uses the same ridge waveguide as the junction output waveguide, while filter 2 uses a smaller one since it has a higher center

frequency. A matched transform is therefore added between the junction and filter 2 to connect them, which is also shown in Fig. 3(b). These two filters are initially chosen as 8-pole, 0.02 dB ripple, doubly terminated Tchebycheff filters. The initial design is based on *k*-inverters method. Basically the initial dimensions can be found by matching the *k*-values on the coupling curve of Ridge-Rectangular-Ridge waveguide coupling sections. The optimization procedure by MMM is then applied to improve the filters performance. Detail information about designing such filters can be found in [4].

Shown in Fig. 4(a) are the 3d and side views of the diplexer structure. The optimized junction and channel filters are connected together to have the initial design of the diplexer. The reflection and transmission coefficients of the diplexer are computed by cascading the GSMs of the junction and filters together. If the higher order resonant modes of channel filter 1 do not exist inside the passband of channel filter 2, the initial diplexer response (only adjusting the connection waveguide lengths) will be a very good starting point for optimization. If it is not the case, the higher order resonant modes of channel filter 1 must be managed to move out of the passband of channel filter 2.

The optimization procedure by MMM is also applied to improve the diplexer performance. The lengths of cavities and coupling sections are optimized. The objective function used in the optimization is weighted least square sums of the deviation of the return loss and insertion loss from their specified values. The optimized diplexer response is shown in Fig. 4(b). The S_{11} response by HFSS shows a very good agreement with MMM. The housing dimensions of the whole diplexer are about: $a \times b \times l$ = 260mil × 168.3mil × 2130mil.

B. Triplexer Design and Modeling

The specifications of the triplexer design are: 1) Pass bands of three channel filters: 6.0 – 6.6 GHz for filter 1, 7.6 – 8.4 GHz for filter 2, 9.0 – 10.0 GHz for filter 3; 2) Minimum passband return loss: 20 dB; 3) Maximum passband insertion loss: 2.5 dB; 4) Minimum stopband attenuation of one channel filter inside other channel filters: 60 dB. The relative bandwidth of the whole triplexer is 50% and each channel filter is about 10%. The triplexer is also designed to be manufactured in LTCC technology. The LTCC parameters are identical as the ones for the previous diplexer design.

The presented ridge waveguide junction is a three-port network component which is proper for diplexer design. To make a triplexer design with such junctions, the configuration as in Fig. 5 is proposed. Basically two diplexers, diplexer 1 and diplexer 2, are cascaded together to fulfill the triplexer. Both diplexers use the presented junctions. The two channels of diplexer 1 are: 6.0 – 6.6 GHz and 7.6 – 10.0 GHz, with the second channel covering the whole frequency band of channel filter 2 and 3 of the triplexer. Diplexer 2 consists of two channels same as channel filter 2 and 3 of the triplexer. A triplexer is expected if well designed diplexer 1 and diplexer 2

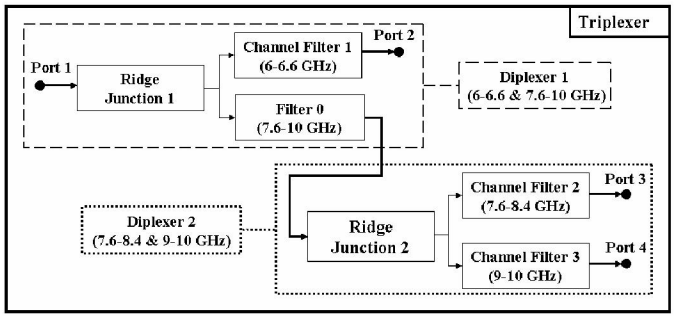

Fig. 5. Triplexer configuration by cascading two diplexers.

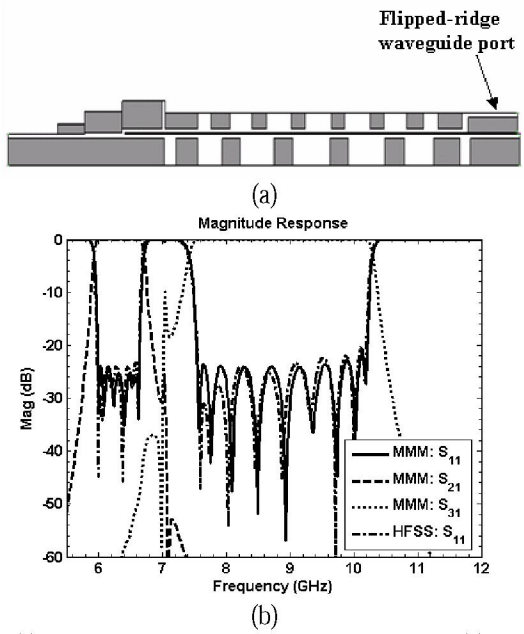

Fig. 6. (a) Side view of diplexer1 for the triplexer; (b) Magnitude response of diplexer 1 by MMM and HFSS.

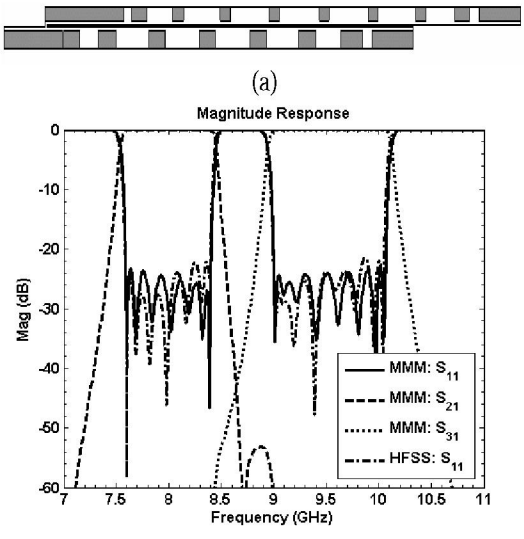

Fig. 7. (a) Side view of diplexer2 for the triplexer; (b) Magnitude response of diplexer 2 by MMM and HFSS.

are cascaded together. The second channel filter of diplexer 1 is named as filter 0 in Fig. 5 for later discussion. This configuration of triplexer maintains the advantage of compactness and is appropriate for system integration.

Fig. 6(a) shows the structure of diplexer 1 which consists of filter 0 (upper branch) and filter 1 (lower branch). Fig. 7(a) shows the structure of diplexer 2 which consists of filter 2 (lower branch) and filter 3 (upper branch). All the filters are ridge waveguide evanescent mode bandpass filters. The output waveguide of filter 0 is a flipped ridge waveguide (as in Fig. 6(a)) with respect to other ridge waveguide resonators inside the filter. The purpose by doing this is to be able to connect it with diplexer 2. The design procedure of the two diplexers is similar as the previous diplexer example. Fig. 6(b) and Fig. 7(b) are simulated responses by MMM and HFSS for diplexer 1 and 2, respectively. HFSS response shows very good agreement with MMM for both designs.

The triplexer is realized by cascading the two designed diplexers together. Usually the triplexer response will satisfy the requirements if the two diplexers are well designed. It is possible that the performance is slightly worse than the requirements. In this case, the connection waveguides between components can be optimized to improve the performance. There is usually no need to change other dimensions. The simulated triplexer response by MMM is shown in Fig. 8, which satisfies all the desired requirements. The housing dimensions of the whole diplexer are about: $a \times b \times l$ = 200mil × 149.6mil × 4276mil.

IV. Transition Design

To be able to test or utilize the designed diplexer/triplexer, transitions from single ridge waveguide to other compatible 50 ohm port components should be designed. In LTCC technology, usually transitions from strip-line to single ridge waveguide are employed. A typical structure of such transition is shown in Fig. 9(a) and detail design procedure can be found in [5]. In metallic form, a coax to ridge waveguide transition can be applied. A typical structure is shown in Fig. 9(b) and a design example is presented in [6].

V. Conclusion

Ridge waveguide divider junctions are described and applied to wide-band multiplexer designs. The design procedure by MMM of such junctions is discussed. One diplexer with total 95% bandwidth and one triplexer with total 50% bandwidth are designed to be manufactured in LTCC technology. The analysis and optimization procedure is fully implemented by MMM, which dramatically reduces the computation time without sacrificing accuracy. Multiplexer using such junctions can also be built in metallic form.

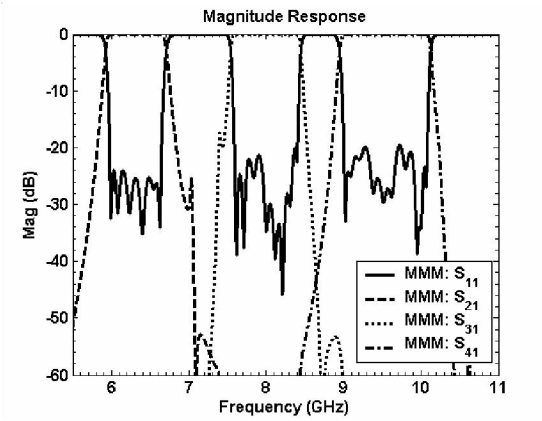

Fig. 8. Magnitude response of the triplxer by MMM. The triplxer housing dimensions are a=200 mil, b=149.6 mil (40 layers), l=4276 mil.

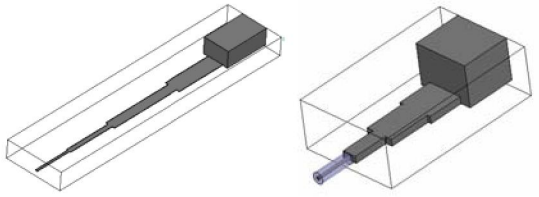

(a) (b)

Fig. 9. (a) Strip-line to Ridge waveguide transition in LTCC technology; (b) Coax to Ridge waveguide transition in metallic form.

Acknowledgement

The authors wish to acknowledge the assistance of Andrew Piloto, Kyocera America, Inc, San Diego, CA, USA, for the LTCC technology. This work has been partially supported by National Science Foundation Grant #ECS0531113.

References

[1] J. Uher, J. Bornemann, and U. Rosenberg, *Waveguide Components for Antenna Feed Systems: Theory and CAD*, Boston, London: Artech House, 1993.

[2] H. Yao, X. Liang, K. A. Zaki, and A. Martin, "Wide-band waveguide and ridge waveguide T-junctions for diplexer applications," *IEEE Trans. Microw. Theory Tech.*,vol. 41, No. 12, pp. 2166-2173, Dec. 1993.

[3] Y. Rong, and K. A. Zaki, "Characteristics of generalized rectangular and circular ridge waveguides," *IEEE Trans. Microw. Theory Tech.*,vol. 48, No. 2, pp. 258-265, Feb. 2000.

[4] Y. Rong, K. A. Zaki, M. Hageman, D. Stevens, and J. Gipprich, "Low-temperature cofired ceramic (LTCC) ridge waveguide bandpass chip filters," *IEEE Trans. Microw. Theory Tech.*,vol. 47, No. 12, pp. 2317-2324, Dec. 1999.

[5] M. A. El Sabbagh, H. Hsu, K. A. Zaki, P. Pramanick, and T. Dolan, "Full wave optimization of stripline tapped-in ridge waveguide bandpass filters," *IEEE MTT-s Dig.*, vol. 3, pp. 1445-1448, June 2002.

[6] Z. Liu, J. A. Ruiz-Cruz, C. Wang, and K. A. Zaki, "An extremely wideband ridge waveguide filter," *IEEE MTT-s Dig.*, vol. 2, pp.615-618, June 2004.

Millimeter-Wave *Ka*-Band *H*-Plane Diplexers and Multiplexers

Yu Rong, *Senior Member, IEEE,* Hui-wen Yao, *Senior Member, IEEE*, Kawthar A. Zaki, *Fellow, IEEE*, and Tim G. Dolan

***Abstract*—Millimeter-wave H-plane diplexers/multiplexers are designed using modified H-plane waveguide T-junctions and modified inductive window bandpass filters. Modeling of the diplexers/multiplexers are performed using the full-wave mode-matching method to obtain the generalized scattering matrices of the building blocks and by the cascading procedure to provide the overall frequency response. A complete systematic optimization procedure leads to the desired diplexer/multiplexer design. The validity of employing the modified H-plane T-junctions in the diplexer/multiplexer configurations are demonstrated by the design examples. A millimeter-wave Ka upper band diplexer based on the simulated results was built and tested. Without any tuning, excellent experimental results are obtained, which verified the full-wave mode-matching-based precise design.**

I. Introduction

THE increasing development of millimeter-wave technology greatly stimulates the need for compact low-loss millimeter-wave diplexing or multiplexing components, which serve as channel separators. H-plane T-junction connected diplexers/multiplexers, shown in Fig. 1, are commonly used [1], [2], where the channel filters are either inductive-window or metal-insert bandpass filters. In the literature, the diplexer/multiplexer design is usually performed by following one of two methods. For each of these two methods, the channel filters are usually designed first to achieve the required channel performances before they are plugged into the diplexer/multiplexer configurations. In the first method [1], the channel filters are re-optimized within the diplexer/multiplexer environment, which includes the T-junction discontinuity effect as well as the interaction between the channel filters. For the second method [2], the original channel filter designs are maintained and additional matching elements are incorporated into the channel paths to obtain an acceptable return loss of the diplexer/multiplexer unit.

The standard H-plane T-junction, shown in Fig. 2(a), has poor characteristics in the upper band that present problems in the diplexer/multiplexer design. The conventional design is not successful for upper band frequency if the above-mentioned first method is used [2]. On the other hand, the overall dimension of the designed diplexer/multiplexer using the second method is too long due to the matching elements, especially for wide-band applications. Recent contributions [3], [4] may be applied to the design of the H-plane diplexers/multiplexers, however, the resultant structures are cumbersome and cannot meet the system compactness requirement for certain applications. The round corners in the E-plane, resulting from the manufacturing process in the inductive windows channel filters, as shown in Fig. 2(b), are unavoidable due to the finite tool radius. This problem is not serious for diplexers/multiplexers operating at lower frequency bands. As the operation frequency increases, especially to millimeter-wave frequency, the dimension of the diplexer/multiplexer is small. The influence of these round corners on the performance of the diplexer/multiplexer becomes critical. Very small radius for these corners is required; otherwise the performance of

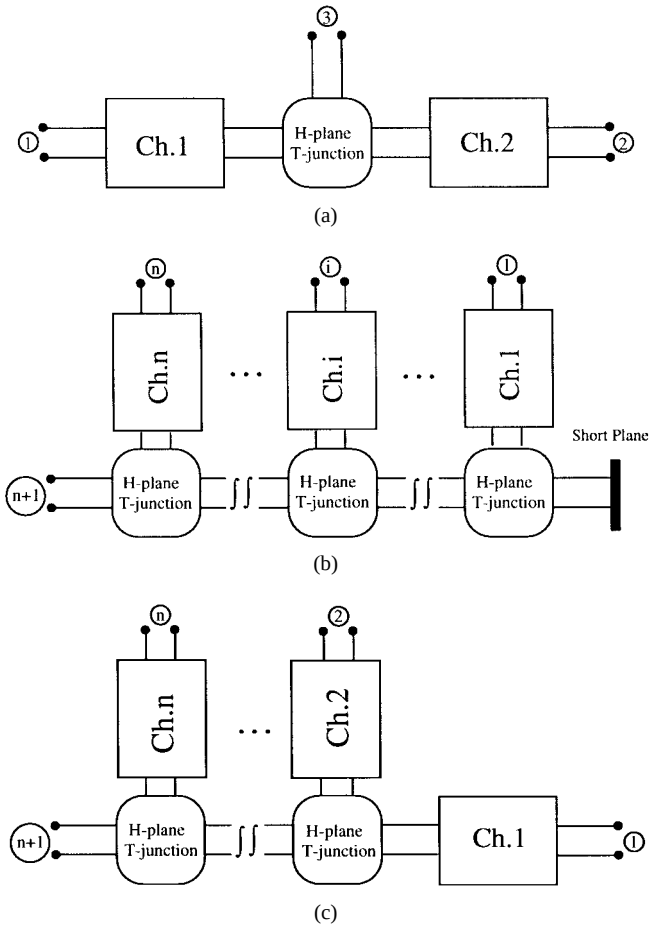

Fig. 1. Configurations of the millimeter-wave H-plane diplexers/multiplexers.

Manuscript received March 26, 1999; revised July 15, 1999.

Y. Rong was with the Department of Electrical Engineering, University of Maryland at College Park, College Park, MD 20742 USA. He is now with Paratek Microwave Inc., Columbia, MD 21045 USA.

H. Yao is with Orbital Sciences Inc., Germantown, MD 20874 USA.

K. A. Zaki is with the Department of Electrical Engineering, University of Maryland at College Park, College Park, MD 20742 USA.

T. G. Dolan is with K&L Microwave Inc., Salisbury, MD 21801 USA.

Publisher Item Identifier S 0018-9480(99)08427-6.

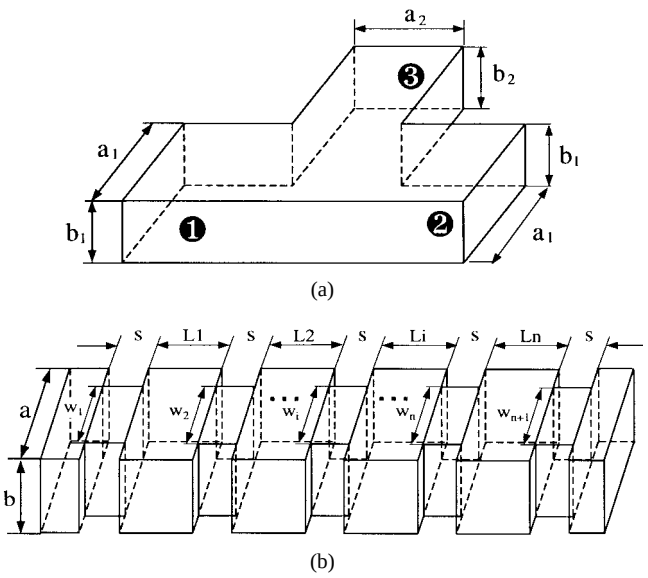

Fig. 2. (a) Standard H-plane T-junction. (b) Standard inductive window bandpass filters.

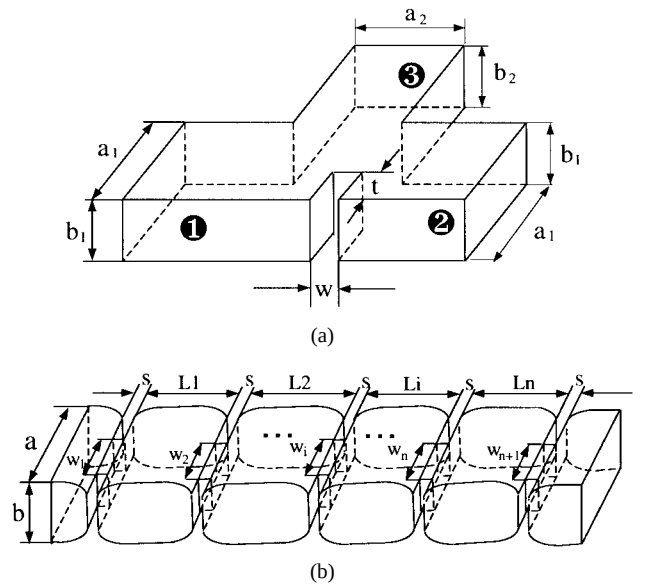

Fig. 3. (a) Modified H-plane T-junction. (b) Modified inductive window bandpass filters with round corners in the E-plane.

the diplexer/multiplexer will deteriorate. However, this often presents problems in practice, especially for the applications where production in quantity is needed.

To overcome the above-mentioned problems, the following strategies are proposed for the design. The standard H-plane T-junction, shown in Fig. 2(a), in the diplexer/multiplexer configurations is replaced by the modified T-junction, shown in Fig. 3(a), which is preferred to the structures described in [5] and [6] because it avoids complexities of manufacturing. The standard inductive window bandpass filters, shown in Fig. 2(b), are replaced by the modified inductive window bandpass filters, as shown in Fig. 3(b). The performance of the modified T-junction can be controlled by varying the dimension of the inserted metal slab. This leads to the design of the diplexers/multiplexers with wider band channel filters becoming possible. The inclusion of the E-plane round corners of the modified inductive window bandpass filters in the modeling allows the use of relatively large radius tools, and thus avoids the manufacturing difficulty for these corners.

A full-wave mode-matching method is employed in the analysis of the diplexer/multiplexers. By computing the generalized scattering matrices of all the discontinuities involved and cascading the generalized scattering matrices of all the building blocks, the performance of the diplexers/multiplexers can be obtained. In order to drastically reduce the computation time, special techniques [7] are applied. A systematic optimization approach leads to the desired multiplexer design. Design examples of optimized diplexers /multiplexers operating in the Ka upper band are given to demonstrate the validity of employing the modified H-plane T-junction in the diplexer/multiplexer configurations. Based on the simulation, a Ka upper band diplexer was manufactured and tested. Measurements showed excellent agreement with the theoretical results. Without any tuning, all the specifications are met and -20-dB return losses in both of the channels of the diplexer are obtained.

II. T-Junction Design Criteria

The basic building block of the configurations shown in Fig. 1 is a lossless reciprocal three-port network, whose two ports (ports 1 and 2) are connected by the two channel filters: Filters 1 and 2. Suppose that the lossless reciprocal three-port junction, i.e., generalized T-junction, is characterized by its dominant mode scattering matrix $[S(f)]_{3\times 3}$. By following the same arguments used in [4], it can be easily shown that if the generalized T-junction has the following properties, channel filters of the desired building block will have maximum bandwidths:

1) $S'_{11}(f) \approx 0$, $S'_{12}(f) \approx 0$, and $S'_{13}(f) \approx 0$, where the prime indicates derivative with respect to f;
2) larger transmissions $|S_{12}(f)|$ and $|S_{13}(f)|$ and $|S_{12}(f)| \approx |S_{13}(f)|$;
3) reflections $|S_{11}(f)| \approx |S_{22}(f)| \approx |S_{33}(f)| \neq 0$.

The above conditions are the same as [4], where symmetrical T-junctions are considered.

III. Modeling

The first step in modeling the diplexer/multiplexer is to model the key building blocks, i.e., the modified H-plane T-junction and modified inductive window channel filters, individually to find their generalized scattering matrices.

To model the modified H-plane T-junction, the three-plane mode-matching method [8] was employed. In this method, the side arm (port 3) of the T-junction is terminated by three different lengths of shorted waveguide. The resultant structures are three two-port waveguide networks. Each of the three two-port networks is a cascade of waveguide step discontinuities. The three-port scattering matrix of the T-junction can be extracted from the scattering matrices of the three two-port waveguide networks. Based on the T-junction design criteria given above, appropriate values of w and t in Fig. 3(a) are obtained by simple optimization. Fig. 4 shows the computed

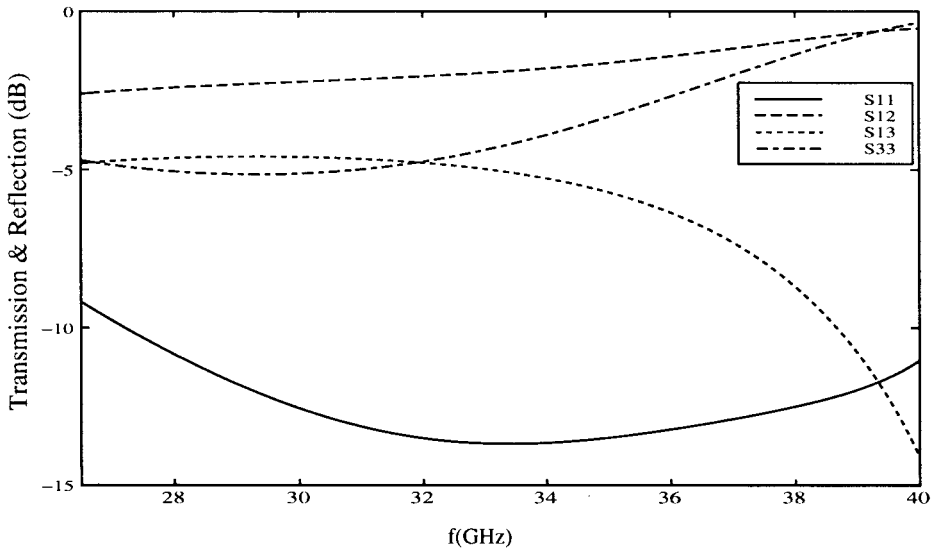

(a)

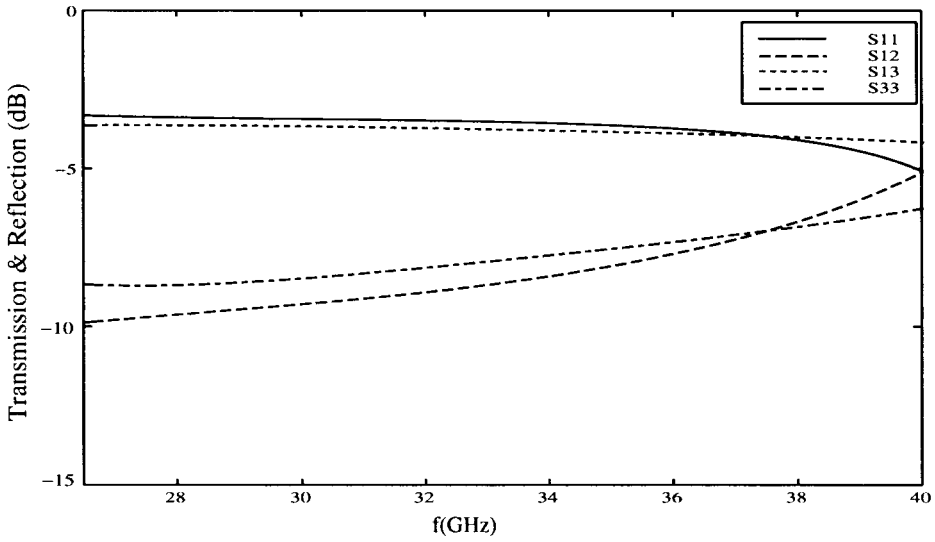

(b)

Fig. 4. Performance comparison of: (a) the standard waveguide WR28 H-plane T-junction and (b) the modified waveguide WR28 H-plane T-junction, where $w = 0.08$ in, $t = 0.14$ in.

S-parameters of the standard and designed modified H-plane T-junctions. Much better characteristics of the modified T-junction approximating the desired design criteria have been obtained.

To model the modified inductive window bandpass filter, the E-plane round-corner inductive windows, shown in Fig. 3(b), should be modeled first. To do that, the E-plane round corners are discritized as a number of waveguide steps, as shown in Fig. 5. This discontinuity can then be regarded as a cascade of several waveguide steps connected by waveguide sections with different heights. Modeling of this discontinuity can be performed by using the cascading algorithm [9]. By following the same way, the generalized scattering matrices of the whole filter can be derived.

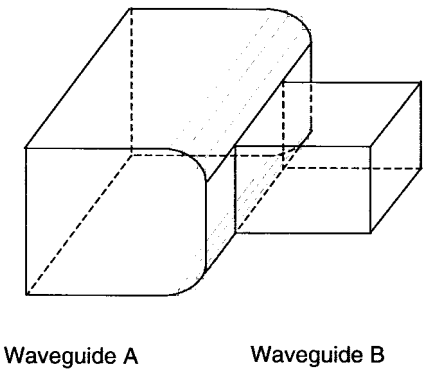

Fig. 5. Configuration of the waveguide step with E-plane round corners, where the round corners are discretized for analysis.

The final step of modeling the diplexers/multiplexers is to get the return losses at all ports and the transmissions from the common port to channel filters. To do that, matching loads should be connected to the corresponding ports in the configurations. Since the three-port modified H-plane T-junction and the modified inductive window channel filters

are characterized by their generalized s-parameters, the overall s-parameters of the resultant networks can be obtained by cascading their network parameters, where terminal connection conditions between networks can be applied.

IV. Optimum Design

The optimum design of the generalized diplexer/multiplexer is primarily based on the optimization. A carefully constructed objective function and a prudent strategy of the optimization are necessary. The objective function must be constructed in such a way that the error between the computed performance of the designed diplexer and the required specifications must be efficiently expressed. Assume that the required specifications for the ℓth channel input reflection in the passband and transmissions in the transition/stopband are $R_\ell^{\rm in}(f)$ and $T_\ell^{\rm out}(f)$, respectively. The computed return loss and the transmission of the ℓth channel are $R_\ell(f,\vec{x})$ and $T_\ell(f,\vec{x})$, respectively, where $\vec{x}$ are a set of diplexer/multiplexer parameters. The following objective function can be defined in the mean-square sense:

$$E_{\rm err}(\vec{x}) = E_R^{\rm in}(\vec{x}) + E_T^{\rm out}(\vec{x})$$

where

$$E_R^{\rm in}(\vec{x}) = \frac{1}{N}\sum_{\ell=1}^{n+1} w_{R,{\rm in}}^{\ell} \sum_{i=1}^{M_\ell} \delta(i)\Big[R_\ell(f_i,\vec{x}) - R_\ell^{\rm in}(f_i)\Big]^2$$

$$E_T^{\rm out}(\vec{x}) = \frac{1}{N}\sum_{\ell=1}^{n} w_{T,{\rm out}}^{\ell} \sum_{k=1}^{N_\ell} \delta(k)\Big[T_\ell(f_k,\vec{x}) - T_\ell^{\rm out}(f_k)\Big]^2$$

$\vec{x} \in [\vec{x}_L, \vec{x}_U]$, the sets of the lower bounds and upper bounds of the optimization variables. M_ℓ and N_ℓ are the sample points taken in the ℓth passband and transition/stopband of the diplexer/multiplexer, respectively. δ equals zero if the computed values at the sampled frequencies satisfy the specification, otherwise one. $w_{R,{\rm in}}$ and $w_{T,{\rm out}}$ are corresponding weighting factors. n is the total number of the multiplexer channels (for diplexers, $n = 2$). N is the total number of the sampled frequency points. Obviously, the design becomes a constrained nonlinear optimization problem.

The computer-aided design is carried out in a two-step optimization procedure by using an IMSL[1] optimization program, where the quasi-Newton gradient algorithm is applied. To apply the optimization to the design of the diplexers/multiplexers, initial values of the diplexers/multiplexers must be provided. The initial dimensions of the channel filters can be obtained based on the individual filter designs satisfying the given specifications using the procedures in [9]. The initial lengths of the connecting waveguides in the manifold are chosen based on [2]. In the first step of the optimization, only the manifold parameters, i.e., lengths of the connecting waveguides, are optimized. In the second step of optimization, more diplexer parameters are needed to be included in the optimization. The resonators and inverters in the channel filters closer to the modified H-plane T-junctions in the manifold should be included earlier in the optimization. The obtained parameters of the resonators and inverters after the present iteration are used as the initial values of the following iteration of the optimization. This step is repeated until all the required diplexer/multiplexer specifications are satisfied.

[1] *IMSL Math/Library User's Manual*, version 1.0, IMSL, Houston, TX, 1987.

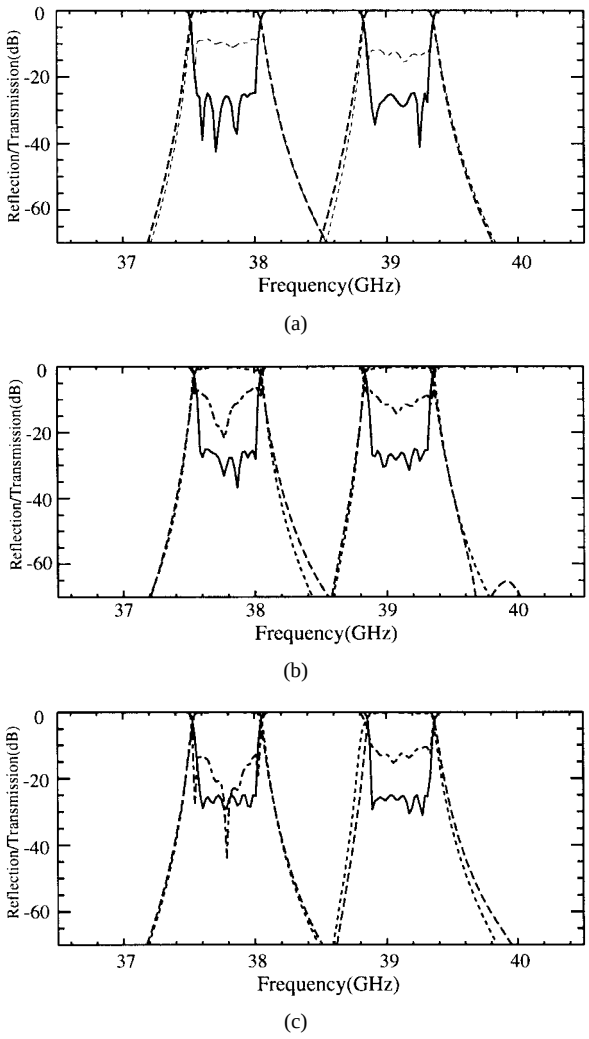

Fig. 6. The frequency responses (a)–(c) of H-plane diplexers of the configurations shown in Fig. 1(a)–(c), respectively. [First step optimization: reflection (dashed–dotted line), transmission (dotted line). Final optimization: reflection (solid line), transmission (dashed line)].

V. Numerical Results

To verify the validity of employing the modified H-plane T-junction in the multiplexer configurations, diplexer designs of the three configurations shown in Fig. 1 are performed first to achieve the following specifications:

Center frequencies	37.8 GHz for Ch. 1;
	39.1 GHz for Ch. 2;
Passband ripple	less than 0.2 dB;
0.2 dB bandwidth	450 MHz excluding;
Rejection at $f_0 \pm$ 1.1 GHz	larger than 65 dB;
Insertion loss at f_0	less than 1.2 dB;
VSWR at all ports in the passbands	18 dB min.

The first optimization step requires less than 1 min of execution time on a SUN ultra-10 work station. The second optimization step requires additional several minutes. The

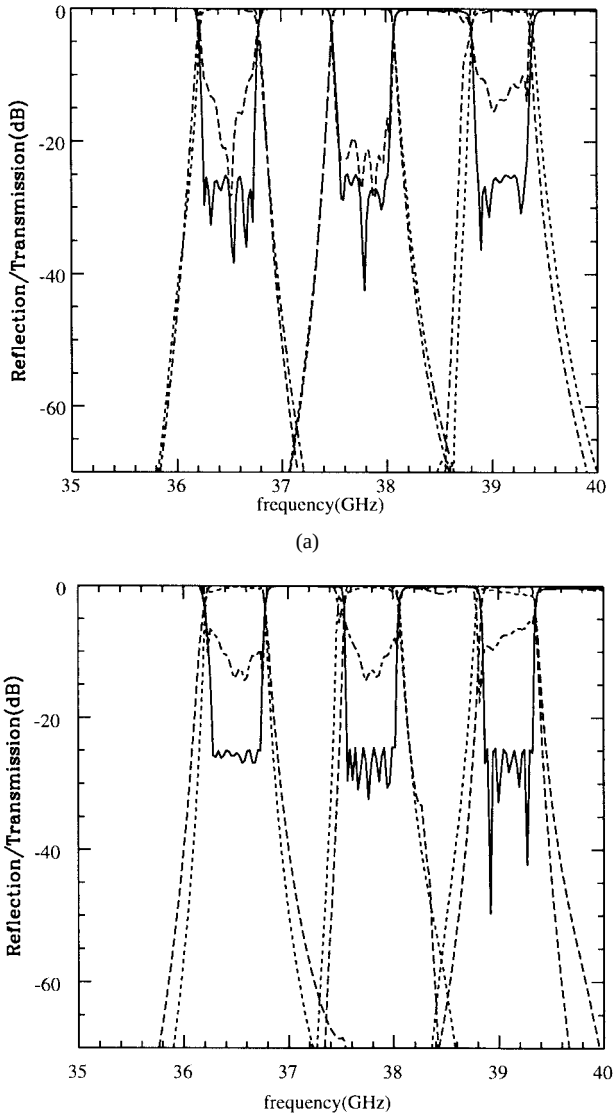

Fig. 7. Frequency response of the H-plane triplexer of the configurations shown in Figs. 1(b) and (c), respectively. [First step optimization: reflection (dashed–dotted line), transmission (dotted line), final optimization: reflection (solid line), transmission (dashed line)].

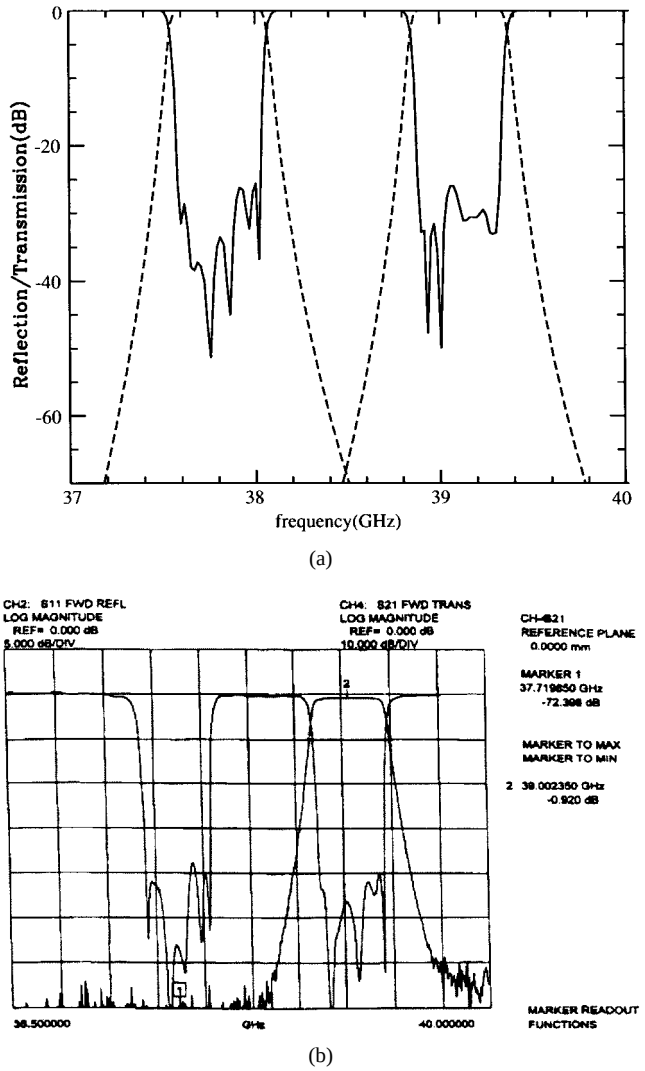

Fig. 8. (a) Simulated performance and (b) experimental performance of the no tuning H-plane diplexer of the configuration shown in Fig. 1(a).

computed frequency responses of the diplexers are presented in Fig. 6. The optimized diplexers of the three configurations have better than −25-dB return loss in the passbands of the channels. All of the three configurations have −10-dB return loss in the passbands of the channels after the first optimization step. This indicates that good initial values of diplexer parameters are obtained through the process described above.

The triplexer designs is performed to demonstrate the validity of employing the modified H-plane T-junction in the upper band multiplexer design. The center frequency and bandwidth of the additional channel is 36.5 GHz and 450 MHz, respectively. The rejection and return-loss requirements maintain the same as those for the diplexer design. Following the full-wave mode-matching-based design procedures, the designs of two upper band H-plane triplexers of the configurations, shown in Figs. 1(b) and (c), respectively, can also be readily obtained. Both of the triplexers have better than −25-dB return losses in the channels, as shown in Fig. 7. By performing the first optimization step, almost −10-dB return losses in the passbands of the triplexers are obtained.

To verify the accuracy of the design process, the above designed diplexer of the configuration, shown in Fig. 1(a), was built and tested. The measured results of the built diplexer is presented in Fig. 8. Excellent agreement between the theory and experiment is observed. All the required specifications are satisfied and −20-dB return losses in the passbands of the diplexer channels in this millimeter-wave upper band are obtained without any tuning.

VI. Conclusion

Millimeter-wave H-plane diplexers or multiplexers constructed by using modified H-plane waveguide T-junctions and modified inductive window channel filters are described. A full-wave mode-matching method is performed to model the diplexers/multiplexers, rigorously taking into account the curvature in the corners of the inductive window bandpass filters. An efficient design algorithm for diplexers/multiplexers

are presented. Validation of employing the modified H-plane T-junction in the diplexer/multiplexer configurations is demonstrated by design examples. A millimeter wave Ka upper band diplexer was simulated, built, and tested. Excellent experimental results of the designed diplexers are obtained without any tuning, which confirms the accuracy of the optimum design.

ACKNOWLEDGMENT

The authors thank Dr. Ali E. Atia, Orbital Sciences Corporation, Germantown, MD, for his kind review of this paper.

REFERENCES

[1] G. L. Matthaei, L. Young, and E. M. T. Jones, *Microwave Filters, Impedance-Matching Networks, and Coupling Structures.* New York: McGraw-Hill, 1964, chs. 13 and 16.

[2] J. Uher, J. Bornemann, and U. Rosenberg, *Waveguide Components for Antenna Feed Systems: Theory and CAD.* Norwood, MA: Artech House, 1993, ch. 3.

[3] A. Morini, T. Rozzi, and M. Mongiardo, "Efficient CAD of wide-band contiguous channel multiplexers," in *IEEE MTT-S Int. Microwave Symp. Dig.*, 1996, pp. 1651–1654.

[4] A. Morini and T. Rozzi, "Constraints to the optimum performance and bandwidth limitations of diplexer employing symmetric three-port junction," *IEEE Trans. Microwave Theory Tech.*, vol. 46, pp. 242–248, Feb. 1996.

[5] K. Ogusu, "Dielectric waveguide corner and power divider with a metallic reflector," *IEEE Trans. Microwave Theory Tech.*, vol. MTT-32, pp. 113–116, Jan. 1984.

[6] J. Hirokawa, K. Sakurai, M. Ando, and N. Goto, "An analysis of waveguide T-junction with an inductive post," *IEEE Trans. Microwave Theory Tech.*, vol. 39, pp. 563–566, Mar. 1991.

[7] J.-F. Liang and K. A. Zaki, "CAD of microwave junctions by polynomial curve fitting," in *IEEE MTT-S Int. Microwave Symp. Dig.*, 1993, pp. 451–454.

[8] X.-P. Liang, K. A. Zaki, and A. E. Atia, "A rigorous three plane mode-matching technique for characterizing waveguide T-junctions, and its application in multiplexer design," *IEEE Trans. Microwave Theory Tech.*, vol. 29, pp. 2138–2147, Dec. 1991.

[9] H.-W. Yao, A. E. Abdelmonem, J.-F. Liang, X.-P. Liang, and K. A. Zaki, "Wide-band waveguide and ridge waveguide T-junctions for diplexer applications," *IEEE Trans. Microwave Theory Tech.*, vol. 41, pp. 2166–2173, Dec. 1993.

Yu Rong (S'97–SM'99), for photograph and biography, see this issue, p. 2324.

Hui-wen Yao (S'92–M'95–SM'97) received the B.S. and M.S. degrees from Beijing Institute of Technology, Beijing, China, in 1983 and 1986, respectively, and the Ph.D. degree from the University of Maryland at College Park, in 1995, all in electrical engineering.

From 1986 to 1991, he was a Lecturer in the Department of Electrical Engineering, Beijing Institute of Technology, where his research dealt mainly with electromagnetic (EM) radiation, scattering, and antenna design. From 1991 to 1992, he was a Teaching Assistant in the Electrical Engineering Department, Wright State University, Dayton, OH, where he was involved with microstrip circuits and transient scattering by cylinders. From 1992 to 1995, he was a Research Assistant in the Department of Electrical Engineering, Microwave Laboratory, University of Maryland at College Park, where he was involved with the analysis, modeling, and design of microwave and millimeter-wave devices and circuits. From December 1995 to August 1997, he was with the Space System Group, CTA Inc., Rockville, MD. Since August 1997, he has been with Orbital Sciences Corporation, Germantown, MD, where he is involved with telecommunications and satellite communications.

Kawthar A. Zaki (SM'85-F'91), for photograph and biography, see this issue, p. 2324.

Tim G. Dolan received the B.S. degree in electrical engineering from Pennsylvania State University, University Park, in 1982.

He possesses over 15 years experience in the electronics field. Since 1994, he has been with K&L Microwave Inc., Salisbury, MD, where he is currently the Vice President of Engineering. His responsibilities include research and development and corporate administration of the engineering department, and is also involved in the design of components and systems.

Efficient Electromagnetic Optimization of Microwave Filters and Multiplexers Using Rational Models

Alejandro García-Lampérez, *Student Member, IEEE*, Sergio Llorente-Romano, *Student Member, IEEE*, Magdalena Salazar-Palma, *Senior Member, IEEE*, and Tapan K. Sarkar, *Fellow, IEEE*

***Abstract*—A method is presented for the efficient optimization of microwave filters and multiplexers designed from an ideal prototype. The method is based on the estimation of a rational function adjusted to a reduced number of samples of the microwave device response obtained either through electromagnetic analysis or measurements. From this rational function, a circuital network having the previously known topology of the microwave device is synthesized and compared to a circuital network with the desired response but including nonidealities. All of the process of analysis and model extraction can be seen as a model function that relates the physical parameters of the microwave device with the extracted circuital network parameters. Then, the error vector of the circuital parameters is used to generate a correction vector of the physical parameters through an estimation of the inverse of the Jacobian matrix of the complete model function. The Jacobian estimation is updated at each iteration of the optimization process with no need for additional evaluations of the model function. Two numerical examples of the proposed technique corresponding to the synthesis of a filter and a diplexer are presented, demonstrating the increased efficiency of the proposed technique with respect to direct electromagnetic optimization.**

***Index Terms*—Characteristic function, electromagnetic optimization, Jacobian estimation, microwave filters, parameter estimation, rational model extraction, tuning.**

I. Introduction

In the last several years, direct electromagnetic optimization has been demonstrated as a real possibility in order to synthesize and tune passive microwave devices [1]–[3]. The strength of electromagnetic analysis, namely the rigorous analysis of general structures, makes the optimization valid for complex devices with geometries that can be arbitrarily irregular. Another advantage is the fact that all second-order effects are taken into account, effects that are partially or completely neglected by parametric models, if available. Yet another advantage is that these latter models become unnecessary.

The big obstacle to generalize the use of full electromagnetic simulations as a tool for the design and tuning of passive devices is the high requirements in time and computation resources. Even relatively small and simple structures can take quite long to be analyzed with sufficient accuracy. A full optimization of a filter response that involves the iterated analysis at a set of frequency points can therefore be impracticable in a reasonable time.

In recent times, some efforts have been made to overcome this problem. In [4], a method of error diagnosis and tuning, based on estimation of a lumped-elements model and multilevel optimization, is presented. An alternative technique based on space mapping is detailed in [2]. Some techniques of computer-aided filter tuning based on the optimization of resonators and couplings have also been used [3], [5]. A related problem, the extraction of individual values of resonant frequencies and coupling coefficients of a filter, is treated in [6].

In this paper, a novel model-based optimization method that allows a very efficient and fast tuning of multiple coupled resonators filters is presented. As usual, the procedure starts from an ideal lumped-elements prototype [7] from which a microwave device with a given topology, coupling matrix, and physical dimensions is derived. Obviously the microwave device frequency response will not coincide with that of the lumped-element prototype. The model optimization technique is applied to this microwave device. The technique is based on the extraction of a circuital model, the response of which fits the microwave device reflection and transfer functions, S_{11} and S_{21}, using a set of points at some frequency values as input data. This set of samples can be obtained from the electromagnetic analysis or even from the measurement of the microwave device. The first step to obtain the model uses the Cauchy's method [8]–[12]. This consists of making extraction of an analytical rational interpolant of the filter characteristic function K that fits the data samples minimizing the model error in a least-squares sense. The degrees of the characteristic polynomials of the model are fixed by the number of resonators n that constitute the filter and the number of finite transmission zeros n_z given by the coupling topology of the filter [7], [13].

The rational model is then improved in order to fit the filter responses that are not strictly rational or rational with nonlimited polynomial degrees, as is the case for microwave filters where nonidealities are present (higher order frequency pass bands, dispersive effects, and so on). This is achieved by increasing the order of the model. From this increased order model, additional reflection zeros are identified. Then, with this information, two coupling matrices are computed [7], [14]. The first one corresponds to the reduced order model obtained by removing those additional reflection zeros and is called in this paper the *extracted coupling matrix*. The coefficients of this coupling matrix are related to the resonant frequencies and mutual coupling coefficients of the microwave filter. The second one corresponds

Manuscript received April 8, 2003; revised August 7, 2003. This work was supported by the Spanish Ministry of Science and Technology under Project TIC2002-02657.

A. García-Lampérez, S. Llorente-Romano, and M. Salazar-Palma are with the Department of Signals, Systems and Radiocommunications, Polytechnical University of Madrid, 28040 Madrid, Spain.

T. K. Sarkar is with the Department of Electrical Engineering and Computer Science, Syracuse University, NY 13210 USA.

Digital Object Identifier 10.1109/TMTT.2003.822021

to the new *objective prototype* derived from the ideal one but including the effect of the additional reflection zeros that allow the modeling of the nonidealities of the microwave filter. The corresponding coupling matrix is called in this paper the *objective coupling matrix*. The coefficients of this coupling matrix are related to the resonant frequencies and mutual coupling coefficients of the objective prototype.

Both coupling matrices are then compared. The result of the comparison is a vector of errors associated with the extracted coupling matrix. From this vector, another vector of corrections of the physical parameters of the microwave filter is generated. The complete coupling matrix extraction process, from the electromagnetic analysis to the extracted coupling matrix, can be seen as a vector function with the physical parameters of the microwave filter as input and the electrical parameters as output. The inverse of the Jacobian of this function relates the circuital errors with the physical corrections. Of course, the Jacobian (or its inverse) is *a priori* unknown. An estimation of the Jacobian that after a first analysis does not require additional model function evaluations has been implemented based on Broyden's method [15].

The application of the computed corrections of the physical parameters leads to a new filter design. This modified design is used as input for the next iteration of the optimization process, that is completed when the correction vector is sufficiently small.

The optimization procedure proposed in this paper is novel in a number of ways. To start with the use of an increased order model [16] to obtain both the extracted and the objective coupling matrices represents a novelty by itself. Also, the approach based on a rational model of the filter characteristic function K is new and shows some advantages when compared to other methods.

- Since only the numerators of S_{11} and S_{21} that form K are directly extracted, the characteristic polynomials of the filter can be enforced to be correct. Namely, the poles of the filter can be forced to be common to S_{11} and S_{21} and have a negative real part, and the passiveness of the extracted model can also be ensured. If, instead of K, S_{11} and S_{21} are used as functions to fit, additional mechanisms to guarantee the properties of the polynomials must be implemented as done in [4].
- The ensured good behavior of the polynomials allows the use of analytical techniques for the synthesis of the coupling matrix instead of the optimization procedure (i.e., nonanalytical) utilized in [4].
- There is no need of an iterative optimization fitting process at each model extraction, as is the case of direct extraction of the coupling matrix coefficients from the data samples [5].

Finally, it should be highlighted that the method for the estimation of the Jacobian after a first analysis does not imply in general additional evaluations of the model function (i.e., additional electromagnetic simulations or explicit sensitivity calibrations) in contrast with other procedures where it is required [5]. Also, this technique makes unnecessary the use of precomputed tables relating physical dimensions and circuital coefficients as done in [3]. Only a reasonable initial estimation of the Jacobian is needed.

This paper begins by describing the complete model extraction procedure (Section II), from the generation of a rational model of the characteristic function using the sampled data, to the synthesis of the extracted and objective coupling matrices. Next, in Section III, the filter optimization procedure is detailed, including the estimation of the Jacobian matrix that relates the computed error and the corrections applied to the filter parameters. Finally, Section IV includes two numerical application examples of the presented technique, consisting of the optimization of a filter and a diplexer.

II. Circuit Model Extraction

A. Polynomial Identification Using the Cauchy Method

A microwave filter response can be characterized by the scattering parameters $S_{11}(f)$ and $S_{21}(f)$, where f is the frequency variable. As usual, the required low-pass frequency transformation is utilized so that the corresponding low-pass scattering parameters will be used. These transmission and reflection coefficients can be approximated using two independent rational interpolants, but in doing so some useful redundancies in the system may be wasted, since the two parameters are related to each other. Using two rational interpolants with a common denominator, a low-pass filter response of order n with n_z finite transmission zeros (that can be obtained from a bandpass to low-pass transformation) is modeled as

$$\begin{cases} \widehat{S}_{11}(s) = \dfrac{F(s)}{E(s)} = \dfrac{\sum_{k=0}^{n} a_k^{(1)} s^k}{\sum_{k=0}^{n} b_k s^k} \approx S_{11}(s) \\ \widehat{S}_{21}(s) = \dfrac{P(s)}{E(s)} = \dfrac{\sum_{k=0}^{n_z} a_k^{(2)} s^k}{\sum_{k=0}^{n} b_k s^k} \approx S_{21}(s) \end{cases} \tag{1}$$

where $S_{11}(s)$, $S_{21}(s)$ and $\widehat{S}_{11}(s)$, $\widehat{S}_{21}(s)$ are the reflection and transmission coefficients of the transformed microwave filter and the model, respectively, and $s = \sigma + j\omega$ is the complex frequency variable. The degree of the polynomials $E(s)$ and $F(s)$ is equal to the order of the low-pass filter n while the degree of $P(s)$ corresponds to its number of transmission zeros at finite complex frequencies n_z.

This model, which is completely defined by the polynomials degrees and coefficients, does not correspond in general to a physically realizable network response, as the condition of passivity

$$\left|\widehat{S}_{11}(j\omega)\right|^2 + \left|\widehat{S}_{21}(j\omega)\right|^2 \leq 1 \tag{2}$$

is not guaranteed. In order to ensure the realizability of the model response, a different approach is taken here. First, only the $n + n_z + 2$ numerator coefficients from (1), $a_k^{(1)}$ and $a_k^{(2)}$, are extracted. The $n + 1$ denominator coefficients b_k are then reconstructed, forcing (2) to be satisfied.

The numerator coefficients completely determine the characteristic function of the model $\widehat{K}(s)$ that will be an approxima-

tion of the characteristic function of the transformed microwave filter $K(s)$ as

$$\widehat{K}(s)=\frac{\widehat{S}_{11}(s)}{\widehat{S}_{21}(s)}=\frac{\sum_{k=0}^{n}a_k^{(1)}s^k}{\sum_{k=0}^{n_z}a_k^{(2)}s^k}\approx\frac{S_{11}(s)}{S_{21}(s)}=K(s). \quad (3)$$

Let the value of S_{11} and S_{21} be given at a set of $N\geq n+n_z+1$ (not necessarily equally spaced) complex frequency points s_i. Then, using the principle of analytical continuation, a system of N linear equations can be established by substituting those values into (3) and rearranging the resulting expression [11], [12] to yield

$$S_{21}(s_i)\sum_{k=0}^{n}a_k^{(1)}s_i^k-S_{11}(s_i)\sum_{k=0}^{n_z}a_k^{(2)}s_i^k=0,\qquad i=1,\ldots,N. \quad (4)$$

The system (4) can be rewritten using a matrix formulation

$$[\boldsymbol{S}_{21}\boldsymbol{V}_n\quad -\boldsymbol{S}_{11}\boldsymbol{V}_{n_z}]\begin{bmatrix}\boldsymbol{a}^{(1)}\\ \boldsymbol{a}^{(2)}\end{bmatrix}=\boldsymbol{X}\begin{bmatrix}\boldsymbol{a}^{(1)}\\ \boldsymbol{a}^{(2)}\end{bmatrix}=0 \quad (5)$$

where $\boldsymbol{a}^{(1)}=[a_0^{(1)},\ldots,a_n^{(1)}]^T$, $\boldsymbol{a}^{(2)}=[a_0^{(2)},\ldots,a_{n_z}^{(2)}]^T$, $\boldsymbol{S}_{11}=\operatorname{diag}\{S_{11}(s_i)\}_{i=1,\ldots,N}$, $\boldsymbol{S}_{21}=\operatorname{diag}\{S_{21}(s_i)\}_{i=1,\ldots,N}$, and $\boldsymbol{V}_r$ is a Vandermonde matrix, defined as

$$\boldsymbol{V}_r=\begin{bmatrix}1 & s_1 & s_1^2 & \cdots & s_1^r\\ 1 & s_2 & s_2^2 & \cdots & s_2^r\\ \vdots & \vdots & \vdots & \ddots & \vdots\\ 1 & s_N & s_N^2 & \cdots & s_N^r\end{bmatrix}\in\mathbb{C}^{N\times(r+1)}. \quad (6)$$

The total least-squares method (TLS) [17] is used to solve the exactly determined or overdetermined system (5) by finding a nontrivial vector of coefficients contained in the null space generated by the columns of the matrix $\boldsymbol{X}\in\mathbb{C}^{N\times(n+n_z+2)}$. A singular value decomposition of $\boldsymbol{X}$ is used to solve the system

$$\boldsymbol{X}\begin{bmatrix}\boldsymbol{a}^{(1)}\\ \boldsymbol{a}^{(2)}\end{bmatrix}=\boldsymbol{U}\boldsymbol{\Sigma}\boldsymbol{V}^H\begin{bmatrix}\boldsymbol{a}^{(1)}\\ \boldsymbol{a}^{(2)}\end{bmatrix}=0 \quad (7)$$

where $\boldsymbol{U}$ and $\boldsymbol{V}$ are unitary matrices, $\boldsymbol{\Sigma}$ is a diagonal matrix of the ordered singular values of $\boldsymbol{X}$, and $(\cdot)^H$ denotes the complex conjugate transpose matrix. The optimum solution is proportional to the last column of the square $(n+n_z+2)$ unitary matrix $\boldsymbol{V}^H$, that is, to the right singular vector of $\boldsymbol{X}$ corresponding to the smallest singular value of $\boldsymbol{X}$. This holds even if $\boldsymbol{X}$ actually does not generate a null space due to noise, measurement errors, or mismatch between the rational model and the real response. Therefore, the solution is

$$\begin{bmatrix}\boldsymbol{a}^{(1)}\\ \boldsymbol{a}^{(2)}\end{bmatrix}=[\boldsymbol{V}^H]_{n+n_z+2}. \quad (8)$$

It should be noted that, although there are a total of $n+n_z+2$ polynomial coefficients to solve, only $n+n_z+1$ data samples are required since one of the coefficients can be arbitrarily fixed, i.e., there is a degree of freedom.

Once the characteristic function $K(s)$ is obtained, the next step consists of constructing the polynomial $E(s)$, the common denominator of both $\widehat{S}_{11}(s)$ and $\widehat{S}_{21}(s)$. In order to achieve this, the condition

$$\left|\widehat{S}_{11}(j\omega)\right|^2+\left|\widehat{S}_{21}(j\omega)\right|^2=1 \quad (9)$$

that ensures the passiveness of a lossless network response is required. Substituting $\widehat{S}_{11}(s)$ and $\widehat{S}_{21}(s)$ by their polynomial representation into (1), an equivalent condition is obtained (Feldtkeller's equation) as follows:

$$F(s)F^*(-s)+P(s)P^*(-s)=E(s)E^*(-s). \quad (10)$$

The left-hand term in (10) is completely determined by the coefficients obtained in (8), and therefore the right-hand polynomial is also known. Since this polynomial is real for all values of s, its complex roots are located in symmetrical pairs with respect to the imaginary axis $j\omega$, i.e., they are of the form $s_{2k-1,2k}=\pm\sigma_k+j\omega_k$, with $k=1,2,\ldots,n$. From each pair, one of the roots corresponds to $E(s)$ and the other one to $E^*(s)$. For the filter to be stable, its natural frequencies, that are precisely the roots of $E(s)$, must be located in the left half of the complex plane s. Hence, the n roots of $E(s)E^*(-s)$ with negative real part $(s_k=-\sigma_k+j\omega_k)$ are chosen as roots of $E(s)$. The roots of the polynomials are obtained from their coefficients by computing the eigenvalues of the companion matrix [18].

In order to complete the characterization of $E(s)$, one of its coefficients must be fixed. Approaching s in (10) to infinity, a relationship among the higher order coefficients of the polynomials is obtained as follows:

$$\left|a_n^{(1)}\right|^2+\left|a_n^{(2)}\right|^2=|b_n|^2. \quad (11)$$

When the condition of phase $\lim_{\omega\to\infty}\sphericalangle S_{11}(j\omega)=0$ is also imposed, the following expression is obtained:

$$b_n=\sqrt{\left|a_n^{(1)}\right|^2+\left|a_n^{(2)}\right|^2}\cdot e^{j\arg\left(a_n^{(1)}\right)}. \quad (12)$$

If the number of finite-frequency transmission zeros n_z is lower than the order of the filter n (i.e., when there is at least one transmission zero at infinity), then $a_n^{(2)}=0$, and (12) is reduced to $b_n=a_n^{(1)}$. This is equivalent to the condition $\lim_{\omega\to\infty}S_{11}(j\omega)=1$. In other cases $(n=n_z)$, the full expression must be taken into account.

The rest of the coefficients $\{b_k\}_{k=0,\ldots,n-1}$ can be reconstructed from the roots of $E(s)$. With them, the characteristic polynomials $P(s)$, $F(s)$, and $E(s)$ from (1) are completely defined, and so are the reflection and transfer function of the model $\widehat{S}_{11}(s)$ and $\widehat{S}_{21}(s)$.

B. Model Error Compensation

Theoretically, a filter response can be represented as a rational expression of polynomials in the complex frequency variable s. In this case, the model extracted in the previous section is exact if the degree of the polynomials of the model are equal to or higher than the degree of the polynomials of the filter response, i.e., $\widehat{S}_{11}(s)=S_{11}(s)$, $\widehat{S}_{21}(s)=S_{21}(s)$, and $\widehat{K}(s)=K(s)$.

In practice, a rational model is a good characterization of a microwave filter response, but only an approximate one. Usually, some features of the response cannot be exactly modeled using a rational interpolant: for example, the presence of spurious passbands due to higher order resonant modes, the effect of the frequency dispersive behavior of waveguides that leads to transfer functions with a different slope at each stopband, the presence of spurious couplings, and so on. Therefore, a nonzero error term between the real response and the model response

will appear. An error term $\epsilon(s)$ relates the characteristic function of the microwave filter and the model filter that may be formally expressed from (3) as

$$K(s) = \widehat{K}(s) + \epsilon(s) = \frac{F(s)}{P(s)} + \epsilon(s). \tag{13}$$

The described polynomial estimation method obtains the best rational approximation in a least-squares sense by minimizing the error term $\epsilon(s)$. The model and the error term depend on the frequency points s_i that have been considered to sample the original function. If the error term $\epsilon(s)$ is an important part of the original function in some of the samples, the complete model will be distorted, affecting all of the frequency points, even those where the rational approximation can be accurate. In the case of filters with asymmetrical slopes of the transfer function, sampled points in the stopband with a large error component distort the reconstruction in the passband, where the rational model can be otherwise adequate.

In order to reduce the model error, the order of the polynomials can be increased. This could be done either by increasing the number of reflection zeros or transmission zeros. The method implemented in this paper proposes the first option because the second one presents a practical drawback that is mentioned later on. It has been observed that the use of extra reflection zeros accurately models a very wide range of nonstrictly rational filter responses. Additional reflection zeros introduce the additional degrees of freedom required to adjust the out-of-band response although they do not correspond to reflection zeros of the microwave filter. If the number of auxiliary reflection zeros is equal to m, the characteristic function of the increased order model is

$$\widehat{K}_{\text{inc}}(s) = \frac{F(s)}{P(s)} \prod_{i=1}^{m} \left(1 - \frac{s}{s_{0i}}\right) \tag{14}$$

where n and n_z are the degrees of $F(s)$ and $P(s)$, respectively, and $\{s_{0i}\}_{i=1,\ldots,m}$ are the complex frequency locations of the additional reflection zeros. It should be noted that the locations of those zeros are unknown *a priori*. Therefore, in (14), they are represented separately only for convenience. Now, the model can be made arbitrarily accurate by increasing m, but $m = 1$, 2, or 3 has been sufficient for all the cases studied. Then the polynomials of the increased order model are obtained using the procedure explained in Section II-A, and then all the reflection zeros are identified.

Of course, this model does not have the right polynomial degrees in order to generate a valid circuital implementation: the order of the filter n and the number of transmission zeros n_z are fixed by the number of resonators, the physical structure, and the coupling topology of the device. Therefore, the next step consists of removing the extra reflection zeros in order to restore the correct degrees of the polynomials, so that the final extracted model is

$$\widehat{K}(s) = \widehat{K}_{\text{inc}}(s) \prod_{i=1}^{m} \left(1 - \frac{s}{s_{0i}}\right)^{-1} = \frac{F(s)}{P(s)}. \tag{15}$$

The identification of $\{s_{0i}\}_{i=1,\ldots,m}$ from the whole set of extracted reflection zeros is usually straightforward. The extra zeros are located at complex frequencies far away from the passband, where they approximate the distortion of the filter response at out-of-band frequencies. On the other hand, the authentic reflection zeros are located in the passband, at frequencies on the imaginary axis ($s = j\omega$), or near it. This simple and robust identification criterion is the reason to prefer the addition of reflection zeros to transmission zeros, as the genuine transmission and/or equalization zeros from the microwave filter response can be located in the entire complex plane s.

The removal of $\{s_{0i}\}_{i=1,\ldots,m}$ restores the model order, however, it also distorts its in-band response, as the term $\prod_{i=1}^{m}(1 - s/s_{0i})^{-1}$ in (15) shows. Hence, to correctly fit the model in (14), one can associate a correct order model, but with distorted characteristic function $\widehat{K}(s)$. Note that the distortion term is known. The objective circuital network, with the characteristic function $\widetilde{K}(s)$

$$\widetilde{K}(s) = \frac{\widetilde{F}(s)}{\widetilde{P}(s)} \tag{16}$$

where $\widetilde{F}(s)$ and $\widetilde{P}(s)$ have degrees n and n_z, respectively, must present the same distortion with respect to the ideal prototype, i.e., it will be a predistorted model function. $\widetilde{K}(s)$ should be generated from a function with correct in-band response and m additional reflection zeros, namely $\{s_{0i}\}_{i=1,\ldots,m}$, that are subsequently removed. This is not practical, as there are no available analytic methods to synthesize equiripple characteristic functions with additional reflection zeros. Instead, this response can be approximated by an equiripple filter with additional transmission zeros, i.e., a quasi-elliptic filter.

Each of the terms of $\prod_{i=1}^{m}(1-s/s_{0i})^{-1}$ can be approximated in the passband by its pth-order Taylor expansion around $s = 0$ as

$$\begin{aligned}\left(1 - \frac{s}{s_{0i}}\right)^{-1} &\approx \sum_{k=0}^{p} \left(\frac{s}{s_{0i}}\right)^{k} \\ &= 1 + \frac{s}{s_{0i}} + \left(\frac{s}{s_{0i}}\right)^{2} + \left(\frac{s}{s_{0i}}\right)^{3} + \cdots\end{aligned} \tag{17}$$

i.e., the effect of removing one reflection zero is equivalent to the effect of removing p transmission zeros, which are roots of the Taylor polynomial in (17). Thus, the objective function $\widetilde{K}(s)$ may be obtained from an equiripple quasi-elliptic filter with $m \cdot p$ prescribed additional transmission zeros, which are roots of each of the m Taylor polynomials of order p. The characteristic function of this quasi-elliptic filter $\widetilde{K}_{\text{qe}}(s)$ is given by

$$\widetilde{K}_{\text{qe}}(s) = \frac{\widetilde{F}(s)}{\widetilde{P}(s)} \prod_{i=1}^{m} \left[\sum_{k=0}^{p} \left(\frac{s}{s_{0i}}\right)^{k}\right]^{-1}. \tag{18}$$

Then, after the removal of the extra transmission zeros, it results in

$$\widetilde{K}(s) = \frac{\widetilde{\widetilde{F}}(s)}{\widetilde{\widetilde{P}}(s)} = \widetilde{K}_{\text{qe}}(s) \prod_{i=1}^{m} \left[\sum_{k=0}^{p} \left(\frac{s}{s_{0i}}\right)^{k}\right]. \tag{19}$$

From $\widehat{F}(s)$ and $\widehat{P}(s)$, and $\widetilde{F}(s)$ and $\widetilde{P}(s)$, $\widehat{E}(s)$ and $\widetilde{E}(s)$ will be computed, respectively, as shown in Section II-A. This

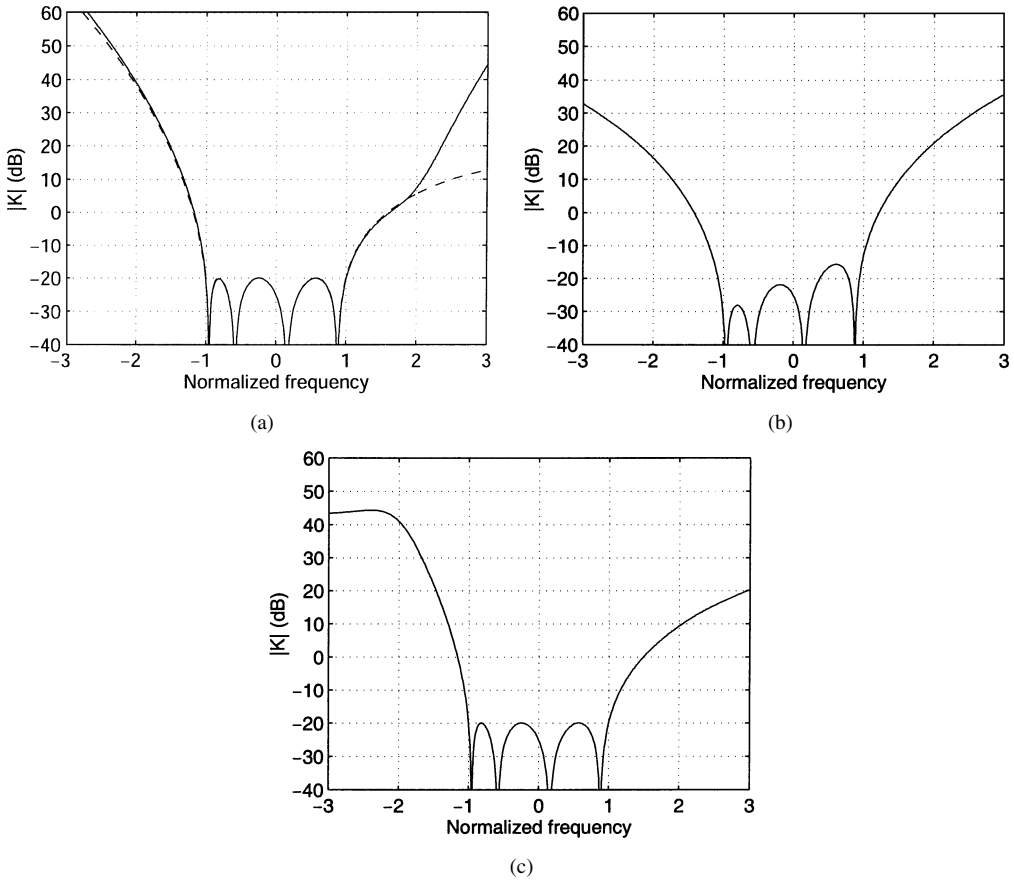

Fig. 1. Distortion of the characteristic function $|K(f)| = |S_{11}(f)|/|S_{21}(f)|$ due to the increment of the order of the rational model, and correction of this effect. (a) Increased-order model with two additional reflection zeros, at complex frequencies $s_{0(1,2)} = \pm\sigma + j\omega$ ($|\widehat{K}_{inc}|$, solid line), compared to the microwave filter response (dashed line). (b) Model after removal of the two additional reflection zeros ($|\widehat{K}|$ that must coincide for the optimized filter with $|\widetilde{K}|$). Now, the bandpass ripple is not constant, but the polynomial degrees are correct. (c) Equivalent increased-order model with two additional transmission zeros at complex frequencies $s'_{0(1,2)} = \pm\sigma - j\omega$ ($|\widetilde{K}_{\rm qe}|$).

concludes the procedure to obtain a predistorted objective model function.

As an example of this method of compensation for the error term from (13), the case for $p = 1$ is considered, i.e., the case when only the first-order term of the Taylor expansion is taken into account. Then (18) results in

$$\widetilde{K}_{\rm qe}(s) = \frac{\widetilde{F}(s)}{\widetilde{P}(s)} \prod_{i=1}^{m} \left(1 + \frac{s}{s_{0i}}\right)^{-1}. \tag{20}$$

Comparing with (14), it can be seen that the first-order equivalent approximation of the characteristic function consists of replacing the additional reflection zeros with transmission zeros of opposite sign.

Fig. 1 illustrates the process described above for $p = 1$, $m = 2$, and an already optimized filter. Fig. 1(a) shows the characteristic function of a fourth-order microwave filter with no finite transmission zeros and the corresponding rational model with two additional reflection zeros ($\widehat{K}_{\rm inc}(s)$ above) that fits the response of the microwave device. Fig. 1(b) shows the distorted function after removing the extra reflection zeros thus with correct polynomials degrees, $\widehat{K}(s)$, that in an optimized filter must coincide with the predistorted objective model $\widetilde{K}(s)$. $\widetilde{K}(s)$ is obtained from an equiripple quasi-elliptic filter, as shown in Fig. 1(c), i.e., $\widetilde{K}_{\rm qe}(s)$, after eliminating its transmission zeros. It can be observed that Fig. 1(c) is very similar to the microwave filter response in Fig. 1(a) in the frequency interval (−2,2) that includes the passband. It can also be observed that outside this band Fig. 1(c) is not accurate. As a consequence, all of the frequency points used in the generation of the model must be chosen into this region where the models are precise, i.e., in or near the passband.

C. Characterization and Synthesis of the Coupling Matrix

Fig. 2 shows the low-pass equivalent of a bandpass coupled resonator filter, with possibly more than one source/load coupling. The network is composed of n inductively coupled lossless series resonator, with frequency-invariant coupling coefficients between resonators denoted as M_{ij} and couplings with the source and load denoted respectively as M_{Si} and M_{iL}. Each resonator is formed by an inductance and a frequency-invariant admittance jM_{ii} that models the shifting between the resonant frequency f_i and the central frequency of the filter f_0. Direct coupling between the source and the load, necessary if the number of zeros n_z is equal to the filter order n, can also be included. Using the impedance scaling property of the couplings, the loop inductances are normalized to unity without loss of generality. The source and load impedances can also be normalized.

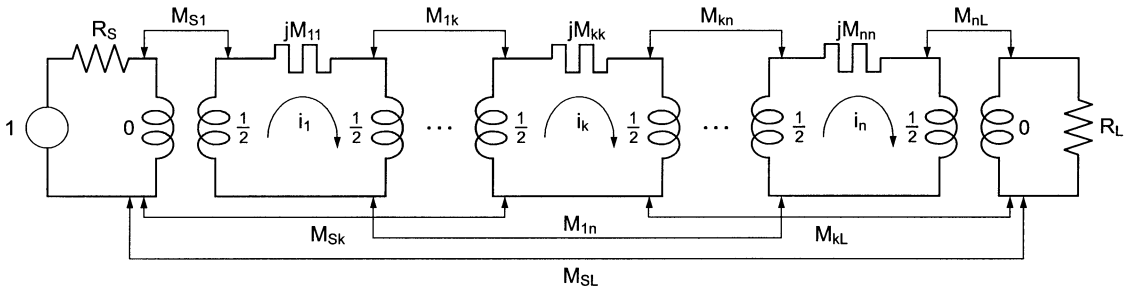

Fig. 2. Low-pass prototype of a lossless coupled resonator filter, with unitary resonator inductances, and frequency-invariant admittances that are responsible for frequency shifts. Couplings between the source/load and multiple resonators (M_{Sk} and M_{kL}) or even the source-to-load coupling (M_{SL}) are represented and taken into account by the model. Without loss of generality, $R_S = R_L = 1$.

The coupling coefficients and the resonator-invariant inductance can be embedded into an extended $(n+2) \times (n+2)$ symmetrical coupling matrix

$$\boldsymbol{M} = \begin{bmatrix} 0 & M_{S1} & M_{S2} & \cdots & M_{Sn} & M_{SL} \\ M_{S1} & M_{11} & M_{12} & \cdots & M_{1n} & M_{1L} \\ M_{S2} & M_{12} & M_{22} & \cdots & M_{2n} & M_{2L} \\ \vdots & \vdots & \vdots & \ddots & \vdots & \vdots \\ M_{Sn} & M_{1n} & M_{2n} & \cdots & M_{nn} & M_{nL} \\ M_{SL} & M_{1L} & M_{2L} & \cdots & M_{nL} & 0 \end{bmatrix}. \quad (21)$$

The $n+2$ loop current equations of the low-pass prototype in Fig. 2 can be expressed using matrix notation

$$\boldsymbol{I} = -j\boldsymbol{A}^{-1}\boldsymbol{E} \quad (22)$$

where $\boldsymbol{I} \in \mathbb{R}^{n+2}$ is the loop current vector, $\boldsymbol{E}$ is the unitary excitation vector, $\boldsymbol{E} = [1, 0, \ldots, 0] \in \mathbb{R}^{n+2}$, and

$$\boldsymbol{A} = [\omega \boldsymbol{U}_0 + \boldsymbol{M} - j\boldsymbol{R}]. \quad (23)$$

In the previous equation, $\boldsymbol{U}_0 \in \mathbb{R}^{(n+2)\times(n+2)}$ is identical to the identity matrix, except for the elements $[\boldsymbol{U}_0]_{11} = [\boldsymbol{U}_0]_{(n+2),(n+2)} = 0$, and $\boldsymbol{R} \in \mathbb{R}^{(n+2)\times(n+2)}$ is also a diagonal matrix, $\boldsymbol{R} = \mathrm{diag}\{1, 0, \ldots, 0, 1\}$.

Therefore, the extended $(n+2) \times (n+2)$ coupling matrix completely characterizes the filter prototype. In order to synthesize a valid coupling matrix, the analytic method originally presented in [19] and [20] and later generalized to extended coupling matrices [21] has been used. The input data for this algorithm are any set of characteristic polynomials $P(s)$, $F(s)$, and $E(s)$, obtained from Section II-A.

The synthesis method generates a coupling matrix corresponding to a network formed by n coupled shunt resonators, with nonzero couplings between each resonator, the source, and the load. In general, this network is not physically realizable. Moreover, for the purpose of this work, a determined coupling topology, related to the physical structure of the device under study, must be forced. The network can include desired and spurious coupling coefficients, but a previous knowledge of the electrical topology of the network is necessary. This knowledge can be represented as a topology matrix $\boldsymbol{T} \in \mathbb{Z}^{(n+2)\times(n+2)}$, with elements $T_{ij} = 1$ if M_{ij} has to be nonzero, and $T_{ij} = 0$ otherwise.

The synthesized coupling matrix can be reduced to a suitable matrix with the topology defined by the matrix $\boldsymbol{T}$ using a series of elemental similarity transformations, as described in [14]. This procedure leads to a new matrix with the undesired couplings reduced to zero, with the same electrical response. If the number of transmission zeros at finite frequencies is the maximum feasible for the given topology [13], the synthesis will be unique or at least a limited number of filter realizations will be possible. Using this procedure, the extracted coupling matrix $\widehat{\boldsymbol{M}}$ is obtained from $\widehat{K}(s)$ and the objective matrix $\widetilde{\boldsymbol{M}}$ from $\widetilde{K}(s)$.

III. Optimization Through Model Extraction

All of the process of analysis and model extraction can be seen as a model function that relates the physical parameters of the device $\boldsymbol{x}$ with the circuital ones $\widehat{\boldsymbol{y}}$ as follows:

$$\widehat{\boldsymbol{y}} = \boldsymbol{f}(\boldsymbol{x}). \quad (24)$$

The elements of $\widehat{\boldsymbol{y}}$ are the significant coefficients of the coupling matrix $\widehat{\boldsymbol{M}}$, i.e., the shiftings of the resonant frequencies and the coupling coefficients. The optimization procedure tries to find a set of physical parameters $\boldsymbol{x}$ so that the circuital parameters of the extracted model $\widehat{\boldsymbol{y}}$ coincide with those of the objective model $\widetilde{\boldsymbol{y}}$ (the significant coefficients of the objective coupling matrix $\widetilde{\boldsymbol{M}}$).

With the evaluation of this function for the initial design $\boldsymbol{x}_0$, the difference between the extracted circuital parameters $\widehat{\boldsymbol{y}}_0 = \boldsymbol{f}(\boldsymbol{x}_0)$ and the objective ones $\widetilde{\boldsymbol{y}}_0$ is evaluated in order to calculate the error of the circuital model that describes the physical implementation of the filter. Then the inverse function of $\boldsymbol{f}$ must be used to translate this error to the correction that must be applied to the physical design parameters

$$\Delta\boldsymbol{y}_0 = \widetilde{\boldsymbol{y}}_0 - \widehat{\boldsymbol{y}}_0 = \widetilde{\boldsymbol{y}}_0 - \boldsymbol{f}(\boldsymbol{x}_0) \quad (25)$$

$$\Delta\boldsymbol{x}_0 = \boldsymbol{x}_1 - \boldsymbol{x}_0 = \boldsymbol{f}^{-1}(\Delta\boldsymbol{y}_0 + \widehat{\boldsymbol{y}}_0) - \boldsymbol{x}_0 \quad (26)$$

where $\boldsymbol{x}_1$ stands for the physical parameters of an improved design.

The inverse function $\boldsymbol{f}^{-1}$ can be estimated with the linear approximation of $\boldsymbol{f}$ as

$$\widehat{\boldsymbol{y}} = \boldsymbol{f}(\boldsymbol{x}) \simeq \boldsymbol{J}_0 \Delta\boldsymbol{x}_0 + \widehat{\boldsymbol{y}}_0. \quad (27)$$

Taking into account (26), one obtains

$$\Delta\boldsymbol{x}_0 \simeq \boldsymbol{J}_0{}^{-1} \Delta\boldsymbol{y}_0 \quad (28)$$

where $\boldsymbol{J}_0$ is the Jacobian matrix of $\boldsymbol{f}$ evaluated for $\boldsymbol{x}_0$. Therefore, the physical parameters of the new design, $\boldsymbol{x}_1 = \boldsymbol{x}_0 + \Delta\boldsymbol{x}_0$, are obtained. The circuital model of this new implementation $\widehat{\boldsymbol{y}}_1$ must be closer to the circuit which was used to begin the design

process; thus the response of the new filter must be more similar to the desired one $\widetilde{\boldsymbol{y}}_1$. The circuital parameters of the new filter are extracted again in order to make a finer correction, and the process is repeated in an iterative scheme until the norm of the correction vector becomes small enough. In this work, the norm used is

$$||\Delta \boldsymbol{x}||_\infty = \max_i \{[\Delta \boldsymbol{x}]_i\}. \tag{29}$$

A. Jacobian Estimation

The Jacobian of the function that maps the physical dimensions of the designed filter to the couplings and the resonant frequencies of the prototype can be calculated numerically by forward differences

$$[\boldsymbol{J}]^i = \frac{\partial \boldsymbol{f}}{\partial x_i} \simeq \frac{\boldsymbol{f}(\boldsymbol{x} + h\boldsymbol{e}_i[\boldsymbol{x}]_i) - \boldsymbol{f}(\boldsymbol{x})}{h[\boldsymbol{x}]_i} \tag{30}$$

where $\boldsymbol{x}$ is the vector of the design physical parameters, h is the finite difference step length, $\boldsymbol{e}_i$ is the ith column of the unitary matrix, i.e.,

$$[\boldsymbol{e}_i]_j = \begin{cases} 0, & \text{if } i \neq j \\ 1, & \text{if } i = j \end{cases} \tag{31}$$

and $[\boldsymbol{J}]^i$ denotes the ith column of the Jacobian matrix. The optimum step length h is the one that minimizes the combination of two error sources: the truncation error due to the linear approximation of the derivative, and the error of the computation or measurements. If this second error is only due to the use of a finite number of digits (roundoff error), the optimum for the forward differences scheme is $h = \mathcal{O}(10^{-n_d/2})$, where n_d is the number of significant digits.

This numerical estimation approach implies $l+1$ evaluations of the function $\boldsymbol{f}(\boldsymbol{x})$, where l is the number of physical parameters, i.e., the number of columns of the Jacobian matrix. Each evaluation requires at least $n + n_z + 1$ frequency samples of the device response. Since $\boldsymbol{f}(\boldsymbol{x})$ is not a linear function, the coefficients of the Jacobian matrix will change at each iteration. However, in order to reduce the computational effort at each iteration, an updating scheme of the Jacobian based on the information obtained from the previous iterations is used.

Every iteration in the optimization algorithm is finished with a variation of the design parameters in a given direction, $\Delta \boldsymbol{x}_k = \boldsymbol{x}_{k+1} - \boldsymbol{x}_k$, that must produce a variation of the extracted circuital parameters $\Delta \widehat{\boldsymbol{y}}_k = \widehat{\boldsymbol{y}}_{k+1} - \widehat{\boldsymbol{y}}_k$. This variation provides an approximation of the directional derivative along $\Delta \boldsymbol{x}_k$ that can be used to update the Jacobian matrix. The new Jacobian must be in agreement with the observed directional derivative, so it must satisfy

$$\Delta \boldsymbol{x}_k = \boldsymbol{J}_{k+1} \Delta \widehat{\boldsymbol{y}}_k. \tag{32}$$

If $\Delta \boldsymbol{x}_k$ is proportional to the unitary vector $\boldsymbol{e}_i$, then (32) can be satisfied by the substitution of the ith column of $\boldsymbol{J}_k$ by $\Delta \widehat{\boldsymbol{y}}_k ||\Delta \boldsymbol{x}_k||^{-1}$, where $||\cdot||$ stands for the Euclidean norm. For an arbitrary correction vector, the basis of the linear transformation represented by the matrix $\boldsymbol{J}_k$ can be changed to align the first vector of the basis with the vector $\Delta \boldsymbol{x}_k$. The transformation matrix $\boldsymbol{P}$ that defines this change of basis applied to the vector $\Delta \boldsymbol{x}_k$ must annihilate all but the first component of the vector $\Delta \boldsymbol{x}_k$. The Householder reflector matrix given by

$$\boldsymbol{P} = \boldsymbol{I} - 2\frac{\boldsymbol{w}\boldsymbol{w}^T}{\boldsymbol{w}^T\boldsymbol{w}} \Rightarrow \boldsymbol{P}\Delta \boldsymbol{x_k} = ||\Delta \boldsymbol{x}_k||\boldsymbol{e}_1 \tag{33}$$

where

$$\boldsymbol{w} = \Delta \boldsymbol{x}_k \pm ||\Delta \boldsymbol{x}_k||\boldsymbol{e}_1 \tag{34}$$

and $\boldsymbol{I}$ is the corresponding identity matrix) achieves this property. The resulting matrix $\boldsymbol{P}$ is orthogonal and symmetric. Thus, $\boldsymbol{P}$ is also the inverse transformation matrix and transforms vectors and matrices between the two bases using the following equations:

$$\begin{aligned} \boldsymbol{P} &= \boldsymbol{P}^T = \boldsymbol{P}^{-1} \\ \boldsymbol{x}^r &= \boldsymbol{P}\boldsymbol{x} \\ \boldsymbol{x} &= \boldsymbol{P}\boldsymbol{x}^r \\ \boldsymbol{J}^r &= \boldsymbol{P}\boldsymbol{J}\boldsymbol{P} \\ \boldsymbol{J} &= \boldsymbol{P}\boldsymbol{J}^r\boldsymbol{P} \end{aligned} \tag{35}$$

where $\boldsymbol{x}^r$ and $\boldsymbol{J}^r$ stand for the transformed vector and Jacobian matrix, respectively.

Applying the linear transformation defined by $\boldsymbol{P}$ to (32), one obtains

$$\boldsymbol{P}\Delta \boldsymbol{x}_k = ||\Delta \boldsymbol{x}_k||\boldsymbol{e}_1 = \boldsymbol{P}\boldsymbol{J}_k\boldsymbol{P}\boldsymbol{P}\Delta \widehat{\boldsymbol{y}}_k \Rightarrow \boldsymbol{e}_1 = \boldsymbol{J}_k^r \frac{\Delta \widehat{\boldsymbol{y}}_k^r}{||\Delta \boldsymbol{x}_k||}. \tag{36}$$

Then, the transformed Jacobian matrix can be updated directly by replacing the first column of the matrix $\boldsymbol{J}_k^r$ by the estimated directional derivative given by $\Delta \widehat{\boldsymbol{y}}_k^r$ as follows:

$$\begin{aligned} \left[\boldsymbol{J}_{k+1}^r\right]^i &= [\boldsymbol{J}_k^r]^i \qquad \text{if } i \neq 1 \\ \left[\boldsymbol{J}_{k+1}^r\right]^1 &= \frac{\Delta \widehat{\boldsymbol{y}}_k^r}{||\Delta \boldsymbol{x}_k||}. \end{aligned} \tag{37}$$

Finally, the new Jacobian is obtained after applying the inverse transformation

$$\boldsymbol{J}_{k+1} = \boldsymbol{P}\boldsymbol{J}_{k+1}^r\boldsymbol{P}. \tag{38}$$

Using this approach, the estimated directional derivative obtained from the last iteration is inserted into the Jacobian matrix without modifying the directional derivatives along vectors orthogonal to vector $\Delta \boldsymbol{x}_k$. However, the vectors $\{\Delta \boldsymbol{x}_{k-1}, \Delta \boldsymbol{x}_{k-2}, \ldots\}$ in the previous iterations are not necessarily orthogonal to $\Delta \boldsymbol{x}_k$, therefore the component along $\Delta \boldsymbol{x}_k$ of the estimated directional derivatives of the previous iterations will be lost by the insertion of the new estimation of the directional derivative. This effect can be avoided if the component of $\Delta \boldsymbol{x}_k$ contained in the vector space defined by the correction vectors of the previous iterations is removed before applying the updating scheme of the Jacobian matrix. Hence, the equations

$$\Delta \boldsymbol{x}_k = (\boldsymbol{x}_{k+1} - \boldsymbol{x}_k) - \mathrm{Proj}_{\mathcal{V}}(\boldsymbol{x}_{k+1} - \boldsymbol{x}_k) \tag{39}$$

$$\Delta \widehat{\boldsymbol{y}}_k = (\widehat{\boldsymbol{y}}_{k+1} - \widehat{\boldsymbol{y}}_k) - \boldsymbol{J}_k \mathrm{Proj}_{\mathcal{V}}(\widehat{\boldsymbol{y}}_{k+1} - \widehat{\boldsymbol{y}}_k) \tag{40}$$

are used in (32), where $\mathrm{Proj}_{\mathcal{V}}(\cdot)$ is the projection of the argument on the vector space defined as

$$\mathcal{V} = \mathcal{L}(\Delta \boldsymbol{x}_{k-1}, \Delta \boldsymbol{x}_{k-2}, \ldots, \Delta \boldsymbol{x}_{k-m}), \qquad m < l \tag{41}$$

where $\mathcal{L}$ stands for the linear variety generated by a set of vectors and l is the dimension of the Jacobian matrix.

The initial estimation of the Jacobian can be done following (30). However, in most designs, each coupling and resonant frequency is strongly determined by just one physical parameter, while the effect of the variation of the rest of the physical parameters is a second-order effect. Therefore, if the vectors $\boldsymbol{x}$ and $\widehat{\boldsymbol{y}}$ are ordered properly, an almost diagonal Jacobian matrix is expected, and $\boldsymbol{J}_0$ can be estimated with just two evaluations of the modeling function (24) as follows:

$$[\boldsymbol{J}_0]_{ii} = \frac{[\boldsymbol{f}(\boldsymbol{x}_0 + h\boldsymbol{x}_0) - \boldsymbol{f}(\boldsymbol{x}_0)]_i}{h[\boldsymbol{x}_0]_i}$$
$$[\boldsymbol{J}_0]_{ij} = 0, \qquad \text{if } i \neq j \tag{42}$$

instead of $l+1$. The update scheme, though not exact, will improve the accuracy of the Jacobian matrix with respect to the original one. This estimation technique is an example of a more general class, called Broyden methods [15], used in nonlinear optimization. It should be mentioned that, if the required corrections are too large, i.e., if the elements of $\Delta\boldsymbol{x}$ are high, the estimation of the Jacobian becomes invalid, and it must be restarted from (30) or (42).

B. Optimization Algorithm

The following is the step-by-step complete filter optimization algorithm. It also corresponds to the diagram in Fig. 3.

1) Generation of the ideal characteristic polynomials, $F(s)$, $P(s)$, $E(s)$, from specifications [7], [14].
2) Synthesis of the ideal coupling matrix $\boldsymbol{M}$ (Section II-C).
3) Computation of initial dimensions of the microwave device physical implementation.
4) Acquisition of N samples of the physical response, $S_{11}(s_i)$, $S_{21}(s_i)$ (through measurements or electromagnetic analysis).
5) Computation of a circuital model with distorted response.
   a) Extraction of an increased-order model $\widehat{K}_{inc}(s)$ (Section II-A).
   b) Identification of the auxiliary reflection zeros $\{s_{0i}\}_{i=1,\ldots,m}$ (Section II-B).
   c) Order reduction of the model in order to obtain $\widehat{K}(s)$ (Section II-B).
   d) Synthesis of the extracted model coupling matrix $\widehat{\boldsymbol{M}}$ (Section II-C).
6) Computation of an objective predistorted circuital model.
   a) Generation of the objective increased-order quasi-elliptic response $\widetilde{K}_{\mathrm{qe}}(s)$, with auxiliary transmission zeros related to $\{s_{0i}\}_{i=1,\ldots,m}$ and correct in-band response (Section II-B).
   b) Order reduction of the objective model in order to obtain $\widetilde{K}(s)$ (Section II-B).
   c) Synthesis of the objective coupling matrix $\widetilde{\boldsymbol{M}}$ (Section II-C).
7) Computation of the error matrix between the extracted model and the objective, $\widehat{\boldsymbol{M}} - \widetilde{\boldsymbol{M}}$, and generation of an error vector of the circuital parameters, $\Delta\boldsymbol{y}$ (Section III).

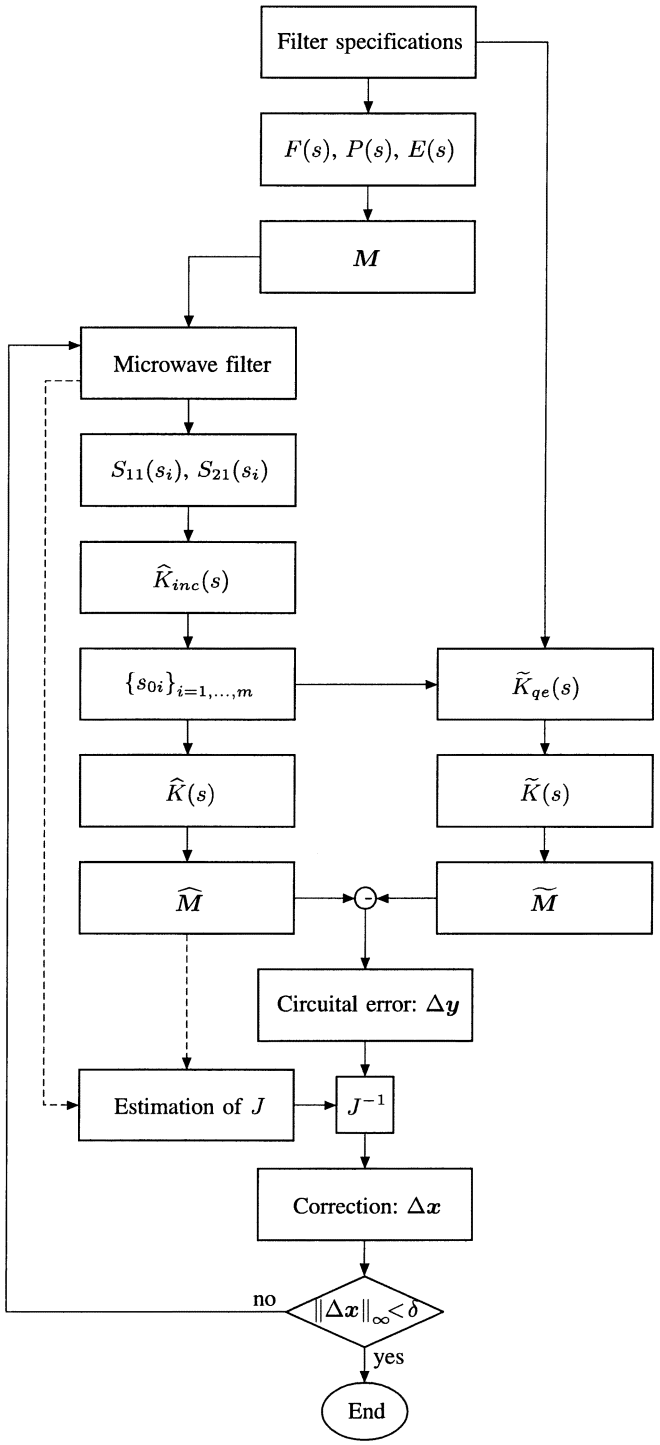

Fig. 3. Flow diagram of the proposed filter optimization algorithm.

8) Estimation or update of the Jacobian matrix $\boldsymbol{J}$ (Section III-A).
9) Estimation of a correction vector for the physical parameters $\Delta\boldsymbol{x} = \boldsymbol{J}^{-1}\Delta\boldsymbol{y}$ (Section III).
10) If $\|\Delta\boldsymbol{x}\|_\infty < \delta$ (where δ is a termination condition), exit.
11) Update of the filter physical parameters.
12) Return to 4).

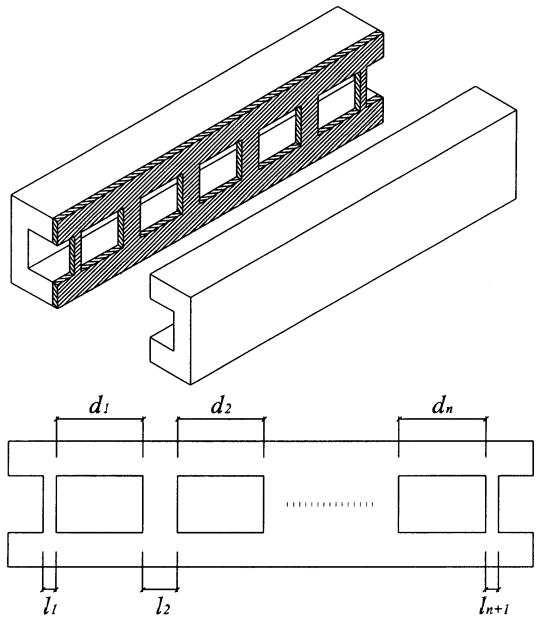

Fig. 4. Waveguide E-plane filter with all-metal inserts.

IV. Numerical Examples

To illustrate the capabilities of the described algorithm, different examples of filters and multiplexers have been designed and optimized. Two representative examples have been chosen. First, an isolated filter is presented, where the application of the method is straightforward. Next, the method is applied to the response of two filters integrated in a diplexer, so that the global diplexer response is optimized.

A. Filter

The method is tested with the design of a fifth-order waveguide E-plane filter with all-metal inserts (see Fig. 4), where the design parameters are the lengths of the metal inserts (l_i in Fig. 4) and the distances between them (d_i in Fig. 4). The center frequency of the specified filter is 29 GHz with a bandwidth of 500 MHz and in-band return losses equal to -25 dB. The section of the waveguide where the filter is constructed is 7.112 mm $\times$ 3.556 mm (WR28), while the thickness of the inserts is 100 μm. The design procedure for this type of filter is described in [22]. However, in order to test the robustness of the optimization method, a very simple initial design was chosen: the length of all metal inserts in Fig. 4 was set to 1 mm, and the distance between two consecutive metal inserts was considered to be equal to a half wavelength at the center frequency (6.5253 mm). The simulated frequency response of this initial design is presented in Fig. 5, where a large mismatch with the desired one is evident. For the full-wave electromagnetic analysis, a mode-matching procedure was utilized. The extended coupling matrix (21) that is extracted at this initial step is given in (43), and the response of the corresponding circuital model is shown in Fig. 6.

Note that the response of the filter and the response of the extracted model are very close. The small disagreement is due to the distortion produced by the process of inserting and removing reflection zeros used to model the error term of (13) in Section II-B. This distortion does not affect the optimization process since a predistorted objective coupling matrix has been used. It should be noted that only nine samples of the scattering

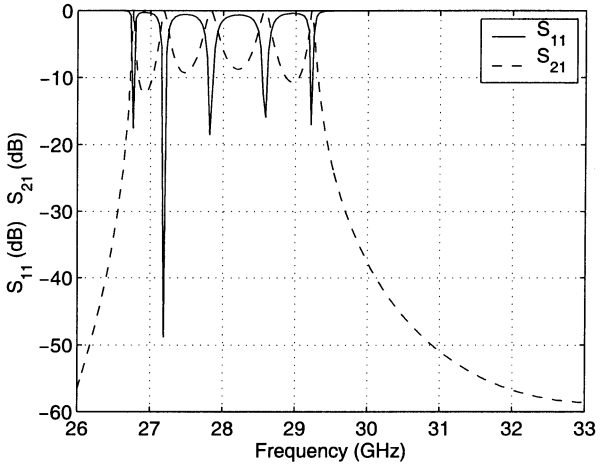

Fig. 5. Full-wave electromagnetic analysis of the scattering parameters of the initial design for the waveguide E-plane filter with all-metal inserts.

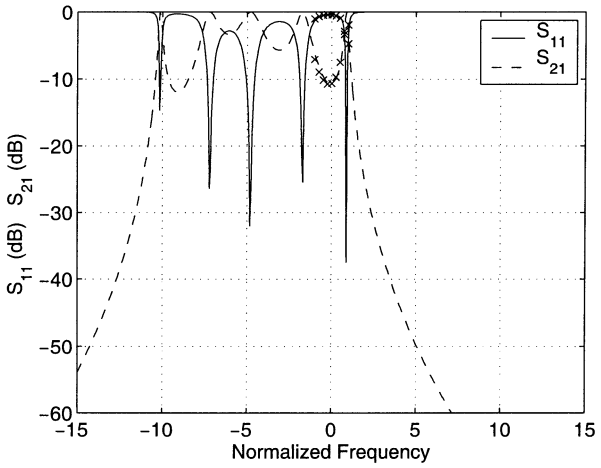

Fig. 6. Scattering parameters of the extracted circuit model of the initial design (solid line) and samples of the scattering parameters of the waveguide E-plane filter used to extract the model (crosses).

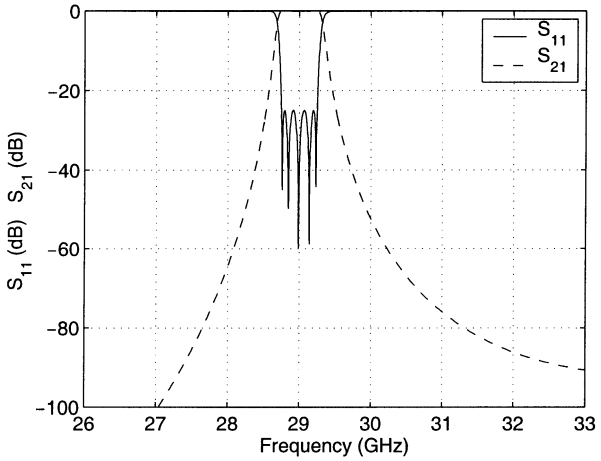

Fig. 7. Scattering parameters of the optimized waveguide E-plane filter of order 5, passband between 28.75 and 29.25 GHz, and return loss level of -25 dB.

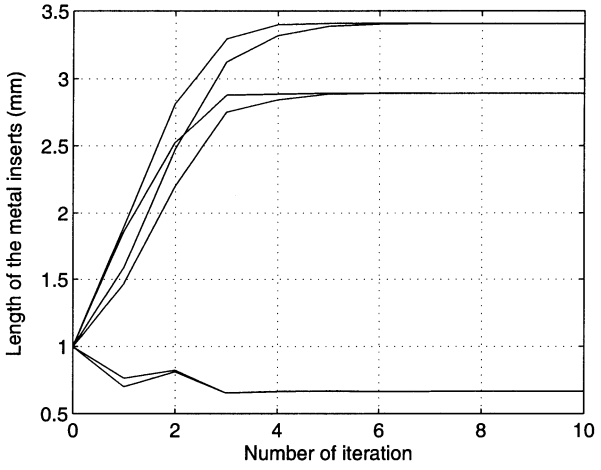

(a)

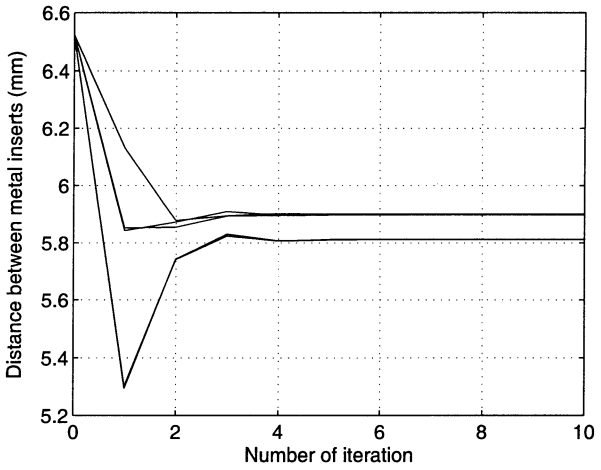

(b)

Fig. 8. Geometric dimensions of the waveguide E-plane filter through the optimization process. (a) Evolution of the lengths of the metal inserts (l_i). (b) Evolution of the distances between the metal inserts (d_i).

parameters uniformly distributed in the specified passband (represented with crosses in Fig. 6) are used to extract the circuital model, showing the good performance of Cauchy's method and its insensitivity to the location of the samples.

Using the initial coupling matrix M_0 of (43), shown at the bottom of the following page, and the ideal one, the optimization method obtain a correction of the physical parameters of the filter as explained in the previous sections. Then a new design and a new coupling matrix are obtained and the same procedure is applied following an iterative scheme. The optimization was completed after only ten iterations. Besides the initial analysis and the ten full-wave electromagnetic analyses for each iteration (at only nine frequency points) only six more electromagnetic analyses (again at only nine frequency points) were required to compute the Jacobian matrix. It may be mentioned that in this case the computation of the Jacobian required to be restarted six times because of the initial poor design. Otherwise, only the first computation is necessary. The process was finished when all the relative errors on the dimensions of the device were lower than 10^{-5}. Fig. 7 refers to the response of the optimized filter, which

TABLE I
FINAL DESIGN PARAMETERS OF THE FILTER

Distances (mm)		Inserts (mm)	
d_1	5.8122	l_1	0.6652
d_2	5.8984	l_2	2.8917
d_3	5.9008	l_3	3.4083
d_4	5.8984	l_4	3.4083
d_5	5.8122	l_5	2.8917
		l_6	0.6652

TABLE II
PERFORMANCE COMPARISON BETWEEN THE MODEL-BASED ELECTROMAGNETIC OPTIMIZATION AND A GRADIENT OPTIMIZATION

	Filter (IV-A)		Diplexer (IV-B)	
	Model	Gradient	Model	Gradient
Number of iterations	10	27	10	82
EM frequency sweeps	17	280	37	2710
Points per sweep	9	30	22	36
Total computed EM points	153	8400	814	97560
CPU time (seconds)	90	4950	420	50350

shows the equiripple shape corresponding to a Chebyshev filter in the prescribed passband. Fig. 8 shows the convergence of the geometric dimensions of the filter and Table I includes their final optimized values. The extended coupling matrix extracted from the optimized filter is given in (44), shown at the bottom of the following page.

The first column of Table II shows the performance comparison between the presented optimization and a standard optimization of the same filter based on a quasi-Newton (BFGS) gradient technique. It should be noted that the gradient technique is not able to converge to the optimum solution using the starting filter with the response shown in Fig. 5. Therefore, the solution of the third iteration of the model-based optimization has been used as the starting point. Even with these different evaluation criteria, the computation time is reduced to 1.82% of the original time when the proposed method is used. The CPU computation times are measured in a Pentium III 1-GHz computer with 512 MB of RAM running MATLAB.

B. Diplexer

The traditional way of electromagnetic optimization of diplexers, based on a least-squares error function, presents some limitations: a high number of data samples and a careful selection of the error function are required, and usually a multistep optimization algorithm is necessary in order to avoid the convergence to a local minimum [23].

The method based on the circuital model presented in this paper can be applied to each channel in a diplexer, since the method can take into account an error term to describe the mutual interaction of the filters. If the common port of the diplexer is defined as port 3, and the ports of channel 1 and channel 2 are defined respectively as port 1 and port 2, then the modeling function presented in Section II can be applied to samples of the scattering parameters S_{11} and S_{31} for channel 1 and the scattering parameters S_{22} and S_{32} for channel 2. Thus, two extracted model coupling matrices are obtained that can be compared with two objective coupling matrices calculated as presented in Section II. The optimization algorithm is applied as

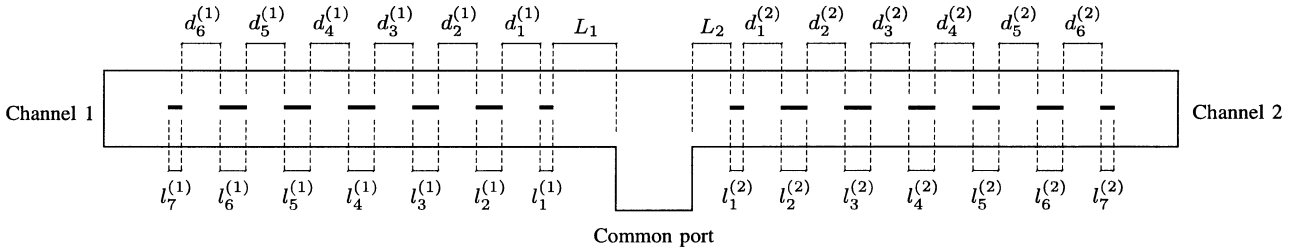

Fig. 9. Top view of a diplexer composed by two waveguide E-plane filters with all-metal inserts and an H-plane T-junction.

in Section III, where the vectors $\boldsymbol{x}$, $\widehat{\boldsymbol{y}}$, and $\widetilde{\boldsymbol{y}}$ include the physical design parameters, the extracted circuital parameters, and the objective circuital parameters of both filters, respectively.

It should be noted that the objective coupling matrices are obtained from the ideal prototype filters that would have been used for optimization of the filters if they were isolated, instead of starting with the model of the complete diplexer structure as is usually done. In fact, the mutual interaction of both filters in the diplexer is reflected in the Jacobian matrix of the modeling function which cannot be almost diagonal, since the variation of the physical dimensions of one filter modifies the electromagnetic behavior of the other filter. Therefore, (30) must be used to calculate the initial Jacobian matrix. However, after this calculation, the Jacobian matrix is updated without additional evaluations of the modeling function, using the scheme of Section III-A.

The diplexer used to test the optimization method consists of two sixth-order E-plane filters connected by an H-plane T-junction as depicted in Fig. 9 with the following specifications:

- Channel 1:
  - center frequency: 28.75 GHz;
  - bandwidth: 0.5 GHz;
  - return loss in the passband: 25 dB.
- Channel 2:
  - center frequency: 30 GHz;
  - bandwidth: 1 GHz;
  - return loss in the passband: 25 dB.
- Waveguide section: WR28 (7.112 mm $\times$ 3.556 mm).
- Thickness of metal inserts: 100 μm.

TABLE III
INITIAL DESIGN PARAMETERS OF THE DIPLEXER

Channel 1				Channel 2			
Distances (mm)		Inserts (mm)		Distances (mm)		Inserts (mm)	
L_1	6.0060	$l_1^{(1)}$	0.6517	L_2	4.8000	$l_1^{(2)}$	0.4101
$d_1^{(1)}$	5.9526	$l_2^{(1)}$	2.8913	$d_1^{(2)}$	5.2612	$l_2^{(2)}$	2.2548
$d_2^{(1)}$	6.0435	$l_3^{(1)}$	3.4464	$d_2^{(2)}$	5.3727	$l_3^{(2)}$	2.8229
$d_3^{(1)}$	6.0457	$l_4^{(1)}$	3.5332	$d_3^{(2)}$	5.3773	$l_4^{(2)}$	2.9139
$d_4^{(1)}$	6.0457	$l_5^{(1)}$	3.4464	$d_4^{(2)}$	5.3773	$l_5^{(2)}$	2.8229
$d_5^{(1)}$	6.0435	$l_6^{(1)}$	2.8913	$d_5^{(2)}$	5.3727	$l_6^{(2)}$	2.2548
$d_6^{(1)}$	5.9526	$l_7^{(1)}$	0.6517	$d_6^{(2)}$	5.2612	$l_7^{(2)}$	0.4101

The initial design of the diplexer is synthesized following the method proposed in [24]. This method starts from the optimized design of the two filters and then fixes the distances from the reference planes of the T-junction to the reference plane of each filter (indicated as L_1 and L_2 in Fig. 9). The geometrical dimensions of the initial design are given in Table III, and the full-wave electromagnetic analyzed response of this initial design is shown in Fig. 10. The mutual interaction between the filters through the T-junction produces high return losses, as is observed in the response. The optimization method modifies the parameters of the filter in order to compensate for this mutual interaction and recover the frequency response of the isolated original filters. The process optimizes the couplings and the resonant frequencies of each filter, but not the distances between the filters and the T-junction (i.e., L_1 and L_2 remain constant during the optimization routine).

$$\widehat{\boldsymbol{M}}_0 = \begin{bmatrix} 0 & 0.9571 & 0 & 0 & 0 & 0 & 0 \\ 0.9571 & 4.6387 & 2.8306 & 0 & 0 & 0 & 0 \\ 0 & 2.8306 & 4.2822 & 3.3545 & 0 & 0 & 0 \\ 0 & 0 & 3.3545 & 5.0356 & 3.3545 & 0 & 0 \\ 0 & 0 & 0 & 3.3545 & 4.2822 & 2.8306 & 0 \\ 0 & 0 & 0 & 0 & 2.8306 & 4.6387 & 0.9571 \\ 0 & 0 & 0 & 0 & 0 & 0.9571 & 0 \end{bmatrix} \tag{43}$$

$$\widehat{\boldsymbol{M}}_{10} = \begin{bmatrix} 0 & 1.1210 & 0 & 0 & 0 & 0 & 0 \\ 1.1210 & 0.0215 & 0.9739 & 0 & 0 & 0 & 0 \\ 0 & 0.9739 & 0.0130 & 0.6826 & 0 & 0 & 0 \\ 0 & 0 & 0.6826 & 0.0112 & 0.6826 & 0 & 0 \\ 0 & 0 & 0 & 0.6826 & 0.0130 & 0.9739 & 0 \\ 0 & 0 & 0 & 0 & 0.9739 & 0.0215 & 1.1210 \\ 0 & 0 & 0 & 0 & 0 & 1.1210 & 0 \end{bmatrix} \tag{44}$$

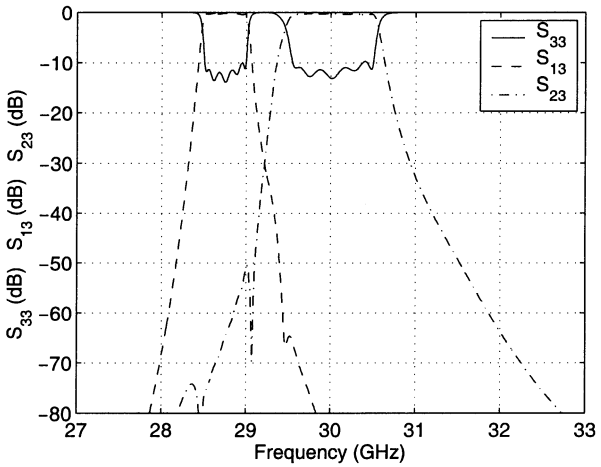

Fig. 10. Scattering parameters of the initial design of the diplexer.

TABLE IV
OPTIMIZED DESIGN PARAMETERS OF THE DIPLEXER

Channel 1				Channel 2			
Distances (mm)		Inserts (mm)		Distances (mm)		Inserts (mm)	
L_1	6.0060	$l_1^{(1)}$	0.8172	L_2	4.8000	$l_1^{(2)}$	0.2817
$d_1^{(1)}$	5.8792	$l_2^{(1)}$	2.8304	$d_1^{(2)}$	4.8079	$l_2^{(2)}$	1.6296
$d_2^{(1)}$	6.0198	$l_3^{(1)}$	3.3659	$d_2^{(2)}$	5.2516	$l_3^{(2)}$	2.6676
$d_3^{(1)}$	6.0413	$l_4^{(1)}$	3.4735	$d_3^{(2)}$	5.3628	$l_4^{(2)}$	2.8466
$d_4^{(1)}$	6.0449	$l_5^{(1)}$	3.3864	$d_4^{(2)}$	5.3747	$l_5^{(2)}$	2.7567
$d_5^{(1)}$	6.0427	$l_6^{(1)}$	2.8343	$d_5^{(2)}$	5.3705	$l_6^{(2)}$	2.2085
$d_6^{(1)}$	5.9474	$l_7^{(1)}$	0.6251	$d_6^{(2)}$	5.2542	$l_7^{(2)}$	0.3939

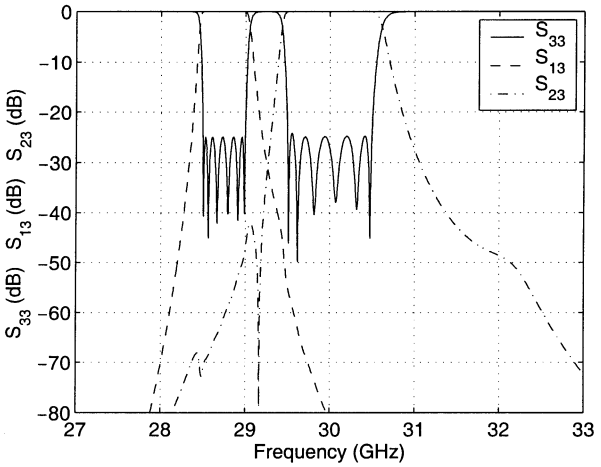

Fig. 11. Scattering parameters of the optimized design of the diplexer.

The geometric dimensions after optimizing the diplexer are shown in Table IV, and the scattering parameters of the modified design are presented in Fig. 11, where the equiripple response is almost completely recovered. As expected, the most modified geometrical dimensions are those located closer to the T-junction, in order to compensate the reactive load that each filter presents to the other. The complete optimization process of the 26 parameters took only ten iterations and the total number of full-wave electromagnetic simulations executed was 37 (11 for the initial design and the ten iterations and 2×13 for the computation of the initial Jacobian, since there are 13 geometrical parameters in each filter). Only 22 frequency samples (11 in the passband of each channel) were calculated in every electromagnetic simulation.

The second column of Table II shows the performance comparison of this process and the equivalent optimization using a conventional gradient-based method as in the example of the isolated filter. In this case, the optimum can be reached using both optimization techniques, but the computation time is reduced to only 0.83% using the proposed method. It should be noted the large reduction of the number of evaluated frequency sweeps due to the Jacobian update scheme, compared to the explicit computations of the gradient of the error function using a forward differences method.

V. CONCLUSION

In this paper, an efficient method for the direct electromagnetic optimization of microwave passive devices, based on the extraction of a rational model from a reduced number of data samples of the frequency response, has been described. Some particular advantages of this method is the possibility to approximate nonrational responses and the adaptive update of the mapping between the circuital model parameters and the dimensions of the physical device. The current implementation restricts the application of the method to lossless networks due to two limitations:

- the use of the lossless Feldtkeller equation;
- the analytical method used to synthesize a coupling matrix.

However, the usual approach for synthesizing microwave devices requires only the use of lossless models, as losses are introduced in a last step after the proper optimization.

Two numerical application examples have shown remarkable improvements in computation efficiency. This reduction of the total time required for the optimization is achieved in two ways. First, the number of required optimization iterations is greatly reduced. Second, the number of needed data samples at each iteration is minimized thanks to the use of Cauchy's method. One of the examples consists of the optimization of a complete diplexer, showing the flexibility of the method, that can be applied to structures different from isolated filters.

REFERENCES

[1] J. Herbert and L. Thal, "Computer-aided filter alignment and diagnosis," *IEEE Trans. Microwave Theory Tech.*, vol. MTT-26, pp. 958–963, Dec. 1978.

[2] M. Bakr, J. Bandler, N. Georgieva, and K. Madsen, "A hybrid aggressive space-mapping algorithm for EM optimization," *IEEE Trans. Microwave Theory Tech.*, vol. 47, pp. 2440–2449, Dec. 1999.

[3] S. Bila, D. Baillargeat, M. Aubourg, S. Verdeyme, P. Guillon, F. Seyfert, J. Grimm, L. Baratchart, C. Zanchi, and J. Sombrin, "Direct electromagnetic optimization of microwave filters," *IEEE Microwave Mag.*, vol. 2, pp. 46–51, Mar. 2001.

[4] M. Kahrizi, S. Safavi-Naeini, S. K. Chaudhuri, and R. Sabry, "Computer diagnosis and tuning of RF and microwave filters using model-based parameter estimation," *IEEE Trans. Circuits Syst.*, vol. 49, pp. 1263–1270, Sept. 2002.

[5] P. Harscher, R. Vahldieck, and S. Amari, "Automated filter tuning using generalized low-pass prototype networks and gradient-based parameter extraction," *IEEE Trans. Microwave Theory Tech.*, vol. 49, pp. 2532–2538, Dec. 2001.

[6] A. E. Atia and H.-W. Yao, "Tuning and measurements of couplings and resonant frequencies for cascaded resonators," in *Proc. IEEE MTT-S Int. Microwave Symp.*, vol. 3, Boston, MA, June 2000, pp. 1637–1640.

[7] A. García Lampérez, M. Salazar Palma, M. Padilla, and I. Hidalgo Carpintero, "Software tool for the design of narrow band band-pass filters," in *Proc. IEEE MTT-S Int. Microwave Symp.*, vol. 3, Phoenix, AZ, May 2001, pp. 2103–2106.
[8] K. Kottapalli, T. K. Sarkar, Y. Hua, E. K. Miller, and G. J. Burke, "Accurate computation of wide-band response of electromagnetic systems utilizing narrow-band information," *IEEE Trans. Microwave Theory Tech.*, vol. 39, pp. 682–687, Apr. 1991.
[9] R. S. Adve and T. K. Sarkar, "Generation of accurate broadband information from narrowband data using the Cauchy method," *Microwave Opt. Technol. Lett.*, vol. 6, no. 10, pp. 569–573, Aug. 1993.
[10] S. F. Peik, R. R. Mansour, and Y. L. Chow, "Multidimensional Cauchy method and adaptive sampling for an accurate microwave circuit modeling," *IEEE Trans. Microwave Theory Tech.*, vol. 46, pp. 2364–2371, Dec. 1998.
[11] A. García Lampérez, T. K. Sarkar, and M. Salazar Palma, "Robust computation and modeling of wide-band system responses using the Cauchy method," in *Proc. IEEE Antennas and Propagation Soc. Int. Symp.*, vol. 2, San Antonio, TX, June 2002, pp. 720–723.
[12] ——, "Filter model generation from scattering parameters using the Cauchy method," in *Proc. 32nd Eur. Microwave Conf.*, vol. 1, Milan, Italy, Sept. 2002, pp. 413–416.
[13] S. Amari and J. Bornemann, "Maximum number of finite transmission zeros of coupled resonator filters with source/load-multiresonator coupling and a given topology," in *Proc. 2000 Asia–Pacific Microwave Conf.*, Sydney, Australia, 2000, pp. 1175–1177.
[14] R. J. Cameron, "General coupling matrix synthesis methods for Chebyshev filtering functions," *IEEE Trans. Microwave Theory Tech.*, vol. 47, pp. 433–442, Apr. 1999.
[15] C. G. Broyden, "A class of methods for solving nonlinear simultaneous equations," *Math. Comput.*, vol. 19, no. 92, pp. 577–593, Oct. 1965.
[16] E. K. Miller and T. K. Sarkar, "Model-order reduction in electromagnetics using model-based parameter estimation," in *Frontiers in Electromagnetics*. Piscataway, NJ: IEEE Press, 1999, pp. 371–436.
[17] S. Van Huffel and J. Vandewalle, *The Total Least Squares Problem: Computational Aspects and Analysis*. Philadelphia, PA: SIAM, 1991.
[18] A. Edelman and H. Murakami, "Polynomial roots from companion matrix eigenvalues," *Math. Comput.*, vol. 64, no. 210, pp. 763–776, 1995.
[19] A. E. Atia and A. E. Williams, "Narrow-bandpass waveguide filters," *IEEE Trans. Microwave Theory Tech.*, vol. MTT-20, pp. 258–265, Apr. 1972.
[20] A. E. Atia, A. E. Williams, and R. W. Newcomb, "Narrow-band multiple coupled cavity synthesis," *IEEE Trans. Circuits Syst.*, vol. CAS-20, pp. 649–655, Sept. 1974.
[21] R. J. Cameron, "Advanced coupling matrix synthesis techniques for microwave filters," *IEEE Trans. Microwave Theory Tech.*, vol. 51, pp. 1–10, Jan. 2003.
[22] D. Budimir, *Generalized Filter Design by Computer Optimization*. Boston, MA: Artech House, 1998.
[23] Y. Rong, H. Wen Yao, K. A. Zaki, and T. G. Dolan, "Millimeter-wave Ka-band H-plane diplexers and multiplexers," *IEEE Trans. Microwave Theory Tech.*, vol. 47, pp. 2325–2330, Dec. 1999.
[24] A. Morini and T. Rozzi, "Constraints to the optimum performance and bandwidth limitations of diplexers employing symmetric three-port junctions," *IEEE Trans. Microwave Theory Tech.*, vol. 44, pp. 242–248, Feb. 1996.

Alejandro García-Lampérez (S'98) was born in Madrid, Spain, in 1976. He received the Ingeniero de Telecomunicación (M.S.E.E.) degree from the Universidad Politécnica de Madrid (UPM), Madrid, Spain, in 2000, and is currently working toward the Ph.D. degree at the UPM.

Since September 1999, he has been with the Microwave and Radar Group, Departamento de Señales, Sistemas y Radiocomunicaciones (SSR), UPM, where he carried out his graduate work on techniques for the design of microwave filters. His research activities and interests are in the area of passive microwave devices design and simulation and application of numerical methods to electromagnetic problems.

Sergio Llorente-Romano (S'01) was born in Madrid, Spain, in 1977. He received the Ingeniero de Telecomunicacíon (M.S.E.E.) degree from the Universidad Politécnica de Madrid (UPM), Madrid, Spain, in 2000, and is currently working toward the Ph.D. degree at UPM.

Since September 1999, he has been with the Microwave and Radar Group, Departamento de Señales, Sistemas y Radiocomunicaciones (SSR), UPM, where he carried out his graduate work on techniques for the simulation and design of filters and diplexers in waveguide technology. His research activities and interests are in the area of numerical methods applied to electromagnetic problems related to the design of microwave devices.

Magdalena Salazar-Palma (M'89–SM'01) was born in Granada, Spain. She received the Ingeniero de Telecomunicación and Ph.D. degrees from the Universidad Politécnica de Madrid (UPM), Madrid, Spain.

She is currently a Profesor Titular with the Departamento de Señales, Sistemas y Radiocomunicaciones, Escuela Técnica Superior de Ingenieros de Telecomunicación, UPM. She has taught courses on electromagnetic-field theory, microwave and antenna theory, circuit networks and filter theory, analog and digital communication systems theory, numerical methods for electromagnetic-field problems, as well as related laboratories. She has developed her research within the Grupo de Microondas y Radar in the areas of electromagnetic-field theory, computational and numerical methods for microwave structures, passive components, and antenna analysis; design, simulation, optimization, implementation, and measurements of hybrid and monolithic microwave integrated circuits; and network and filter theory and design. On numerous occasions, she has been a Visiting Professor with the Department of Electrical Engineering and Computer Science, Syracuse University, Syracuse, NY. She has authored three books and has authored or coauthored a total of 15 contributions for chapters and papers in books published internationally, 30 papers in international journals, and 140 papers in international conferences, symposiums, and workshops, plus a number of national publications and reports. She has served in different academic committees at the department, school, and university level. She has delivered a number of invited presentations, lectures, and seminars. She has lectured on several short courses, some of them in the frame of European Community Programs. She has participated as a researcher or director in 45 research projects and contracts, financed by international, European, and national institutions and companies. She has assisted the Comisión Interministerial de Ciencia y Tecnología (Spain National Board of Research) in the evaluation of projects. She is serving as reviewer of the Grant Project Office of the Italian Ministero dell'Universita e della Ricerca Scientifica e Tecnologica (Ministry of Universities and Scientific and Technological Research). She has also served in several evaluation panels of the Commission of the European Communities. She was Topical Editor for the disk of references of the triennial *Review of Radio Science* for three times. She has been a member of the Editorial Board of three scientific journals.

Prof. Salazar-Palma is a Registered Ingeniero de Telecomunicación in Spain. She is an associate editor for the IEEE ANTENNAS AND WIRELESS PROPAGATION LETTERS (AWPL). She is a correspondent of the International Union of Radio Science (URSI). She has served as vice-chairman and chairman of the IEEE Microwave Theory and Techniques Society (IEEE MTT-S)/IEEE Antennas and Propagation Society (IEEE AP-S) Spain joint chapter and chairman of the IEEE Spain Section. She is currently the IEEE Spain Section membership development officer. She has been a member of the IEEE Region 8 Nominations and Appointments Committee. She is currently the chairperson of the IEEE Region 8 Conference Coordination Subcommittee. She has been a member of the IEEE Ethics and Member Conduct Committee. Since 2001, she has been a member of the IEEE Women in Engineering Committee (WIEC). She has acted as liaison between the IEEE Regional Activities Board and the IEEE WIEC. She is currently the chairperson of the IEEE WIEC. She is a member of the Technical Program Committee of several international and national symposiums and reviewer for different international scientific journals, symposiums, and editorial companies. She has received two individual research awards and, together with the rest of her department, another research award, all from national institutions.

Tapan K. Sarkar (S'69–M'76–SM'81–F'92) received the B.Tech. degree from the Indian Institute of Technology, Kharagpur, India, in 1969, the M.Sc.E. degree from the University of New Brunswick, Fredericton, NB, Canada, in 1971, and the M.S. and Ph.D. degrees from Syracuse University, Syracuse, NY, in 1975.

From 1975 to 1976, he was with the TACO Division, General Instruments Corporation. He was with the Rochester Institute of Technology, Rochester, NY, from 1976 to 1985. He was a Research Fellow with the Gordon McKay Laboratory, Harvard University, Cambridge, MA, from 1977 to 1978. He is currently a Professor with the Department of Electrical and Computer Engineering, Syracuse University. His current research interests deal with numerical solutions of operator equations arising in electromagnetics and signal processing with application to system design. He has authored or coauthored over 250 journal papers and numerous conference papers and has authored 28 chapters in books and ten books, including *Iterative and Self Adaptive Finite-Elements in Electromagnetic Modeling* (Boston, MA: Artech House, 1998), *Applications of Wavelets in Electromagnetic and Signal Analysis* (Boston, MA: Artech House, 2002), and *Smart Antennas* (New York: Wiley/IEEE Press, 2003). He is on the editorial board of *Journal of Electromagnetic Waves and Applications* and *Microwave and Optical Technology Letters*.

Dr. Sarkar is a Registered Professional Engineer in the State of New York. He is a member of Sigma Xi and International Union of Radio Science Commissions A and B. He was an associate editor for feature articles of the *IEEE Antennas and Propagation Society Newsletter*, and he was the Technical Program chairman for the 1988 IEEE Antennas and Propagation Society International Symposium and URSI Radio Science Meeting. He has been appointed a U.S. Research Council Representative to many URSI General Assemblies. He was the Chairman of the Intercommission Working Group of International URSI on Time Domain Metrology (1990–1996). He was the recipient of the Best Paper Award of the IEEE TRANSACTIONS ON ELECTROMAGNETIC COMPATIBILITY in 1979 and at the 1997 National Radar Conference. He received the College of Engineering Research Award in 1996 and the Chancellor's Citation for Excellence in Research in 1998 at Syracuse University. He received the title Docteur Honoris Causa from Universite Blaise Pascal, Clermont Ferrand, France in 1998 and the Medal of the City of Clermont Ferrand, France, in 2000.

Analytical synthesis of microwave multiport networks

Alejandro García-Lampérez*, Magdalena Salazar-Palma*, Tapan K. Sarkar†

*Dpto. Señales, Sistemas y Radiocomunicaciones, ETSI Telecomunicación,
Universidad Politécnica de Madrid, Ciudad Universitaria s/n, 28040 Madrid, Spain
Tel: 34-91-336-7358, e-mail: lamperez@ieee.org
†Dept. of ECE, Syracuse University, Syracuse, NY 13244, USA

***Abstract*— An analytical, exact method for the synthesis of multiport microwave networks formed by coupled resonators is proposed. The method is based on the definition of a novel class of coupling matrix with non-resonant nodes and an arbitrary number of input/output ports. The use of this coupling matrix allows a synthesis procedure analogous to the one used for filters. Some applications of the presented technique are the design of power dividers, multiplexers and diplexers. A synthesis example of a diplexer formed by two box-section filters with one transmission zero at a specified frequency for each one is included.**

***Index Terms*— Microwave network synthesis, resonators, multiport, diplexer, coupling matrix, box-section.**

I. Introduction

Multiplexers and diplexers are key components in a wide range of communication systems. Combination of transmission and reception signals or channel separation are examples of application of this kind of multiport networks. Traditionally, the design of microwave multiplexer networks is performed in two steps: first, the filters for each channel are independently synthesized. Second, a power divider or manifold network is designed so that the responses of the isolated filters are minimally affected when integrated into the whole device. Usually this network is formed by lengths of transmission lines that introduce phase shifts to each channel [1], [2]. Extra decoupling resonators have been also proposed [3]. Usually an additional optimization step of the complete network is carried out in order to further improve the response of each channel [4], [5].

In the present work a different approach has been followed. Multiport networks are synthesized using techniques analogous to that ones traditionally restricted to two port networks, that is, filters. The complete network is formed by electromagnetically coupled microwave resonators, with an arbitrary number of ports. Instead of the response of each filter, the complete multiport network response must be specified in the form of scattering or open-circuit admittance parameters. The resulting coupling matrix can be manipulated in the same way as coupling matrices of filters are, in order to generate the desired coupling topology.

II. Definition of the Coupling Matrix for Multiport Networks

The synthesis technique presented in this work is valid for networks formed by n resonators and p non-resonant nodes, in this case the input/output ports. For networks with $p > 2$, the conventional $n \times n$ [6] or even the extended $(n+2) \times (n+2)$ [7] coupling matrices are no longer valid. Therefore, it is necessary to define a new kind of coupling matrix suitable for networks with an arbitrary number of ports. This generalized coupling matrix $\boldsymbol{M} \in \mathbb{R}^{(n+p)\times(n+p)}$ is defined by blocks,

$$\boldsymbol{M} = \begin{bmatrix} \boldsymbol{M}_p & \boldsymbol{M}_{pn} \\ \boldsymbol{M}_{pn}^T & \boldsymbol{M}_n \end{bmatrix} \tag{1}$$

where

- $\boldsymbol{M}_p \in \mathbb{R}^{p\times p}$: matrix of direct couplings between non-resonant nodes (ports). The diagonal coefficients of this matrix are zero.
- $\boldsymbol{M}_n \in \mathbb{R}^{n\times n}$: matrix of the network couplings, that is, couplings between pairs of resonators (conventional $n \times n$ coupling matrix).
- $\boldsymbol{M}_{pn} \in \mathbb{R}^{p\times n}$: matrix of couplings between ports and resonators.

Given the previous definition of the coupling matrix the loop equations of the network are expressed using matrix notation

$$[s\boldsymbol{U}_0 + \boldsymbol{M} - j\boldsymbol{R}_0] \cdot \boldsymbol{I} = \boldsymbol{A} \cdot \boldsymbol{I} = -j\boldsymbol{E} \tag{2}$$

where $s = j\frac{f_0}{\Delta f}\left(\frac{f}{f_0} - \frac{f_0}{f}\right)$ is the normalized complex frequency variable and f_0 and Δf are respectively the center frequency and the bandwidth used for the band-pass to low-pass transformation. Here, the unknown $\boldsymbol{I} \in \mathbb{R}^{(n+p)}$ is the vector of loop currents, $\boldsymbol{E}$ is the unit excitation vector (i.e. $\boldsymbol{E} = [1, 0, \ldots, 0]^T$ if only the first port is excited), and $\boldsymbol{U}_0$ and $\boldsymbol{R}_0$ are diagonal matrices defined by blocks with the same dimensions as $\boldsymbol{M}$,

$$\boldsymbol{U}_0 = \begin{bmatrix} \boldsymbol{0} & \boldsymbol{0} \\ \boldsymbol{0} & \boldsymbol{U}_n \end{bmatrix} \qquad \boldsymbol{R}_0 = \begin{bmatrix} \boldsymbol{U}_p & \boldsymbol{0} \\ \boldsymbol{0} & \boldsymbol{R}_n \end{bmatrix} \tag{3}$$

where $\boldsymbol{U}_n$ is the $(n\times n)$ identity matrix and $\boldsymbol{R}_n$ is a $(n\times n)$ diagonal matrix of the loss resistances of each resonator (zero for lossless networks). As $\boldsymbol{U}_p$ is the $(p \times p)$ identity

matrix, the definition of $\boldsymbol{R}_0$ as presented corresponds to a network with unit reference impedances at each port.

The loop currents of the multiport network are obtained by solving (2). In the case of excitation of the first port, $I_k = -j\left[\boldsymbol{A}^{-1}\right]_{k1}$. From the currents I_k the transmission and reflection coefficients are given by

$$\begin{aligned} S_{11} &= 1 - 2I_1 = 1 + 2j\left[\boldsymbol{A}^{-1}\right]_{11} \\ S_{k1} &= 2I_k = -2j\left[\boldsymbol{A}^{-1}\right]_{k1}, \qquad k \in \{2, \ldots, p\}. \end{aligned} \tag{4}$$

The rest of scattering parameters are computed in a similar way by exciting the remaining ports of the network and solving the corresponding current equations.

A different kind of coupling matrix for diplexers has been previously presented [8]. The main difference with the method proposed here is the lack of non-resonant nodes, that causes the coupling matrix to be less structured. This block structure is the key for the straightforward synthesis algorithm presented in the next section.

III. Coupling Matrix Synthesis Procedure

The synthesis technique for microwave multiport networks is based on an analogous method recently presented [9] for two-port networks, that is, filters. In fact, the method for filters is a particular case of the most general technique for networks with p ports. In this work the presented algorithm will be particularized to $p = 3$ for greater clarity, but it is easily generalizable.

The initial required data for the synthesis are the short-circuit admittance parameters, represented as rational polynomials with a common denominator. The matrix $\boldsymbol{Y}$ of these admittance parameters can be computed from the specified scattering parameters through the following matrix equation,

$$\boldsymbol{Y} = \boldsymbol{Z}_0^{-1}(\boldsymbol{U} - \boldsymbol{S})(\boldsymbol{U} - \boldsymbol{S})^{-1}\boldsymbol{Z}_0^{-1} \tag{5}$$

where $\boldsymbol{S}$ is the scattering matrix, $\boldsymbol{U}$ is the identity matrix and $\boldsymbol{Z}_0$ is the diagonal matrix of reference impedances at each port of the network [10]. In order to compute a rational representation of the admittance parameters (5) is particularized for a set of discrete frequency values, and then the complete functions reconstructed by rational polynomial identification [11].

The partial fraction expansion of the admittance matrix takes the following form,

$$\boldsymbol{Y} = \boldsymbol{Y}^{(\infty)} + \sum_{k=1}^{n} \frac{1}{s - j\lambda_k} \begin{bmatrix} r_{11k} & r_{12k} & r_{13k} \\ r_{21k} & r_{22k} & r_{23k} \\ r_{31k} & r_{32k} & r_{33k} \end{bmatrix} \tag{6}$$

where $\left[\boldsymbol{Y}^{(\infty)}\right]_{ij} = y_{ij}^{(\infty)} = \lim_{s \to j\infty} y_{ij}(s)$, $\{j\lambda_k\}_{k=1,\ldots,n}$ are the purely imaginary common poles of y_{ij} (that is, λ_k are the eigenvalues of the system) and $\{r_{ijk}\}_{k=1,\ldots,n}$ are the real residues of each y_{ij}.

Following an approach analogous to [9], the admittance matrix can also be synthesized from a canonical transversal network, with the general structure shown in Fig. 1. The network is formed by n resonators connected in parallel to each of the p ports through admittance inverters. The low-pass prototype of each resonator comprises one capacitor and one frequency invariant susceptance connected in parallel. Using the impedance-scaling property of the inverters the capacitor is normalized to unity without loss of generality. Additionally, fully canonical transfer functions are obtained if direct couplings between each possible pair of ports are included, as shown in Fig. 1. Therefore, using the notation presented in Section II the network is completely defined by the following parameters:

- Frequency invariant susceptances of each resonator, M_{ii}, $i \in \{1, \ldots, n\}$.
- Coupling coefficients between each resonator and each port of the network M_{ij}, $i \in \{1, \ldots, n\}$, $j \in \{A, B, C\}$.
- Coupling coefficients between each pair of ports, M_{ij}, $i, j \in \{A, B, C\}$.

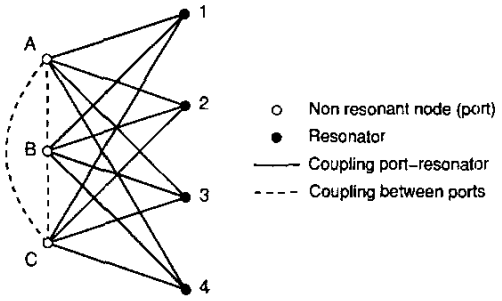

Fig. 1. Multiport canonical transversal network for $p = 3$ and $n = 4$.

A circuital analysis of the three-port transversal network gives rise to the following equation for its admittance matrix:

$$\boldsymbol{Y} = j \begin{bmatrix} 0 & M_{AB} & M_{AC} \\ M_{AB} & 0 & M_{BC} \\ M_{AC} & M_{BC} & 0 \end{bmatrix} + \sum_{k=1}^{n} \frac{1}{s + jM_{kk}} \begin{bmatrix} M_{Ak}^2 & M_{Ak}M_{Bk} & M_{Ak}M_{Ck} \\ M_{Ak}M_{Bk} & M_{Bk}^2 & M_{Bk}M_{Ck} \\ M_{Ak}M_{Ck} & M_{Bk}M_{Ck} & M_{Ck}^2 \end{bmatrix} \tag{7}$$

The elements of the coupling matrix are solved by equating (6) and (7) and identifying each matrix coefficient,

$$\begin{aligned} M_{kk} &= -\lambda_k \\ M_{AB} &= -jy_{12}^{(\infty)} \\ M_{AC} &= -jy_{13}^{(\infty)} \\ M_{BC} &= -jy_{23}^{(\infty)} \\ M_{Ak} &= \sqrt{r_{11k}} \\ M_{Bk} &= r_{21k}/\sqrt{r_{11k}} \\ M_{Ck} &= r_{31k}/\sqrt{r_{11k}} \end{aligned} \tag{8}$$

with $k \in \{1, \ldots, n\}$. The previous equations can be used to compute all the non-zero coefficients of the coupling matrix of the transversal network prototype from its admittance parameters. Therefore, they constitute the method to synthesize the coupling matrix from a specified response. It should be noted that the residues of only three admittance parameters (from a total of six) are required for the synthesis.

In general, the transversal structure is not the desired coupling topology for the network. In this case a sequence of similarity transformations is applied in order to generate the required structure [6].

IV. Numerical Example: Diplexer with Box-Section Filters

A diplexer response has been synthesized in order to illustrate the presented technique. The diplexer is formed by two fourth-order filters with box-section coupling topology [12]. One terminal of each filter is directly connected to the common port of the diplexer, as shown in Fig. 2. Therefore, the complete network is formed by $n = 8$ resonators, with $p = 3$ non-resonant nodes that constitute the common port and the port of each channel.

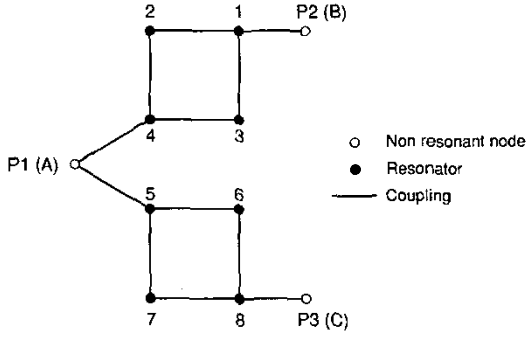

Fig. 2. Diagram of resonators and couplings of a diplexer formed of two box-section filters.

Fig. 3 shows the specified reflection parameter at the common port and the transmission parameter of each one of the diplexer channels. Each channel, symmetrically centered at ± 1.66 rad/s has a normalized bandwidth of 2 rad/s. Reflection losses better than -25 dB are specified at the pass-bands. The coupling topology of the filters allows the generation of one transmission zero for each filter response at specified frequencies. The locations of these transmission zeros are chosen so that an isolation better than 40 dB is obtained at the opposite channel passband. Additional, non-complete transmission zeros appear as a consequence of the interaction between the two channels, as can be seen in Fig. 3. The prescribed response corresponds to the admittance parameters whose coefficients are included in Table I.

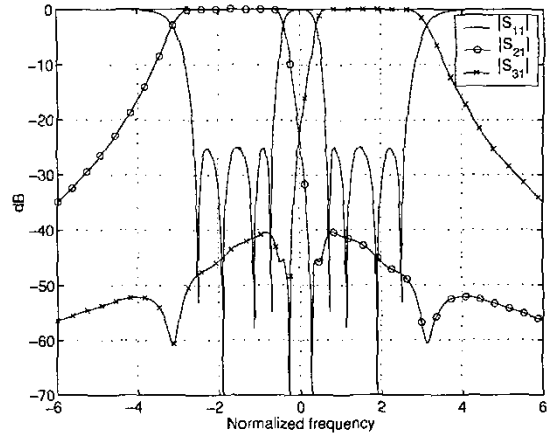

Fig. 3. Diplexer: return-loss at the common port (S_{11}) and atenuation of each channel (S_{21} and S_{31}).

TABLE I
Diplexer: Coefficients of the Admittance Parameters.

Order	Denominator	Numerators		
		$y_{11}(s)$	$y_{21}(s)$	$y_{31}(s)$
0	5.4425	0	$0.3232j$	$0.3232j$
1	0	$9.8721j$	$-2.6927j$	$2.6927j$
2	-52.1473	0	$7.5372j$	$7.5372j$
3	0	$-56.7869j$	$-8.2765j$	$8.2765j$
4	69.1126	0	$3.5421j$	$3.5421j$
5	0	$28.3158j$	$-0.5031j$	$0.5031j$
6	-16.5872	0		
7	0	$-2.5567j$		
8	1.0000			

The application of the synthesis method generates a transversal network with the topology shown in Fig. 4. The corresponding coupling matrix is structured as shown in Fig. 5(a). It should be noted that some of the residues of the admittance parameters are zero, and therefore as (8) indicates, not all the possible couplings are present in the network.

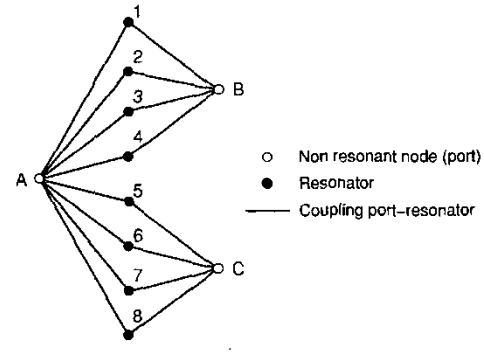

Fig. 4. Diagram of resonators and couplings of a diplexer with transversal topology.

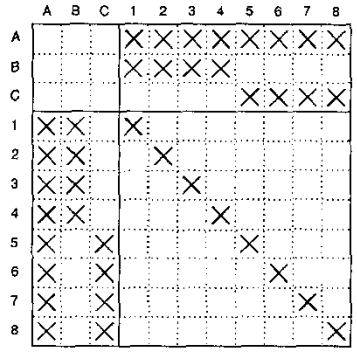

(a) Transversal network.

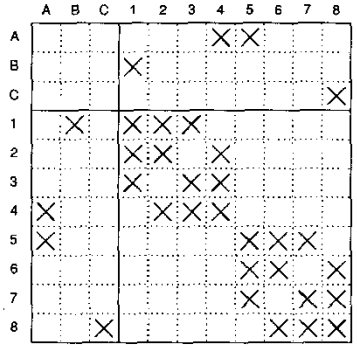

(b) Two box-section network.

Fig. 5. Diplexer: structure of the coupling matrix (crosses represent non-zero coupling coeffi cients.

Fig. 5(b) shows the structure of the coupling matrix required for the diplexer in Fig. 2. In order to transform the transversal coupling matrix into this one a sequence of similarity matrix transformations is required. Due to the reduced number of coupling coefficients between the resonators and the ports B and C, the two fourth-order subnetworks formed by resonators $1-4$ and $5-8$ can be independently modified. Two operations as described in [12] have been applied in order to obtain the box-sections. The resulting coupling coefficients are shown in Table II.

V. Conclusions

A novel method for the exact synthesis of multiport networks formed by coupled resonators have been presented. The technique is based on the generalization of the coupling matrix from two-port networks to an arbitrary number of ports. This matrix allows the formulation of a synthesis procedure similar to the one for filters. An example of application to the synthesis of a diplexer formed by two box-section fourth-order filters with one transmission zero each one has been also presented.

TABLE II

DIPLEXER: COEFFICIENTS OF THE COUPLING MATRIX.

Diagonal coeffi cients		
i	j	M_{ij}
1	1	1.6944
2	2	2.1848
3	3	0.7332
4	4	2.1523
5	5	-2.1523
6	6	-0.7332
7	7	-2.1848
8	8	-1.6944

Off-diagonal coeffi cients		
i	j	M_{ij}
A	4	1.1306
A	5	
B	1	
C	8	
1	2	-0.8368
7	8	
1	3	0.5538
6	8	
2	4	0.7974
5	7	
3	4	0.4938
5	6	

Acknowledgments

This work has been financed by the Projects TIC2002–02657 and TIC2002-04569–C02–C01 of the Spanish Ministry of Science and Technology.

References

[1] J. D. Rhodes and R. Levy, "A generalized multiplexer theory," *IEEE Trans. Microwave Theory Tech.*, vol. 27, no. 2, pp. 99–111, Feb. 1979.

[2] ——, "Design of general manifold multiplexers," *IEEE Trans. Microwave Theory Tech.*, vol. 27, no. 2, pp. 111–123, Feb. 1979.

[3] G. L. Matthaei, L. Young, and E. M. T. Jones, *Microwave Filters, Impedance-Matching Networks, and Coupling Structures.* Artech House, Feb. 1980.

[4] A. E. Atia, "Computer-aided design of waveguide multiplexers," *IEEE Trans. Microwave Theory Tech.*, vol. 22, no. 3, pp. 332–336, Mar. 1974.

[5] R. G. Egri, A. E. Williams, and A. E. Atia, "A contiguous-band multiplexer design," in *IEEE MTT-S Int. Microwave Symp. Digest*, vol. 83, May 1983, pp. 86–88.

[6] R. J. Cameron, "General coupling matrix synthesis methods for Chevyshev fi ltering functions," *IEEE Trans. Microwave Theory Tech.*, vol. 47, no. 4, pp. 433–442, Apr. 1999.

[7] J. R. Montejo-Garai, "Synthesis of N-even order symmetric fi lters with N transmission zeros by means of source-load cross coupling," *Electronic Letters*, vol. 36, no. 3, pp. 232–233, Feb. 2000.

[8] G. Tudoise, E. Ofi, and R. Vahldieck, "Hybrid EM-simulator based optimization of microwave and millimeter wave diplexers and multiplexers," in *2003 IEEE MTT-S Int. Microwave Symp. Digest*, vol. 2, Philadelphia, PA, June 2003, pp. 1219–1222.

[9] R. J. Cameron, "Advanced coupling matrix synthesis techniques for microwave fi lters," *IEEE Trans. Microwave Theory Tech.*, vol. 51, no. 1, pp. 1–10, Jan. 2003.

[10] D. M. Pozar, *Microwave engineering*, 2nd ed. John Wiley & sons, 1998.

[11] A. García Lampérez, T. K. Sarkar, and M. Salazar Palma, "Filter model generation from scattering parameters using the Cauchy method," in *32nd European Microwave Conference Proceedings*, vol. 1, Milan, Italy, Sept. 2002, pp. 413–416.

[12] R. J. Cameron, A. R. Harish, and C. J. Radcliffe, "Synthesis of advanced microwave fi lters without diagonal cross-couplings," *IEEE Trans. Microwave Theory Tech.*, vol. 50, no. 12, pp. 2862–2872, Dec. 2002.

A Theorem on Complex-Normalized Reflection Coefficient and Its Application

YI-SHENG ZHU AND WAI-KAI CHEN

Abstract—**Given an n-port lossless network terminated in n non-Foster positive-real impedances and its augmented n-port network terminated in n 1-Ω resistors, an expression is given relating the complex-normalized scattering matrix of the n-port network to that of its augmented n-port normalizing to the n 1-Ω resistances, from which the scattering matrix of a diplexer or a multiplexer is obtained.**

I. Introduction

Consider a lossless two-port network E terminated in two frequency-dependent non-Foster positive-real impedances $Z_G(s)$ and $Z_L(s)$, which according to the Darlington theory can be represented by the lossless two-port networks G and L terminated in the 1-Ω resistors, respectively, as shown in Fig. 1. In the paper, we study the relationships of the reflection coefficients of E normalized to $Z_G(s)$ and $Z_L(s)$ and the unit-normalized reflection coefficients of the composite two-port network composed of G, E, and L connected in cascade (GEL).

A theorem closely related to Carlin and Yarman's approach [1] to the design of a doubly matched equalizer is presented. Instead of using the complex-normalized scattering matrix, as suggested by Chien [2] or Chen and Satyanarayana [3], Carlin and Yarman employed the real normalized reflection coefficients to avoid the use of the complicated Wohler's conditions [4]. They first extract G from the front-end and then L from the back under certain constraints. The idea was later extended to the problem of reciprocal reactance $2n$-port cascade decomposition [5]. In these works, the expressions for the unit-normalized reflection coefficients of GEL in terms of those of E normalized to $Z_G(s)$ and $Z_L(s)$ are the corner stone of their technique [1].

In the paper, we show the limitation of their theory and give a complete solution to their problem. The present result is crucial to the understanding of Carlin and Yarman's CAD technique of double matching [1]. The theorem will also solve the problems of compatible impedances and multiport network synthesis and decomposition.

II. Limitations of the Carlin and Yarman Theory

Referring to Fig. 1, write

$$R_G(s) = \tfrac{1}{2}[Z_G(s) + Z_G(-s)] \tag{1}$$

$$R_L(s) = \tfrac{1}{2}[Z_L(s) + Z_L(-s)] \tag{2}$$

and define

$$b_G(s) = \prod_k \frac{\mu_{Gk} - s}{\mu_{Gk} + s} \tag{3}$$

$$b_L(s) = \prod_m \frac{\mu_{Lm} - s}{\mu_{Lm} + s} \tag{4}$$

where μ_{Gk} and μ_{Lm} are the right half of the s-plane (RHS) poles of $Z_G(-s)$ and $Z_L(-s)$, respectively, and

$$\eta_G(s) = \prod_u \frac{\lambda_{Gu} - s}{\lambda_{Gu} + s} \tag{5}$$

$$\eta_L(s) = \prod_v \frac{\lambda_{Lv} - s}{\lambda_{Lv} + s} \tag{6}$$

where λ_{Gu} and λ_{Lv} are the RHS transmission zeros of G and L, respectively, i.e., the RHS zeros of $R_G(s)$ and $R_L(s)$. With (3) and (4), the bounded-real regular Youla functions at ports 11′ and 22′ of E are found to be [6][1]

$$S_G(s) = b_G(s)\frac{Z_{EG}(s) - Z_G(-s)}{Z_{EG}(s) + Z_G(s)} \tag{7}$$

$$S_L(s) = b_L(s)\frac{Z_{EL}(s) - Z_L(-s)}{Z_{EL}(s) + Z_L(s)} \tag{8}$$

where $Z_{EG}(s)$ and $Z_{EL}(s)$ are the input impedances of the equalizer E looking into ports 11′ and 22′ with the other ports terminated in $Z_L(s)$ and $Z_G(s)$, respectively, as depicted in Fig. 1. Let

$$\boldsymbol{S}_a(s) = [S_{ija}(s)] \tag{9}$$

be the unit-normalized scattering matrix of the lossless two-port network composed of G, E, and L in cascade. Carlin and Yarman [1] showed that

$$S_{11a}(s) = \eta_G(s) S_G(s) \tag{10}$$

$$S_{22a}(s) = \eta_L(s) S_L(s). \tag{11}$$

As an example, consider the network of Fig. 2. The desired functions are found to be

$$Z_G(s) = \frac{s^4 + 178s^3 + 11s^2 + 25s + 1}{16s^4 + s^3 + 18s^2 + s + 1} \tag{12}$$

$$Z_L(s) = 1 \tag{13}$$

$$b_G = \frac{16s^4 - s^3 + 18s^2 - s + 1}{16s^4 + s^3 + 18s^2 + s + 1} \tag{14}$$

$$\eta_G(s) = \frac{(2s^2 - \sqrt{2}s + 1)^2}{(2s^2 + \sqrt{2}s + 1)^2} \tag{15}$$

$$S_G(s) = \frac{-3s^6 + 581s^5 + 157s^4 + 295s^3 + 26s^2 + 26s}{3s^6 + 583s^5 + 231s^4 + 319s^3 + 60s^2 + 30s + 2}. \tag{16}$$

Using Carlin and Yarman's results (10) and (11), we obtain

$$S_{11a}(s) = \frac{(2s^2 - \sqrt{2}s + 1)^2}{(2s^2 + \sqrt{2}s + 1)^2} \cdot \frac{-3s^6 + 581s^5 + 157s^4 + 295s^3 + 26s^2 + 26s}{3s^6 + 583s^5 + 231s^4 + 319s^3 + 60s^2 + 30s + 2}. \tag{17}$$

By definition [6], $S_{11a}(s)$ is also found to be

$$S_{11a}(s) = \frac{Z_{GEL}(s) - 1}{Z_{GEL}(s) + 1} \tag{18}$$

Manuscript received April 13, 1988; revised October 31, 1988. This paper was recommended by Associate Editor J. Mavor.

The authors are with the Department of Electrical Engineering and Computer Science, University of Illinois at Chicago, Chicago, IL 60680.

IEEE Log Number 8929298.

[1] Instead of (3) and (4), Youla defines: $b_G = \Pi_k(s - \mu_{Gk})/(s + \mu_{Gk})$ and $b_L(s) = \Pi_m(s - \mu_{Lm})/(s + \mu_{Lm})$.

0098-4094/89/0900-1238$01.00 ©1989 IEEE

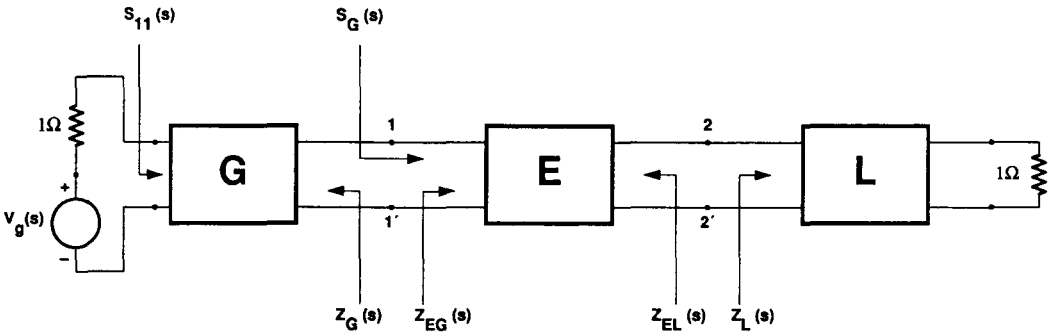

Fig. 1. A terminated lossless reciprocal two-port network.

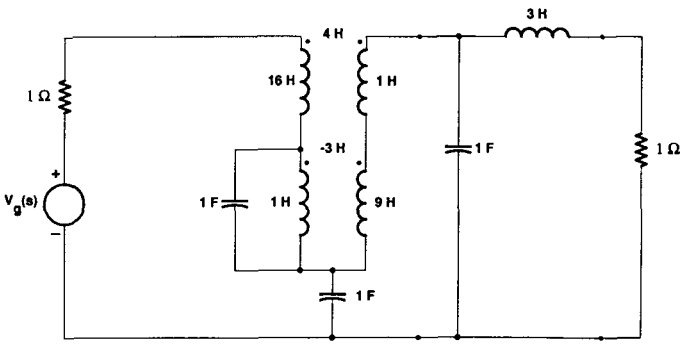

Fig. 2. A network used to illustrate the complex-normalized reflection coefficients.

where

$$W_k(s)W_{k*}(s) = \tfrac{1}{2}[p_k(s)q_{k*}(s) + p_{k*}(s)q_k(s)] \quad (23)$$

$$W_{k*}(s) = W_k(-s). \quad (24)$$

The zeros of the polynomial $W_k(s)$ are restricted to the left half of the s-plane (LHS), whereas the zeros on the imaginary axis are equally divided between $W_k(s)$ and $W_{k*}(s)$. Then we have

Theorem 1: Let $\boldsymbol{S}(s) = [S_{ij}(s)]$ be the scattering matrix of a lossless reciprocal n-port network N of Fig. 3 normalized to n non-Foster positive-real impedances $z_k(s)$, $(k = 1,2,\cdots,n)$. Then the unit-normalized scattering matrix $\boldsymbol{S}_a(s)$ of the augmented n-port network N_a of Fig. 3 is given by

$$\boldsymbol{S}_a(s) = \begin{bmatrix} \pm\frac{W_1}{W_{1*}}S_{11} & \left(\pm\frac{W_1}{W_{1*}}\right)^{1/2}\left(\pm\frac{W_2}{W_{2*}}\right)^{1/2}S_{12} & \cdots & \left(\pm\frac{W_1}{W_{1*}}\right)^{1/2}\left(\pm\frac{W_n}{W_{n*}}\right)^{1/2}S_{1n} \\ \left(\pm\frac{W_2}{W_{2*}}\right)^{1/2}\left(\pm\frac{W_1}{W_{1*}}\right)^{1/2}S_{21} & \pm\frac{W_2}{W_{2*}}S_{22} & \cdots & \left(\pm\frac{W_2}{W_{2*}}\right)^{1/2}\left(\pm\frac{W_n}{W_{n*}}\right)^{1/2}S_{2n} \\ \vdots & \vdots & \vdots & \vdots \\ \left(\pm\frac{W_n}{W_{n*}}\right)^{1/2}\left(\pm\frac{W_1}{W_{1*}}\right)^{1/2}S_{n1} & \left(\pm\frac{W_n}{W_{n*}}\right)^{1/2}\left(\pm\frac{W_2}{W_{2*}}\right)^{1/2}S_{n2} & \cdots & \pm\frac{W_n}{W_{n*}}S_{nn} \end{bmatrix} \quad (25)$$

where $Z_{GEL}(s)$ is the input impedance of the network composed of G, E, and L in cascade, and is given by

$$Z_{GEL}(s) = \frac{582s^5 + 194s^4 + 307s^3 + 43s^2 + 28s + 1}{3s^6 + s^5 + 37s^4 + 12s^3 + 17s^2 + 2s + 1}. \quad (19)$$

Substituting (19) in (18) yields

$$S_{11a}(s) = \frac{-3s^6 + 581s^5 + 157s^4 + 295s^3 + 26s^2 + 26s}{3s^6 + 583s^5 + 231s^4 + 319s^3 + 60s^2 + 30s + 2}. \quad (20)$$

Comparing (17) and (20) shows that Carlin and Yarman's relations (10) and (11) are not really correct. In this regard, a more general relation will be presented below.

III. Theory

Given a lossless reciprocal n-port network N terminated in n non-Foster positive-real impedances $z_k(s)$, $k = 1,2,\cdots,n$, as shown in Fig. 3. Write

$$z_k(s) = \frac{p_k(s)}{q_k(s)}, \qquad k = 1,2,\cdots,n \quad (21)$$

$$r_k(s) = \frac{W_k(s)W_{k*}(s)}{q_k(s)q_{k*}(s)} \quad (22)$$

where $(\pm W_k/W_{k*})$ is a complete square. When all the zeros of W_kW_{k*} are on the $j\omega$-axis, $(\pm W_k/W_{k*})^{1/2} = \pm 1$. When the minus sign inside the parentheses is used, a minus is assigned to $S_{kk}(s)$.

Proof: Consider the kth lossless reciprocal two-port N_k of Fig. 4. Let the input impedance of N_k be $z_k(s)$, when the output is terminated in the 1-Ω resistor. Let $A_k(s)/\xi_k(s)$, $B_k(s)/\xi_k(s)$, $C_k(s)/\xi_k(s)$ and $D_k(s)/\xi_k(s)$ be the transmission parameters of N_k defined by

$$\begin{bmatrix} V_{k1}(s) \\ I_{k1}(s) \end{bmatrix} = \frac{1}{\xi_k(s)}\begin{bmatrix} A_k(s) & B_k(s) \\ C_k(s) & D_k(s) \end{bmatrix}\begin{bmatrix} V_{k2}(s) \\ -I_{k2}(s) \end{bmatrix}. \quad (26)$$

For a lossless two-port N_k, $A_k(s)$, and $D_k(s)$ are even polynomials, $B_k(s)$ and $C_k(s)$ are odd, or vice versa. Then

$$z_k(s) = \frac{A_k(s) + B_k(s)}{C_k(s) + D_k(s)}. \quad (27)$$

If, in addition, N_k is reciprocal, $A_k(s)D_k(s) - B_k(s)C_k(s)$ is a

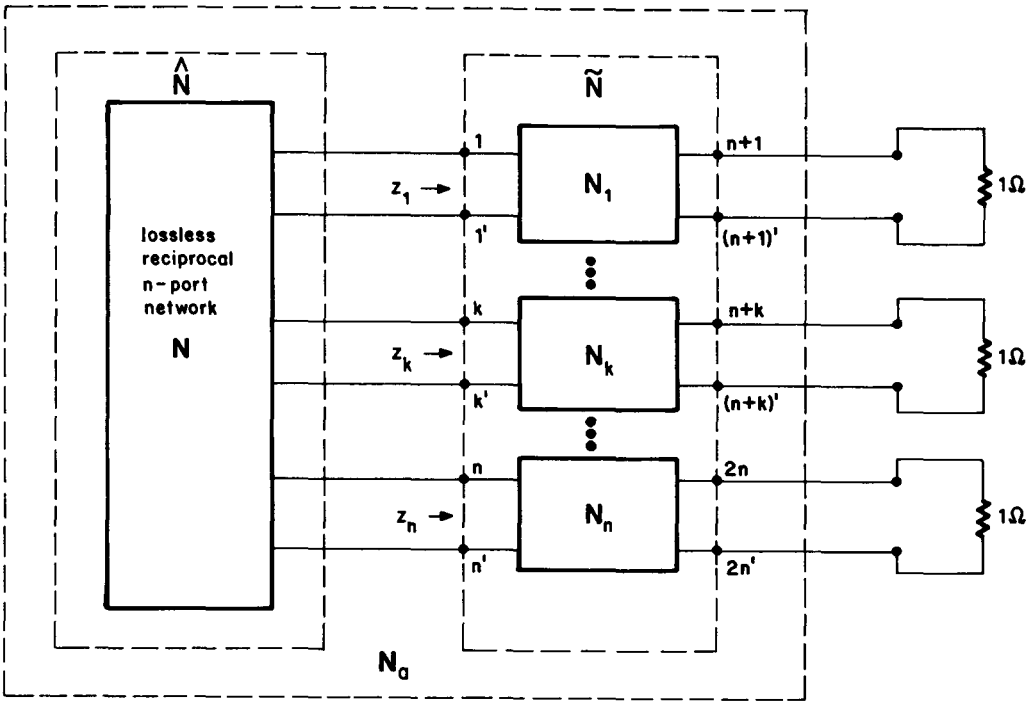

Fig. 3. An n-port terminated in n non-Foster positive-real impedances.

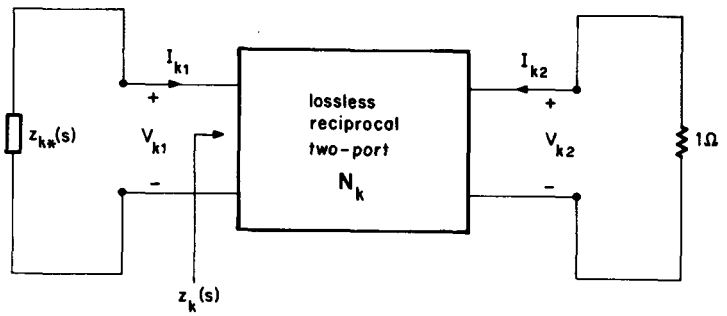

Fig. 4. A lossless reciprocal two-port network terminated in z_{k*} and 1 Ω.

complete square and equals to [7]

$$\begin{aligned} &A_k(s)D_k(s) - B_k(s)C_k(s) \\ &\quad = \xi_k^2(s) \\ &\quad = s^{2m}\prod_n (s^2+\omega_n^2)^2 \prod_i (s^2-a_i^2)^2 \\ &\qquad \cdot \prod_j \left\{ \left[(s+b_j)^2 + c_j^2 \right]^2 \left[(s-b_j)^2 + c_j^2 \right]^2 \right\} \end{aligned} \tag{28}$$

where ω_n, a_i, b_j, and c_j are all real and positive; m, n, i, and j are nonnegative integers. Comparing (21) with (27) and substituting the resulting function in (23) give

$$W_k(s)W_{k*}(s) = \pm \xi_k^2(s) \tag{29}$$

$$W_k(s) = s^m \prod_n (s^2+\omega_n^2) \prod_i (s+a_i)^2 \prod_j \left[(s+b_j)^2 + c_j^2 \right]^2 \tag{30}$$

$$\begin{aligned} W_{k*}(s) &= (-1)^m s^m \prod_n (s^2+\omega_n^2) \prod_i (s-a_i)^2 \\ &\quad \cdot \prod_j \left[(s-b_j)^2 + c_j^2 \right]^2. \end{aligned} \tag{31}$$

In (29) we choose the plus sign if $A_k(s)$ and $D_k(s)$ are even, and the minus sign if they are odd. By (26), the scattering matrix $\tilde{S}_k(s)$ of N_k normalizing to $z_{k*}(s)$ and the 1-Ω resistance is found to be

$$\tilde{S}_k(s) = \begin{bmatrix} 0 & \left(\pm \dfrac{W_k(s)}{W_{k*}(s)} \right)^{1/2} \\ \left(\pm \dfrac{W_k(s)}{W_{k*}(s)} \right)^{1/2} & 0 \end{bmatrix}. \tag{32}$$

Substituting (30) and (31) in (32) yields

$$\left(\pm \frac{W_k(s)}{W_{k*}(s)} \right)^{1/2} = \pm \frac{\prod_i (s+a_i) \prod_j \left[(s+b_j)^2 + c_j^2 \right]}{\prod_i (s-a_i) \prod_j \left[(s-b_j)^2 + c_j^2 \right]}. \tag{33}$$

We remark that (33) is not a real regular all-pass function since $z_{k*}(s)$ is not positive-real. When $a_i = b_j = c_j = 0$, all zeros of (28) lie on the $j\omega$-axis, and $(\pm W_k/W_{k*})^{1/2} = \pm 1$.

The overall matrix composed of these n matrices (32) constitutes the $2n \times 2n$ scattering matrix of the $2n$-port network $\tilde{N}$ of Fig. 3 normalizing to $z_{1*}(s), z_{2*}(s), \cdots, z_{n*}(s)$ and the n 1-Ω

resistances:

$$\tilde{S}(s)=\left[\begin{array}{cccc|cccc} 0 & 0 & \cdots & 0 & \left(\pm\frac{W_1}{W_{1*}}\right)^{1/2} & 0 & \cdots & 0 \\ 0 & 0 & \cdots & 0 & 0 & \left(\pm\frac{W_2}{W_{2*}}\right)^{1/2} & \cdots & 0 \\ \vdots & \vdots & \cdots & \vdots & \vdots & \vdots & \cdots & \vdots \\ 0 & 0 & \cdots & 0 & 0 & 0 & \cdots & \left(\pm\frac{W_n}{W_{n*}}\right)^{1/2} \\ \hline \left(\pm\frac{W_1}{W_{1*}}\right)^{1/2} & 0 & \cdots & 0 & 0 & 0 & \cdots & 0 \\ 0 & \left(\pm\frac{W_2}{W_{2*}}\right)^{1/2} & \cdots & 0 & 0 & 0 & \cdots & 0 \\ \vdots & \vdots & \cdots & \vdots & \vdots & \vdots & \cdots & \vdots \\ 0 & 0 & \cdots & \left(\pm\frac{W_n}{W_{n*}}\right)^{1/2} & 0 & 0 & \cdots & 0 \end{array}\right] \tag{34}$$

Write explicitly the scattering matrix of the n-port N of Fig. 3 normalized to $z_1(s), z_2(s), \cdots, z_n(s)$ as

$$S(s)=\left[S_{ij}(s)\right]_{n\times n}. \tag{35}$$

If the n-port N is viewed as a $2n$-port $\hat{N}$ with n of these $2n$ ports being open-circuited, its $2n\times 2n$ scattering matrix can be partitioned as

$$\hat{S}(s)=\left[\begin{array}{c|c} \hat{S}_{11}(s) & \hat{S}_{12}(s) \\ \hline \hat{S}_{21}(s) & \hat{S}_{22}(s) \end{array}\right]=\begin{array}{c} \\ n \\ n \end{array}\overset{\begin{array}{cc} n & n \end{array}}{\left[\begin{array}{c|c} \mathbf{0} & \mathbf{0} \\ \hline \mathbf{0} & S(s) \end{array}\right]}. \tag{36}$$

The augmented n-port network N_a of Fig. 3 is composed of a $2n$-port network $\tilde{N}$ in cascade with a $2n$-port network $\hat{N}$. According to Chen [8], we can express the submatrices $\hat{S}_{ija}(s)$ of the scattering matrix $\hat{S}_a(s)$ of the extended $2n$-port of N_a in terms of those $\hat{S}_{ij}(s)$ and $\hat{S}_{ij}(s)$, $(i, j=1,2)$, of $\tilde{S}(s)$ and $\hat{S}(s)$, as follows:

$$\hat{S}_{11a}(s)=\hat{S}_{11}(s)+\hat{S}_{12}(s)\left[U_n-\tilde{S}_{11}(s)\hat{S}_{22}(s)\right]^{-1}\cdot\tilde{S}_{11}(s)\hat{S}_{21}(s) \tag{37a}$$

$$\hat{S}_{12a}(s)=\hat{S}_{12}(s)\left[U_n-\tilde{S}_{11}(s)\hat{S}_{22}(s)\right]^{-1}\tilde{S}_{12}(s) \tag{37b}$$

$$\hat{S}_{21a}(s)=\tilde{S}_{21}(s)\left[U_n-\hat{S}_{22}(s)\tilde{S}_{11}(s)\right]^{-1}\hat{S}_{21}(s). \tag{37c}$$

$$S_{22a}(s)=\tilde{S}_{22}(s)+\tilde{S}_{21}(s)\left[U_n-\hat{S}_{22}(s)\tilde{S}_{11}(s)\right]^{-1}\cdot\hat{S}_{22}(s)\tilde{S}_{12}(s). \tag{37d}$$

Substituting (34) and (36) in (37) yields the $n\times n$ scattering matrix (25). Q.E.D.

Now we apply Theorem 1 to the network of Fig. 1. Let

$$T_x(s)=\frac{1}{\xi_x(s)}\begin{bmatrix} A_x(s) & B_x(s) \\ C_x(s) & D_x(s) \end{bmatrix},\qquad x=G,\ E, \text{ or } L \tag{38}$$

be the transmission matrices of the lossless reciprocal two-port networks G, E, and L, respectively. From Fig. 1, we have

$$Z_G(s)=\frac{D_G(s)+B_G(s)}{A_G(s)+C_G(s)} \tag{39}$$

$$Z_L(s)=\frac{A_L(s)+B_L(s)}{C_L(s)+D_L(s)}. \tag{40}$$

The transmission matrix of the composite network GEL becomes

$$T(s)=T_G(s)T_E(s)T_L(s)=\frac{1}{\xi(s)}\begin{bmatrix} A(s) & B(s) \\ C(s) & D(s) \end{bmatrix}. \tag{41}$$

By definition [6], [9], the reflection coefficients at ports $11'$ and $22'$ of E in Fig. 1 normalized to $Z_G(s)$ and $Z_L(s)$ are given by

$$S_{11}(s)=\frac{H_G(s)}{H_G(-s)}\cdot\frac{Z_{EG}(s)-Z_G(-s)}{Z_{EG}(s)+Z_G(s)} \tag{42}$$

$$S_{22}(s)=\frac{H_L(s)}{H_L(-s)}\cdot\frac{Z_{EL}(s)-Z_L(-s)}{Z_{EL}(s)+Z_L(s)} \tag{43}$$

respectively, where

$$\frac{H_G(s)}{H_G(-s)}=\pm\frac{W_G(-s)}{W_G(s)}\cdot\frac{A_G(s)-C_G(s)}{A_G(s)+C_G(s)} \tag{44}$$

$$\frac{H_L(s)}{H_L(-s)}=\pm\frac{W_L(-s)}{W_L(s)}\cdot\frac{-C_L(s)+D_L(s)}{C_L(s)+D_L(s)}. \tag{45}$$

We choose the plus sign when $A_x(s)$ and $D_x(s)$ are even, and the minus sign if they are odd; and $W_x(s)$ is defined the same as in (23) with $x=G$ or L.

Substituting (39), (40) and (41) in (42) and (43) in conjunction with (44) and (45) gives

$$S_{11}(s)=\pm\frac{W_G(-s)}{W_G(s)}\cdot\frac{A(s)+B(s)-C(s)-D(s)}{A(s)+B(s)+C(s)+D(s)} \tag{46}$$

$$S_{22}(s)=\pm\frac{W_L(-s)}{W_L(s)}\cdot\frac{D(s)+B(s)-A(s)-C(s)}{A(s)+B(s)+C(s)+D(s)}. \tag{47}$$

Appealing to the para-unitary property of the scattering matrix

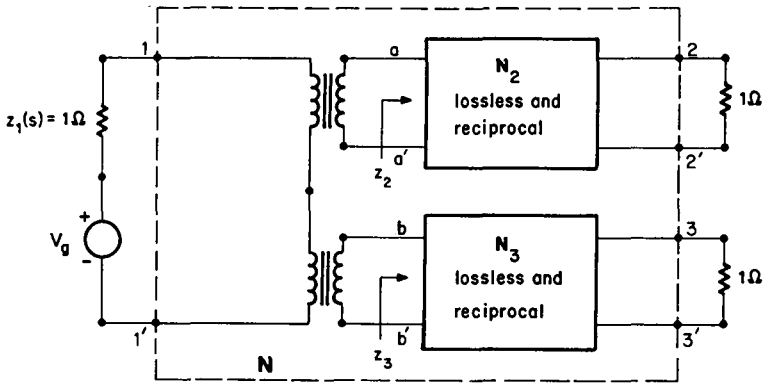

Fig. 5. The ideal transformer and two lossless reciprocal two-port networks N_2 and N_3 constitute the diplexer.

of a lossless two-port network, we obtain

$$S_{12}(s) = S_{21}(s) = \left[\pm \frac{W_G(-s)}{W_G(s)}\right]^{1/2} \cdot \left[\pm \frac{W_L(-s)}{W_L(s)}\right]^{1/2} \cdot \frac{2[A(s)D(s) - B(s)C(s)]^{1/2}}{A(s)+B(s)+C(s)+D(s)}. \quad (48)$$

From Theorem 1, the unit-normalized scattering parameters of *GEL* are found to be

$$S_{11a}(s) = \frac{A(s)+B(s)-C(s)-D(s)}{A(s)+B(s)+C(s)+D(s)} \quad (49)$$

$$S_{22a}(s) = \frac{D(s)+B(s)-A(s)-C(s)}{A(s)+B(s)+C(s)+D(s)} \quad (50)$$

$$S_{12a}(s) = S_{21a}(s) = \frac{2[A(s)D(s) - B(s)C(s)]^{1/2}}{A(s)+B(s)+C(s)+D(s)}. \quad (51)$$

They possess the following attributes.

1) Substituting (38) in (41) in conjunction with (28)–(31) yields

$$[A(s)D(s) - B(s)C(s)]^{1/2} = \prod_{x=G,E,L} [A_x(s)D_x(s) - B_x(s)C_x(s)] = \prod_{x=G,E,L} [\pm W_x(s)W_x(-s)]^{1/2}. \quad (52)$$

The rules for the composition of the transmission zeros can be found in [1, lemma 1].

2) Let

$$U(s) = A(s) + B(s) - C(s) - D(s) \quad (53)$$

$$\pm U(-s) = D(s) + B(s) - A(s) - C(s). \quad (54)$$

If $U(s)$ has a factor $s + a$, $\mathrm{Re}\, a \geq 0$, then $\pm U(-s)$ will have the factor $\pm(-s + a)$. As a result, the common factor $(s + a)^{2m}$ of the numerator and denominator polynomials of $S_{11a}(s)$ will yield a real regular all-pass function $[(-s + a)/(s + a)]^{2m}$ in $S_{22a}(s)$, $\pm[(-s + a)/(s + a)]^m$ in $S_{21a}(s)$; or vice versa.

3) The numerator polynomial of $S_{21a}(s)$ is either even or odd. Choosing only those zeros in the LHS, as in Carlin and Yarman [1, eq. (A-5)], may lead to an erroneous result.

IV. Application

A diplexer or, in general, a multiplexer, may be formed by connecting filters either in series or in parallel. When these filters are complemented to approximate the desired responses, an expression for the scattering matrix of the above-mentioned multi-port network is often required. With Theorem 1, this scattering matrix can easily be expressed in terms of the filter input impedances. For example, consider the diplexer given in Fig. 5, which is composed of a three-port ideal transformer and two lossless reciprocal two-port networks N_2 and N_3 terminated in the 1-Ω resistors. Let $z_1(s)$ be the source impedance, and $z_2(s)$ and $z_3(s)$ be the input impedances of N_2 and N_3, when the output port is terminated in the 1-Ω resistors, respectively. We first write the scattering matrix of the three-port ideal transformer normalized to $z_1(s)$, $z_2(s)$ and $z_3(s)$ at ports 11′, *aa′* and *bb′*, as shown in Fig. 5, and then use Theorem 1 to obtain the unit-normalized scattering matrix of the diplexer at ports 11′, 22′ and 33′. From definition [8], the scattering matrix of the three-port ideal transformer normalized to $z_1(s)$, $z_2(s)$ and $z_3(s)$ is found to be

$$S(s) = \begin{bmatrix} \frac{h_1}{h_{1*}} \cdot \frac{z_2+z_3-z_{1*}}{z_1+z_2+z_3} & \frac{2h_1h_2}{z_1+z_2+z_3} & \frac{2h_1h_3}{z_1+z_2+z_3} \\ \frac{2h_1h_2}{z_1+z_2+z_3} & \frac{h_2}{h_{2*}} \cdot \frac{z_1+z_3-z_{2*}}{z_1+z_2+z_3} & \frac{-2h_2h_3}{z_1+z_2+z_3} \\ \frac{2h_1h_3}{z_1+z_2+z_3} & \frac{-2h_2h_3}{z_1+z_2+z_3} & \frac{h_3}{h_{3*}} \cdot \frac{z_1+z_2-z_{3*}}{z_1+z_2+z_3} \end{bmatrix} \quad (55)$$

where

$$h_i(s) = \frac{W_{i*}(s)}{q_i(s)}, \qquad i = 1,2,3 \tag{56}$$

and $W_i(s)$ is given in (23) and $q_i(s)$ in (21). Assume that $z_1(s) = 1$ and write the impedances $z_2(s)$ and $z_3(s)$ explicitly as

$$z_2(s) = \frac{p_2(s)}{q_2(s)} \tag{57a}$$

$$z_3(s) = \frac{p_3(s)}{q_3(s)}. \tag{57b}$$

Substituting (56) and (57) with $z_1(s) = 1$ in (55) gives

$$\boldsymbol{S}(s) = \frac{1}{p_2q_3 + p_3q_2 + q_2q_3} \begin{bmatrix} p_2q_3 + p_3q_2 - q_2q_3 & \frac{W_{2*}}{W_2} \cdot 2W_2q_3 & \frac{W_{3*}}{W_3} \cdot 2W_3q_2 \\ \frac{W_{2*}}{W_2} \cdot 2W_2q_3 & \frac{W_{2*}}{W_2} \cdot (p_3q_{2*} + q_3q_{2*} - q_3p_{2*}) & \frac{W_{2*}W_{3*}}{W_2W_3} \cdot (-2W_2W_3) \\ \frac{W_{3*}}{W_3} \cdot 2W_3q_2 & \frac{W_{2*}W_{3*}}{W_2W_3} \cdot (-2W_2W_3) & \frac{W_{3*}}{W_3} \cdot (p_2q_{3*} - q_2p_{3*} + q_2q_{3*}) \end{bmatrix} \tag{58}$$

Applying Theorem 1, the unit-normalized scattering matrix of the diplexer N at ports 11′, 22′ and 33′ is found to be

$$\boldsymbol{S}_a(s) = \frac{1}{p_2q_3 + p_3q_2 + q_2q_3} \begin{bmatrix} p_2q_3 + p_3q_2 - q_2q_3 & \left(\pm \frac{W_{2*}}{W_2}\right)^{1/2} 2W_2q_3 & \left(\pm \frac{W_{3*}}{W_3}\right)^{1/2} 2W_3q_2 \\ \left(\pm \frac{W_{2*}}{W_2}\right)^{1/2} 2W_2q_3 & \pm(p_3q_{2*} + q_3q_{2*} - q_3p_{2*}) & \left(\pm \frac{W_{2*}W_{3*}}{W_2W_3}\right)^{1/2} (-2W_2W_3) \\ \left(\pm \frac{W_{3*}}{W_3}\right)^{1/2} 2W_3q_2 & \left(\pm \frac{W_{2*}W_{3*}}{W_2W_3}\right)^{1/2} (-2W_2W_3) & \pm(p_2q_{3*} - q_2p_{3*} + q_2q_{3*}) \end{bmatrix} \tag{59}$$

or

$$\boldsymbol{S}_a(s) = \frac{1}{p_2q_3 + p_3q_2 + q_2q_3} \begin{bmatrix} p_2q_3 + p_3q_2 - q_2q_3 & 2(\pm W_2W_{2*})^{1/2} q_3 & 2(\pm W_3W_{3*})^{1/2} q_2 \\ 2(\pm W_2W_{2*})^{1/2} q_3 & \pm(p_3q_{2*} + q_3q_{2*} - q_3p_{2*}) & -2(\pm W_2W_{2*})^{1/2} (\pm W_3W_{3*})^{1/2} \\ 2(\pm W_3W_{3*})^{1/2} q_2 & -2(\pm W_2W_{2*})^{1/2} (\pm W_3W_{3*})^{1/2} & \pm(p_2q_{3*} - q_2p_{3*} + q_2q_{3*}) \end{bmatrix}. \tag{60}$$

From (59) and (60), we arrive at the following conclusions.

1) Since $p_i(s)/q_i(s)$ is non-Foster and positive-real, the polynomial $p_2q_3 + p_3q_2 + q_2q_3$ is strictly Hurwitz; and since N_2 and N_3 of Fig. 5 are reciprocal, $(\pm W_{i*}/W_i)$ or $(\pm W_iW_{i*})$ is a complete square. $\boldsymbol{S}_a(s)$ is rational and bounded-real and possesses the para-unitary property for a linear, lumped, lossless and reciprocal diplexer.

2) At a frequency ω_i, if

$$p_2(j\omega_i)\,q_3(j\omega_i) + p_3(j\omega_i)\,q_2(j\omega_i) - q_2(j\omega_i)\,q_3(j\omega_i) = 0 \tag{61}$$

$$z_2(j\omega_i) + z_3(j\omega_i) = 1 \tag{62}$$

we obtain a perfect match at port 11′ at ω_i. Likewise, we have

$$1 + z_3(j\omega_j) = z_2(-j\omega_j) \tag{63}$$

for port 22′ at the frequency ω_j and

$$1 + z_2(j\omega_k) = z_3(-j\omega_k) \tag{64}$$

for port 33′ at the frequency ω_k.

3) The zeros of $\mathrm{Ev}\,z_2(s) = \pm W_2W_{2*}$ on the $j\omega$-axis and in the RHS are also the zeros of transmission of $S_{12a}(s)$ and $S_{23a}(s)$, respectively. The zeros of $\mathrm{Ev}\,z_3(s) = \pm W_3W_{3*}$ on the $j\omega$-axis and in the RHS are the zeros of transmission of $S_{13a}(s)$ and $S_{23a}(s)$, respectively.

4) In (59), when all the zeros of W_iW_{i*} are on the $j\omega$-axis, $(\pm W_{i*}/W_i)^{1/2} = \pm 1$. When the minus sign inside the parentheses is used, a minus is assigned to $S_{iia}(s)$.

As a special case, assume that $z_2(s)$ possesses a low-pass all-pole transmission characteristic, and $z_3(s)$ a high-pass all-pole one. Then

$$W_2(s) = 1 \tag{65}$$

$$W_3(s) = s^m. \tag{66}$$

Substituting (65) and (66) in (64) yields

$$S_a(s) = \frac{1}{p_2q_3 + p_3q_2 + q_2q_3} \times \begin{bmatrix} p_2q_3 + p_3q_2 - q_2q_3 & 2q_3 & 2s^m q_2 \\ 2q_3 & p_3q_{2*} + q_3q_{2*} - q_3p_{2*} & -2s^m \\ 2s^m q_2 & -2s^m & (-1)^m(p_2q_{3*} - q_2p_{3*} + q_2q_{3*}) \end{bmatrix} \tag{67}$$

V. Conclusions

In this paper, we studied the scattering matrix of a lossless reciprocal n-port network terminated in n non-Foster positive-real impedances and its augmented n-port network. A theorem relating the complex-normalized scattering matrix of the n-port network to that of its augmented n-port normalizing to the n 1-Ω resistors was given, from which the scattering matrix of a diplexer or a multiplexer was obtained.

References

[1] H. J. Carlin and B. S. Yarman, "The double matching problem: analytic and real frequency solutions," *IEEE Trans. Circuits Syst.*, vol. CAS-30, pp. 15–28, Jan. 1983.

[2] T. M. Chien, "A theory of broadband matching of a frequency-dependent generator and load," *J. Franklin Inst.*, vol. 298, pp. 181–221, Sept. 1974.

[3] C. Satyanarayana and W. K. Chen, "Theory of broadband matching and the problem of compatible impedances," *J. Franklin Inst.*, vol. 309, pp. 267–280, April 1980.

[4] N. R. Wohlers, "Complex normalization of scattering matrices and the problem of compatible impedances," *IEEE Trans. Circuit Theory*, vol. CT-12, pp. 528–535, Dec. 1965.

[5] D. C. Youla, H. J. Carlin, and B. S. Yarman, "Double broadband matching and the problem of reciprocal reactance $2n$-port cascade decomposition," *Int. J. Circuit Theory Appl.*, vol. 12, pp. 269–281, July 1984.

[6] D. C. Youla, "A new theory of broad-band matching," *IEEE Trans. Circuit Theory*, vol. CT-11, pp. 30–50, Mar. 1964.

[7] Y. S. Zhu and W. K. Chen, "Realizability of lossless reciprocal and nonreciprocal broadband matching networks," *J. Franklin Inst.*, vol. 319, pp. 325–340, Mar. 1985.

[8] W. K. Chen, *Theory and Design of Broadband Matching Networks*. New York: Pergamon, 1976.

[9] ___, *Broadband Matching: Theory and Implementations*. Singapore: World Scientific, 1988

Ridge Waveguide Coupled Stripline Resonator Filters and Multiplexers

Yunchi Zhang, Jorge A. Ruiz-Cruz, and Kawthar A. Zaki

Department of Electrical and Computer Engineering, University of Maryland, College Park, MD 20742, USA (ychzhang@umd.edu)

Abstract **— Stripline resonator bandpass filters with evanescent-mode coupling sections by ridge waveguides are introduced in this paper. Such filters have very compact cross sections, which makes them suitable choices for some integrated systems having cross section constraints. Low Temperature Co-fired Ceramic (LTCC) technology can be employed to build such filters for PCB systems. It is also possible to manufacture them in air-filled metallic structures. Two filter design examples by Mode Matching Method (MMM) are given in this paper. Stepped impedance line resonators are used in one example to improve the spurious. The presented filters can also be applied for multiplexer applications using stripline junctions. One diplexer design example for LTCC application is presented to show the feasibility.**

Index Terms **— Bandpass filter, multiplexer, diplexer, stripline, Ridge Waveguide, LTCC.**

I. Introduction

Modern communication systems have created the need of small size, light weight, high performance, and easy-to-be integrated RF/microwave filters and multiplexers. In integrated PCB circuits, waveguide filters using LTCC technology are recently employed because they usually offer higher quality factors than other planar circuit structures. Typically LTCC technology is suitable for multiple layer structure and other RF/microwave products where high integration level is needed. A LTCC ridge waveguide filter design is presented in [1]. The drawback of such filter is the relative large cross section of the ridge waveguide. Many ceramic layers are usually needed to implement the waveguide, which will lower the filter performance because the variation of the material permittivity parameter is increased with the number of ceramic layers. Therefore, new filter structures with more compact cross sections and high quality need to be found for integrated circuit systems.

On the other hand, in metallic structures, available filters consist of combline filters, interdigital filters, rectangular waveguide filters, ridge waveguide evanescent-mode filters, etc [2]-[4]. Combline and interdigital filters have relative small lengths and usually large cross sections since the resonator length is about quarter wavelength. Rectangular and ridge waveguide filters usually have smaller cross sections than combline and interdigital ones. But their cross sections are constrained by the cutoff frequency of the fundamental mode. In practice, a system may have strict limitations on the size of cross section which can not be satisfied by all these existing kinds of filters. Therefore, new filter structures with smaller cross sections are also required for metallic structures.

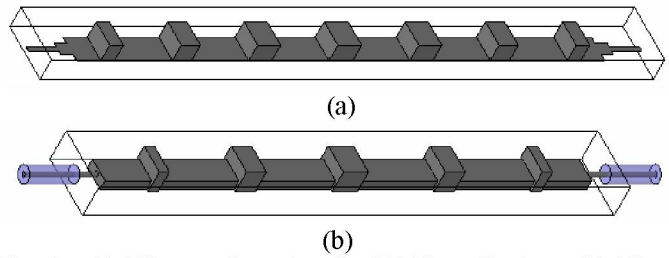

Fig. 1. (a) Filter configuration for LTCC applications; (b) Filter configuration in metallic structures.

In this paper, a new filter configuration using ridge waveguide coupled stripline resonators is presented. The cross section of this filter configuration is much smaller than all the aforementioned filter structures, which makes it a very good choice for LTCC applications since only a few ceramic layers are usually required. This kind of filter in metallic structures is also feasible, which will be a possible solution for some size-demanding applications. Such filters can also be applied for multiplexer designs using stripline junctions. Two filter examples and one diplexer example are given in this paper to show the feasibility. All the examples are designed with MMM and verified by HFSS.

II. Filter Configuration and Modeling

A. Filter Configuration

The filter configuration is shown in Fig. 1 for both LTCC technology and metallic form. Basically stripline resonators are coupled by ridge waveguide evanescent-mode sections to fulfill the filter. The size of filter cross section is not limited by the cutoff frequency of stripline since the TEM mode of stripline is the propagating mode. Actually the cross section is mainly constrained by the ridge waveguide coupling sections. Usually the bigger the cross section, the stronger the coupling. Therefore, for a broader bandwidth filter, a relative bigger cross section will be needed since strong couplings are required. However, the cross section is always smaller than ridge waveguide evanescent-mode filters because all the

0-7803-9542-5/06/$20.00

modes of the ridge waveguides in this presented filter configuration are evanescent modes. Typically the cross section is about half size of the ridge waveguide evanescent-mode filter for a 20% bandwidth filter. If filter bandwidth is smaller, the size of cross section can be reduced more. Usually up to 40% bandwidth filter can be realized by such configuration.

Fig. 2 is a draft showing how to build the filter configuration in LTCC technology. The horizontal walls of ridge waveguides are constructed by printing parallel planar conductors, while the vertical walls are realized by closely spaced metal filled vias. The stripline is implemented by one metallization layer. Thus, the filter can be embedded into multilayer ceramics and integrated with other PCB circuits.

B. Filter design and modeling

To design a filter with the presented configuration, dimensions of the cross sections of stripline and ridge waveguide should be determined first according to the filter specifications, such as center frequency f_0 and bandwidth. Typically the cutoff frequency of the fundamental mode of ridge waveguide can be chosen around $2f_0$ for 15% - 20% bandwidth filters, which will generate enough couplings between stripline resonators.

The filter design consists of two steps after the cross sections are determined. The first step is to obtain the initial dimensions of the filter based on the impedance inverter method [2], [5]. Physical realizations of the input/output couplings are shown in Fig. 3(a) and 3(b) for LTCC technology and metallic structure. Stripline tapped-in excitation is used for LTCC application and coaxial cable probe excitation is used in metallic form. In these two models, the loading effect from the first resonator is taken into account. The actual external coupling is obtained as in [6]

$$R = -\frac{4}{f_l \left.\frac{d\phi}{df}\right|_{\min}} \qquad (1)$$

where ϕ is the phase angle of the reflection coefficient at the reference plane of the first discontinuity and f_l is the loaded resonant frequency that corresponds to the minimum phase angle variation. The analysis of both cases is made by MMM (Stepped structures are used to approximate the coaxial cable and probe). The inter-coupling sections are shown in Fig. 3(c). The generalized S parameters between the two discontinuities of stripline to ridge waveguide can be calculated by MMM [6]. The impedance inverter is related to the S-parameter as in [5]

$$K = \sqrt{\frac{1-|S_{11}|}{1+|S_{11}|}} \qquad (2)$$

The length of the ridge waveguide can be swept to find the dimensions for the required impedance inverter values. Phase

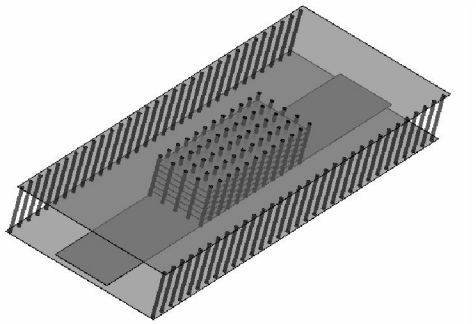

Fig. 2. Draft of LTCC physical realization of a part of the presented filter configuration as in Fig. 1(a) (Stripline-Ridge-Stripline).

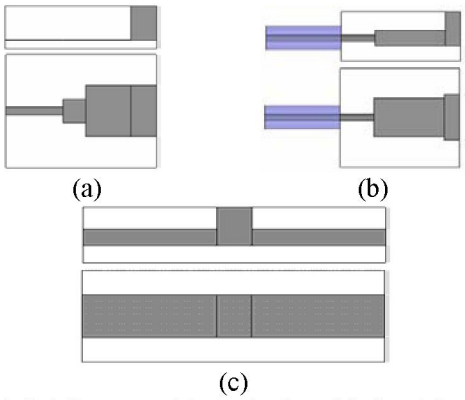

Fig. 3. (a) Stripline tapped-in excitation; (b) Coaxial cable probe excitation; (c) Stripline-Ridge waveguide-Stripline coupling section.

information of the S-parameter should be also considered to adjust the stripline resonator lengths to compensate the loading effects.

The second step is the full wave optimization by MMM to get the optimum filter parameters. Usually only the lengths of the resonators and coupling sections are optimized. By properly defining an objective function, the optimization of the filer performance can be done very efficiently using a gradient optimization method.

III. Filter Examples

To show the feasibility of the presented filter configuration, two filter examples are given in this paper. One filter is in LTCC technology, the other one is in metallic structures. To improve the spurious response of the filter in LTCC, the stepped impedance stripline resonators are applied.

A. Filter using LTCC Technology

The requirements of the filter are: 1) Passband: 8 – 10 GHz; 2) Minimum return loss: 22 dB; 3) Maximum insertion loss: 2 dB. The relative bandwidth of the filter is about 22%. The filter is designed for LTCC applications. The parameters of the employed LTCC technology are: ε_r=5.9; thickness of dielectric layer: 3.74mil; thickness of metallization layer: 0.4mil. The design procedure in section II is followed to

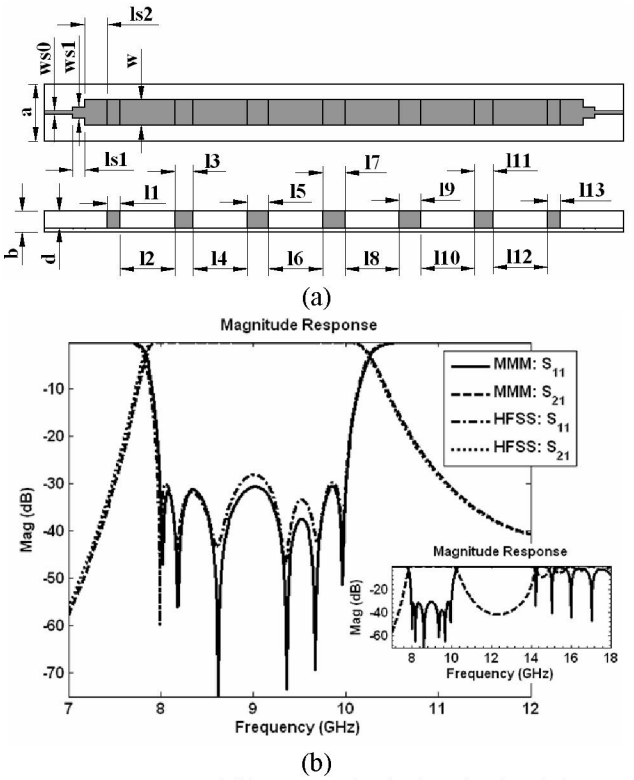

Fig. 4. (a) Structure of filter example *A*; (b) Simulated frequency responses by MMM and HFSS. The filter is designed for LTCC application. ε_r=5.9; Thickness of each dielectric layer: 3.74mil; Thickness of metallization strip: 0.4mil; Dimensions of the filter are: a=100mil; b=37.4mil; d=29.92mil; ws0=7mil; ws1=20mil; w=45mil; ls1=40.88mil; ls2=79.66; l1=l13=44.73mil; l2=l12=192.12mil; l3=l11=63.37mil; l4=l10=189.38mil; l5=l9=76.25mil; l6=l8=188.9mil; l7=78.92mil.

design the filter. Fig. 3 shows the optimized filter dimensions and the simulated response in MMM and HFSS. HFSS response shows a good agreement with MMM.

The spurious response of the designed filter in Fig. 4(a) is poor, which can be seen in Fig. 4(b). To improve the spurious response, the idea of stepped impedance resonators can be applied [7], [8]. Basically a wider-strip lower-impedance stripline is introduced in the middle of the original stripline resonator (as in Fig. 5(a)). Therefore, one resonator will consist of three striplines, which are in the order of high impedance, low impedance and high impedance. The new resonator now behaves like a lowpass filter, which is expected to be able to improve the bandpass filter spurious response.

From the other point of view, the spurious response is caused by the higher order resonant modes of the stripline resonators. Adding a wider stripline in the middle of the resonator will reduce the total length of the resonator to have the dominant resonant mode at center frequency because the field of dominant mode is concentrating in the middle of the resonator and the added stripline introduces very strong coupling effects for this dominant mode. While for the first higher order resonant mode, the field is very weak in the middle of stripline and is very strong close to the two ends of

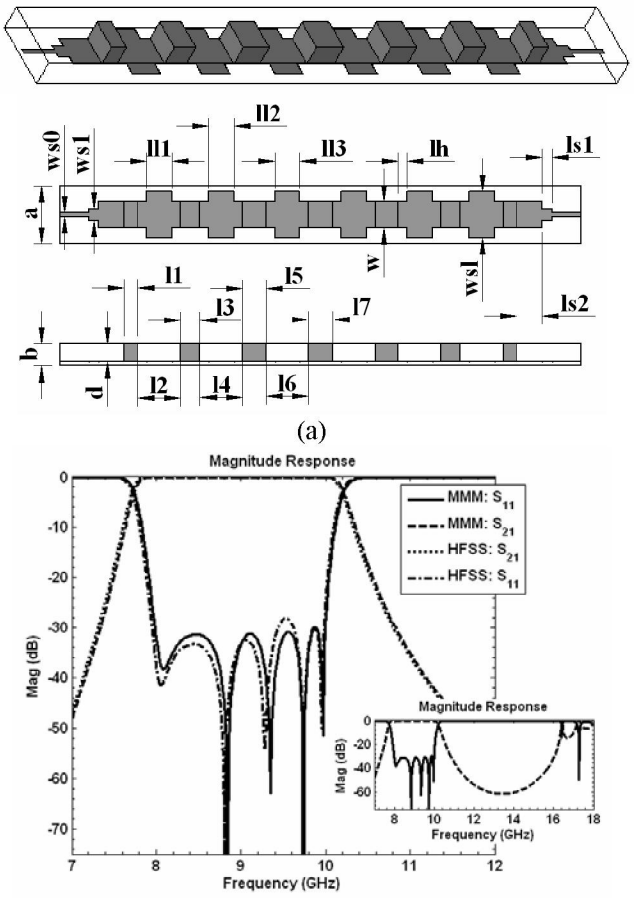

Fig. 5. (a) Structure of filter example *A* with stepped impedance stripline resonators; (b) Simulated frequency responses by MMM and HFSS. The filter is a symmetric structure. All the high impedance striplines in the resonators have the same length lh. Dimensions of the filter are: a=100mil; b=37.4mil; d=29.92mil; ws0=7mil; ws1=20mil; w=45mil; wsh=80mil; ls1=33.99mil; ls2=87.65; lh=30mil l11=87.83mil; l12=87.03mil l13=85.92mil l1=46.33mil; l2=147.83mil; l3=66.99mil; l4=147.03mil; l5=80.4mil; l6=145.92mil; l7=84.26mil.

the stripline, so this mode will be pushed further away from filter passband by the added wider stripline since the length of the new resonator is shorter and the added stripline introduces very small coupling effect on this mode.

The improved filter dimensions and responses are shown in Fig. 5(a) and Fig. 5(b), respectively. The spurious response is indeed improved. If more stepped impedance striplines are used as one resonator, the spurious response might be improved more.

B. Filter in Metallic Structures

The requirements of the filter are: 1) Passband: 3 – 3.5 GHz; 2) Minimum return loss: 22 dB; 3) Maximum insertion loss: 0.5 dB. The relative bandwidth of the filter is about 15%. The filter is designed in air-filled metallic structures. The designed filter dimensions and responses are shown in Fig. 6. HFSS response shows a good agreement with MMM.

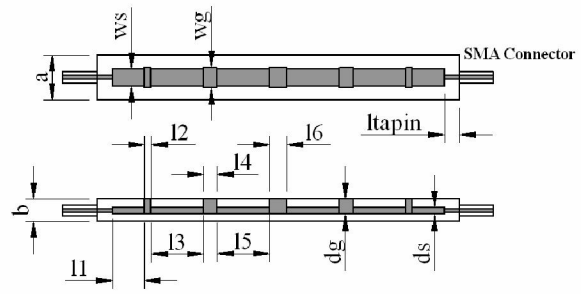

(a)

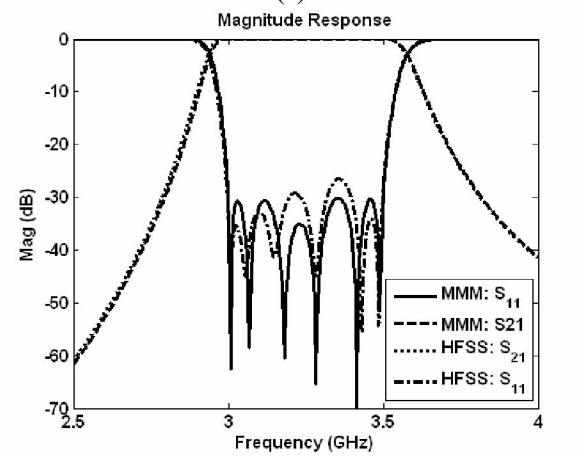

(b)

Fig. 6. (a) Structure of filter example *B*; (b) Simulated frequency responses by MMM and HFSS. The filter is a symmetric structure and in metallic structures. Dimensions of the filter are: a=650mil; b=325mil; ws=230mil; wg=300mil; ds=100mil; dg=225mil; ltapin=445mil; l1=932mil; l2=102mil; l3=1536mil; l4=217mil; l5=1531mil; l6=250mil.

IV. Multiplexer Applications

The presented stripline resonator filters have compact cross sections which makes them also suitable choices for multiplexer applications, especially in LTCC technology. Two kinds of stripline junctions can be employed for diplexer/multiplexer designs. One is stripline H-plane T junction as in Fig. 7(a), the other one is stripline H-plane bifurcation/multifurcation junction as in Fig. 7(b). One diplexer design example using H-plane bifurcation is presented in Fig. 7(c). The analysis and optimization process by MMM is applied to improve the diplexer performance.

V. Conclusion

Ridge waveguide coupled stripline resonator filters are presented in this paper. Such filters have compact cross sections and are suitable choices for some RF/microwave systems having demanding size limitations. The given filter examples show that the presented filter configuration is feasible and can be manufactured in either LTCC technology or metallic structures. Such filters can also be applied to multiplexer application, which is proved by the given diplexer example.

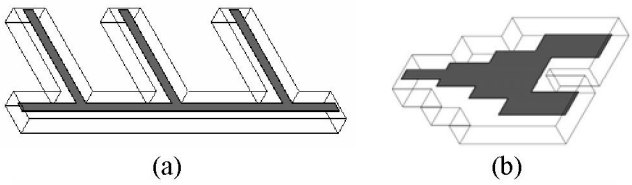

(a) (b)

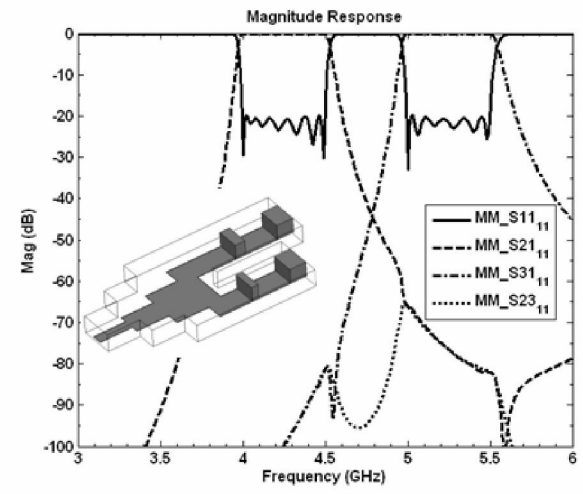

(c)

Fig. 7. (a) Stripline T junction; (b) Stripline bifurcation junction; (c) Diplexer structure (part structure) and simulated responses.

References

[1] Y. Rong, K. A. Zaki, M. Hageman, D. Stevens, and J. Gipprich, "Low-temperature cofired ceramic (LTCC) ridge waveguide bandpass chip filters," *IEEE Trans. Microw. Theory Tech.*,vol. 47, No. 12, pp. 2317-2324, Dec. 1999.

[2] G. L. Matthaei, L. Young, and E. M. T. Jones, *Microwave Filters Impedance-Matching Networks and Coupling Structures.* Norwood, MA: Artech House, 1980.

[3] J. Uher, J. Bornemann, and U. Rosenberg, *Waveguide Components for Antenna Feed Systems: Theory and CAD*, Boston, London: Artech House, 1993..

[4] R. Levy, R. V. Snyder, and G. Matthaei, "Design of Microwave Filters," *IEEE Trans. Microw. Theory Tech.*,vol. 50, No. 3, pp. 783-793, Mar. 2002.

[5] H. Yao, X. Liang, K. A. Zaki, and A. Martin, "Wide-band waveguide and ridge waveguide T-junctions for diplexer applications," *IEEE Trans. Microw. Theory Tech.*,vol. 41, No. 12, pp. 2166-2173, Dec. 1993.

[6] M. A. El Sabbagh, H. Hsu, K. A. Zaki, P. Pramanick, and T. Dolan, "Full wave optimization of stripline tapped-in ridge waveguide bandpass filters," *IEEE MTT-s Dig.*, vol. 3, pp. 1445-1448, June 2002.

[7] M. Sagawa, M. Makimoto, and S. Yamashita, "A design method of bandpass filters using dielectric-filled coaxial resonators," *IEEE Trans. Microw. Theory Tech.*,vol. 33, pp. 152-157, Feb. 1985.

[8] H. W. Yao, K. A. Zaki, A. E. Atia, and T. Dolan, "Improvement of spurious performance of combline filters," *IEEE MTT-s Dig.*, vol. 2, pp. 1099-1102, June 1997.

RIGOROUS DESIGN OF SEPTATE E-PLANE MULTIPLEXERS WITH PRINTED CIRCUIT ELEMENTS

Joachim Dittloff, and Fritz Arndt

Microwave Department
University of Bremen
Kufsteiner Str., NW1, D-2800 Bremen, West-Germany

ABSTRACT

A new design of compact, low-cost and low-insertion loss millimeter wave multiplexers is introduced utilizing metallic E-plane filters integrated in the septate waveguide sections of wide-band E-plane n-furcated power dividers. A rigorous simulation technique, which is based on the modal scattering matrix method, comprises the complete component including the E-plane transformer, the septum as well as the filter sections, and takes the influences of the higher-order mode interaction at all discontinuities into account. Computer optimized data are given for Ku- and E-band di- and triplexer design examples with five-, or seven-resonator metal-insert filters, respectively.

INTRODUCTION

Recent advances in the design of channelized receivers have stirred the need for compact, low-cost and low-insertion-loss millimeter wave diplexers and multiplexers. Common designs utilizing printed circuit filter technology [1] - [7] include hybrid, [1] - [3], E-plane T-junction, [4], H-plane T-junction, [3], [5], and suspended probe coupling techniques, [6], [7]. Hybrid and probe coupling methods require additional structures and, hence, may cause additional costs and losses, [1] - [3], [6] - [8]; T-junction feeds are relatively narrow-band and it is often difficult to compensate for the rapid reactance variation, [3] - [5].

In this paper, we will describe a new design of a millimeter wave multiplexer (Fig. 1) which is capable to avoid these disadvantages by utilizing the wide-band low-insertion loss properties of E-plane n-furcated power dividers [9]. The design is well compatible with metallic E-plane filters providing low insertion losses because of the absence of supporting dielectrics, [10], [11]. Moreover, the technique leads to very compact and low-cost multiplexer performances as the metal-etched filters may be directly integrated in the septate E-planes of a common split-block waveguide housing (Fig. 1).

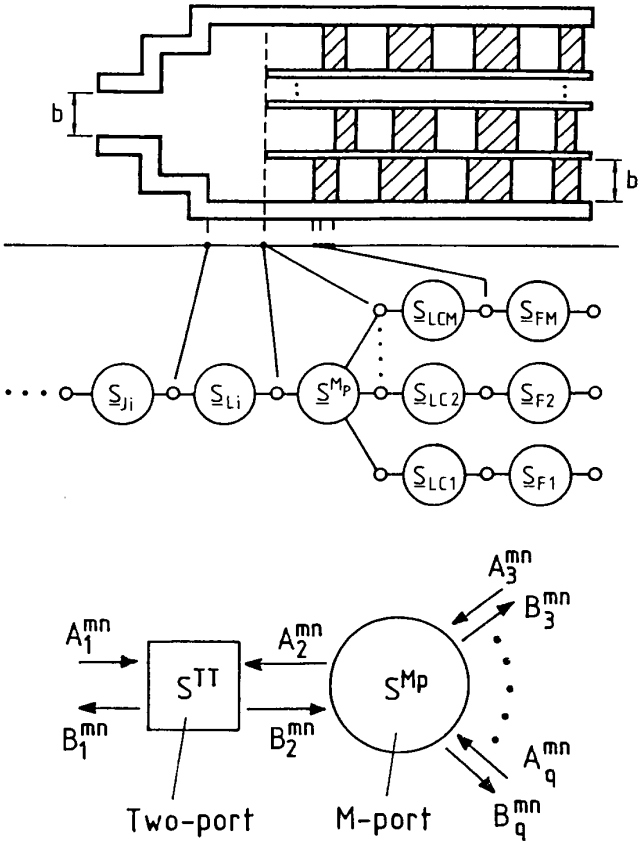

Fig. 1: Septate E-plane multiplexer with metallic E-plane filters

0149-645X/88/0000-0431$01.00 © 1988 IEEE

Usual design methods of millimeter wave multiplexers are based on empirical studies [1], equivalent circuit techniques [2], [3], [12], or approximate theories for the transitions [6], [7]. However, loading effects of the filter structures as well as the higher-order mode interactions between them and the feeding transition must be rigorously included in the design of the multiplexer to ensure good overall performance, especially for millimeter wave designs. Moreover, it may be desirable to take advantage of the full low-insertion loss and mutual compensation potential inherent to the technology by utilizing adequate exact simulation and optimization theories for the total millimeter wave multiplexer structure.

This paper presents a rigorous modal scattering matrix method for the design of the complete multiplexer component comprising the E-plane transformer, the septum and the filter section (Fig. 1). As higher-order mode interactions at millimeter waves have turned out to be of increasing importance, already for designing single filters [11], these effects, as well as the septum and metallization thicknesses, are taken into account for the complete component. Relevant influences, such as the transformer step heights and lengths, the septum distance to the transformer section, as well as the individual distances of the filters to the power divider section, are utilized for the optimization process as additional design parameters. Moreover, the exact design theory enables the high-precision manufacturing by computer controlled milling machines and etching techniques without the necessity of post assembly 'trial-and-error' adjustment methods.

THEORY

For the computer-aided design of the complete multiplexer structure (Fig. 1), the modal S-matrix method [9], [11], [13], is applied. The combination of all individual structures (E-plane and H-plane step discontinuities), including the higher-order mode interaction of the cascaded structures, requires all six field components to be considered, at each discontinuity. For a general homogeneous waveguide subregion under consideration, the fields

$$\vec{E} = \frac{1}{j\omega\epsilon} \nabla \times \nabla \times (\vec{Q}_{ez}) + \nabla \times (\vec{Q}_{hz}) \qquad (1)$$
$$\vec{H} = -\frac{1}{j\omega\mu} \nabla \times \nabla \times (\vec{Q}_{hz}) + \nabla \times (\vec{Q}_{ez})$$

are derived from the z-components of the electric (e) and magnetic (h) vector potentials

$$Q^{o}_{ez} = \sum_{i^o} N^{o}_{i^o} \cdot T^{o}_{ei^o} \cdot (A^{o}_{ei^o}{}^{\pm} \cdot e^{\mp jk^{o}_{ze_{i^o}} z})$$
$$Q^{o}_{hz} = \sum_{i^o} N^{o}_{i^o} \cdot T^{o}_{hi^o} \cdot (A^{o}_{hi^o}{}^{\pm} \cdot e^{\mp jk^{o}_{zh_{i^o}} z}) \qquad (2)$$

where $o = 1,2,3,\ldots,M_s$ (M_s = total number of subregions), i^o is the index for all TE-, and TM-modes in each subregion, N are the normalization factors due to the complex power, and T are the eigenfunctions in the corresponding subregions, [9], [11], [13]; $A^{\pm}$ are the amplitude coefficients of the forward and backward waves, and k_z are the wavenumbers of the corresponding TE- and TM-modes.

By matching the tangential field components at the common interfaces at the individual step discontinuities, the wave amplitude coefficients of (2) can be related to each other after multiplication with the appropriate orthogonal function, [9], [11], [13]. This yields the key building block two-port modal scattering matrices (S_{Ji}), (S_{Fi}) of the transformer and filter sections, respectively (cf. Fig. 1), and the M-port modal scattering matrix (S^{Mp}) of the n-furcated waveguide section [9].

In order to preserve numerical accuracy, the direct combination of the modal scattering matrices of all step discontinuities and of the intermediate homogeneous waveguide sections is used. The advantage of this procedure has already been demonstrated for two-port structures, cf. [11], [13]. The more general relations, which may also be used iteratively, for multi-port structures, e.g. including the transformer section two-port modal scattering matrix (S^{TT}), and the M-port modal scattering matrix (S^{Mp}), to calculate the scattered wave vectors B of the mn modes considered at the ports 1, s, (s=3,4,...,q), cf. Fig. 1, are given by

$$B_1 = [S^{TT}_{11} + S^{TT}_{12} \cdot W \cdot S^{Mp}_{11} \cdot S^{TT}_{21}] \cdot A_1 + S^{TT}_{12} \cdot W \cdot K ,$$
$$B_s = S^{Mp}_{s-1,1} \cdot [S^{TT}_{21} + S^{TT}_{22} \cdot W \cdot S^{Mp}_{11} \cdot S^{TT}_{21}] \cdot A_1 + S^{Mp}_{s-1,1} \cdot S^{TT}_{22} \cdot W \cdot K + P, \qquad (3)$$

with

$$W=(U-S_{11}^{Mp}S_{22}^{TT})^{-1},\quad K=\sum_{r=2}^{q-1} S_{1,r}^{Mp}\cdot A_{r+1},$$

$$P=\sum_{p=2}^{q-1} S_{s-1,p}^{Mp}\cdot A_{p+1},$$

and where the indices denote the related submatrices.

A computer program was written using the preceding relations and utilizing the evolution strategy method, cf. [13], for optimizing the geometrical parameters for given specifications. Sufficient asymptotic behaviour has been obtained by consideration of 15 TE- and TM-modes for the E-plane transformer and n-furcated waveguide section, and up to 40 TE_{m0}-modes for the filter sections.

RESULTS

A computer optimized Ku-band diplexer design example with two five-resonator metallic E-plane filters in the septate waveguide regions is shown in Fig. 2. Due to the inclusion of all relevant design parameters in the optimization process, only a one-step transformer is required to provide the desired pass-band return loss of about 26 dB. This holds also for thicker septa thicknesses as is demonstrated by a design example with t = 3mm. For higher frequencies, cf. the E-band diplexer design example in Fig. 3, a two-step transformer section has been chosen. The efficiency of the design method, also for more complicated structures, is demonstrated by the E-band triplexer design example shown in Fig. 4.

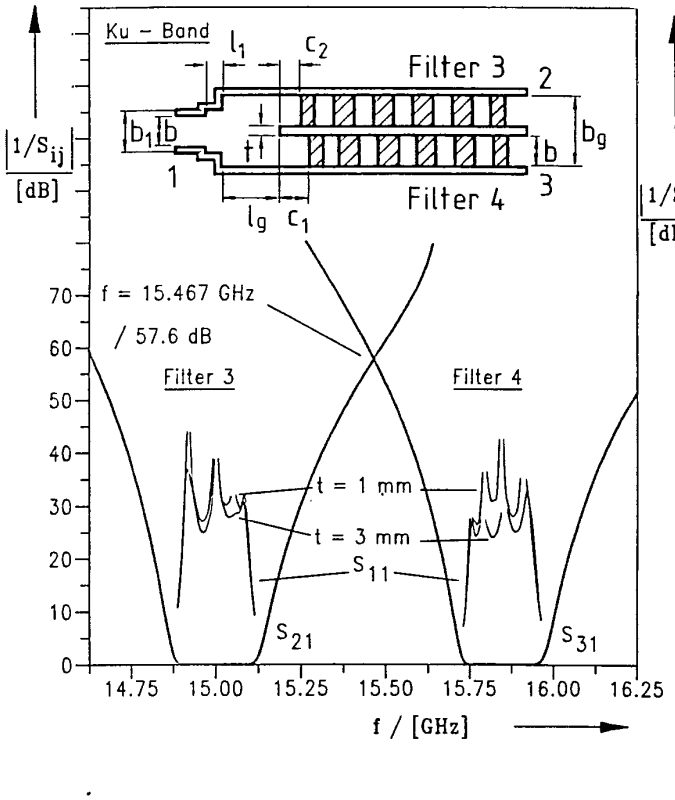

Fig. 2: Computer-optimized septate E-plane diplexer for Ku-band with two 5-resonator metallic E-plane filters.
Filter 3: f_{03} = 15.00 GHz,
filter 4: f_{04} = 15.85 GHz.

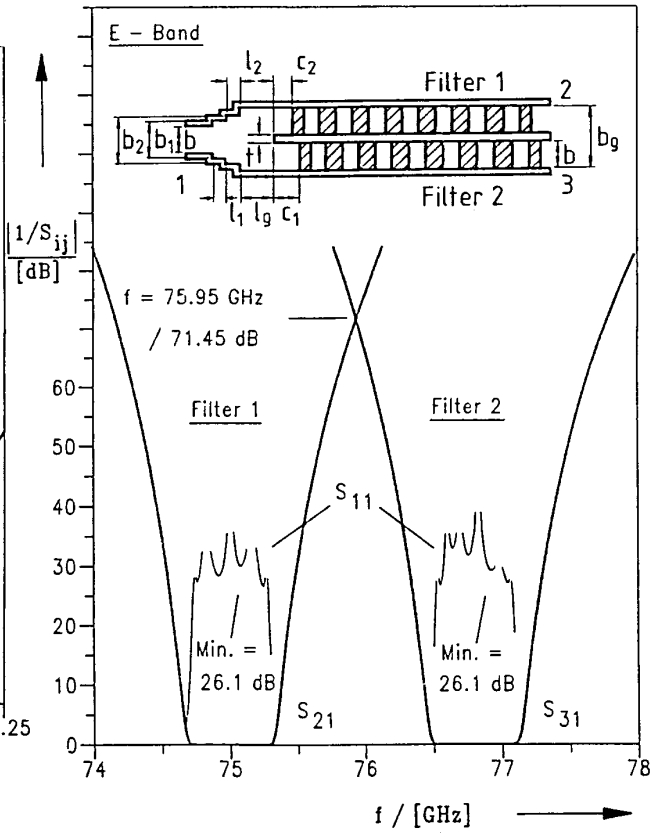

Fig. 3: Computer-optimized septate E-plane diplexer for E-band with two 7-resonator metallic E-plane filters.
Filter 1: f_{01} = 75.00 GHz,
filter 2: f_{02} = 76.80 GHz.

Measurements are available for the typical single components. The metallic E-plane filters have been fabricated and measured up to 144 GHz [11], [13], and the n-furcated waveguide power dividers have already been utilized for practical antenna feeding networks in the R120 waveguide-band (10 - 15 GHz), [9]. Excellent agreement between theory and measurements verifies the modal S-matrix design method. For diplexer designs with metallic E-plane filters, based on E-plane T-junction feeds, measured pass-band insertion losses of typically about 0.5 - 0.8 dB in the R120-band have been reported [4]. The E-plane diplexers designed may be fabricated utilizing computer controlled milling machines for the split-block housing of the filters and the transformer section, and using metal-etching techniques for the filter elements.

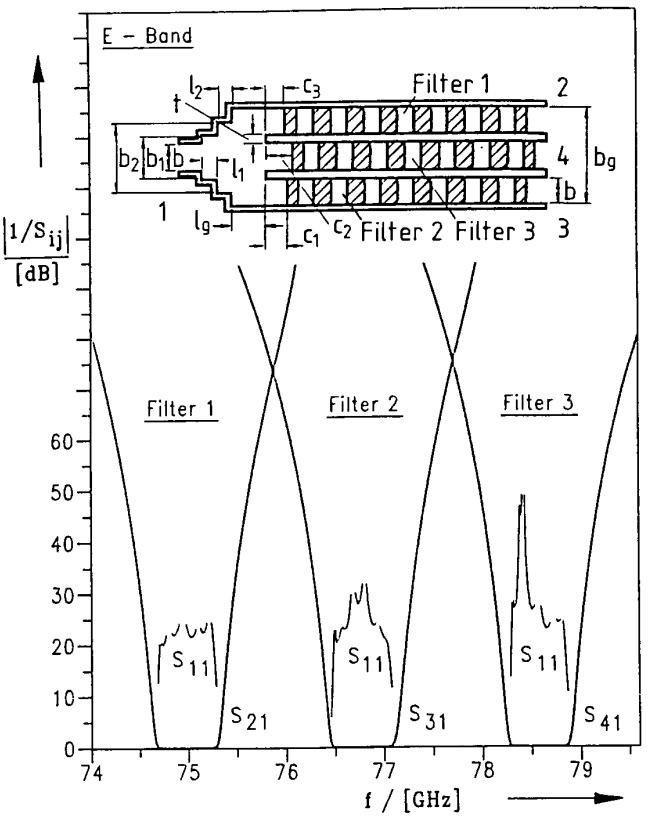

Fig. 4: Computer-optimized septate E-plane multiplexer for E-band with three 7-resonator metallic E-plane filters.
Filter 1: f_{01} = 75 GHz,
filter 2: f_{02} = 76.8 GHz,
filter 3: f_{03} = 78.6 GHz.

REFERENCES

[1] J. Reindel, "Printed WG circuits trim component costs", Microwaves, pp. 60 - 63, Oct. 1980.

[2] K.D. Breuer, and N. Worontzoff, "Low cost multiplexer for channelized receiver front ends at millimeter waves," in IEEE MTT-S Int. Symp. Digest, pp. 150 - 152, 1980.

[3] L.D.Cohen, N. Worontzoff, J. Levy, and A. Harvey, "Millimeter wave multiplexer with printed circuit elements for the 88 to 100 GHz frequency range," in IEEE MTT-S Int. Symp. Digest, pp. 233 - 235, 1984.

[4] F. Arndt, J. Bornemann, D. Grauerholz, D. Fasold, and N. Schroeder, "Waveguide E-plane integrated-circuit diplexer, " Electronics Letters, vol. 21, pp. 615 - 617, 4th July 1985.

[5] C. Nguyen, and K. Chang, "W-band wideband low loss planar integrated circuit diplexer," Microwave Journal, pp. 157 - 161, July 1985.

[6] Y.-C. Shih, and T. Itoh, "Millimeter-wave diplexers with printed circuit elements," IEEE Trans. Microwave Theory Tech., vol. MTT-33, pp. 1465 - 1469, Dec. 1985.

[7] Y.-C. Shih, L.Q Bui, and T. Itoh, "Mm-wave contiguous diplexer designed with printed circuit elements," Micowave System News & CT, pp. 46 - 53, Feb. 1987.

[8] D. Rubin, and A.R. Hislop, "Millimeter-wave coupled line filters," Microwave Journal, pp. 67 - 78, Oct. 1980.

[9] J. Dittloff, J. Bornemann, and F. Arndt, "Computer aided design of optimum E- or H-plane n-furcated waveguide power dividers," in Proc. Europ. Microwave Conf., Rome, pp. 181 - 186, Sept. 1987.

[10] Y. Konishi, and K. Uenakada, "The design of a bandpass filter with inductive strip - Planar circuit mounted in waveguide," IEEE Trans. Microwave Theory Tech., vol. MTT-22, pp. 869 - 873, Oct. 1974.

[11] R. Vahldieck, J. Bornemann, F. Arndt, and D. Grauerholz, "Optimized waveguide E-plane metal insert filters for millimeter-wave applications," IEEE Trans. Microwave Theory Tech., vol. MTT-31, pp. 65 - 69, Jan. 1983.

[12] J.W.Bandler, S. Daijavad, and Q.-J. Zhang, "Exact simulation and sensitivity analysis of multiplexing networks," IEEE Trans. Microwave Theory Tech., vol. MTT-34, pp. 93 - 101, Jan. 1986.

[13] F. Arndt et al., "Modal S-matrix method for the optimum design of inductively direct-coupled cavity filters," IEE Proceedings, vol. 133; Pt. H, pp. 341 - 350, Oct. 1986.

Published in IET Microwaves, Antennas & Propagation
Received on 8th September 2010
Revised on 23rd December 2010
doi: 10.1049/iet-map.2010.0447

ISSN 1751-8725

Synthesis of multiple output coupled resonator circuits using coupling matrix optimisation

T.F. Skaik M.J. Lancaster F. Huang

School of Electronic, Electrical and Computer Engineering, University of Birmingham, Birmingham B15 2TT, UK
E-mail: talalskaik@gmail.com

Abstract: Coupled resonator circuits are the basis for the design of many bandpass microwave filters. Design techniques used for two-port coupled resonator circuits are extended here to multiple output circuits such as power dividers and diplexers. The design approach is based on synthesis of coupling matrix for multiple coupled resonators with multiple outputs using gradient-based optimisation. It allows the synthesis of power dividers with arbitrary power division, as well as diplexers and multiplexers with novel topologies. Since there is no need to use separate energy distribution networks such as circulators, manifolds or other junctions, the components can be miniaturised. An X-band unequal power divider and diplexer have been designed and realised using waveguide cavity resonators to confirm the new design methodology.

1 Introduction

In communications systems, microwave filters are used as individual components, as well as parts of multiplexers [1]. Coupled resonator filters have been extensively presented in the literature for many applications. There is a general technique for designing these filters that can be applied to any type of resonator regardless of its physical structure [2]. Such a technique is based on coupling coefficients for coupled resonators arranged in a topology representing a two-port network. Optimisation techniques are employed to synthesise the coupling matrix by minimisation of a scalar cost function [3–5].

Coupled resonator circuits with multiple ports were first presented in [6]. The synthesis of multiport microwave coupled resonator networks using a procedure analogous to filters has been presented in [7, 8]. *N*-port devices such as power splitters and directional couplers formed from magneto-inductive waveguides based on coupled loop resonators have been reported in [9].

In the current work, a general coupling matrix for n coupled resonators with multiple ports is presented. Three-port microwave components such as power dividers with arbitrary power division and diplexers with novel topologies are demonstrated in particular. The synthesis of these devices employs similar coupling matrix optimisation techniques to those of coupled resonator filters.

Power dividers are passive microwave components used to divide an input signal into two or more signals of less power [10]. Examples of widely used power dividers are T-junctions [10], and Wilkinson divider [11]. An approach to design three-port filtering power dividers with arbitrary power division is proposed here. It is based on coupled resonator T-topology, and realisation is possible using microstrip resonators or waveguide cavities or other types of resonators. The synthesis of polynomials and coupling matrices of the proposed power divider is presented. In [12], we presented a 3 dB power divider, and here we present an unequal power divider realised using waveguide cavity resonators to demonstrate the approach.

The common approach to synthesise multiplexers is to design each channel filter individually and then to design a distribution network. The most commonly used distribution configurations are multiple-way or cascaded dividers, circulators [13] and manifold structures [14]. These configurations have drawbacks of large volume and footprints, high cost and time-consuming optimisation. Diplexers without distribution networks have also been reported in [7, 15, 16]. In [7], a diplexer is designed with the common port directly connected to two resonators. However, this may have practical difficulties in implementation. In [15], miniaturised microstrip diplexers designed using stepped impedance resonators by integrating two bandpass filters with common resonator sections have been proposed. In [16], the synthesis of diplexers employing a resonant junction (an extra resonator in addition to the channel filters) has been reported.

In this paper, we present diplexers with novel topologies that can be implemented using any type of resonators. The synthesis of the diplexers is based on optimisation of coupling matrices for topologies without using any external junctions for the distribution of energy. This gets rid of the drawbacks mentioned earlier. A simple X-band waveguide diplexer has been designed, fabricated and tested to verify the proposed approach.

2 General coupling matrix for multiple coupled resonators with multiple outputs

A similar approach to the derivation of coupling matrix of coupled resonator filters in [2] has been adopted in the

current work to derive general coupling matrix of n coupled resonators circuit with multiple ports. Both electric and magnetic coupling have been considered separately and later a solution has been generalised for both types of coupling.

The equivalent circuit considered for each type of coupling assumes that each resonator can be connected to one port, with the input port connected to resonator 1. In the case of magnetically coupled resonators, using Kirchoff's voltage law, the loop equations are derived and represented in impedance matrix form. Similarly, for electrically coupled resonators, using Kirchoff's current law, node equations are derived and represented in admittance matrix form. The derivations show that the normalised admittance matrix has a form identical to that of the normalised impedance matrix [2]. Accordingly, regardless of the type of coupling, a general normalised matrix $[\boldsymbol{A}]$ in terms of coupling coefficients and external quality factors is derived as shown in

$$[\boldsymbol{A}] = \begin{bmatrix} \frac{1}{q_{e1}} & \cdots & 0 & 0 \\ \vdots & \vdots & \vdots & \vdots \\ 0 & \cdots & \frac{1}{q_{e(n-1)}} & 0 \\ 0 & \ldots & 0 & \frac{1}{q_{en}} \end{bmatrix} + P \begin{bmatrix} 1 & \cdots & 0 & 0 \\ \vdots & \vdots & \vdots & \vdots \\ 0 & \cdots & 1 & 0 \\ 0 & \ldots & 0 & 1 \end{bmatrix} - j \begin{bmatrix} m_{11} & \cdots & m_{1(n-1)} & m_{1n} \\ \vdots & \vdots & \vdots & \vdots \\ m_{(n-1)1} & \cdots & m_{(n-1)(n-1)} & m_{(n-1)n} \\ m_{n1} & \ldots & m_{n(n-1)} & m_{nn} \end{bmatrix} \quad (1)$$

where q_{ei} is the scaled external quality factor ($q_{ei} = Q_{ei}\,\mathrm{FBW}$) of resonator i, P is the complex lowpass frequency variable, m_{ij} is the normalised coupling coefficient ($m_{ij} = M_{ij}/\mathrm{FBW}$), FBW is the fractional bandwidth and the diagonal entries m_{ii} account for asynchronous tuning, so that resonators can have different self-resonant frequencies. Considering a three-port network with n coupled resonators, with port 1 at resonator 1, port 2 at resonator a and port 3 at resonator b, the S-parameters will have the form

$$S_{11} = 1 - \frac{2}{q_{e1}}[\boldsymbol{A}]^{-1}_{11}, \quad S_{21} = \frac{2}{\sqrt{q_{e1}q_{ea}}}[\boldsymbol{A}]^{-1}_{a1}, \quad S_{31} = \frac{2}{\sqrt{q_{e1}q_{eb}}}[\boldsymbol{A}]^{-1}_{b1} \quad (2)$$

3 Power divider synthesis

3.1 Power divider polynomials synthesis

Since the proposed divider is based on filtering functions, its response can be described by polynomial transfer functions. Therefore for a three-port power divider consisting of n coupled resonators, the reflection and transmission functions may be defined as the ratio of two polynomials as follows

$$S_{11}(\omega) = \frac{F(\omega)}{E(\omega)}, \quad S_{21}(\omega) = \frac{P(\omega)/\varepsilon_1}{E(\omega)}, \quad S_{31}(\omega) = \frac{P(\omega)/\varepsilon_2}{E(\omega)} \quad (3)$$

where ω is the real frequency variable, the polynomials $F(\omega)$, $P(\omega)$ and $E(\omega)$ are assumed to be normalised so that their highest degree coefficients are unity. $F(\omega)$ and $E(\omega)$ are Nth-order polynomials, where N is the order of the filtering function, whereas $P(\omega)$ has an order equal to the number of prescribed transmission zeros. The maximum number of transmission zeros that can be realised in the suggested network is $N-2$. The roots of $F(\omega)$ correspond to the reflection zeros of the filtering function and can be found by a recursive technique [17], whereas the roots of $P(\omega)$ correspond to the positions of transmission zeros of the filtering function. For a Chebyshev function, the constants ε_1 and ε_2 normalise $S_{21}(\omega)$ and $S_{31}(\omega)$, respectively, to the specified insertion loss levels at $\omega = \pm 1$. The polynomial $E(\omega)$ has its complex roots corresponding to the filter pole positions and can be constructed if the polynomials $F(\omega)$, $P(\omega)$ and the constants ε_1 and ε_2 are known.

Expressions for ε_1 and ε_2 will be derived next, followed by a discussion on determining $E(\omega)$. If the input power is to be divided such that $|S_{31}(\omega)|^2 = \alpha|S_{21}(\omega)|^2$, then for a lossless system

$$|S_{11}(\omega)|^2 + (1+\alpha)|S_{21}(\omega)|^2 = 1 \quad (4)$$

From (3) and (4), the constant ε_1 is evaluated as

$$\varepsilon_1 = \left|\frac{S_{11}(\omega)}{S_{21}(\omega)}\right|\left|\frac{P(\omega)}{F(\omega)}\right| = \frac{\sqrt{1+\alpha}|S_{11}(\omega)|}{\sqrt{1-|S_{11}(\omega)|^2}}\left|\frac{P(\omega)}{F(\omega)}\right|$$

When $\omega = \pm 1$, $|S_{11}(\omega)|$ is equal to the maximum passband reflection coefficient, whose value is known from the specification. ε_1 can be expressed in terms of the polynomials $F(\omega)$ and $P(\omega)$, and the prescribed return loss level in dB, RL, in the passband as follows

$$\varepsilon_1 = \sqrt{\frac{1+\alpha}{10^{\mathrm{RL}/10}-1}}\left|\frac{P(\omega)}{F(\omega)}\right|_{\omega=\pm 1} \quad (5)$$

Similarly, ε_2 can be expressed as

$$\varepsilon_2 = \sqrt{\frac{1+\alpha}{\alpha(10^{\mathrm{RL}/10}-1)}}\left|\frac{P(\omega)}{F(\omega)}\right|_{\omega=\pm 1} \quad (6)$$

Once the polynomials F and P, and the constants ε_1 and ε_2 are known, the denominator polynomial E can be derived by substitution of $F(s)$, $P(s)$ and $E(s)$, where $s = \mathrm{j}\omega$ is the complex frequency variable, into the conservation of energy formula, as follows

$$F(s)F(s)^* + \frac{P(s)P(s)^*}{\varepsilon_1^2} + \frac{P(s)P(s)^*}{\varepsilon_2^2} = E(s)E(s)^* \quad (7)$$

$E(s)E(s)^*$ is constructed by polynomials multiplications in the left-hand side of (7), which must be polynomial of the order $2N$ with real coefficients. The roots of $E(s)E(s)^*$ will be symmetric about the imaginary axis in the complex plane, and they can be found using numerical analysis software such as MATLAB [18]. Since $E(s)$ is strictly Hurwitz, then its roots are those in the left half-plane, whereas the roots of $E(s)^*$ are those in the right half-plane. The polynomial $E(s)$ is then constructed by choosing the N roots in the left half-plane.

doi: 10.1049/iet-map.2010.0447

3.2 Power divider coupling matrix synthesis

The synthesis procedure of the coupling matrix of the proposed power divider is similar to that of a filter with n coupled resonators. It is based on minimisation of a cost function that is evaluated at frequency locations of reflection and transmission zeros. The formulation of the cost function used here is similar, in principle, to that in [5], which is used to optimise coupling matrices for coupled resonator filters. Here the cost function has an extra term to satisfy the power division ratio requirement. The initial cost function is written in terms of the polynomials F and P and is evaluated at critical frequencies as follows

$$\Omega = \sum_{i=1}^{T} |P(s_{ti})|^2 + \sum_{j=1}^{R} |F(s_{rj})|^2 + \sum_{j=1}^{R} \left(\left| \frac{P(s_{rj})}{\varepsilon_1 E(s_{rj})} \right| - \sqrt{\frac{1}{1+\alpha}} \right)^2 \quad (8)$$

where T is the number of transmission zeros, R is the number of reflection zeros, s_{ti} and s_{rj} are the complex lowpass prototype transmission and reflection zeros, respectively. The lowpass prototype frequency positions of reflection zeros are found using Cameron's recursive technique [17]. The last term in the cost function is used to achieve the required power division ratio, and is evaluated at the peaks of $|S_{21}|$, where α is the power ratio as given earlier. This cost function does not involve the ripple in the optimisation parameters, and hence the external quality factors have to be calculated analytically at the desired return loss. The calculations of the external quality factors and the right locations of the return zeros enforce the peaks of $|S_{11}|$ to be at the required return loss level.

The polynomials P and F can be evaluated in terms of the coupling matrix by equating the scattering parameters in (2) to their equivalent in (3). In (2), the inverse of the matrix $[\boldsymbol{A}]$ can be described in terms of the adjoint and determinant as $[\boldsymbol{A}]^{-1} = \text{adj}(\boldsymbol{A})/\Delta_{\boldsymbol{A}}$, where adj($\boldsymbol{A}$) is the adjoint of the matrix $[\boldsymbol{A}]$, and $\Delta_{\boldsymbol{A}}$ is its determinant. Using this, and noting that the adjoint is the transpose of the matrix cofactors, the cost function can be rewritten as given in (9), where $[\boldsymbol{A}]$ is the matrix derived and given in (1), $\Delta_{\boldsymbol{A}}(S_{rj})$ is the determinant of the matrix $[\boldsymbol{A}]$ evaluated at the frequency variable S_{rj}, and $\text{cof}_{kh}\{[\boldsymbol{A}(s=x)]\}$ is the cofactor of matrix $[\boldsymbol{A}]$ evaluated by removing the kth row and the hth column of $[\boldsymbol{A}]$ and finding the determinant of the resulting matrix at the frequency variable $s = x$

$$\Omega = \sum_{i=1}^{T} \left| \frac{2}{\sqrt{q_{e1} q_{ea}}} \text{cof}_{1a}([\boldsymbol{A}(S_{ti})]) \right|^2 + \sum_{j=1}^{R} \left| \Delta_{\boldsymbol{A}}(S_{rj}) - \frac{2\text{cof}_{11}([\boldsymbol{A}(S_{rj})])}{q_{e1}} \right|^2 + \sum_{j=1}^{R} \left| \frac{2}{\sqrt{q_{e1} q_{ea}}} \frac{\text{cof}_{1a}([\boldsymbol{A}(S_{rj})])}{\Delta_{\boldsymbol{A}}(S_{rj})} - \sqrt{\frac{1}{1+\alpha}} \right|^2 \quad (9)$$

The external quality factors are analytically evaluated at specific order and ripple using the equations of a coupled resonator filter [2], and their values are set at the outset of optimisation.

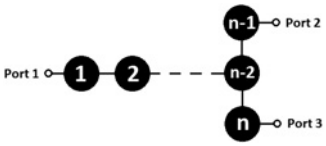

Fig. 1 *Power divider T-topology*

A gradient-based optimisation technique has been used to synthesise the coupling matrix of the proposed power divider, whereby the coupling matrix elements are the optimisation variables. A proposed topology for a three-port power divider with n coupled resonators with Chebyshev filtering response is shown in Fig. 1. Although there are many possible topologies, the topology shown has been suggested since it has large number of shared resonators, so that the order of the filtering function at each output is equal to $(n-1)$, where n is the total number of resonators. This is due to the existence of two signal paths with $(n-1)$ resonators in each; the first contains the resonators (1, 2, 3, …, $n-2$, $n-1$) and the second contains the resonators (1, 2, 3, …, $n-2$, n). The coupling coefficients $m_{(n-2),(n-1)}$ and $m_{(n-2),n}$ will have equal values in case of 3 dB power division, and differing values for arbitrary power division. The initial guess of all coupling coefficients that exist in the divider topology was 0.5, and those that do not exist were set to zero.

It should be noted that the proposed divider is not matched at all ports, and the output ports are not isolated. In consequence, matching is only achieved at port 1, and the output return loss $|S_{22}|$ and $|S_{33}|$ and the isolation $|S_{23}|$ are around 6 dB in the passband. This is a typical problem of lossless reciprocal three-port junctions [19].

3.3 Power divider example

Power dividers with different power division ratios and different number of resonators have been synthesised successfully with the proposed method. An example of 3 dB power divider is presented here. The divider has a return loss of 20 dB and it has the topology in Fig. 1 with $n = 12$. Both the reflection zeros and the external quality factors have been evaluated for 11th-order filter, which is the order of the filtering function at each output, and their values have been set in the optimisation algorithm. The reflection zeros have been calculated using Cameron's recursive technique as follows, $s_{rj} = 0,\ \pm 0.2817\text{j},\ \pm 0.5406\text{j},$

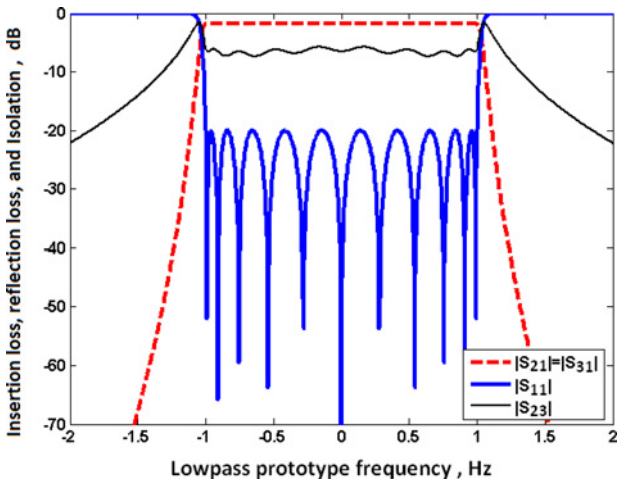

Fig. 2 *Filtering power divider response*

± 0.7557j, ± 0.9096j and ± 0.9898j Hz. The values of external quality factors are $q_{e1} = q_{e11} = q_{e12} = 1.0331$. The synthesised normalised coupling coefficients are $m_{12} = 0.8103$, $m_{23} = 0.5817$, $m_{34} = 0.5419$, $m_{45} = 0.5289$, $m_{56} = 0.5245$, $m_{67} = 0.5244$, $m_{78} = 0.5290$, $m_{89} = 0.5418$, $m_{9,10} = 0.5817$ and $m_{10,11} = m_{10,12} = 0.5730$, and the power divider ideal response is shown in Fig. 2. The response shows that the output ports are not isolated as expected, with $|S_{23}|$ of 5.3 dB or better in the passband.

4 Diplexer synthesis

4.1 Coupling matrix synthesis of diplexer

An approach similar to the power divider cost function formulation has been followed to derive a cost function for diplexers. Assuming that the polynomials $F(s)$, $P_1(s)$, $P_2(s)$ and $E(s)$ along with ripple constant ε completely define the response of the diplexer, where the roots of $F(s)$ correspond to the reflection zeros, the roots of and $P_1(s)$, $P_2(s)$ correspond to the transmission zeros of the filter frequency response at ports 2 and 3, respectively, and the roots of $E(s)$ correspond to the pole positions of the filtering function, the initial cost function may be written in terms of the characteristic polynomials as follows

$$\Omega = \sum_{i=1}^{T_1} |P_1(s_{ti})|^2 + \sum_{k=1}^{T_2} |P_2(s_{tk})|^2 + \sum_{j=1}^{R} |F(s_{rj})|^2 + \sum_{v=1}^{R-2} \left| \left| \frac{F(s_{pv})}{E(s_{pv})} \right| - 10^{L_R/20} \right|^2 \quad (10)$$

where s_{ti}, s_{tk} are the frequency locations of transmission zeros of S_{21}, S_{31}, respectively, T_1, T_2 are the numbers of the transmission zeros of S_{21}, S_{31} respectively, R is the total number of resonators in the diplexer, L_R is the desired return loss in dB ($L_R < 0$), and s_{rj} and s_{pv} are the reflection zeros and the peaks' frequency values of $|S_{11}|$ in the passband. The last term in the cost function is used to set the peaks of $|S_{11}|$ to the required return loss level.

Assuming that the common port of the diplexer is connected to resonator 1, port 2 is connected to resonator a and port 3 is connected to resonator b, the cost function in (10) may be rewritten in terms of determinants and cofactors of the matrix $[A]$ in a similar way to the cost function of power divider as follows

$$\Omega = \sum_{i=1}^{T_1} \left| \frac{2}{\sqrt{q_{e1} q_{ea}}} \mathrm{cof}_{1a}([A(s_{ti})]) \right|^2 + \sum_{k=1}^{T_2} \left| \frac{2}{\sqrt{q_{e1} q_{eb}}} \mathrm{cof}_{1b}([A(s_{tk})]) \right|^2 + \sum_{j=1}^{R} \left| \Delta_A(s_{rj}) - \frac{2\mathrm{cof}_{11}([A(s_{rj})])}{q_{e1}} \right|^2 + \sum_{v=1}^{R-2} \left| \left| 1 - \frac{2\mathrm{cof}_{11}([A(s_{pv})])}{q_{e1}\Delta_A(s_{pv})} \right| - 10^{\frac{L_R}{20}} \right|^2 \quad (11)$$

where q_{e1}, q_{ea} and q_{eb} are the external quality factors at ports 1, 2 and 3, respectively. The first two terms in the cost function are used if the diplexer characteristics contain transmission zeros. However, for a Chebyshev response, these terms may be used to minimise the transmission of each channel at the passband of the other channel, thus increasing the isolation between channel ports. The frequency locations s_{ti} are chosen to be the band edges of the channel at port 3, and similarly the frequency locations s_{tk} are chosen to be the band edges of the channel at port 2.

The lowpass frequency positions of the reflection zeros of the diplexer are initially set to be equally spaced in the optimisation algorithm, and later these positions are moved until an equiripple level at specified insertion loss is achieved. The variables in the optimisation algorithm are the coupling matrix elements and the frequency locations of the reflection zeros.

The external quality factors are numerically calculated, and their values are set at the beginning of the algorithm. This reduces the optimisation parameters set and decreases the convergence time. In order to find the normalised external quality factors of the proposed diplexer, assume we have two lowpass prototype filters with the same order and filtering function but different bandwidth, the first with frequency edges of ± 1 Hz and a bandwidth of $\mathrm{BW}_{\pm 1}$, and the second with frequency edges of x and 1 Hz and a bandwidth of BW_{x1}. The normalised external quality factors of these filters are related by

$$q_{ex1} = \frac{\mathrm{BW}_{\pm 1}}{\mathrm{BW}_{x1}} q_{e\pm 1} = \frac{2}{1-x} q_{e\pm 1} \quad (12)$$

where q_{ex1} is the normalised external quality factor of the second filter, and $q_{e\pm 1}$ is the normalised external quality factor of the first filter, which is known for lowpass prototype filters [2]. Accordingly, for a symmetrical diplexer with channel edges of $(-1, -x)$ and $(x, 1)$, the normalised external quality factors at ports 2 and 3 are calculated from (12), and the normalised external quality factor at the common port is equal to $q_{ex1}/2$. This works for all the examples of symmetrical diplexers presented throughout this paper.

Coupling matrices of symmetrical diplexers have been successfully optimised using the gradient-based technique for possible topologies shown in Fig. 3, where n is the total number of resonators, and $\pm x$ define the inner edges of the two channels.

In the T-topology in Fig. 3*a*, r is the number of resonators located between either output port or the junction resonator

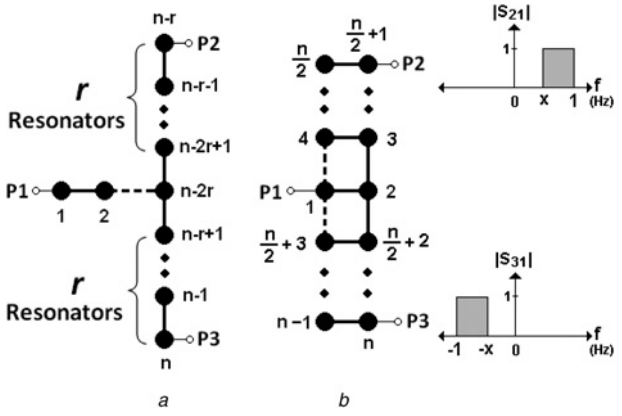

Fig. 3 *Proposed general topologies for coupled resonator diplexers*
a T-topology
b Canonical topology

doi: 10.1049/iet-map.2010.0447

$(n - 2r)$. These resonators should have different self-resonant frequencies to separate the diplexer channels from each other. Different values of r make it possible to realise many topologies with n coupled resonators. The optimisation algorithm has been successful in producing non-distorted diplexer responses for the T-topology in Fig. 3*a* with values of r from $r = \lceil n/4 \rceil$ to $r = [(n/2) - 1]$. A comparison between diplexers with T-topology, with the same number of resonators n, and different value of r will be shown in the next section.

All the resonators in the T-topology shown in Fig. 3*a* are directly coupled (no cross coupling), and hence only Chebyshev response can be obtained. The resonators in the vertical branch apart from the junction resonator should have different self-resonant frequencies; this is to achieve disjoint frequency bands at ports 2 and 3. Consequently, for the high-frequency channel to be at port 2, the resonators above the junction resonator should have positive frequency offsets ($M_{ii} > 0$), and for the low-frequency channel to be at port 3, the resonators below the junction resonator should have negative frequency offsets ($M_{ii} < 0$).

In the canonical topology shown in Fig. 3*b*, solid lines represent direct coupling, and dashed lines represent cross coupling, and a quasi-elliptic filter response can be achieved. The resonators $(3, 4, \ldots, n/2 + 1)$ have positive frequency offsets ($M_{ii} > 0$), and the resonators $(n/2 + 2, n/2 + 3, \ldots, n)$ have negative frequency offsets ($M_{ii} < 0$).

It has been found that by using local optimisation techniques for relatively large structures, the optimisation algorithm may converge to a local minimum. To solve this problem, the optimisation has been done in two stages. In the first stage, the optimisation is carried out by using the cost function in (11) without the last term, and with equally spaced reflection zeros. In the second stage, the full cost function in (11) is used, and the resulting coupling coefficients from the first stage are used as initial values, and the locations of the reflection zeros are allowed to move until equiripple insertion loss is achieved. This has been successful for symmetrical diplexer topologies up to 12 resonators. Moreover, assigning different weights to the terms of the cost function has been found useful for convergence, especially for large structures.

4.2 Diplexer examples

Coupling matrices of diplexers with the same specification and different topologies have been synthesised. Fig. 4 represents three topologies for diplexers with non-contiguous bands with $n = 8$, $x = 0.5$. The structures in Figs. 4*a* and *b* are examples of the general T-topology in Fig. 3*a* with $r = 2$ and 3, respectively, and the structure in Fig. 4*c* is a conventional diplexer with the common port assumed as a shunt connection of the inputs of the two filters composing the diplexer (the addition of a frequency-invariant susceptance representing a three-port junction is possible). The synthesis of the third diplexer is presented in [16].

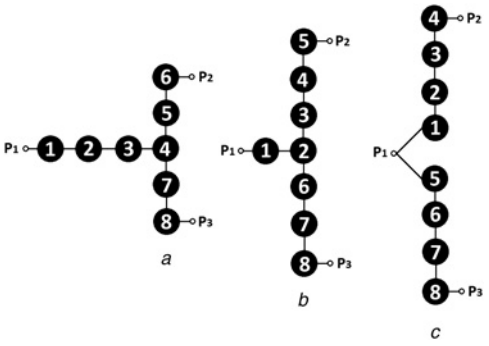

Fig. 4 *Topologies for diplexers*

a T-topology with $r = 2$
b T-topology with $r = 3$
c Conventional topology

In both examples in Figs. 4*a* and *b*, the initial values of the lowpass prototype frequency locations of the zeros of $|S_{11}|$ have been set with equal spacing, and the required return loss has been taken as 20 dB. The external quality factors are numerically calculated as previously described and the frequency locations of $|S_{11}|$ peaks at the passbands are evaluated by numerical differentiation at each iteration in the optimisation algorithm. The initial reflection zeros are $s_{rj} = \pm 0.52\text{j}$, $\pm 0.6733\text{j}$, $\pm 0.8267\text{j}$ and $\pm 0.98\text{j}$, and the external quality factors are 1.863 at port 1, and 3.726 at both ports 2 and 3. The optimised normalised coupling coefficients for the structure in Fig. 4*a* are: $m_{12} = 0.8218$, $m_{23} = 0.4224$, $m_{34} = 0.7117$, $m_{45} = m_{47} = 0.2553$, $m_{56} = m_{78} = 0.2315$, $m_{55} = -m_{77} = 0.7112$ and $m_{66} = -m_{88} = 0.7414$, whereas the optimised normalised coupling coefficients for the structure in Fig. 4*b* are: $m_{12} = 0.8256$, $m_{23} = m_{26} = 0.2981$, $m_{34} = m_{67} = 0.1786$, $m_{45} = m_{78} = 0.2284$, $m_{33} = -m_{66} = 0.6963$, $m_{44} = -m_{77} = 0.7428$ and $m_{55} = -m_{88} = 0.7462$.

In the example in Fig. 4*c*, the return loss is set to 20 dB, and each channel filter is initially designed individually, and then the full coupling matrix of the diplexer is synthesised by integrating the common port in the optimisation. The optimised normalised coupling coefficients for the structure in Fig. 4*c* are: $q_{e1} = q_{e4} = q_{e5} = q_{e8} = 3.7258$, $m_{12} = m_{56} = 0.2279$, $m_{23} = m_{67} = 0.1750$, $m_{34} = m_{78} = 0.2242$, $m_{11} = m_{22} = -m_{55} = -m_{66} = 0.75$, $m_{33} = -m_{77} = 0.7511$ and $m_{44} = -m_{88} = 0.7976$.

The responses of the diplexers in Fig. 4 are shown in Fig. 5. Comparing these responses, it is noticed that the diplexer in Fig. 4*c* has better isolation than the diplexer in Fig. 4*b*, and that the diplexer in Fig. 4*b* has better isolation than the diplexer in Fig. 4*a*. In other words, the higher the number of resonators between ports 2 and 3, the better the isolation is. However, far out of band, the response is better for structures in Figs. 4*a* and *b*. Accordingly, in the proposed general T-topology in Fig. 3*a*, the value of r that gives the best isolation performance is $r = [(n/2) - 1]$, where n is the total number of resonators. This is due to the existence of more resonators between the output ports.

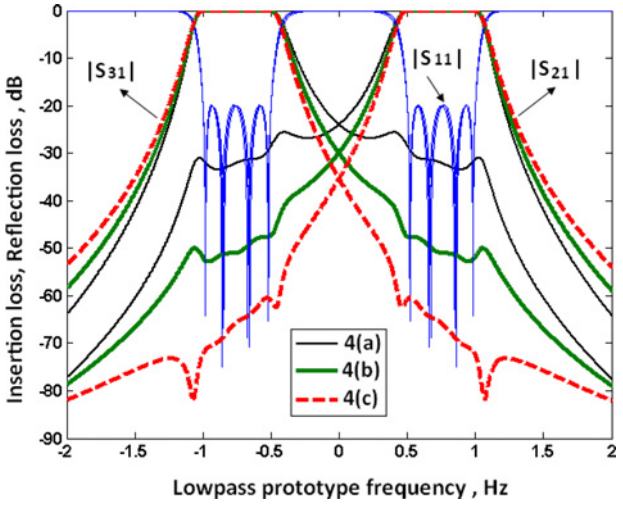

Fig. 5 *Responses of diplexers in Fig. 4*

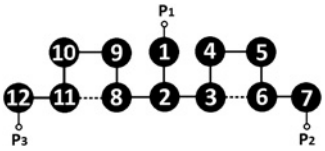

Fig. 6 *Twelve-resonator diplexer structure*

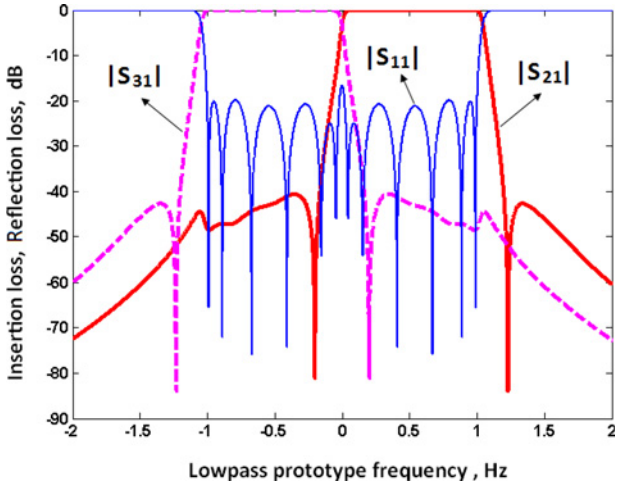

Fig. 7 *Response of contiguous diplexer*

Although the isolation performance degrades in comparison with the conventional diplexers, an advantage of the proposed diplexers is that the source is directly coupled to the input resonator (number 1). This is distinct from the diplexers reported in the literature, since there is no need to use an external junction (T-junction, manifold etc.) as in conventional diplexers, or to add a resonant junction (an extra resonator in addition to the channel filters) as in [16], or to directly connect the common port to one terminal of each of the channel filters, which may have practical constraints in implementation, as in [7]. Thus, the proposed diplexer exhibits a trade-off between design complexity and isolation performance.

A contiguous band diplexer has also been synthesised. The structure of the diplexer is shown in Fig. 6 and it is an example of the general topology in Fig. 3*b* with cross-coupling, $n = 12$ and $x = 0$. The cross-coupling (dashed line) between resonators 3 and 6, and resonators 8 and 11 generate transmission zeros to obtain a quasi-elliptic response.

The optimised normalised coupling coefficients are: $m_{12} = 0.8224$, $m_{23} = m_{28} = 0.4150$, $m_{34} = m_{89} = 0.2785$, $m_{45} = m_{9,10} = 0.3304$, $m_{56} = m_{10,11} = 0.2865$, $m_{67} = m_{11,12} = 0.4136$, $m_{36} = m_{8,11} = -0.0652$, $m_{33} = -m_{88} = 0.4638$ and $m_{44} = -m_{99} = 0.5148$, $m_{55} = -m_{10,10} = 0.5154$, $m_{66} = -m_{11,11} = 0.5088$, $m_{77} = -m_{12,12} = 0.5024$, and the normalised external quality factors are 0.994 at port 1 and 1.9881 at both ports 2 and 3. The response of the diplexer is shown in Fig. 7.

5 Implementation of unequal power divider

5.1 Power divider design and fabrication

A five-resonator unequal power divider has been designed, fabricated and tested. The divider has been designed according to the coupled resonator design methodology proposed here. It is designed at the X-band with a centre frequency of 10.15 GHz, bandwidth of 925 MHz, a reflection loss of 20 dB at the passband and $\alpha = 1.5$. The divider topology is that shown in Fig. 1 with $n = 5$, and the synthesised normalised coupling coefficients using optimisation are as follows: $m_{12} = 0.9116$, $m_{23} = 0.7005$, $m_{34} = 0.5766$, $m_{35} = 0.7061$ and $q_{e1} = q_{e4} = q_{e5} = 0.931$.

The power divider has been implemented using waveguide cavity resonators coupled together using capacitive irises. A photograph of the divider is shown in Fig. 9*a*. The device has been made of two mirror image pieces of copper, and metal screws have been used to tune its response.

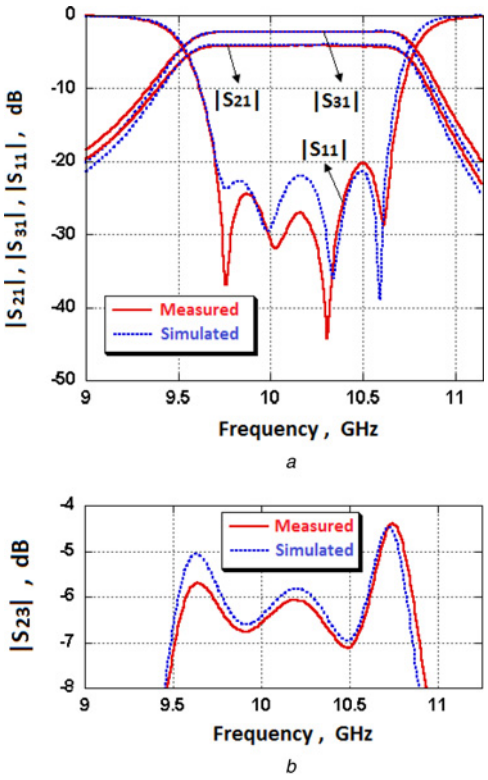

Fig. 8 *Power divider performance*

a Measured and simulated results of the power divider
b Power divider isolation

5.2 Power divider measurement

The simulated and measured results of the power divider are depicted in Fig. 8. The measured response has been tuned using metal screws and it is in good agreement with the simulated response. The experimental results show that the maximum return loss within the passband is 20 dB and the minimum insertion loss is 2.28 dB for S_{31} and 4.29 dB for S_{21}. The measured isolation between the output ports is more than 4.4 dB in the passband.

6 Implementation of X-band diplexer

6.1 Diplexer design and fabrication

An X-band non-contiguous diplexer has been designed using the new methodology presented with the following specifications: passband centre frequency of 9.5 GHz for channel 1 and 10.5 GHz passband centre frequency for

doi: 10.1049/iet-map.2010.0447

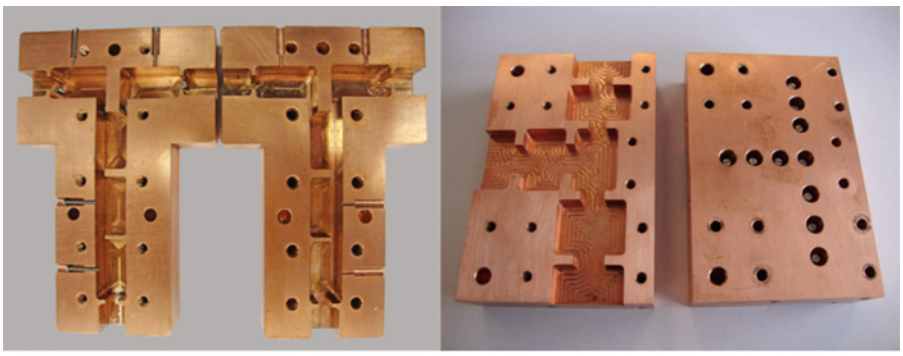

Fig. 9 *Photographs of the power divider and the diplexer*

a Unequal power divider
b Diplexer

channel 2, bandwidth of each channel is 52 MHz, and desired return loss at the passband of each channel is 20 dB.

The diplexer topology is that given in Fig. 3*a* with $n = 4$ and $r = 1$. The optimised normalised coupling coefficients are: $m_{12} = 1.3044$, $m_{23} = m_{24} = 0.1666$, $m_{33} = -m_{44} = 1.2894$ and the calculated normalised external quality factors are $q_{e1} = 4.651$, $q_{e3} = q_{e4} = 9.302$.

The diplexer has been implemented using waveguide cavity resonators coupled together using inductive apertures. A photograph of the physical diplexer is shown in Fig. 9*b*.

6.2 Diplexer measurement

The simulated and measured results of the diplexer are depicted in Fig. 10. The tuned measured response is in very good agreement with the simulated response. The measurements show that the passband of channel 1 has maximum return loss of 22 dB and minimum insertion loss of 0.38 dB, and that the passband of channel 2 has maximum return loss of 22 dB and minimum insertion loss of 0.43 dB. The losses in diplexer channels are mainly because of the conductor loss in small fractional bandwidth of each channel.

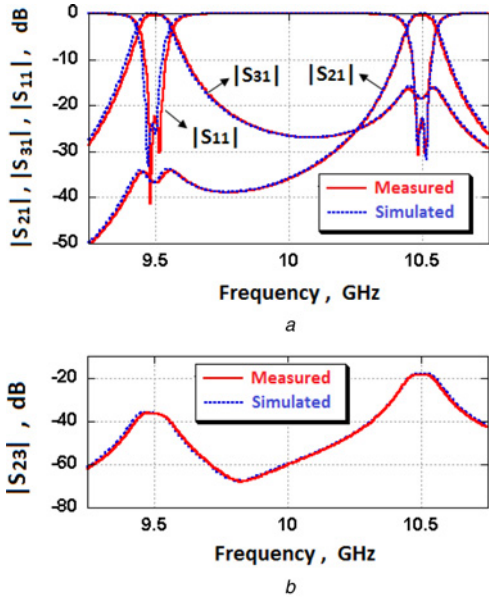

Fig. 10 *Performance of the diplexer*

a Measured and simulated results of the diplexer
b Diplexer isolation

7 Conclusion

The synthesis of multiple output coupled resonator circuits is presented in this study. Coupled resonator power dividers with arbitrary power division and diplexers with novel topologies have been synthesised using the coupling matrix optimisation technique. An X-band unequal power divider and diplexer have been designed, fabricated and tested to verify the design approach. More devices such as triplexers and multiplexers will be designed in the future using the same methodology.

8 Acknowledgments

The authors would like to thank Clifford Ansell for fabrication of devices. The UK Engineering and Physical Science Research Council supported part of this work.

9 References

1 Cameron, R., Kudsia, C., Mansour, R.: 'Microwave filters for communication systems' (Wiley, 2007)
2 Hong, J.S., Lancaster, M.J.: 'Microstrip filters for RF/microwave applications' (Wiley, 2001)
3 Amari, S.: 'Synthesis of cross-coupled resonator filters using an analytical gradient-based optimization technique', *IEEE Trans. Microw. Theory Tech.*, 2000, **48**, (9), pp. 1559–1564
4 Atia, W.A., Zaki, K.A., Atia, A.E.: 'Synthesis of general topology multiple coupled resonator filters by optimization'. IEEE MTT-S Int. Microwave Symp., Baltimore, USA, 1998, pp. 821–824
5 Jayyousi, A.B., Lancaster, M.J.: 'A gradient-based optimization technique employing determinants for the synthesis of microwave coupled filters'. IEEE MTT-S Inter. Microwave Symp., USA, June 2004, pp. 1369–1372
6 Lancaster, M.J.: 'Radio frequency filter'. W.I.P.O patent WO/01/69712, 2001
7 Garcia-Lamperez, A., Salazar-Palma, M., Sarkar, T.K.: 'Analytical synthesis of microwave multiport networks'. IEEE MTT-S Int. Microwave Symp. Digest, USA, June 2004, pp. 455–458
8 Garcia-Lamperez, A., Salazar-Palma, M., Sarkar, T.K.: 'Compact multiplexer formed by coupled resonators with distributed coupling'. IEEE Antennas and Propagation Society Int. Symp., USA, 2005, pp. 89–92
9 Syms, R.R.A., Shamonina, E., Solymar, L.: 'Magneto-inductive waveguide devices', *IEE Proc. Microw. Antennas Propag.*, 2006, **153**, (2), pp. 111–121
10 Pozar, D.M.: 'Microwave engineering' (Wiley, 1998, 2nd edn.)
11 Wilkinson, E.J.: 'An N-way hybrid power divider', *IRE Trans. Microw. Theory Tech.*, 1960, **8**, (1), pp. 116–118
12 Skaik, T., Lancaster, M., Huang, F.: 'Coupled-resonator 3-dB power divider'. Proc. IET seminar on Passive RF and Microwave Components, Birmingham, UK, April 2010

13 Mansour, R.R., Ye, S., Dokas, V., *et al.*: 'Design considerations of superconductive input multiplexers for satellite applications', *IEEE Trans. Microw. Theory Tech.*, 1996, **44**, (7), pp. 1213–1229
14 Rhodes, J.D., Levy, R.: 'Design of general manifold multiplexers', *IEEE Trans. Microw. Theory Tech.*, 1979, **27**, (2), pp. 111–123
15 Chi-Feng, C., Ting-Yi, H., Chi-Ping, C., Ruey-Beei, W.: 'Microstrip diplexers design with common resonator sections for compact size, but high isolation', *IEEE Trans. Microw. Theory Tech.*, 2006, **54**, (5), pp. 1945–1952
16 Macchiarella, G., Tamiazzo, S.: 'Novel approach to the synthesis of microwave diplexers', *IEEE Trans. Microw. Theory Tech.*, 2006, **54**, (12), pp. 4281–4290
17 Cameron, R.J.: 'General coupling matrix synthesis methods for Chebyshev filtering functions', *IEEE Trans. Microw. Theory Tech.*, 1999, **47**, (4), pp. 433–442
18 Mathworks Inc.: 'MATLAB 9 user's guide'. Available at http://www.mathworks.com
19 Collin, R.E.: 'Foundations for microwave engineering' (John Wiley & Sons, 2001, 2nd edn.)

doi: 10.1049/iet-map.2010.0447

MILLIMETER WAVE MULTIPLEXER WITH PRINTED CIRCUIT ELEMENTS FOR THE 88 TO 100 GHZ FREQUENCY RANGE

L. D. Cohen, N. Worontzoff, J. Levy and A. Harvey

Eaton Corporation AIL Division
Deer Park, N.Y. 11729

ABSTRACT

An 88 to 100 GHz contiguous triplexer that uses printed circuit elements has been developed and demonstrates the practicality of millimeter wave multiplexers. The triplexer is composed of an E-plane, 7-pole, dual band-pass filter, a common junction diplexer and two H-plane quadrature hybrids. The filter and hybrid circuit elements are printed on metal cards. This multiplexer technology is extendible to 140 GHz.

INTRODUCTION

There is an emerging need for high performance multiplexers for millimeter wave channelized receivers. The practicality of such receivers has been advanced with the development of an 88 to 100 GHz contiguous triplexer that uses printed circuit elements. The triplexer demonstrates that high quality performance, simple fabrication and assembly, small size and low cost can be achieved at millimeter wavelengths.

DISCUSSION

The configuration of the 88 to 100 GHz triplexer is shown in Figure 1. It consists of a hybrid coupled dual band-pass filter that passes the 92 to 96 GHz portion of the input frequency band and a common junction diplexer for separation of the remaining band into the 88 to 92 GHz and 96 to 100 GHz channels. This sequence of channel dropping provided a 4 GHz guard band between the channels to be seprated in the common junction diplexer and thereby minimized channel interaction effects.

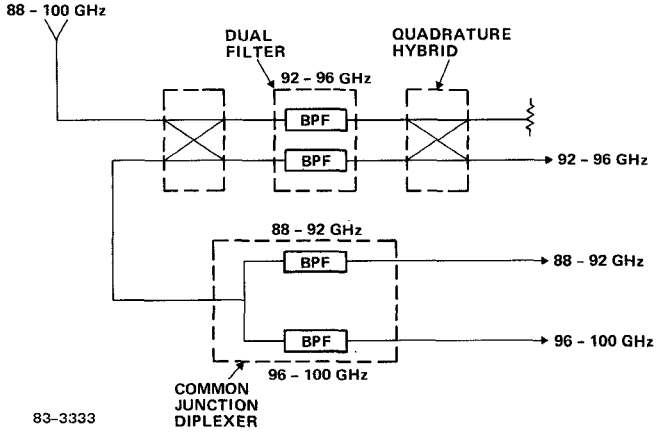

Figure 1. Block Diagram of Printed Element 88 to 100 GHz Triplexer

The work to be reported with the 88 to 100 GHz triplexer both enhances and extends previously reported multiplexer results in the 26 to 60 GHz range (ref. 1 to 4) in which cascaded sections of printed element, hybrid coupled filters were used for the channelization process. The present work extends multiplexer realization to 100 GHz, and includes the development of a common junction diplexer that provides a means to simplify multiplexer construction and reduce its size for the channelization process. The common junction diplexer is used in combination with hybrid coupled filters. This approach is advantageous in the millimeter waveguide bands where a large number of channels may be involved. As compared to multiplexing by use of only hybrid coupled filters, the combined approach provides for smaller size and lower channel loss by eliminating many hybrids. This multiplexer technology is also significantly less mechanically complex and less costly then a waveguide cavity type millimeter wave multiplexer that has been reported (ref. 6). Performance characteristics of the multiplexer technology over a temperature range of -54 to +95°C will also be reported.

The triplexer shown in Figure 1 used E-plane filters and H-plane (broadwall) qudrature hybrids couplers. The band-pass filters were printed on 1 mil thick copper cards and were designed for 7-pole, 0.1 dB ripple Tchebycheff response. The design follows the procedure described in ref. 2 which is based on Knoishi's model (ref. 5). The all metal printed cards offers about 50 percent higher Q than a metal clad dielectric backed card (ref. 7) and was a key factor in maintaining low passband loss (1 dB) at 100 GHz. The hybrid was printed on a 3-mil thick copper card and consisted of a 2 x 10 array of coupling apertures.

The filter and hybrid cards were printed by standard photolithographic and chemical etching techniques. Typical printed filter and hybrid cards, from batch processed sheets, that were used in the millimeter triplexer are shown in the right side of Figure 2. Filter and hybrid cards used in

0149-645X/84/0000-0187 $01.00 © 1984 IEEE

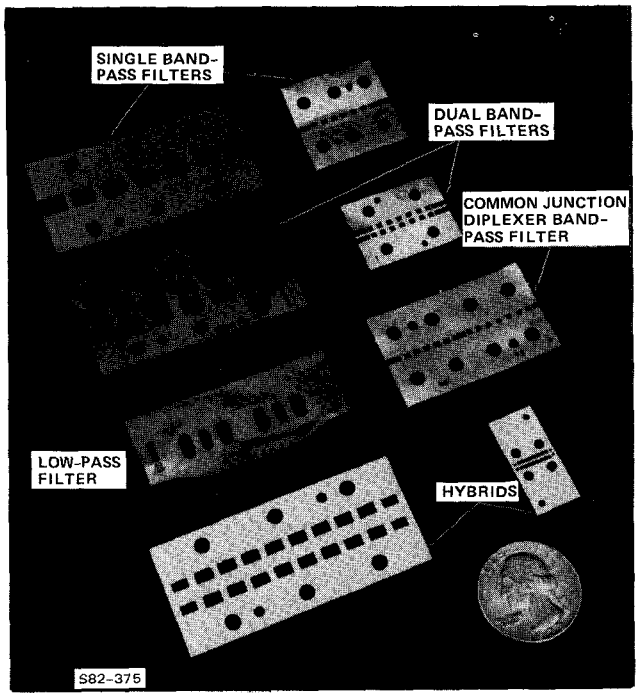

Figure 2. Typical Printed Filter and Hybrid Cards for Microwave and Millimeter Band Multiplexers

a K-band (18 to 26 GHz) multiplexer are shown in the left side of the figure. This figure illustrates the broad frequency range (18 to 100 GHz) over which this technology has been used and the relative size of the filter and hybrid elements at microwave and millimeter wavelengths. Our experience has shown that filters can be realized with smaller size in the microwave region by use of other transmission mediums, such as suspended substrate stripline, but with a tradeoff on performance. Comparative measurements in Ka-band (26 to 40 GHz) of E-plane and suspended substrate filters showed that suspended substrate filters exhibited approximately 0.4 dB higher passband loss and 50 percent higher frequency/temperature sensitivity ($\pm$18 ppm/°C). Dimensional constraints and mode problems make transmission mediums such as suspended substrate stripline impractical for filters and hybrids in W-band (75 to 110 GHz). However, the all metal E-plane filters and H-plane hybrids have remained a viable approach through the microwave region and have exhibited mode free, high quality performance and fabrication simplicity to 100 GHz. Based on the results obtained with the triplexer, it is projected that this multiplexer technology is usable to 140 GHz.

Beryllium copper was used for the K- and Ka-band filter and hybrid cards, but pure copper was used for the millimeter triplexer cards because of its lower dissipative loss. Triplexer filter cards fabricated from beryllium copper exhibited 0.8 dB higher loss than cards fabricated from pure copper. The 92 to 96 GHz dual band-pass filter element shown in Figure 1 was printed on a common card and was assembled in a housing with a common broadwall. A dual filter assembly is shown in Figure 3. The filter card is self jigging on dowel pins in the housing. The simple mechanical form, fabrication and assembly at millimeter wavelengths is noteworthy. The quadrature hybrid and common junction diplexer were of similar constructional form. The hybrid was one half the volume of the dual filter assembly shown in Figure 3. The hybrid was split along the H-plane and its printed card with coupling apertures formed the common broadwall between parallel waveguide sections.

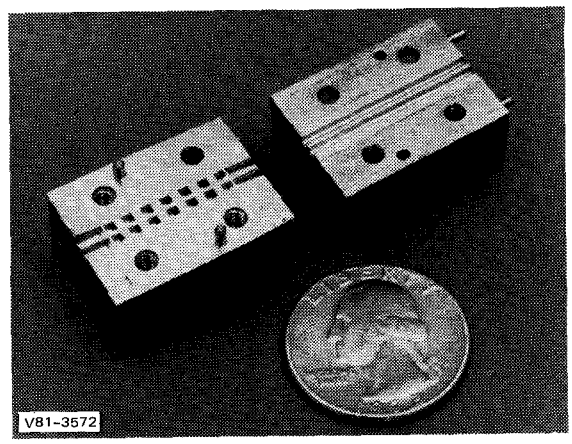

Figure 3. MM Wave Dual Band-Pass Filter

A diagrammatic representation of the common junction diplexer and its filter card is shown in Figure 4. A printed filter card is shown in Figure 2. The filter card contains two 7-pole band-bass filters that are suitably spaced from each other to minimize their interaction.

The performance of the band-pass filters is typified by the measured performance of a 96 to 100 GHz filter shown in Figure 5. The average midband insertion loss was 1 db and return loss was 15 to 30 dB over the 4 GHz passband. Out of band rejection was greater than 40 dB to the measurement frequency limits of 90 to 104 GHz.

The swept response of the triplexer over the 91 to 104 GHz frequency limits of a sweep generator is shown in Figure 6. The average passband loss was 2 dB in the 92 to 96 GHz channel, which is the combined loss of the dual filter (1 dB) and the input and output hybrids (0.5 dB/hybrid). The average passband loss of the 96 to 100 GHz channel was 2.5 dB which comprises the loss of the common junction diplexer and two passes through the input hybrid. Channel response in the 88 to 92 GHz band is not shown in Figure 6 due to sweeper limitations, but its response was similar to that shown for the 96 to 100 GHz channel (complementary common junction diplexer channels).

The fabrication experience and performance obtained with the 88 to 100 GHz triplexer indicate that is is feasible to extend this multiplexer technology to 140 GHz.

Frequency/temperature performance of the triplexer filters has not been measured. However,

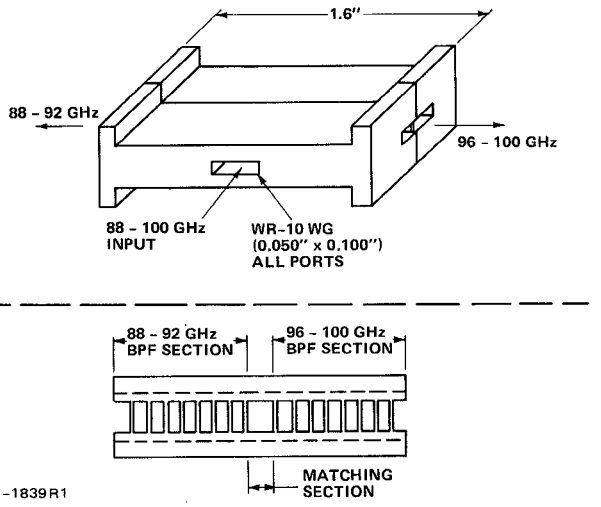

Figure 4. MM Wave Common Junction Diplexer

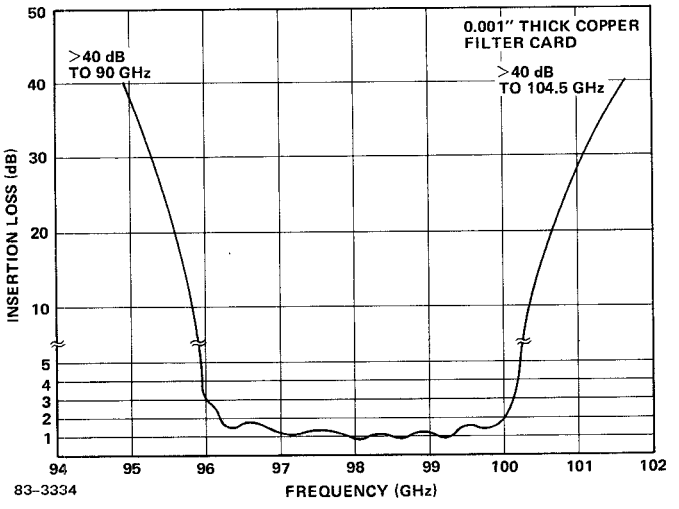

Figure 5. Printed E-plane Band-Pass Filter Measured Performance

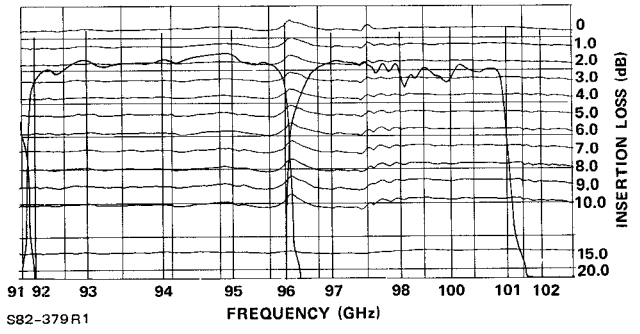

Figure 6. Swept Frequency Response of Millimeter Wave Triplexer

performance should be comparable to the measured performance of printed filters of a similar design for the 18 to 40 GHz range which exhibited a frequency/temperature sensitivity of ±12.5 ppm/°C over a temperature range of -54 to +95°C. Amplitude tracking between individual multiplexers in this lower frequency range was within ±0.3 dB and the variation in crossover frequency between units was within ±25 MHz. The close tracking performance and good frequency/temperature stability was the result of the printing of the multiplexer circuit elements and the absence of any adjustable tuning elements, technology features that were also in the 88 to 100 GHz triplexer.

SUMMARY

The design and performance of an 88 to 100 GHz triplexer has been described. The basic components comprising the triplexer are a common junction diplexer and a hybrid coupled channel dropping filter. The use of printed filter and hybrid circuit elements has reduced multiplexer fabrication to a simple and low-cost level, while providing a high level of performance and small size at millimeter wavelengths. The results obtained indicate that the technology is extendible to 140 GHz. The practicality of channelized receivers at millimeter wavelengths has been advanced by the reported triplexer technology and should have wide application in the emerging needs for receivers in the millimeter bands.

ACKNOWLEDGEMENTS

This work was performed at the Eaton Corporation AIL Division in Melville, NY, under the direction of J. Whelehan and G. Irvin. Technical consultation was provided by J. Taub. Technical assistance was provided by A. Cooley and J. Pfeifer.

REFERENCES

1. J. Reindel, "Printed Circuit Waveguide Components," NOSC Technical Note 581, December 1978.

2. K. Breuer and N. Worontzoff, "A Low-Cost Multiplexer for Channelized Receiver Front-Ends at Millimeter Waves," 1980 IEEE MTT-S International Microwave Symposium Digest, p. 150.

3. J. Reindel, "Printed WG Circuits Trim Component Costs," Microwaves, October 1980, pp. 60-63.

4. P. Meier, L. Cohen, et al., "Millimeter Wave Channelized Receiver with Planar Integrated Circuit Components," Microwave System News, December 1981, Vol. II, No. 12.

5. Y. Konishi and K. Uenakada, "The Design of a Band-Pass Filter with Inductive Strip--Planar Circuit Mounted in Waveguide," IEEE Trans. MTT, Vol. MTT-22, No. 10, pp. 869-873, October 1974.

6. J. Bratherton, "Waveguide Filters for MM Wavelengths, " Microwave Journal, Vol, 25, No. 7, July 1982, pp. 91-95.

7. P.J. Meier, "New Developments with Integrated Fin-Line and Related Printed Millimeter Circuits," Digest of IEEE 1975 MTT-S International Microwave Symposium, pp. 143-145, May 1975.

REFERENCES

[1] J. D. Rhodes, "Direct design of symmetrical interacting bandpass channel diplexers," *Inst. Elec. Eng. J. Microwaves, Opt. Acous.*, vol. 1, no. 1, pp. 34–40, Sept. 1976.

[2] J. L. Haine and J. D. Rhodes, "Direct design formulas for asymmetric bandpass channel diplexers," *IEEE Trans. Microwave Theory Tech.*, vol. MTT-25, pp. 807–813, Oct. 1977.

[3] J. D. Rhodes and R. Levy, "General manifold multiplexers," this issue, pp. 111–123.

[4] J. D. Rhodes, *Theory of Electrical Filters*. New York: Wiley, 1976.

[5] R. J. Wenzel and W. G. Erlinger, "Narrowband contiguous multiplexing filters with arbitrary amplitude and delay response," *1976 IEEE MTT-S Int. Microwave Symp. Digest*, pp. 116–118.

[6] G. L. Matthaei and E. G. Cristal, "Theory and design of diplexers and multiplexers," in *Advances in Microwaves*, vol. 2, Leo Young, Ed. New York and London: Academic Press, 1967, pp. 237–326.

[7] R. Sato and E. G. Cristal, "Simplified analysis of coupled transmission-line networks," *IEEE Trans. Microwave Theory Tech., vol. MTT-18, pp.* 122–131, *Mar.* 1970.

[8] E. G. Cristal, "New design equations for a class of microwave filters," *IEEE Trans. Microwave Theory Tech.*, vol. MTT-19, pp. 486–490, May 1971.

Design of General Manifold Multiplexers

J. DAVID RHODES, MEMBER, IEEE, AND RALPH LEVY, FELLOW, IEEE

Abstract—**The direct analytical design process for arbitrary multiplexers given in a previous paper is extended to the case of bandpass channel filters connected to a uniform-impedance manifold (e.g., a length of waveguide or transmission line). The previous approximations are greatly improved by adding immittance compensation in a way which not only preserves the canonic form of the network but also assists in the physical construction by spacing the filters along a manifold. The phase shifters between channels are themselves sufficient to compensate the filter interactions to such an extent that contiguous channeling cases are designable. The results are presented mainly in closed form requiring minimal computer optimization.**

Analysis of multiplexers with frequency-dependent manifolds indicate that there are restrictions on the total bandwidth, but a ten-channel multiplexer is probably feasible, suitable for input and output multiplexers required in typical communications systems. Practical results on a simple manifold triplexer are presented.

I. INTRODUCTION

In the previous paper [1] it was shown that there are inherent limitations to the canonic matching of a multiplexer consisting of a number of filters connected directly in series or parallel. We may define canonic matching as that requiring only changes to the parameters of the filters and not adding extra immittance compensation networks. In this paper immittance compensation is introduced, but in a way which not only preserves the canonic form of the network but also assists in the physical construction by spacing the filters along a manifold. The phase shifters between channels are sufficient to compensate the multiplexer to such an extent that contiguous channeling cases are designable by the theory.

It is interesting to consider various approaches to the design of multiplexers, particularly on a manifold feed. Due to requirements in communication satellites and elsewhere, many attempts have been made to produce such multiplexers. One important and difficult requirement is that of an output multiplexer on a waveguide manifold with bandpass channels separated to yield guardbands of only 10 percent. Most design techniques have adopted an approach based upon singly terminated bandpass channels resulting in 3-dB crossover points between channels, e.g., [2], [3]. Such designs exhibit good return loss over the channel bandwidths and the guardbands. Also, dummy channels have to be included to simulate channels at the edges of the total multiplexer bandwidth, forming an additional annulling network. Thus redundant elements are necessary, and the channel interactions are compensated to produce a channel performance comparable to the individual channels based upon a singly terminated prototype.

The need for contiguous band multiplexers originally arose in receiver design for countermeasures where the incoming signal was unknown and complete band coverage was necessary with good match at all frequencies. Here all channels have to be designed on a singly terminated basis and must provide a prescribed level of attenuation over the major part of other bands.

However, the requirements for multiplexers in communication systems are different since they must provide

Manuscript received April 3, 1978; revised July 24, 1978.

J. D. Rhodes is with the Department of Electrical and Electronic Engineering, the University of Leeds, Leeds LS2 9JT, England.

R. Levy is with the Microwave Development Laboratories, Natick, MA 01760.

0018-9480/79/0200-0111$00.75 ©1979 IEEE

good reflection and transmission only over each channel bandwidth while maintaining high attenuation over all other channels. For typically realizable passband return loss specifications (e.g., 20–25 dB), the *optimum* solution leads to attenuation in excess of 10 dB at the crossover frequencies independent of the guardband bandwidth. Thus contiguous band multiplexers are *nonoptimum* in this situation and have probably been used because a design procedure was known. They result in a higher degree filter than necessary in each channel in addition to the annulling network. Furthermore, if one attempts to use singly terminated designs for crossover levels in excess of 3 dB, the passband return loss rapidly deteriorates if further annulling networks are not used.

The significant difference between the optimum design approach and the contiguously designed solution to the above type of problem may be illustrated by the simple diplexer examples presented in [4, Figs. 4 and 5]. For the case of two noncontiguous bandpass channels of bandwidth 2 and guardband of 1, five-cavity Chebyshev filters may produce a return loss >25 dB over each passband while >34-dB attenuation is achieved over the opposite channel [4, Fig. 4], whereas the contiguous approach using similar five-cavity filters gives an attenuation level over the opposite channel of only 19 dB [4, Fig. 5]. Thus the price paid for preserving the good 25-dB return loss at the common port over the guardband region is a 15-dB reduction in the attenuation level in the stopband! Hence, for most applications in communication systems, contiguous band multiplexers result in designs far from the optimum solution.

The alternative approach described here is an extension of the companion paper [1] and similarly commences from doubly terminated prototype filters. Modifications are then made to all elements when the manifold is designed. Criteria used in this approach are that multiplexers having an arbitrary number of channels with different bandwidths and variable center frequency spacings should be designable, and that the individual passband performances should be maintained from the case of large guardbands down to contiguous crossovers. In addition to the 6-dB improvement in stopband attenuation levels over frequency bands where a passband exists elsewhere in the multiplexer (given by any type of design due to power division between the in-band and out-of-band channels), further improvement in attenuation due to compensation of the interaction between channels should be expected.

II. Manifold Theory Applied to Frequency-Independent Manifolds

The theory for the manifold multiplexer is identical with that of the directly coupled multiplexer up to (15) and (17) of [1], which form the in-band and out-of-band input admittances of the channel filters. It is necessary to refer also to [1, Figs. 1–4] for definitions of the terminology. However, rather than employing direct parallel connection as in [1, Fig. 4], we form the manifold multiplexer

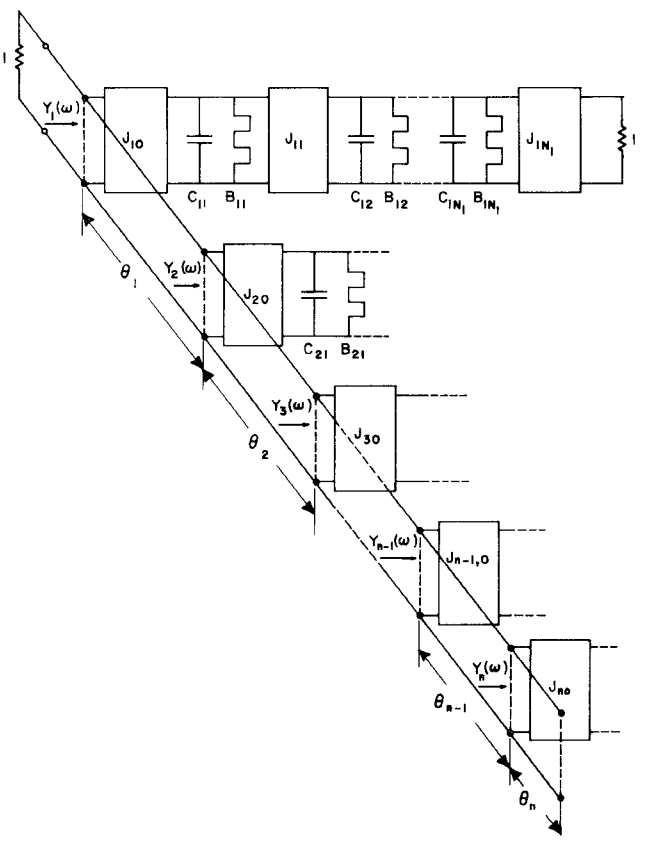

Fig. 1. Prototype manifold multiplexer.

shown in Fig. 1. $Y_m(\omega)$ is the imput admittance of the mth channel as a function of frequency. The transfer matrix of the mth, unity impedance phase shifter may be written as

$$\frac{1}{\sqrt{1+B_m^2\alpha^{-2}}}\begin{bmatrix} 1 & jB_m\alpha^{-1} \\ jB_m\alpha^{-1} & 1 \end{bmatrix} \tag{1}$$

where

$$\theta_m = \tan^{-1}\left(B_m\alpha^{-1}\right). \tag{2}$$

Initially the manifold is assumed to be frequency independent and of uniform inpedance. Modifications to the design process will be made at a later stage to account for the frequency dependence of the manifold. Note that as $\alpha\to\infty$ (the case of decoupled channels), $\theta_m\to 0$ or an integral multiple of π, i.e., the channels are effectively connected in parallel as in [1]. $\alpha=1$ gives the actual situation to be determined.

An additional n parameters $B_1, B_2, \cdots, B_n$ appear to have been obtained by connecting the filters on to a manifold, but later it will be shown that one of these is redundant.

If the rth channel is in band, then

$$Y_r = Y_r(\Omega_r\alpha + \omega_t) \tag{3}$$

as given by [1, eq. (15)] while the admittance of the rest of the channels which are out of band are given by

$$\overline{Y}_m = Y_m(\Omega_m\alpha + \omega_t) \tag{4}$$

with $m=1,\cdots,r-1,r+1,\cdots,n$ and $\bar{Y}_m$ is given by [1, eq. (17)]. The transfer matrix of the network at the set of frequencies $(\Omega_r\alpha+\omega_i)$ will now be derived. The transfer matrix for the mth channel admittance followed by the mth phase shifter is

$$[T_m]=\frac{1}{\sqrt{1+B_m^2\alpha^{-2}}}\cdot\begin{bmatrix}1 & jB_m\alpha^{-1}\\ jB_m\alpha^{-1}+\bar{Y}_m & 1+\dfrac{\alpha^{-2}B_m}{C_{m1}(\Omega_r-\Omega_m)}-\dfrac{\omega_i\alpha^{-3}B_m}{C_{m1}(\Omega_r-\Omega_m)^2}\end{bmatrix} \tag{5}$$

and the matrix possesses an error of order α^{-4}.

For the first $r-1$ channels we have a transfer matrix

$$\frac{1}{F}\begin{bmatrix}A & B\\ C & D\end{bmatrix}=\prod_{m=1}^{r-1}[T_m] \tag{6}$$

where by analysis, for errors up to α^{-4}, we have a lossless transfer matrix of the form

$$\begin{aligned}F&=1+\frac{1}{2}\sum_{m=1}^{r-1}B_m^2\alpha^{-2}\\ A&=1+a_1\alpha^{-2}-a_2\omega_i\alpha^{-3}\\ B&=j\sum_{m=1}^{r-1}B_m\alpha^{-1}+jb_1\alpha^{-3}\\ C&=j\sum_{m=1}^{r-1}B_m\alpha^{-1}+\sum_{m=1}^{r-1}\bar{Y}_m-jc_1\alpha^{-3}\\ D&=1+d_1\alpha^{-2}-\omega_i d_2\alpha^{-3}\end{aligned} \tag{7}$$

where

$$\begin{aligned}a_1&=\sum_{m=2}^{m-1}\frac{\sum_{i=1}^{m-1}B_i}{C_{m1}(\Omega_r-\Omega_m)}-\sum_{m=2}^{r-1}\left(B_m\sum_{i=1}^{m=1}B_i\right)\\ a_2&=\sum_{m=2}^{r-1}\frac{\sum_{i=1}^{m-1}B_i}{C_{m1}(\Omega_r-\Omega_m)^2}\\ b_1&=\sum_{m=2}^{r-1}B_m\cdot\left[\sum_{j=2}^{m}\frac{\sum_{i=1}^{j-1}B_i}{C_{j1}(\Omega_r-\Omega_j)}-\sum_{j=2}^{m-1}\left(B_j\sum_{i=1}^{j-1}B_i\right)\right]\\ c_1&=\sum_{m=2}^{r=1}\left[\left(\frac{1}{C_{m1}(\Omega_r-\Omega_m)}-B_m\right)\right.\\ &\quad\left.\cdot\left[\sum_{j=1}^{m=1}\frac{\sum_{i=j}^{m-1}B_i}{C_{j1}(\Omega_r-\Omega_j)}-\sum_{j=2}^{m=1}\left(B_j\cdot\sum_{i=1}^{j-1}B_i\right)\right]\right]\end{aligned}$$

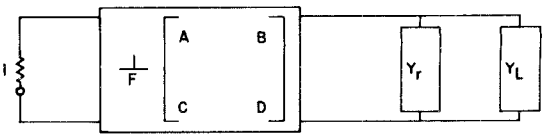

Fig. 2. Approximate equivalent circuit of manifold at frequencies in the rth-channel passband.

$$\begin{aligned}d_1&=\sum_{m=1}^{r-1}\frac{\sum_{i=m}^{r-1}B_i}{C_{m1}(\Omega_r-\Omega_m)}-\sum_{m=2}^{r-1}\left(B_m\cdot\sum_{i=1}^{m=1}B_i\right)\\ d_2&=\sum_{m=1}^{r=1}\frac{\sum_{i=m}^{r-1}B_i}{C_{m1}(\Omega_r-\Omega_m)^2}.\end{aligned} \tag{8}$$

We may proceed with a similar analysis for the network after the rth channel. However, we require only the input admittance which is given by

$$Y_L=\frac{C'}{A'} \tag{9}$$

with

$$\begin{aligned}A'&=1+a_1'\alpha^{-2}-a_2'\omega_i\alpha^{-3}\\ C'&=j\sum_{m=r}^{n}B_m\alpha^{-1}+\sum_{m=r+1}^{n}\bar{Y}_m-jC_1'\alpha^{-3}\end{aligned} \tag{10}$$

where

$$\begin{aligned}a_1'&=\sum_{m=r+1}^{n}\frac{\sum_{i=r}^{m-1}B_i}{C_{m1}(\Omega_r-\Omega_m)}-\sum_{m=r+1}^{n}\left(B_m\cdot\sum_{i=}^{m=1}B_i\right)\\ a_2'&=\sum_{m=r+1}^{n}\frac{\sum_{i=r}^{m-1}B_i}{C_{m1}(\Omega_r-\Omega_m)^2}\\ C_1'&=\sum_{m=r+2}^{n}\left[\left(\frac{1}{C_{m1}(\Omega_r-\Omega_m)}-B_m\right)\right.\\ &\quad\left.\cdot\left[\sum_{j=r+1}^{m}\frac{\sum_{i=4}^{m=1}B_i}{C_{j1}(\Omega_r-\Omega_j)}-\sum_{j=r+1}^{m}\left(B_j\cdot\sum_{i=r}^{j-1}B_i\right)\right]\right]\end{aligned} \tag{11}$$

and Y_L is a reactance function up to the order α^{-4}.

We now have the network shown in Fig. 2, and at the set of frequencies $\omega=\Omega_r\alpha+\omega_i$ we require the common port reflection coefficient and the rth channel port reflection coefficient to be zero. Since up to the order of approximation the networks given by (6) and (9) are lossless, we need only apply the condition of a conjugate match at any plane in the network. Applying this condition at the junction with the rth port we have

$$Y_r=\frac{A-C}{D-B}-\frac{C'}{A'}. \tag{12}$$

Expanding the right-hand side of the equation as a power series in α^{-1} and comparing with the expansion of Y_r in [1, (15)] yields

1) α^{-1} *term:*

$$C_{r1}\beta_{r11} = \sum_{m=1\neq r}^{n} \frac{1}{C_{m1}(\Omega_r - \omega m)} - \sum_{m=r}^{n} B_m \tag{13}$$

2) $\alpha^{-2}\omega_t$ *term:*

$$\gamma_{r12}C_{r1} = \sum_{m=1\neq r}^{n} \frac{1}{C_{m1}(\Omega_r - \Omega_m)^2} \tag{14}$$

3) α^{-2} *term:*

$$\gamma_{r12} - \gamma_{r02} - C_r^2 1\beta_{r11}^2 = a_1 - d_1 - \sum_{m=1}^{r-1} B_m \cdot \sum_{m=1}^{r-1} \frac{1}{C_{m1}(\Omega_r - \Omega_m)} \tag{15}$$

4) $\alpha^{-3}\omega_t^2$ *term:*

$$\frac{C_{r1}^2 C_{r2}\beta_{r23}}{J_{r1}^2} = \sum_{m=1\neq r}^{n} \frac{1}{C_{m1}(\Omega_r - \Omega_m)^3} \tag{16}$$

5) $\alpha^{-3}\omega_t$ *term:*

$$\frac{-2C_{r1}C_{r2}\beta_{r23}}{J_{r1}^2} + 2C_{r1}^2\beta_{r11}\gamma_{r12} = d_2 - a_2 + \sum_{m=1}^{r-1} B_m \cdot \sum_{m=1}^{r-1} \frac{1}{C_{m1}(\Omega_r - \Omega_m)^2} \tag{17}$$

6) α^{-3} *term:*

$$C_{r1}\beta_{r13} - \frac{C_{r2}\beta_{r23}}{J_{r1}^2} + 2C_{r1}\beta_{r11}\gamma_{r12} - \gamma_{r02}C_{r1}\beta_{r11} - C_{r1}^3\beta_{r11}^3 = \sum_{m=1\neq r}^{n} \left[\frac{1}{C_{m1}(\Omega_r - \Omega_m)} \left(-\gamma_{m02} + \frac{\beta_{m11}}{(\Omega_r - \Omega_m)} + \frac{J_{m1}^2}{C_{m1}C_{m2}(\Omega_r - \Omega_m)^2} \right) \right] + c_1 + c_1' - a_1' \cdot \sum_{m=r+1}^{n} \frac{1}{C_{m1}(\Omega_r - \Omega_m)} + a_1' \sum_{m=r}^{n} B_m + b_1 - d_1 \sum_{m=1}^{r-1} \frac{1}{C_{m1}(\Omega_r - \Omega_m)} + (a_1 + d_1) \sum_{m=1}^{r-1} B_m - \left(\sum_{m=1}^{r-1} B_m \right)^2 \sum_{m=1}^{r-1} \frac{1}{C_{m1}(\Omega_r - \Omega_m)} \cdot \tag{18}$$

Applying the above set of equations for $r = 1 \rightarrow n$ leads to $6n$ equations with up to $6n$ unknowns. Since these are linear simultaneous equations we may attempt to obtain direct expressions for the unknown quantities.

Substituting for a_2 and d_2 from (8) into (17) gives

$$\frac{-C_{r1}C_{r2}\beta_{r23}}{J_{r1}^2} + C_{r1}^2\beta_{r11}\gamma_{r12} = \sum_{m=1}^{r-1} \frac{\sum_{\iota=m}^{r-1} B_\iota}{C_{m1}(\Omega_r - \Omega_m)^2} \cdot \tag{19}$$

Defining a new function P_r as

$$P_r = \sum_{m=1\neq r}^{n} \frac{1}{C_{m1}(\Omega_r - \Omega_m)^2} \cdot \sum_{m=1\neq r}^{n} \frac{1}{C_{m1}(\Omega_r - \Omega_m)} - \frac{1}{C_{r1}} \cdot \sum_{m=1\neq r}^{n} \frac{1}{C_{m1}(\Omega_r - \Omega_m)^3} \tag{20}$$

and substituting for β_{r23} and γ_{r12} from (16) and (14), respectively, into (19) results in the set of equations

$$P_r - \sum_{m=r}^{n} B_m \cdot \sum_{m=1\neq r}^{n} \frac{1}{C_{m1}(\Omega_r - \Omega_m)^2} = \sum_{m=1}^{r-1} \frac{\sum_{\iota=m}^{r-1} B_\iota}{C_{m1}(\Omega_r - \Omega_m)^2} \qquad (r = 1, 2, \cdots, n). \tag{21}$$

If

$$H_r = \sum_{m=r}^{n} B_m \tag{22}$$

then (21) may be rearranged as

$$H_r = \frac{P_r - \sum_{m=1}^{r-1} \frac{H_m}{C_{m1}(\Omega_r - \Omega_m)^2}}{\sum_{m=r+1}^{n} \frac{1}{C_{m1}(\Omega_r - \Omega_m)^2}} \tag{23}$$

and hence H_r may be obtained for $r = 1 \rightarrow n-1$. H_n is, in general, indeterminate since the set of equations (21) on close inspection represent n equations with $n-1$ unknowns. From a network viewpoint this may readily be appreciated by considering the network shown in Fig. 1. The last phase shifter θ_n represents a frequency invariant reactance in parallel with the nth channel admittance $Y_n(\omega)$. Since this may be readily absorbed into the modification to the first admittance inverter and resonant frequency of the first cavity, this element is redundant and may be made zero, i.e.,

$$B_n = 0. \tag{24}$$

In the very special case of the diplexer

$$P_1 = \frac{(C_{11} - C_{12})}{C_{11}C_{12}^2(\Omega_1 - \Omega_2)^2} \qquad P_2 = \frac{C_{12}}{C_{11}} P_1 \tag{25}$$

and, consequently,

$$P_2 - \frac{H_1}{C_{11}(\Omega_2 - \Omega_1)^2} = 0 \tag{26}$$

enabling both equations given in (21) to be satisfied. For

the triplexer and above in the nth channel at the end of the manifold only five of the six conditions may be satisfied.

Combining (22) and (24) we have the final design for the manifold

$$B_r = H_r - H_{r+1} \tag{27}$$

with $r=1,2,\cdots,n-1$ and $H_n=0$.

Having solved for B_r, we may then substitute into (13) to obtain β_{r11} as

$$\beta_{r11} = \frac{1}{C_{r1}}\left[\sum_{m=1\neq r}^{n} \frac{1}{C_{m1}(\Omega_r-\Omega_m)} - \sum_{m=r}^{n} B_m\right] \tag{28}$$

and from (14) and (16)

$$\gamma_{r12} = \frac{1}{C_{r1}} \sum_{m=1\neq r}^{n} \frac{1}{C_{m1}(\Omega_r-\Omega_m)^2} \tag{29}$$

and

$$\beta_{r23} = \frac{J_{r1}^2}{C_{r1}^2 C_{r2}} \sum_{m=1\neq r}^{n} \frac{1}{C_{m1}(\Omega_r-\Omega_m)^3}. \tag{30}$$

Additionally, the substitution of (8) into (15) gives

$$\gamma_{r02} = \gamma_{r12} - C_{r1}^2\beta_{r11}^2 + 2\sum_{m=1}^{r-1} \frac{\sum_{i=m}^{r-1} B_i}{C_{m1}(\Omega_r-\Omega_m)}. \tag{31}$$

In principle, the set of equations (18) may be used to obtain β_{r13}, but these contain very tedious algebra. Since these equations result from the α^{-3} term, they represent a fine adjustment to the matching of each channel around midband, and, in general, this is more readily done by direct computer optimization of the circuit around the midband frequencies of each channel, as described later. Furthermore, since the $\alpha^{-3}\omega_i$ could not be satisfied for the nth channel, such optimization leads to a slightly improved performance.

A further fine improvement in the design formulas may be obtained by closer inspection of the expansions for Y_r and Y_m as given in [1, eqs. (15) and (17)]. If we assume that the resonant frequencies of all the resonators should be changed, then noting the format of [1, (11)], the following generalization is applied:

$$B_{rk} \rightarrow -C_{rk}(\Omega_r\alpha + \beta_{rkl}\alpha^{-l}) \tag{32}$$

where $l=2k-1$, $k=2,3,\cdots,N_r$. Similarly, if we assume that the admittance inverters should also change, then a generalization of [1, (9)] leads to

$$J_{rk}^2 \rightarrow J_{rk}^2(1-\gamma_{rkl}\alpha^{-l}) \tag{33}$$

where $l=2k$, $k=1,2,\cdots,N_r-1$. Now by expanding [1, (15) and (17)] to α^{-5} it becomes obvious that the extra correction terms above are associated only with the terms of highest degree in ω_i for each coefficient of α^{-l}. Thus in addition to [1, (19), (20), and (22)] which give

1) $\alpha^{-1}\omega_i^0$ *term:*

$$\beta_{r11} = \frac{1}{C_{r1}} \sum_{m=1\neq r}^{n} \frac{1}{C_{m1}(\Omega_r-\Omega_m)} \tag{34}$$

2) $\alpha^{-2}\omega_i$ *term:*

$$\gamma_{r12} = \frac{1}{C_{r1}} \sum_{m=1\neq r}^{n} \frac{1}{C_{m1}(\Omega_r-\Omega_m)^2} \tag{35}$$

3) $\alpha^{-3}\omega_i^2$ *term:*

$$\beta_{r23} = \frac{J_{r1}^2}{C_{r1}^2 C_{r2}} \sum_{m=1\neq r}^{n} \frac{1}{C_{m1}(\Omega_r-\Omega_m)^3} \tag{36}$$

we have also

4) $\alpha^{-4}\omega_i^3$ *term:*

$$\gamma_{r24} = \frac{J_{r1}^2}{C_{r1}^2 C_{r2}} \sum_{m=1\neq r}^{n} \frac{1}{C_{m1}(\Omega_r-\Omega_m)^4} \tag{37}$$

and

5) $\alpha^{-5}\omega_i^4$ *term:*

$$\beta_{r35} = \frac{J_{r1}^2 J_{r2}^2}{C_{r1}^2 C_{r2}^2 C_{r3}} \sum_{m=1\neq r}^{n} \frac{1}{C_{m1}(\Omega_r-\Omega_m)^5}. \tag{38}$$

The general expression for the higher order terms is now obvious. Actually, these are associated with the effect of the first resonators only of each out-of-band channel, since such resonators are responsible for the terms of highest degree in ω_i.

At this point it is useful to summarize the design process step-by-step.

1) Compute the values of P_r given by (20).

2) Compute the values of H_r given by (23) for $r=1,2,\cdots,n-1$ and $H_n=0$.

3) Then the B_r are given by (27).

4) The coefficients β_{r11}, γ_{r12}, β_{r23}, and γ_{r02} are given by (28)–(31).

5) The higher ordered correction terms γ_{rkl} with $l=2k$ and β_{rkl} with $l=2k-1$ which are defined in (32) and (33) are given by formulas such as (37) and (38), which are easily generalized to give

$$\gamma_{rkl} = \frac{1}{C_{rk}}\left(\prod_{s=1}^{k-1} \frac{J_{rs}^2}{C_{rs}^2}\right) \sum_{m=1\neq r}^{n} \frac{1}{C_{m1}(\Omega_r-\Omega_m)^l} \tag{39}$$

where $l=2k$ and

$$\beta_{rkl} = \frac{1}{C_{rk}}\left(\prod_{s=1}^{k-1} \frac{J_{rs}^2}{C_{rs}^2}\right) \sum_{m=1\neq r}^{n} \frac{1}{C_{m1}(\Omega_r-\Omega_m)^l} \tag{40}$$

where $l=2k-1$.

As stated earlier, in addition to the above design process, a further refinement may be made to ensure that the best possible performance is obtained about the band center frequencies. For out-of-band channels, one may truncate the filters after two or three cavities to produce a

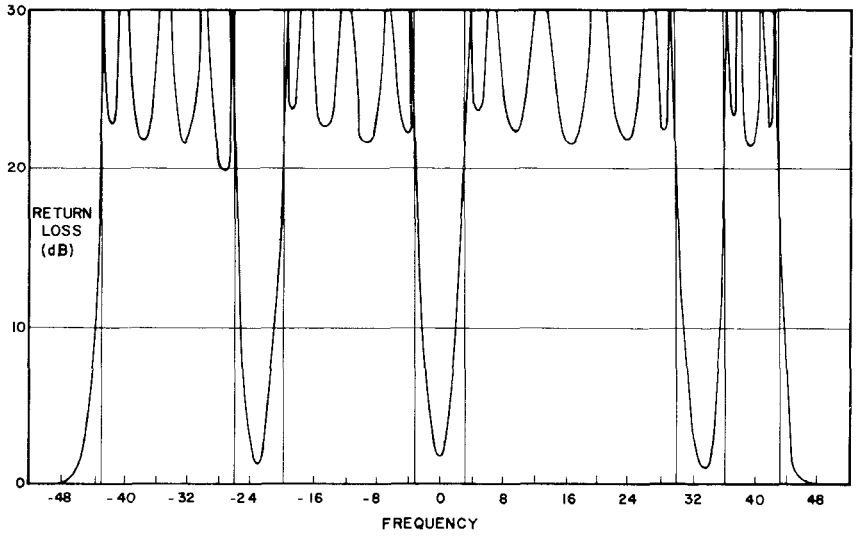

Fig. 3. Computer response for common port return loss of the four-channel manifold multiplexer.

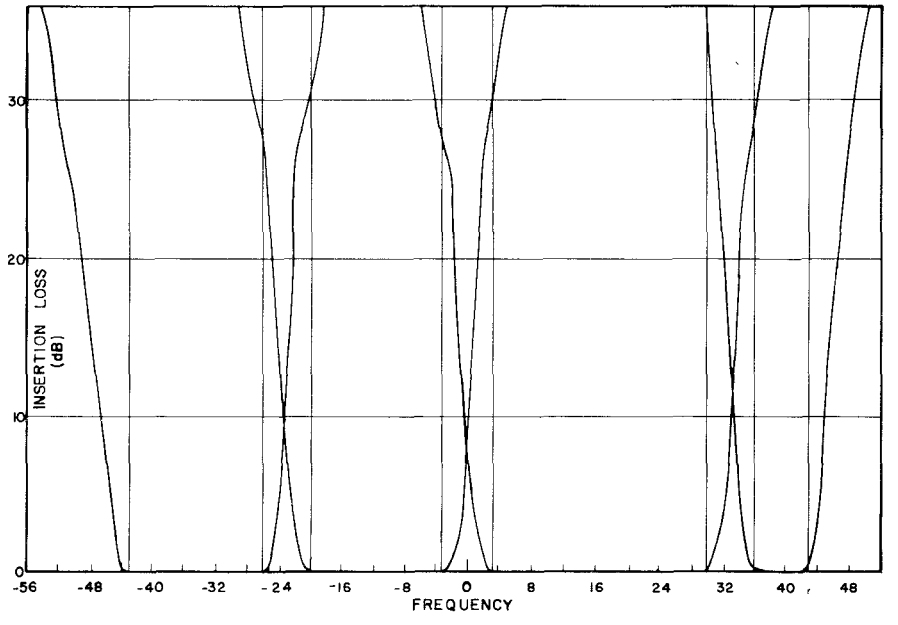

Fig. 4. Insertion loss response for each channel of the four-channel manifold multiplexer.

purely reactive loading on the manifold. Define Ω_{rk} as the resonant frequency of the kth resonator of channel r. Then in the odd-degree case J_{r0} and Ω_{r1} may be slightly modified to produce a conjugate match at the junction with the manifold at midband. For the even-degree case, J_{r1} and Ω_{r2} in addition may be modified to produce a conjugate match at the two frequencies closest to midband. This updating process may be performed channel by channel and, if necessary, may be repeated.

A computer program has been developed to evaluate all of the design formulas with the additional updating process described above. As an example, we may consider a four-channel prototype multiplexer with all channels being of the conventional Chebyshev type. The first channel to be dropped along the manifold from the common port is of fifth degree,[1] passband return loss of 22 dB, bandwidth 17, and center frequency -34.5. The three remaining channels in order are of degree 5, 6, and 4, bandwidths 17, 27, and 7, and center frequencies -11.5, 16.5, and 39.5, all designed with a passband return loss of 22 dB. The guardband between all channels is 6. This multiplexer has much closer relative channel spacings than any of the designs illustrated in [1]. The element values are given in Table I, and the computed response for the common port return loss is shown in Fig. 3 with the return loss at the appropriate channel port being comparable over the corresponding passband. The performance is

[1]Here "degree" corresponds to the number of cavities or resonant elements of the filter.

TABLE I
TABLE OF ELEMENT VALUES OF FOUR-CHANNEL PROTOTYPE MULTIPLEXERS "COUPLING" IS J_{rk}, "ADM" IS C_{rk}, AND "RES. FREQ." IS Ω_{rk}; ELEMENTS ADJACENT TO THE MANIFOLD ARE TABULATED FIRST

CHANNEL	DEGREE	RET.LOSS	BANDWIDTH	CENTRE FREQ.
1	5	22 dB	17	-34.5
COUPLING	ADM.	RES.FREQ.		
0.9665	0.1053	-37.9807		
1.1825	0.2757	-35.0087		
1.6849	0.3408	-34.5264		
1.7011	0.2757	-34.5015		
1.3132	0.1053	-34.5002		
CHANNEL	DEGREE	RET.LOSS	BANDWIDTH	CENTRE FREQ.
2	5	22 dB	17	-11.5
COUPLING	ADM.	RES.FREQ.		
1.0119	0.1053	-13.2129		
1.1246	0.2757	-11.4549		
1.6747	0.3408	-11.4894		
1.7007	0.2757	-11.4991		
1.3112	0.1053	-11.4999		
CHANNEL	DEGREE	RET.LOSS	BANDWIDTH	CENTRE FREQ.
3	6	22 dB	27	16.5
COUPLING	ADM.	RES.FREQ.		
1.6159	0.0680	4.1212		
1.2041	0.1859	16.9914		
1.7760	0.2539	16.4915		
2.0294	0.2539	16.4953		
1.8376	0.1859	16.4991		
1.3367	0.0680	16.4997		
CHANNEL	DEGREE	RET.LOSS	BANDWIDTH	CENTRE FREQ.
4	4	22 dB	7	39.5
COUPLING	ADM.	RES.FREQ.		
0.7698	0.2440	42.5573		
1.2298	0.5890	39.6479		
1.4964	0.5890	39.5007		
1.2737	0.2440	39.5		
MANIFOLD PHASE SHIFTERS (RADIANS)				
-0.3181	-0.8026	0.7818		

very close to the 22-dB return loss level, and the bandwidths and center frequencies are equal to the original channel requirements. The significant improvement in channel performance using this multiplexer design may be observed in Fig. 4 where the insertion loss of each channel is plotted. The 28-dB minimum level of attenuation of the first three channels and 38 dB for the fourth channel over all other channels are 10 dB larger than would have been achieved by the channels operating in isolation. Alternatively, this may be viewed as a saving of one cavity per channel over using individual channel filters and other channel combination procedures to meet the same specification. Many examples have been analyzed, and it has been found that there is very little deterioration in return loss performance even down to contiguous channels.

In most practical realizations of this prototype multiplexer, the manifold will have phase properties which are frequency dependent. We shall consider in detail the case where the manifold possesses a transmission-line frequency dependence, and any other cases could be considered in a similar manner.

III. THE FREQUENCY DEPENDENT MANIFOLD

Incorporation of the frequency dependence of the manifold in a manner compatible with the established design procedure is by no means obvious. The problem is to incorporate correction terms α^{-r} into the circuit description of a length of transmission line in a way which is both physically reasonable and results in a tractable solution. A number of early attempts failed for reasons which became apparant only after successful solutions were obtained.

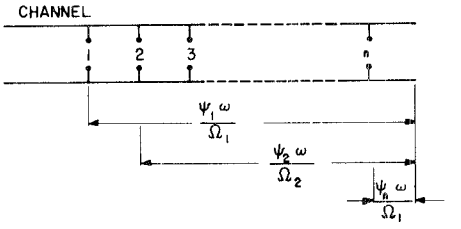

Fig. 5. Definition of phase lengths in manifold.

The first positive results were obtained using a piecewise-constant expression for the phase shift between channels. This is equivalent to an assumption that the individual channel bandwidths are sufficiently small so over any one channel the manifold presents a constant phase shift to the network. Over different channels the manifold possesses different constant values of phase shift.

This approach gives a considerable improvement over the constant phase shifter prototype when implemented into the design equations and applied to practical situations. However, with several channels requiring a long manifold the response deteriorates due to large phase changes of the manifold across the individual channel passbands. It is necessary then to take the frequency dependence of the manifold into account more exactly as follows.

The manifold multiplexer shown schematically in Fig. 5 indicates shunt-connected channels terminated in an open-circuited line. The electrical length between the rth channel and the termination is defined as ψ_r at the frequency Ω_r, leading to the general expressions indicated in the figure valid at any frequency ω. This circuit may be regarded as a prototype, and practical cases using a short-circuit termination may be designed by including slight modifications as described later.

In the constant phase-shifter theory, the transfer matrix of a phase shifter between physically adjacent channels was defined as in (1) and (2). In the frequency-dependent case, it is recognized that the most dominant terms involved in the design equations will be the lengths from each channel to the termination rather than the interchannel spacings. The following transfer matrix is found to give an adequate representation of the mth electrical length (shown in Fig. 5):

$$T(\psi_m) = \frac{1}{\sqrt{1+\alpha^{-2}\tan^2\left(\frac{\psi_m \alpha^{-1}\omega}{\Omega_m}\right)}} \cdot \begin{bmatrix} 1 & j\alpha^{-1}\tan\left(\frac{\psi_m \alpha^{-1}\omega}{\Omega_m}\right) \\ j\alpha^{-1}\tan\left(\frac{\psi_m \alpha^{-1}\omega}{\Omega_m}\right) & 1 \end{bmatrix}. \quad (41)$$

When $\alpha=1$, this matrix represents a length of transmission line. It has the same format as (1) and (2) with the susceptance B_m replaced by $\tan(\psi_m\omega\cdot\alpha^{-1}/\Omega_m)$. Hence the transformation $\alpha\rightarrow-\alpha$ does not change the sign of the electrical length (the B and C terms in (41) do not change sign), which is a physical requirement. It is known that the distance of each channel to the termination is close to an integral multiple of π even for channels spaced fairly closely in frequency, so that the transfer matrix (41) should not vary too rapidly with changes in interchannel frequencies (i.e., with changes in α). The essentially quadratic (α^{-2}) dependence of this transfer matrix ensures that the transfer matrix does indeed vary slowly with α and results in physically valid solutions.

The transfer matrix between channels m and $m+1$ is, by application of (41), given by

$$T(\psi_m)T(-\psi_{m+1})$$

$$=\frac{1}{\sqrt{1+\alpha^{-2}\tan^2\phi_m}}\begin{bmatrix}1 & j\alpha^{-1}\tan\phi_m\\ j\alpha^{-1}\tan\phi_m & 1\end{bmatrix}$$

$$\cdot\frac{1}{\sqrt{1+\alpha^{-2}\tan^2\phi_{m+1}}}\begin{bmatrix}1 & j\alpha^{-1}\tan\phi_{m+1}\\ j\alpha^{-1}\tan\phi_{m+1} & 1\end{bmatrix}$$

$$=\frac{1}{\sqrt{1+\alpha^{-2}B_m^2}}\begin{bmatrix}1 & j\alpha^{-1}B_m\\ j\alpha^{-1}B_m & 1\end{bmatrix} \quad (42)$$

where at $\omega=\Omega_r\alpha+\omega_i$

$$\phi_m=\frac{\psi_m}{\Omega_m}(\Omega_r+\omega_i\alpha^{-1})$$

$$\phi_{m+1}=\frac{\psi_{m+1}}{\Omega_{m+1}}(\Omega_r+\omega_i\alpha^{-1}) \quad (43)$$

$$B_m=\frac{\tan\phi_m-\tan\phi_{m+1}}{1+\alpha^{-2}\tan\phi_m\tan\phi_{m+1}}. \quad (44)$$

This implies that in the previous analysis for the frequency independent manifold as presented in Section II, B_m should be replaced by the expression (44) above, after expansion as a power series in α^{-1}. Thus in the previous analysis we should replace the following quantities containing B_m by the expressions shown:

$$\alpha^{-1}\sum_{m=1}^{r-1}B_m=\alpha^{-1}\left(\tan\left(\frac{\psi_1}{\Omega_1}\Omega r\right)-\tan(\psi_r)\right)$$

$$+\omega_i\alpha^{-2}\left(\frac{\psi_1}{\Omega_1}\left(1+\tan^2\left(\frac{\psi_1}{\Omega_1}\Omega_r\right)\right)-\frac{\psi_r}{\Omega_r}(1+\tan^2\psi_r)\right)$$

$$+\alpha^{-3}\left(G_r+\omega_i^2\left[\left(\frac{\psi_1}{\Omega_1}\right)^2\tan\left(\frac{\psi_1}{\Omega_1}\Omega_r\right)\left(1+\tan^2\left(\frac{\psi_1}{\Omega_1}\Omega_r\right)\right)\right.\right.$$

$$\left.\left.-\left(\frac{\omega_r}{\Omega_r}\right)^2\tan\psi_r(1+\tan^2\psi_r)\right]\right)+\epsilon(\alpha^{-4}) \quad (45)$$

and

$$\alpha^{-1}\sum_{m=r}^{n}B_m=\alpha^{-1}\tan\psi_r+\omega_i\alpha^{-2}\frac{\psi_r}{\Omega_r}(1+\tan^2\psi_r)$$

$$+\alpha^{-3}\left(G_r'+\omega_i^2\left(\frac{\psi_r}{\Omega_r}\right)^2\tan\psi_r(1+\tan^2\psi_r)\right)+\epsilon(\alpha^{-4}). \quad (46)$$

Here G_r, G_r' are undetermined coefficients of α^{-3} which are not required.

If the analysis of the manifold is modified accordingly, then (13)–(17) become

α^{-1} term:

$$C_{r1}\beta_{r11}=\sum_{m=1}^{n}{}_{\neq r}\frac{1}{C_{m1}(\Omega_r-\Omega_m)}-\tan\psi_r \quad (47)$$

$\alpha^{-2}\omega_i$ term:

$$\gamma_{r12}C_{r1}=\sum_{m=1}^{n}{}_{\neq r}\frac{1}{C_{m1}(\Omega_r-\Omega_m)^2}+\frac{\psi_r}{\Omega_r}(1+\tan^2\psi_r) \quad (48)$$

α^{-2} term:

$$\gamma_{r02}=\gamma_{r12}-C_{r1}^2\beta_{r11}^2+2\sum_{m=1}^{r-1}\frac{\tan\left(\frac{\psi_m}{\Omega_m}\Omega_r\right)-\tan(\psi_r)}{C_{m1}(\Omega_r-\Omega_m)}$$

(see also (31)) (49)

$\alpha^{-3}\omega_i^2$ term:

$$\frac{C_{r1}^2C_{r2}\beta_{r23}}{J_{r1}^2}=\sum_{m=1\neq r}^{n}\frac{1}{C_{m1}(\Omega_r-\Omega_m)^3}-\left(\frac{\psi_r}{\Omega_r}\right)^2$$

$$\cdot\tan\psi_r(1+\tan^2\psi_r) \quad (50)$$

$\alpha^{-3}\omega_i$ term:

$$\frac{-2C_{r1}C_{r2}\beta_{r23}}{J_{r1}^2}+2C_{r1}^2\beta_{r11}\gamma_{r12}$$

$$=d_2-\alpha_2+\left(\tan\left(\frac{\psi_1}{\Omega_1}\cdot\psi_r\right)-\tan\psi_r\right)\cdot\sum_{m=1}^{r-1}\frac{1}{C_{m1}(\Omega_r-\Omega_m)^2}$$

$$-\left(\frac{\psi_1}{\Omega_1}\left(1+\tan^2\left(\frac{\psi_1}{\Omega_1}\cdot\Omega_r\right)\right)\right.$$

$$\left.-\frac{\psi_r}{\Omega_r}(1+\tan^2\psi_r)\right)\sum_{m=1}^{r-1}\frac{1}{C_{m1}(\Omega_r-\Omega_m)}$$

$$+\sum_{m=2}^{r-1}\frac{\frac{\psi_1}{\Omega_1}\left(1+\tan^2\left(\frac{\psi_1}{\Omega_1}\Omega_r\right)\right)-\frac{\psi_m}{\Omega_m}\left(1+\tan^2\left(\frac{\psi_m}{\Omega_m}\Omega r\right)\right)}{C_{m1}(\Omega_r-\Omega_m)}$$

$$-\sum_{m=1}^{r-1}\frac{\frac{\psi_m}{\Omega_m}\left(1+\tan^2\left(\frac{\psi_m}{\Omega_m}\Omega_r\right)\right)-\frac{\psi_r}{\Omega_r}(1+\tan^2\psi_r)}{C_{m1}(\Omega_r-\Omega_m)} \quad (51)$$

which reduces to

$$-\frac{C_{r1}C_{r2}\beta_{r23}}{J_{r1}^2}+C_{r1}^2\beta_{r11}\gamma_{r12}=\sum_{m=1}^{r-1}\frac{\tan\left(\frac{\psi_m}{\Omega_m}\Omega_r\right)-\tan\psi_r}{C_{m1}(\Omega_r-\Omega_m)^2}$$
$$-\sum_{m=1}^{r-1}\frac{\frac{\psi_m}{\Omega_m}\left(1+\tan^2\left(\frac{\psi_m}{\Omega_m}\cdot\Omega_r\right)\right)-\frac{\psi_r}{\Omega_r}(1+\tan^2\psi_r)}{C_{m1}(\Omega_r-\Omega_m)}. \quad (52)$$

Substituting (47), (48), and (50) into (52) gives

$$P_r=\tan\psi_r\cdot\sum_{m=r+1}^{n}\frac{1}{C_{m1}(\Omega_r-\Omega_m)^2}$$
$$-\frac{\psi_r}{\Omega_r}(1+\tan^2\psi_r)\cdot\sum_{m=r+1}^{n}\frac{1}{C_{m1}(\Omega_r-\Omega_m)}$$
$$+\frac{\psi_r}{\Omega_r}\tan\psi_r(1+\tan^2\psi_r)$$
$$-\frac{1}{C_{r1}}\left(\frac{\psi_r}{\Omega_r}\right)^2\tan\psi_r(1+\tan^2\psi_r)$$
$$+\sum_{m=1}^{r-1}\frac{\tan\left(\frac{\psi_m}{\Omega_m}\Omega_r\right)}{C_{m1}(\Omega_r-\Omega_m)^2}-\sum_{m=1}^{r-1}\frac{\frac{\psi_m}{\Omega_m}\left(1+\tan^2\left(\frac{\psi_m}{\Omega_m}\Omega r\right)\right)}{C_{m1}(\Omega_r-\Omega_m)} \quad (53)$$

where P_r is defined in (20).

For large phase lengths in the manifold, the second and sixth terms on the right-hand side of this equation can become large. These terms, however, were obtained from a power series expansion in α^{-1} which assumed that these were small as compared to the first and fifth terms. Thus it is important to recombine the terms.

Consider the function

$$\tan\left(\frac{\Omega_m}{\Omega_r}\psi_r\right)=\tan\left(\psi_r+(\Omega_m-\Omega_r)\frac{\psi_r}{\Omega_r}\right). \quad (54)$$

Assuming that $(1-\Omega_m/\Omega_r)$ is small as compared to unity, we may expand (54) as a power series in $(\Omega_m-\Omega_r)$. The first three terms are

$$\tan\left(\frac{\Omega_m}{\Omega_r}\psi_r\right)=\tan\psi_r+(\Omega_m-\Omega_r)$$
$$\cdot\frac{\psi_r}{\Omega_r}(1+\tan^2\psi_r)+(\Omega_m-\Omega_r)^2$$
$$\cdot\left(\frac{\psi_r}{\Omega_r}\right)^2\tan\psi_r(1+\tan^2\psi_r)+\cdots. \quad (55)$$

Hence the first four terms of the right-hand side of (53) may be combined into the form

$$\sum_{m=r+1}^{n}\frac{\tan\left(\frac{\Omega_m}{\Omega_r}\psi_r\right)}{C_{m1}(\Omega_r-\Omega_m)^2}+\left(1-\frac{\psi_r}{\Omega_r}\sum_{m=r}^{n}\frac{1}{C_{r1}}\right)$$
$$\cdot\frac{\psi_r}{\Omega_r}\tan\psi_r(1+\tan^2\psi_r). \quad (56)$$

Combining terms five and six on the right-hand side of (53) in a similar manner results in (53) becoming

$$P_r=\sum_{m=r+1}^{n}\frac{\tan\left(\frac{\Omega_m}{\Omega_r}\psi_r\right)}{C_{m1}(\Omega_r-\Omega_m)^2}+\left(1-\frac{\psi_r}{\Omega_r}\sum_{m=r}^{n}\frac{1}{C_{r1}}\right)$$
$$\cdot\frac{\psi_r}{\Omega_r}\tan\psi_r(1+\tan^2\psi_r)+\sum_{m=1}^{r-1}\frac{\tan\psi_m}{C_{m1}(\Omega_r-\Omega_m)^2}$$
$$-\sum_{m=1}^{r-1}\left(\frac{\psi_m}{\Omega_m}\right)^2\frac{1}{C_{m1}}\tan\psi_m(1+\tan^2\psi_m). \quad (57)$$

In practice, the terms in (57) containing the $(\psi_m/\Omega_m)^2$ factors may now be deleted.

For $r=1$, the only unknown appearing in this transcendental equation is ψ_1 which may be obtained iteratively using, for example, the Newton–Raphson technique for a solution around any integral number of π rad.

Having obtained ψ_1, (57) may then be solved for ψ_2 with $r=2$ under the restriction

$$\frac{\psi_r}{\Omega_r}<\frac{\psi_{r-1}}{\Omega_{r-1}} \quad (58)$$

which is necessary to ensure that a positive length of line separates the two channels along the manifold. This process may be repeated until $r=n-1$, but for $r=n$ the first term on the right-hand side of (57) disappears, and a solution to the equation may be difficult to obtain. This corresponds closely to the result obtained in the frequency independent manifold case. Normally ψ_n would be chosen to be zero.

From the values of ψ_r, (47)–(50) may then be used to obtain the remaining design parameters, and a simple updating process commencing with the nth channel will ensure a good passband match near to the band center of each channel.

Frequently it may be desirable to terminate the manifold in a short circuit approximately $\pi/2$ rad from the last channel. This is achieved readily by replacing

$$\tan\theta\rightarrow-\cot\theta=\tan\left(\theta-\frac{\pi}{2}\right) \quad (59)$$

in (47)–(57) resulting in an increase in each value of ψ_r by approximately $\pi/2$.

These equations have been programmed and applied to the design of several multiplexers having either widely spaced or contiguous channels. As an example of the latter a ten-channel manifold was designed in WR75 to

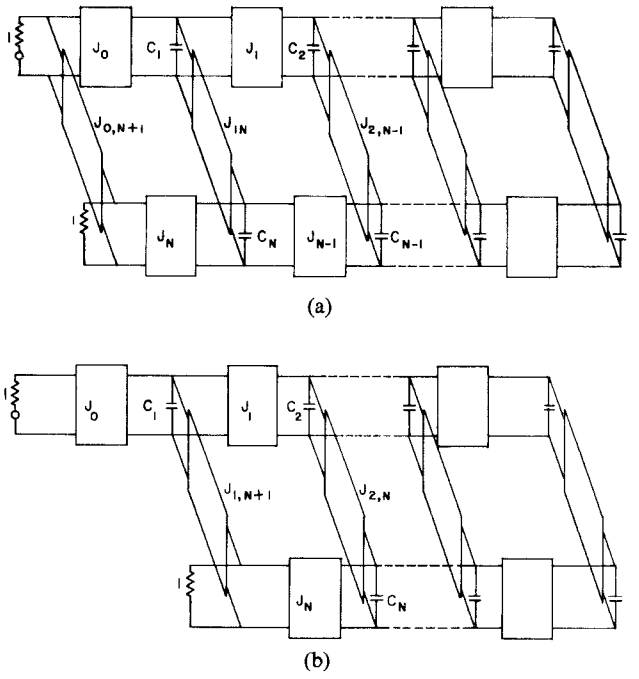

Fig. 6. (a) Realization of general even-degree filter. (b) Realization of general odd-degree filter.

divide the 14–14.5-GHz band into ten contiguous channels. The doubly terminated prototype filters were selected to have six cavities with 22-dB return loss bandwidth of 43 MHz, and the channel center frequencies were spaced by 49 MHz (this gives 3-dB crossover points). The multiplexer synthesized from the design equations was analyzed on the computer, and showed results in good agreement with theory. In fact, the worst return loss at the common port in the entire band is approximately 16 dB, occurring near the passband edges; most of the band has return loss of greater than 22 dB. This multiplexer has not yet been built in practice, but there is good reason to believe that practical versions would work in accordance with theory, since the computer analysis is known to be accurate in predicting practical performance. Presently only relatively simple manifold multiplexers, such as that described in Section IV, have been actually constructed.

A. Extension to Filters with Extra Cross-Couplings

In the most general case of optimum equiripple filters having finite frequency transmission zeros and/or complex conjugate pairs of transmission zeros giving improved phase response, extra cross-couplings are utilized as designated by the cross-coupling admittance inverters included in the low-pass prototypes depicted in Fig. 6. The even-degree case is shown in Fig. 6(a), and the convenient asymmetric realization of the odd-degree case [5] is shown in Fig. 6(b). The question arises of how to treat the extra cross-coupling inverters when such filters are multiplexed. Such filters are often realized using dual-mode cavities to give convenient means of inclusion of the extra cross couplings.

From a practical viewpoint filters will have at least 10-dB attenuation in the stopband and normally considerably more. This implies that the first cross-coupling is very small compared to the main line couplings, and for filters of degree greater than 2, the second cross-coupling will also be small. Thus, in calculating the input impedance of the filter for the purposes of the multiplexer theory, the first and second cross-couplings may be ignored initially. Then, after calculating the correction terms for multiplexing, it can be shown that the scaling factor for the correction on a cross-coupling J_{kq} is the same at the scaling factor on J_k. For example, the correction factor on J_k for the rth channel is given by (33) as $(1-\gamma_{rkl})^{1/2}$, so that the corresponding cross-coupling admittance inverter changes accordingly as

$$J_{(r)kq} \rightarrow J_{(r)kq}(1-\gamma_{rkl})^{1/2}, \qquad k=1,2,\cdots,N_r-1. \quad (60)$$

Here the subscript r has been added in parentheses to indicate the rth channel as in (33).

B. Design of Practical Waveguide Multiplexers

Early waveguide multiplexers constructed on a common manifold were designed on a semiempirical basis and required adjustable phase shifters between channels to take up unknown junction effects, particularly unpredicted phase shifts across the junctions. This is no longer necessary, since it is not difficult to take the junction effects into account by computer analysis, e.g., [6] which describes the design of an aperture-coupled E-plane multiplexer.

Similar excellent results have been obtained both in theory and practice using aperture-coupled H-plane manifolds. The slit-coupled H-plane T junction is a particularly useful circuit for rectangular waveguide filters since the equivalent circuit is very accurate, and the junction provides the first admittance inverter and shunt susceptance of the filter. The equivalent circuit of Marcuvitz [7, Fig. 6.6-2] is easily transformed as indicated in Fig. 7. Here we make the simplification that the broad dimensions of the main line and side arms are equal, giving

$$\frac{X_b}{Z_0} = \frac{a}{\lambda g}\left[\left(\frac{4a}{\pi d}\right)^2 - 1\right] + \frac{2a}{\lambda_g} \quad (61)$$

$$\frac{X_c}{Z_0} = \frac{2a}{\lambda_g}. \quad (62)$$

The capacitive T of Fig. 7(b) is identical to a series reactance $-j(X_b - X_c)$ in cascade with an ideal impedance inverter of impedance X_c, and carrying out a Kuroda-type transformation gives the final equivalent circuit of Fig. 7(c) where

$$\frac{J}{Y_0} = \frac{\lambda_g}{2a} \quad (63)$$

$$\frac{B}{Y_0} = -\frac{\lambda_g}{4a}\left[\left(\frac{4a}{\pi d}\right)^2 - 1\right]. \quad (64)$$

The negative shift in the reference planes, as indicated in

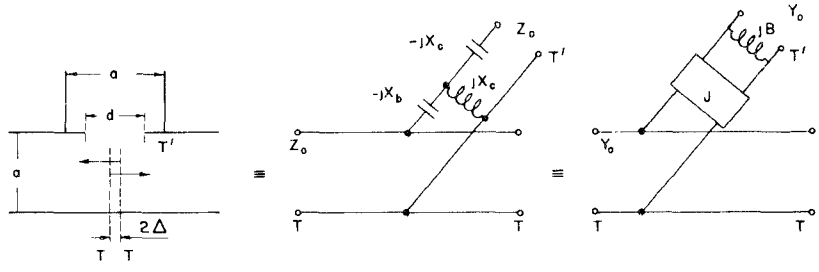

Fig. 7. (a) Slit-coupled H-plane T junction; (b) Marcuvitz equivalent circuit; and (c) Modified equivalent circuit.

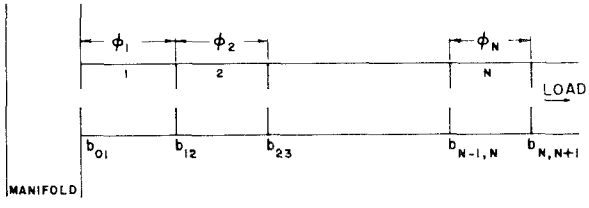

Fig. 8. Typical waveguide channel filter on a manifold.

Fig. 7(a), is given by

$$\Delta = \frac{1}{32\pi}\frac{a}{\lambda_g}\left(\frac{\pi d}{2a}\right)^4. \tag{65}$$

The finite thickness of the iris of width d may be taken into account by inclusion of the short length of waveguide so formed, which may be either below or above cutoff.

The design equations for the susceptances and cavity lengths of a direct-coupled cavity filter connected to the manifold, as illustrated in Fig. 8, may be based on those given in [8] for narrow-band filters. The equations require modification when based on the prototype used in this paper [1, Fig. 2] and are as follows.

Given band-edge guide wavelengths λ_{g1} and λ_{g2}, the fractional bandwidth is defined as

$$w = \frac{2(\lambda_{g1}-\lambda_{g2})}{\lambda_{g1}+\lambda_{g2}}. \tag{66}$$

Defining

$$J_1' = \frac{1}{J_0}\sqrt{\frac{\omega_1' g_1}{(\pi/2)w}} \tag{67}$$

$$J_k' = \frac{1}{J_k}\frac{\omega_1'\sqrt{g_{k-1}g_k}}{(\pi/2)w}, \qquad \text{for } k=2,3,\cdots,N \tag{68}$$

$$J_{N+1}' = \frac{1}{J_N}\sqrt{\frac{\omega_1' g_N}{(\pi/2)w}} \tag{69}$$

then the shunt susceptances are given by

$$b_{01} = J/J_1' - J_1'/J \tag{70}$$

$$b_{k,k+1} = J_k' - 1/J_k', \qquad \text{for } k=1,2,\cdots,N-1 \tag{71}$$

$$b_{N,N+1} = J_{N+1}' - 1/J_{N+1}' \tag{72}$$

$$\phi_k = \pi - 1/2\left(\tan^{-1}\frac{2}{|b_{k-1,k}|} + \tan^{-1}\frac{2}{|b_{k,k+1}|}\right). \tag{73}$$

In (70) above J is the admittance inverter shown in Fig. 8(c), given by (63) with $Y_0 = 1$.

The iris opening d in Fig. 7(a) is given by (64) with B/Y_0 replaced by the value of b_{01} given by (70).

In applying the above formulas to the multiplexer the modified prototype element values given earlier in this section are used, and the cavities are "detuned" from their nominal values given by (73) in accordance with this theory.

In the case of rather broad-band waveguide filters, the improved theory given in [9] should be used to derive equivalent effective prototype values for [67]–[69].

IV. Practical Result: A WR229 Waveguide Triplexer

The theory described in the previous section was applied to the design of a waveguide WR229 manifold triplexer. Each channel consists of a 37-MHz bandwidth six-cavity Chebyshev filter having ripple return loss 26 dB (VSWR 1.1) with center frequencies at 3720, 3800, and 3880 MHz. Although this is not a "severe" contiguous or nearly contiguous case, it is far from trivial from a design viewpoint because the 26-dB return loss is relatively difficult for a multiplexer. The theoretical performance is shown in Fig. 9, which gives the common port return loss and channel insertion losses of the triplexer, taking all practical effects into account. It is seen that all six return loss poles are present in each channel, and the return loss minima are close to the specified level of 26 dB. The physical spacing between channels was approximately one guide wavelength to allow the filters to be all on one side of the manifold, as shown in Fig. 10.

The measured performance was very close to the theoretical prediction, and no problems were experienced in obtaining the five ripples at the 1.1-VSWR level in each channel. In particular, no empirical adjustments to the waveguide manifold were required, e.g., in the relative spacing between the channels. This has been the case also for several manifold multiplexers of this type made in a variety of waveguide sizes.

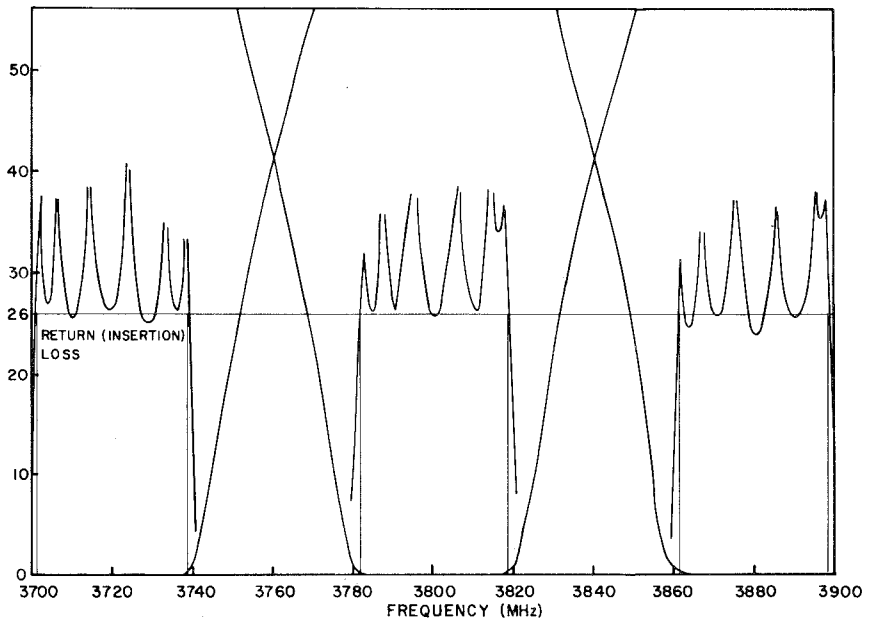

Fig. 9. Analysis of a practical waveguide manifold triplexer.

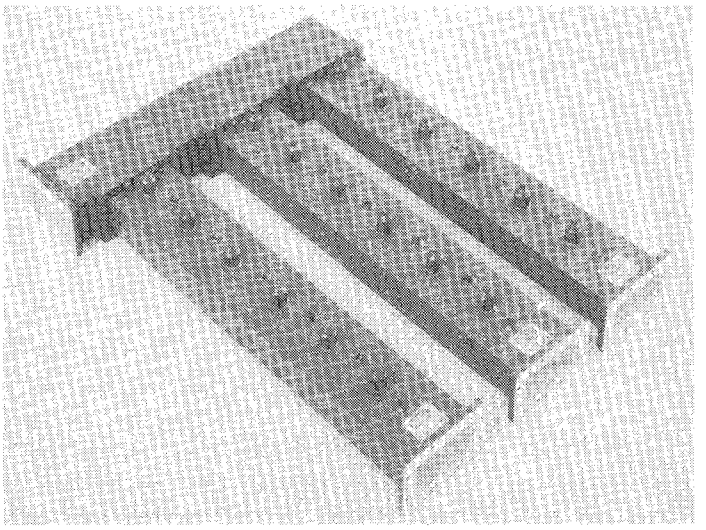

Fig. 10. Photograph of the WR229 triplexer.

V. Conclusions

A new design process has been presented for bandpass channel multiplexers where the channel filters are separated along a manifold. The design process has been found to be valid for a large variety of channel separations from very large guardbands down to contiguous channel operation. In addition to the design process being canonic (i.e., the total degree of the multiplexer is equal to the sum of the individual degrees of the channel filters), a significant improvement in channel performance is achieved over the individual channel filters operating in isolation. For the basic manifold prototype multiplexer with frequency-independent phase shifters, theoretically, there are no limitations upon the number of channels nor the complexity or type of channel filters used.

In practice, the manifold will possess a transmission-line frequency dependence, and modifications to the design process have been presented which are valid for fairly broad-band operation. There are two limitations, namely, the maximum channel bandwidths and the maximum number of channels, the latter normally being more restrictive due to the significant frequency dependence of a long manifold.

Examples have been given indicating that both input and output multiplexers suitable for most communication systems may readily be designed. Practical waveguide manifold multiplexers have been constructed, showing that the theory is reproduced in practice with no empirical adjustments being required to the location of the filters on the manifold.

References

[1] J. D. Rhodes and R. Levy, "A generalized multiplexer theory," this issue, pp. 99–111.
[2] R. J. Wenzel and W. G. Erlinger, "Narrowband contiguous multi-

plexing filters with arbitrary amplitude and delay response," *1976 IEEE MTT-S Int. Microwave Symp. Digest*, IEEE Cat. no. 76CH1087-6MTT, pp. 116–118.
[3] M. H. Chen, F. Assal, and C. Mahle, "A contiguous band multiplexer," *Comsat Tech. Rev.*, vol. 6, no. 2, pp. 285–305, Fall 1976.
[4] J. D. Rhodes, "Direct design of symmetrical interacting bandpass channel diplexers," *Inst. Elec. Eng. Microwaves, Opt., Acoust.*, vol. 1, no. 1, pp. 34–40, Sept. 1976.
[5] R. Levy, "Filters with single transmission zeros at real or imaginary frequencies," *IEEE Trans. Microwave Theory Tech.*, vol. MTT-24, pp. 172–181, Apr. 1976.
[6] A. E. Atia, "Computer-aided design of waveguide mutiplexers," *IEEE Trans. Microwave Theory Tech.*, vol. MTT-22, pp. 332–336, Mar. 1974.
[7] N. Marcuvitz Ed., *Waveguide Handbook*. M.I.T. Radiation Lab. Series, vol. 10. New York: McGraw-Hill, 1951.
[8] S. B. Cohn, "Direct-coupled-resonator filters," *Proc. IRE*, vol 45, pp. 187–196, Feb. 1957.
[9] R. Levy, "Theory of direct-coupled-cavity filters," *IEEE Trans. Microwave Theory Tech.*, vol. MTT-15, pp. 340–348, June 1967.

Tables for Nonminimum-Phase Even-Degree Low-Pass Prototype Networks for the Design of Microwave Linear-Phase Filters

J. H. CLOETE, MEMBER, IEEE

Abstract—**The element values of a selection of even-degree nonminimum-phase low-pass prototype networks with equiripple passband amplitude and constant group delay in the least squares sense over a large percentage of the passband are tabulated. All the prototypes have passband insertion loss ripple $R = 0.01$ dB and cutoff frequency $\omega_c = 1.0$ rad/s at the 0.01-dB point. Five tables contain the element values of networks up to degree $N = 20$. The tables are classified according to the number of transmission zeros at infinite frequency NZ_∞ and the passband frequency to which the group delay is constant in the least squares sense ω_d. The following combinations of NZ_∞ and ω_d are tabulated: $NZ_\infty = 2$ and $\omega_d = 0.9$; $NZ_\infty = 4$ and $\omega_d = 0.8$; $NZ_\infty = 6$ and $\omega_d = 0.7$; $NZ_\infty = 8$ and $\omega_d = 0.6$; and $NZ_\infty = 10$ and $\omega_d = 0.5$. The maximum phase and delay errors for each network are tabulated. Plots of the passband group delay and stopband insertion loss versus frequency, for each network, accompany the tables to facilitate selection of a prototype. The prototypes are suitable for the design of narrow-band generalized interdigital, generalized direct-coupled cavity waveguide, and generalized combline linear-phase filters. A simple algorithm for the analysis of the prototypes is given.**

I. Introduction

THE SYMMETRICAL nonminimum-phase low-pass prototype network introduced by Rhodes [1] is shown for the even-degree case. It is topologically suited to the design of microwave bandpass filters capable of good amplitude selectivity while approximating closely to linear phase over a large percentage of the passband. The microwave filters are realized by providing coupling between nonadjacent resonators. Examples include the generalized interdigital filter [2], the generalized direct-coupled cavity waveguide filter [3]–[5] and the generalized combline filter [6].

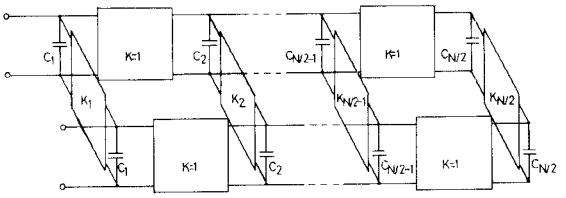

Fig. 1. The symmetrical even-degree nonminimum phase low-pass prototype network consisting of lumped capacitors and ideal admittance inverters. The notation for the network elements is consistent with the notation used in Tables I–V.

The first step in the design of a narrow-band microwave linear-phase filter is to find the element values of a low-pass prototype which satisfies the amplitude and phase or group delay specifications. When this step is completed the elements in the equivalent circuit of the microwave filter may be calculated [2], [3]. A number of approximation theories and techniques have been described for the construction of nonminimum-phase low-pass transfer functions from which the element values of the prototype networks can be synthesized [1], [4], [7]–[10]. These methods generally require considerable computation to achieve a satisfactory prototype. The method of Levy [4], applicable when only one pair of finite zeros provides

Manuscript received February 13, 1978; revised June 27, 1978.
The author was with the Department of Electrical Engineering, University of Stellenbosch, Stellenbosch 7600, South Africa, on leave from the National Institute for Aeronautics and Systems Technology, Council for Scientific and Industrial Research, P.O. Box 395, Pretoria 0001, South Africa.

0018-9480/79/0200-0123$00.75 ©1979 IEEE

A Design Procedure for Bandpass Channel Multiplexers Connected at a Common Junction

JOHN DAVID RHODES, MEMBER, IEEE, AND SAOD A. ALSEYAB, STUDENT MEMBER, IEEE

Abstract—A new general design procedure is presented for multiplexers having any number of Chebyshev channel filters, with arbitrary degrees, bandwidths, and interchannel spacings. The design procedure is developed for bandpass channel filters connected in series at a common junction for narrow-band applications.

Commencing with the closed-form expressions for element values in Chebyshev filters, the multiplexer design process modifies all of the elements in each channel filter and preserves a match at the two points of perfect transmission closest to the band edges of each channel filter, while taking into account the frequency dependence across each channel.

Examples of several multiplexers are given indicating that the design process is valid for most combinations of contiguous and noncontiguous channels.

I. Introduction

MOST OF THE previous multiplexers design techniques have adopted an approach based upon singly terminated bandpass channels inherently resulting in 3-dB crossover points between channels (contiguous), e.g., [1], [2]. Such designs exhibit good return loss over the channel bandwidths and guardbands. However, dummy channels have to be included to imitate absent channels at the edges of the total multiplexer bandwidth, thus forming an additional annulling network. These redundant elements are necessary for the compensation of the channel interactions to produce a channel performance comparable to the individual channels based upon a singly terminated prototype.

In general, contiguous band multiplexers based upon the singly terminated filter design are nonoptimum because they need a higher degree filter than necessary in each channel in addition to an annulling network. Furthermore, if the singly terminated designs are to be used for crossover levels in excess of 3 dB, which is the case in most communication systems, the passband return loss rapidly deteriorates if a further annulling network is not used. A general design procedure was recently presented in [3] for multiplexers based upon doubly terminated channel filters where the parameters associated with the first two resonators of each individual channel filter are modified in terms of a well-defined band separation factor. The process is powerful and flexible but has a number of limitations mentioned in [3] for the simple series connection of channels. For example, the channels may not be spaced too closely in frequency, the procedure will give inaccurate results when the channel return loss is greater than 20 dB, and the lowest and highest frequency channels suffer a severe deterioration for most specifications containing three or more channels.

In this paper a new general design procedure is presented for narrow-band bandpass channel prototype multiplexers having any number of Chebyshev channel filters, with arbitrary degrees, bandwidths, and interchannel spacing without the necessity of having a manifold feed. This design procedure commences from the element values of a doubly terminated low-pass prototype filter satsifying an equiripple response which is obtained from the closed-form formulas given in [4], and the individual channel filters can be realized in a direct coupled cavity form connected in series at a common junction. The multiplexer design procedure modifies all of the elements in each channel filter and preserves a complete match at the two points of perfect transmission closest to the band edges of each channel filter, while taking into account the frequency dependence across each channel. An optimization process has been used to modify the elements of each channel in turn and the convergence of the process is normally achieved if the insertion loss of the neighboring channels cross over at greater than 3 dB. The resulting multiplexer is canonic without an immittance compensating annulling network or a manifold feed. Finally, it is shown that this process gives very good results for a wide variety of specifications, as demonstrated by the computer analysis of several multiplexer examples.

II. The Design Procedure

The design procedure commences from lumped-element doubly terminated channel filters operating in isolation satisfying an equiripple passband amplitude response with the maximum number of ripples. Thus there is perfect transmission at n points $\omega=\omega_i (i=1\rightarrow n)$, where n is the degree of transfer function.

The assumed normalized low-pass prototype filter satisfies an optimum equiripple amplitude passband response (I.L.) sketched in Fig. 1 and given by the formula:

$$\text{I.L.} = 1+\epsilon^2 T_n^2(\omega) \tag{1}$$

where

$$T_n(\omega)=\cos(n\cos^{-1}\omega)$$

Manuscript received June 11, 1979; revised October 17, 1979.

The authors are with the Department of Electrical and Electronic Engineering, The University of Leeds, Leeds LS2 9JT, England.

0018-9480/80/0300-0246$00.75 ©1980 IEEE

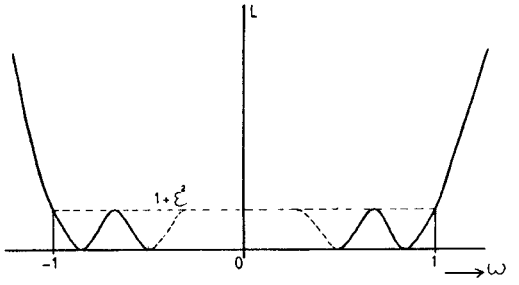

Fig. 1. Insertion-loss response of the low-pass filter.

and has the equivalent circuit shown in Fig. 2, with the explicit design formulas [4]:

$$\left.\begin{aligned} C_r' &= \frac{2\sin\left[\dfrac{(2r-1)\pi}{2n}\right]}{\eta}, \qquad r=1\to n \\ K_{r,r+1} &= \frac{\sqrt{\eta^2+\sin^2(r\pi/n)}}{\eta}, \qquad r=1\to n-1 \\ \eta &= \sinh\left[\frac{1}{n}\sinh^{-1}\left(\frac{1}{\epsilon}\right)\right] \end{aligned}\right\}. \tag{2}$$

The bandpass channels based on this low pass can be designed as individual doubly terminated filters with the corrected bandwidths and center frequencies by applying the frequency transformation

$$\omega' \to (\omega - I_i)/\beta_i \tag{3}$$

where I_i and β_i are the ith channel center frequency and bandwidth scaling factor, respectively.

Assuming the lower and upper band edges frequencies of the individual bandpass channels ω_{1i} and ω_{2i} are known, then

$$I_i = \frac{(\omega_{1i}+\omega_{2i})}{2}. \tag{4}$$

The frequency transformation given in (3) changes all of the capacitors C_r' into capacitors C_{ir} in parallel with a frequency invariant susceptances B_{ir}, where

$$C_{ir} = \frac{C_r'}{\beta_i} \tag{5}$$

$$B_{ir} = -'C_{ir}I_i \tag{6}$$

and preserves the equiripple amplitude response.

The design principle used here modifies all of the elements in each channel filter taking into account the frequency variation across each channel and the interaction due to other channels.

A perfect transmission is preserved with the correct overall phase shift in the auxiliary variable η at the two points of perfect transmission (F_{1i} and F_{2i}) closest to the band edges of each channel. However, when channel $j(j=1,2,3,\cdots,L)$ is modified the remaining channels $i(i=1,2,3,\cdots,\neq j,\cdots L)$ are replaced by their input impedances calculated at F_{1j} and F_{2j} and the modification process may be repeated until no more change in the element values is possible.

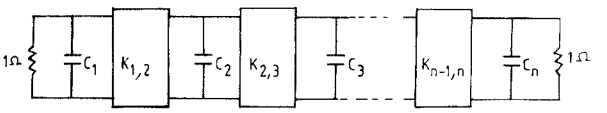

Fig. 2. Low-pass prototype filter.

The two points of perfect transmission closest to the band edges of channel i, (F_{1i} and F_{2i}) can be obtained by solving the following set of linear equations formed by preserving the same argument value of $T_n(\omega)$ at the band edges and the two points of perfect transmission closest to the low-pass band edges, after applying the bandpass frequency transformation given earlier in expression (3). Hence,

$$\frac{I_i-\omega_{1i}}{\beta_i} = 1 \tag{7}$$

$$\frac{I_i-F_{1i}}{\beta_i} = \cos(\pi/2n_i) \tag{8}$$

$$\frac{I_i-\omega_{2i}}{\beta_i} = -1 \tag{9}$$

$$\frac{I_i-F_{2i}}{\beta_i} = -\cos(\pi/2n_i). \tag{10}$$

From (7) and (9)

$$\beta_i = I_i-\omega_{1i} = \omega_{2i}-I_i. \tag{11}$$

From (8)

$$F_{1i} = I_i - \beta_i\cos(\pi/2n_i) \tag{12}$$

and from (10)

$$F_{2i} = I_i + \beta_i\cos(\pi/2n_i). \tag{13}$$

Now, if each bandpass channel i is assumed to be operating in isolation, terminated at both ends by 1-Ω resistors, then at $\omega = F_{1i}$, the transfer matrix for the entire network of channel i would be

$$\prod_{r=1}^{n_i-1} \frac{1}{\sqrt{\eta_i^2+\sin^2\left(\dfrac{r\pi}{n_i}\right)}} \begin{bmatrix} -\sin\left(\dfrac{r\pi}{n_i}\right) & j\eta_i \\ j\eta_i & -\sin\left(\dfrac{r\pi}{n_i}\right) \end{bmatrix}. \tag{14}$$

Also, at $\omega = F_{2i}$ the transfer matrix for the entire network of channel i would be

$$\prod_{r=1}^{n_i-1} \frac{1}{\sqrt{\eta_i^2+\sin^2\left(\dfrac{r\pi}{n_i}\right)}} \begin{bmatrix} \sin\left(\dfrac{r\pi}{n_i}\right) & j\eta_i \\ j\eta_i & \sin\left(\dfrac{r\pi}{n_i}\right) \end{bmatrix}. \tag{15}$$

This has been shown by Rhodes [4] and represents a cascade of passive all-pass sections in the auxiliary parameter $-j\eta$ or $j\eta$.

The insertion-loss characteristics of an L-channel multiplexer indicating the insertion losses from the common port to the L-output ports is shown in Fig. 3, where the

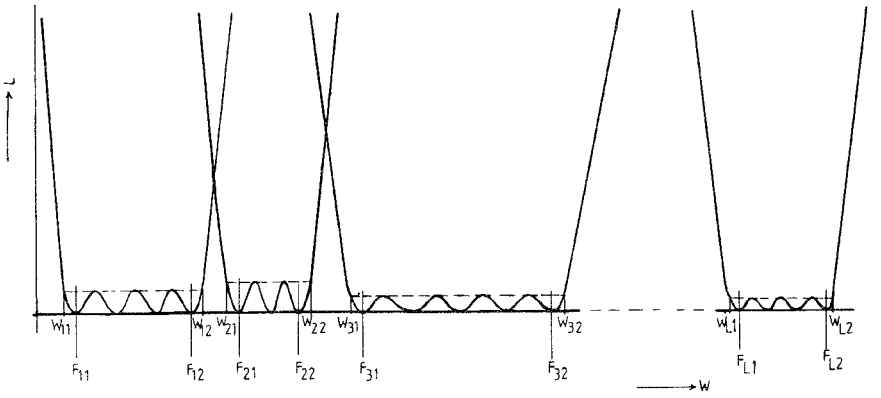

Fig. 3. Insertion loss of a multiplexer.

ripple level of the channels are not necessarily identical. The L-channel series connected multiplexer is shown in Fig. 4. The effect on the passband response of one channel due to the interaction of the others is to create a frequency dependent complex load at one end. Since the value of this load is different at the two critical band edge frequencies where all-pass behavior in the auxiliary parameter occurs, an impedance scaling within the network must occur coupled with additional phase shift. Hence, the transfer matrix for the entire network of channel i operating in a multiplexer of L-channels calculate at $\omega = F_{1i}$ from general image parameter theory for matched sections is given by

$$\prod_{r=1}^{n_i-1} \frac{1}{\sqrt{(\eta_i^2+S_{ir}^2)(1+t_{i,r}^2)}} \begin{bmatrix} \sqrt{Z_{1i,r}} & 0 \\ 0 & \dfrac{1}{\sqrt{Z_{1i,r}}} \end{bmatrix} \cdot \begin{bmatrix} 1 & jt_{i,r} \\ jt_{i,r} & 1 \end{bmatrix} \begin{bmatrix} -S_{i,r} & j\eta_i \\ j\eta_i & -S_{i,r} \end{bmatrix} \begin{bmatrix} \dfrac{1}{\sqrt{Z_{1i,r+1}}} & 0 \\ 0 & \sqrt{Z_{1i,r+1}} \end{bmatrix} \tag{16}$$

or

$$\prod_{r=1}^{n_i-1} \frac{1}{\sqrt{(\eta_i^2+S_{i,r}^2)(1+t_{i,r}^2)}} \cdot \begin{bmatrix} -\sqrt{\dfrac{Z_{1i,r}}{Z_{1i,r+1}}}\,(S_{i,r}+\eta_i t_{i,r}) & j\sqrt{Z_{1i,r}Z_{1i,r+1}}\,(\eta_i - S_{1,r}t_{i,r}) \\ j\dfrac{(\eta_i - S_{i,r}t_{i,r})}{\sqrt{Z_{1i,r}Z_{1i,r+1}}} & -\sqrt{\dfrac{Z_{1i,r+1}}{Z_{1i,r}}}\,(S_{i,r}+\eta_i t_{i,r}) \end{bmatrix}. \tag{17}$$

Similarly at $\omega = F_{2i}$ the transfer matrix for the entire network of channel i may be represented by

$$\prod_{r=1}^{n_i-1} \frac{1}{\sqrt{(\eta_i^2+S_{i,r}^2)(1+t_{i,r}^2)}} \cdot \begin{bmatrix} \sqrt{Z_{2i,r}} & 0 \\ 0 & \dfrac{1}{\sqrt{Z_{2i,r}}} \end{bmatrix} \begin{bmatrix} 1 & jt_{i,r} \\ jt_{i,r} & 1 \end{bmatrix} \cdot \begin{bmatrix} S_{i,r} & j\eta_i \\ j\eta_i & S_{i,r} \end{bmatrix} \begin{bmatrix} \dfrac{1}{\sqrt{Z_{2i,r+1}}} & 0 \\ 0 & \sqrt{Z_{2i,r+1}} \end{bmatrix} \tag{18a}$$

$$\prod_{r=1}^{n_i-1} \frac{1}{\sqrt{(\eta_i^2+S_{i,r}^2)(1+t_{i,r}^2)}} \cdot \begin{bmatrix} \sqrt{\dfrac{Z_{2i,r}}{Z_{2i,r+1}}}\,(S_{i,r}-\eta_i t_{i,r}) & j\sqrt{Z_{2i,r}Z_{2i,r+1}}\,(\eta_i + S_{i,r}t_{i,r}) \\ j\dfrac{(\eta_i + S_{i,r}t_{i,r})}{\sqrt{Z_{2i,r}Z_{2i,r+1}}} & \sqrt{\dfrac{Z_{2i,r+1}}{Z_{2i,r}}}\,(S_{i,r}-\eta_i t_{i,r}) \end{bmatrix} \tag{18b}$$

where $t_{i,r}$ is a phase correcting factor introduced to preserve the all-pass characteristic of channel i at F_{1i} and F_{2i}:

$$S_{i,r} = \sin(r\pi/n_i).$$

$Z_{1i,r}$ and $Z_{2i,r}$ are the image impedances of the rth section of channel i and required to be different at F_{1i} and F_{2i}.

In order to modify the element values of channel j ($j = 1,2,3,\cdots,L$), the remaining channels of the multiplexer $i \neq j$ may be replaced by their equivalent input impedances evaluated at $\omega = F_{1j}$ and $\omega = F_{2j}$ which are connected in series with the 1-Ω generator load, as shown in Fig. 5, and

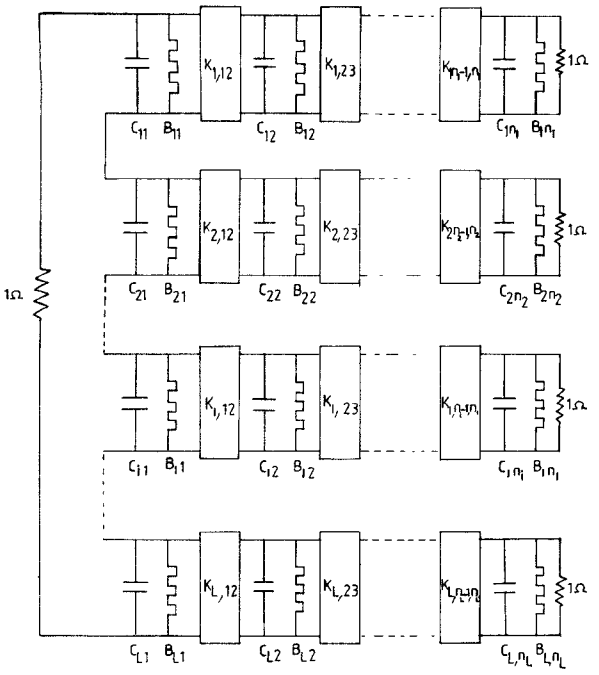

Fig. 4. Series-connected multiplexer.

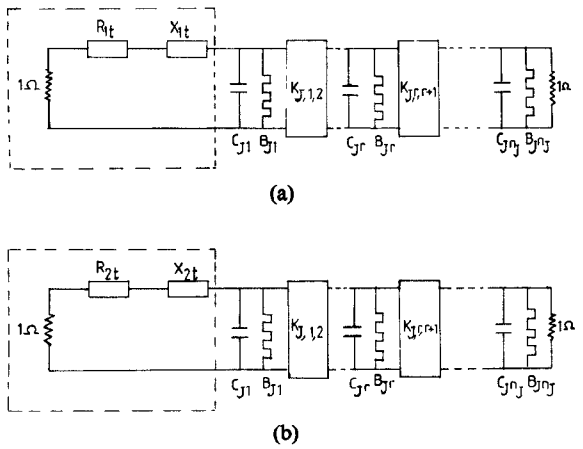

Fig. 5. Equivalent circuit of the multiplexer (series-connected load). (a) At $\omega = F_{1J}$. (b) At $\omega = F_{2J}$.

given by

$$R_{1t}(F_{1j}) = \sum_{i \neq j}^{L} R_{1i}(F_{1j}) \tag{19a}$$

$$X_{1t}(F_{1j}) = \sum_{i \neq j}^{L} X_{1i}(F_{1j}) \tag{19b}$$

$$R_{2t}(F_{2j}) = \sum_{i \neq j}^{L} R_{2i}(F_{2j}) \tag{19c}$$

and

$$X_{2t}(F_{2j}) = \sum_{i \neq j}^{L} X_{2i}(F_{2j}) \tag{19d}$$

where $R_{1t}(F_{1j})$ and $R_{2t}(F_{2j})$ are the sum of the real parts of the input impedances of the individual channels evaluated at F_{1j} and F_{2j}, respectively, and $X_{1t}(F_{1j})$ and $X_{2t}(F_{2j})$ are the sum of the imaginary parts of the input impedances of the individual channels evaluated at F_{1j} and F_{2j}, respectively.

For convenience, the load from the common junction side to channel j is replaced by its shunt equivalent circuit, as shown in Fig. 6, where $G_{1t}(F_{1j})$ and $G_{2t}(F_{2j})$ are the real parts, $Y_{1t}(F_{1j})$ and $Y_{2t}(F_{2j})$ are the imaginary parts. Hence, they are given by

$$G_{1t}(F_{1j}) = \left(1 + R_{1t}(F_{1j})\right) / \left(\left(1 + R_{1t}(F_{1j})\right)^2 + X_{1t}^2(F_{1j})\right) \tag{20a}$$

$$Y_{1t}(F_{1j}) = -X_{1t}(F_{1j}) / \left(\left(1 + R_{1t}(F_{1j})\right)^2 + X_{1t}^2(F_{1j})\right) \tag{20b}$$

$$G_{2t}(F_{2j}) = \left(1 + R_{2t}(F_{2j})\right) / \left(\left(1 + R_{2t}(F_{2j})\right)^2 + X_{2t}^2(F_{2j})\right) \tag{20c}$$

and

$$Y_{2t}(F_{2j}) = -X_{2t}(F_{2j}) / \left(\left(1 + R_{2t}(F_{2j})\right)^2 + X_{2t}^2(F_{2j})\right). \tag{20d}$$

Now let $i = j$ in matrix (17), whose basic section can be decomposed into a transfer matrix of a shunt resonator and an admittance inverter [5]. Hence, the overall admittance of the shunt resonator can be described by

$$C_{j,r}\{F_{1j} - I_{j,r}\} = \frac{-1}{Z_{1j,r}} \left\{ \frac{(S_{j,r} + \eta_j t_{j,r})}{(\eta_j - S_{j,r} t_{j,r})} + \frac{(S_{j,r-1} + \eta_j t_{j,r-1})}{(\eta_j - S_{j,r-1} t_{j,r-1})} \right\} \tag{21}$$

and the characteristic admittance of the inverter is given by

$$K_{j,r,r+1} = \frac{\sqrt{(\eta_j^2 + S_{j,r}^2)(1 + t_{j,r}^2)}}{\sqrt{Z_{1j,r} Z_{1j,r+1}}\,(\eta_j - S_{j,r} t_{j,r})}. \tag{22}$$

Similarly from matrix (18b)

$$C_{j,r}\{F_{2j} - I_{j,r}\} = \frac{1}{Z_{2j,r}} \left\{ \frac{(S_{j,r} - \eta_j t_{j,r})}{(\eta_j + S_{j,r} t_{j,r})} + \frac{(S_{j,r-1} - \eta_j t_{j,r-1})}{(\eta_j + S_{j,r-1} t_{j,r-1})} \right\} \tag{23}$$

and

$$K_{j,r,r+1} = \frac{\sqrt{(\eta_j^2 + S_{j,r}^2)(1 + t_{j,r}^2)}}{\sqrt{Z_{2j,r} Z_{2j,r+1}}\,(\eta_j + S_{j,r} t_{j,r})}. \tag{24}$$

Since $K_{j,r,r+1}$ is characteristic admittance of a frequency independent inverter, from (22) and (24) we have

$$R_{0j,r+1} = \frac{1}{R_{0j,r}} \left(\frac{\eta_j + S_{j,r} t_{j,r}}{\eta_j - S_{j,r} t_{j,r}} \right)^2 \tag{25}$$

where

$$R_{0j,r} = \frac{Z_{1j,r}}{Z_{2j,r}}. \tag{26}$$

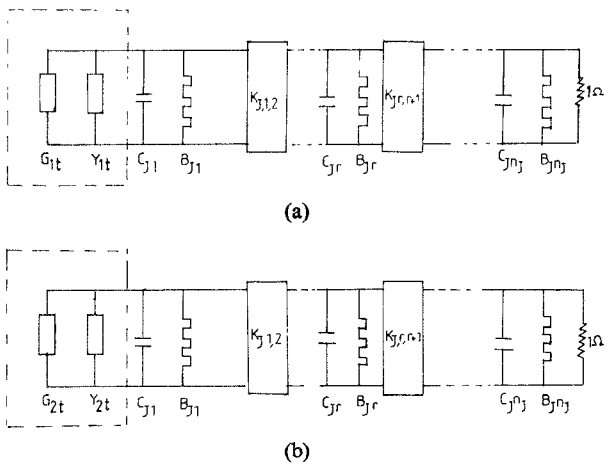

Fig. 6. Equivalent circuit of the multiplexer (parallel-connected load). (a) At $\omega = F_{1j}$. (b) At $\omega = F_{2j}$.

In addition it has been found, after trying different relationships, that if the individual channel network is originally symmetrical, then the required impedance variation level through it can be approximately expressed by the following expressions which give the best possible return-loss response over the entire passband

$$Z_{1j,r+1} = (Z_{1j,r})^{1/4} \tag{27a}$$

$$Z_{2j,r+1} = (Z_{2j,r})^{1/4} \tag{27b}$$

and consequently

$$R_{0j,r+1} = (R_{0j,r})^{1/4}. \tag{27c}$$

Furthermore, for the all-pass behavior in the auxiliary parameter for each channel at its critical frequencies we must have

$$Z_{1j,1} = 1/G_{2t}(F_{1j})$$

and

$$Z_{2j,1} = 1/G_{2t}(F_{2j}).$$

So, from (25) an expression for $t_{j,r}$ can be written as

$$t_{j,r} = (\eta_j / S_{j,r}) \left[\frac{\sqrt{R_{0j,r} R_{0j,r+1}} - 1}{\sqrt{R_{0j,r} R_{0j,r+1}} + 1} \right] \tag{28}$$

and

$$t_{j,0} = 0.$$

The modified values of the elements with the first resonator of channel (j) can be obtained by solving the following two equations for $C_{j,1}$ and $I_{j,1}$:

$$Y_{1t}(F_{1j}) + C_{j1}\{F_{1j} - I_{j1}\} = -A_{0j,1} \tag{29}$$

$$Y_{2t}(F_{2j}) + C_{j1}\{F_{2j} - I_{j1}\} = B_{0j,1} \tag{30}$$

to give

$$C_{j,1} = \frac{Y_{1t}(F_{1j}) - Y_{2t}(F_{2j}) + A_{0j,1} + B_{0j,1}}{(F_{2j} - F_{1j})} \tag{31}$$

and

$$I_{j1} = F_{1j} + \{ Y_{1t}(F_{1j}) + A_{0,j,1} \} / C_{j1} \tag{32}$$

where

$$A_{0j,1} = G_{1t}(F_{1j}) \left(\frac{S_{j,1} + \eta_j t_{j,1}}{\eta_j - S_{j,1} t_{j,1}} \right) \tag{33}$$

$$B_{0j,1} = G_{2t}(F_{2j}) \left(\frac{S_{j,1} - \eta_j t_{j,1}}{\eta_j + S_{j,1} t_{j,1}} \right). \tag{34}$$

The modified value of the remaining resonators of channel (j) can be obtained by solving (21) and (23) for C_{jr} and I_{jr}:

$$C_{jr} = \left\{ \frac{A_{0j,r}}{Z_{1j,r}} + \frac{B_{0j,r}}{Z_{2j,r}} \right\} / (F_{2j} - F_{1j}), \qquad r = 2 \rightarrow n_j \tag{35}$$

$$I_{jr} = F_{1j} + \frac{A_{0j,r}}{Z_{1j,r} C_{jr}}, \qquad r = 2 \rightarrow n_j \tag{36}$$

where

$$A_{0j,r} = \frac{S_{j,r} + \eta_j t_{j,r}}{\eta_j - S_{j,r} t_{j,r}} + \frac{S_{j,r-1} + \eta_j t_{j,r-1}}{\eta_j - S_{j,r-1} t_{j,r-1}} \tag{37}$$

$$B_{0j,r} = \frac{S_{j,r} - \eta_j t_{j,r}}{\eta_j + S_{j,r} t_{j,r}} + \frac{S_{j,r-1} - \eta_j t_{j,r-1}}{\eta_j + S_{j,r-1} t_{j,r-1}}. \tag{38}$$

The modified characteristic impedance of the inverter $K_{j,r,r+1}$ can be obtained by using either (22) or (24).

A computer program has been written to perform the modification process. This process is then repeated channel by channel until all the elements values converge. No proof of convergence is offered but it has been found that if the channel crossover insertion-loss levels are in excess of 3 dB the process appears to converge.

III. Prototype Examples and Computer Analysis

1) The generality of this procedure is demonstrated here by an asymmetric 8-channel multiplexer whose individual filters are designed with varying number of resonators, bandwidths, and interchannel separations, but are identical in their inband return loss of 20 dB. (There is no restriction in this theory against designing the individual filters to have varying inband return loss as well.) The design specifications are given in Table I, and the computer analysis of the common port return loss of the resulting multiplexer is shown in Fig. 7. It may be seen that all of the channels have a good match even for such complicated multiplexer.

2) A triplexer has been designed with each of the three channels having six resonators, bandwidth of 2 rad/s, minimum inband return loss of 26 dB, and center frequencies at $\omega = 1.5$, 4.5, and 7.5. respectively.

The modified elements values are given in Table II and the return-loss and insertion-loss characteristics are plotted in Figs. 8 and 9, respectively. This example demonstrates the applicability of this design procedure to a high return-loss specification and shows that the parame-

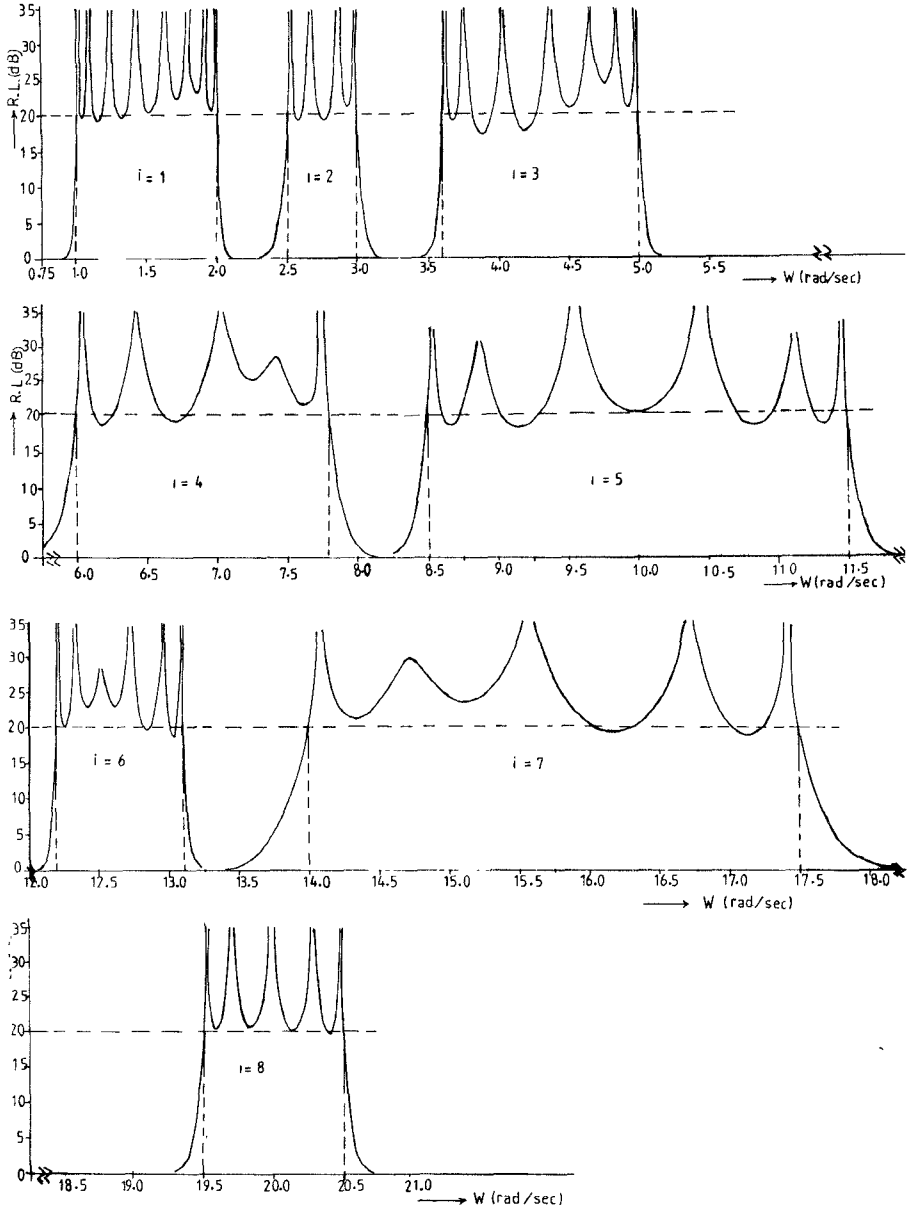

Fig. 7. Return-loss characteristic of 8-channel asymmetric multiplexer; minimum return loss = 20 dB. i = channel number (individual channel specifications are given in Table I).

TABLE I
A SYMMETRIC MULTIPLEXER SPECIFICATION: MINIMUM RETURN LOSS = 20 dB, i = CHANNEL NUMBER, n_i = NUMBER OF RESONATORS, AND ω_{1i} AND ω_{2i} ARE THE LOWER AND UPPER PASSBAND EDGES OF CHANNEL i, RESPECTIVELY

i	n_i	ω_{1i}	ω_{2i}
1	8	1	2
2	4	2.5	3
3	7	3.6	5
4	5	6	7.8
5	7	8.5	11.5
6	6	12.2	13.1
7	5	14	17.5
8	5	19.5	20.5

ters associated with the first resonator of each individual channel suffer the largest modification while the last resonator parameters suffer the least modification.

3) *A Contiguous Diplexer:* The validity of this design procedure has been tested for a limiting contiguous case of a diplexer of degree 5, with a return loss of 26 dB for both channels. The first channel has band edges at $\omega_{11} = 0.175$ and at $\omega_{12} = 2.175$ while the second channel has its band edges at $\omega_{21} = 2.525$ and at $\omega_{22} = 4.525$. The modified values of this diplexer are given in Table III and the computer analysis of the insertion-loss and return-loss characteristics shown in Fig. 10, where the required 3-dB loss at the crossover frequency is observed and the return loss at the common port does not fall below 19.6 dB. This is an acceptable situation for many applications.

From the many examples which have been designed and analyzed by a computer, several points of interest

TABLE II
ELEMENT VALUES OF THREE-CHANNEL MULTIPLEXER (MINIMUM RETURN LOSS = 26 dB FOR ALL CHANNELS)

	r	1	2	3	4	5	6
Channel 1 $n_1=6, \omega_{11}=.5, \omega_{12}=2.5$	C_{1r}	0.587586	1.97644	2.88192	2.93414	2.15776	0.790699
	I_{1r}	0.632983	1.40632	1.48548	1.49618	1.49853	1.49899
	$K_{1,r,r+1}$	1.00325	1.56137	1.79859	1.65239	1.25728	0
Channel 2 $n_2=6, \omega_{21}=3.5, \omega_{22}=5.5$	C_{2r}	1.02058	2.10667	2.9333	2.94736	2.16019	0.790922
	I_{2r}	4.5	4.5	4.5	4.5	4.5	4.5
	$K_{2,r,r+1}$	1.18079	1.63249	1.81896	1.65706	1.25817	0
Channel 3 $n_3=6, \omega_{31}=6.5, \omega_{32}=8.5$	C_{3r}	0.587586	1.97644	2.88192	2.93414	2.15776	0.790699
	I_{3r}	8.36702	7.59368	7.51452	7.50382	7.50147	7.50101
	$K_{3,r,r+1}$	1.00325	1.56137	1.79859	1.65239	1.25728	0

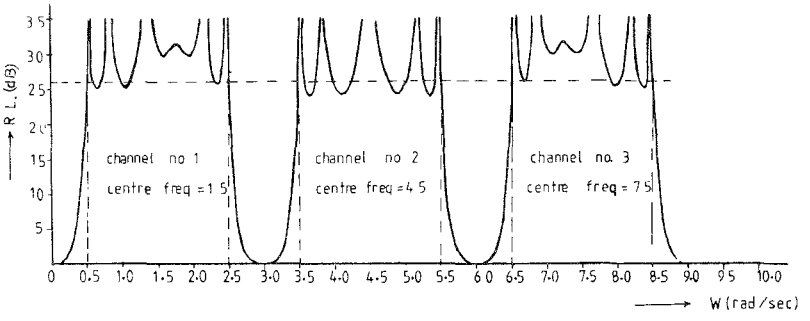

Fig. 8. Return-loss characteristic of three-similar-channel multiplexer $n=6$ resonator; minimum return loss = 26 dB; bandwidth = 2.

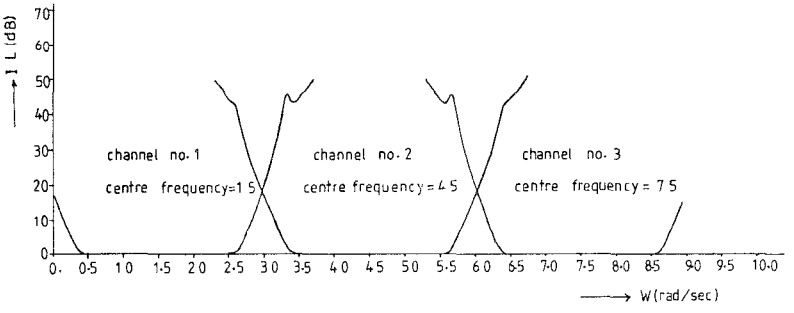

Fig. 9 Insertion-loss characteristic of three-similar channels multiplexer $n=6$ resonator; minimum return loss = 26 dB; bandwidth = 2.

TABLE III
ELEMENT VALUES OF A CONTIGUOUS PROTOTYPE BP/BP DIPLEXER

	Channel 1 $n_1=5$, R.L.=26dB, $\omega_{11}=.175, \omega_{12}=2.175$			Channel 2 $n_2=5$, R.L =26dB, $\omega_{21}=2.525, \omega_{22}=4.525$		
r	C_{1r}	I_{1r}	$K_{1,r,r+1}$	C_{2r}	I_{2r}	$K_{2,r,r+1}$
1	0.428514	-0.132203	0.90002	0.428514	4.8322	0.90002
2	1.77957	0.969964	1.40676	1.77957	3.73004	1.40676
3	2.38908	1.13869	1.50911	2.38908	3.56131	1.50911
4	1.98661	1.16237	1.22983	1.98661	3.53763	1.22983
5	0.764275	1.16664	0	0.764275	3.53336	0

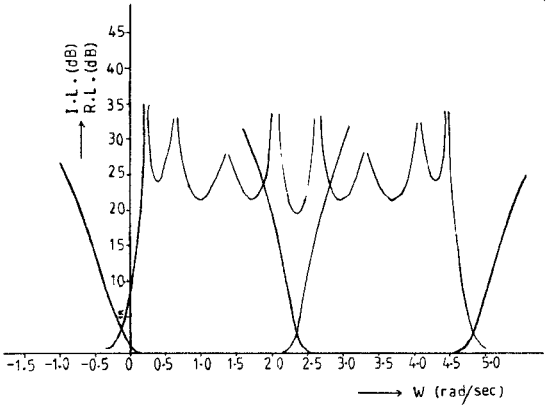

Fig. 10. A contiguous BP/BP channel diplexer $n=5$; minimum return loss = 26 dB.

arise. The design procedure is a very general one in the sense that it can handle the design of complicated asymmetric multiplexer with only a slight mismatch in some channels. The resulting multiplexers designed according to this technique are canonic (the degrees of the multiplexer is equal to the sum of the degrees of the individual channel filters), because there is no necessity for annulling immittance networks or dummy channels to be added to the multiplexer. Furthermore, this optimum doubly terminated design procedure shares the advantage of an increase of at least 6 dB in the attenuation level over the passband regions of all other channels, similar to other common junction multiplex design method based upon doubly terminated prototype, e.g., [3].

IV. CONCLUSIONS

A new general design procedure has been presented for bandpass Chebyshev channel multiplexers without the addition of immittance compensation networks or dummy channels. This design procedure is also an approximate one since an exact synthesis procedure has not yet been found for this type of L-port network. It is believed that a further improvement could be made if an exact expression could be derived for the internal impedance level variation through each individual channel instead of the approximate one given in (27a)–(c). If a correct all-pass equivalent form could be obtained at a third point of perfect transmission different from those closest to the passband edges of each individual channel, an improvement could be made. Attempts to obtain this solution have so far not been successful. However, this design procedure for a direct connection of all channels at a common junction results in an excellent design without the necessity for any annulling network and represents a strictly canonical solution.

REFERENCES

[1] R. J. Wenzel and W. G. Erlinger, "Narrow band contiguous multiplexing filters with arbitrary amplitude and delay response," in *IEEE PG-MTT, 1976 Int. Symp. Dig.*, pp. 116–118.
[2] M. H. Chen, F. Assal, and C. Mahle, "A contiguous band multiplexer," *Comsat Tech. Rev.*, vol. 6, no. 2, pp. 285–305, Fall 1976.
[3] J. D. Rhodes and R. Levy, "A generalized multiplexer theory," *IEEE Trans. Microwave Theory Tech.*, vol. MTT-27, no. 2, Feb., 1979.
[4] J. D. Rhodes, *Theory of Electrical Filters*. New York: Wiley, 1976.
[5] R. K. Brayton, L. O. Chua, J. D. Rhodes, and R. Spence, *Modern Network Theory—An Introduction*. Switzerland: Georgi Pub., 1978.

Design of Manifold-Coupled Multiplexers

Richard J. Cameron and Ming Yu

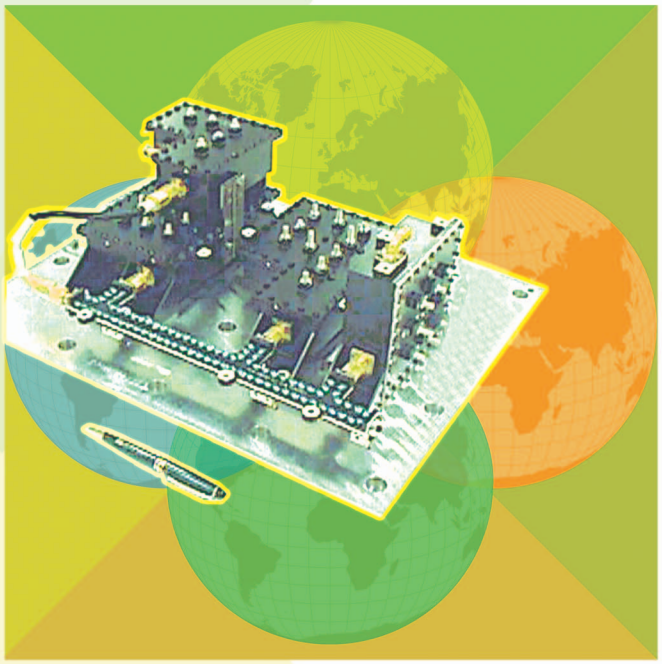

© ARTVILLE

Although the principles of combining or separating frequency diverse microwave signals (channels) for interfacing with a single port of an antenna system have been known for many years now, it was with the advent of satellite communication systems in the 1970s that the greatest technical advances were made. In the satellite transponder itself, the uplinked channel groups from a common antenna need to be separated (demultiplexed) to allow separate routing and processing before power amplification and downlinking to (possibly) different zones on Earth (Figure 1). Here, very high selectivity is most critical to prevent adjacent channel interference and multipath effects. It is usually preferred that the bulk of the channel selectivity task as the channel passes through the transponder is done by the input demultiplexer (IMUX) filters to keep the output multiplexer (OMUX) filters as simple and low-loss as possible.

On the high-power side, the channels for downlinking need to be efficiently combined into one high-power composite output and transferred to the input port of an antenna feed system. Now, lowest possible loss is a priority, with a certain amount of selectivity to suppress out-of-band spectral regrowth caused by nonlinearities in the power amplifiers [traveling wave tube amplifiers (TWTAs) or solid-state power amplifiers (SSPAs)]. Further essential features that will be required of the IMUX and OMUX subsystems and their filters will be noted later.

A third category of multiplexers that have been finding widespread application lately are the transmit/receive diplexers in the basestations of cellular telephony systems. These devices perhaps have the most demanding electrical and build-standard requirements of all, accommodating as they do both high- and low-power signals in close proximity within one housing. In some cases, these diplexers are located at the top of transmitter masts, and there experience the worst of climatic extremes.

This article offers a brief overview of the principles of operation and the main design considerations for four different multiplexer subsystem configurations. The design method for the manifold multiplexer is

Richard J. Cameron and Ming Yu (ming.yu@ieee.org) are with COM DEV in Cambridge, Ontario, Canada.

Digital Object Identifier 10.1109/MMM.2007.904715

 1527-3342/07/$25.00©2007 IEEE

explained in detail, using as an example the design and optimization of a four-channel output multiplexer. A more comprehensive review of waveguide (de)multiplexing systems—including practical information, design formulae, and a good bibliography—may be found in [1].

Multiplexer Configurations

Over the past three decades, there have been many advances in the design and implementation of multiplexing networks [1]–[23]. The most commonly used configurations are:

- hybrid-coupled multiplexers,
- circulator-coupled multiplexers,
- directional filter multiplexers, and
- manifold-coupled multiplexers.

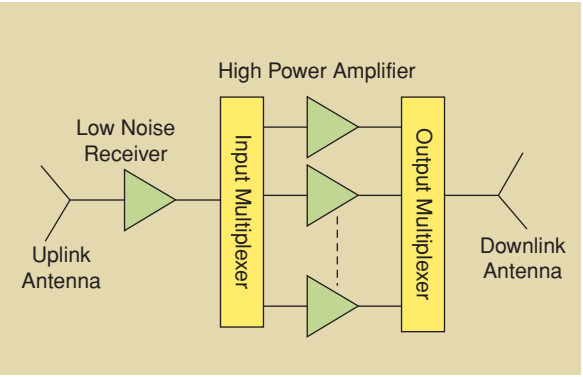

Figure 1. *A simplified block diagram of a satellite payload.*

A summary of the advantages and disadvantages of these multiplexer configurations is given in Table 1 [6].

TABLE 1. A Comparison of Various Multiplexer Configurations.

Hybrid-Coupled Mux Advantages	Circulator-Coupled Mux Advantages	Directional Filter Mux Advantages	Manifold Multiplexer Advantages
–Amenable to a modular concept. –Simple to tune, no interaction between channel filters.	–Requires one filter per channel. –Employs standard design of filters. –Simple to tune. –No interaction between channel filters.	–Requires one filter per channel. –Simple to tune, no interaction between channel filters.	–Requires one filter per channel. Most compact design.
–Total power in transmission modes as well as reflection mode is divided by the hybrid so that only 50% of the power is incident on each filter. Power handling is thus increased and susceptibility to voltage breakdown is reduced.	–Amenable to a modular concept.	–Amenable to a modular concept.	–Capable of realizing optimum performance, both in terms of absolute insertion loss and amplitude and group delay response.
Disadvantages	**Disadvantages**	**Disadvantages**	**Disadvantages**
–Two identical filters and two hybrids are required for each channel.	–Signals must pass in succession through circulators, incurring extra loss per trip.	–Restricted to realize all- pole functions such as Butterworth and Chebyshev.	–Complex design.
–Line lengths between hybrids and filters require precise balancing to preserve circuit directivity.	–Low-loss, high-power ferrite circulators are expensive.	–Difficult to realize bandwidths greater than 1%.	–Tuning of the multiplexer can be time-consuming and expensive.
–The physical size and weight of the multiplexer is greater than other approaches.	–Higher level of passive intermodulation (PIM) products than other configurations.	–Restricted to the use of single-mode filters.	–Not amenable to a flexible frequency plan, i.e., change of a channel frequency will require a new multiplexer design.

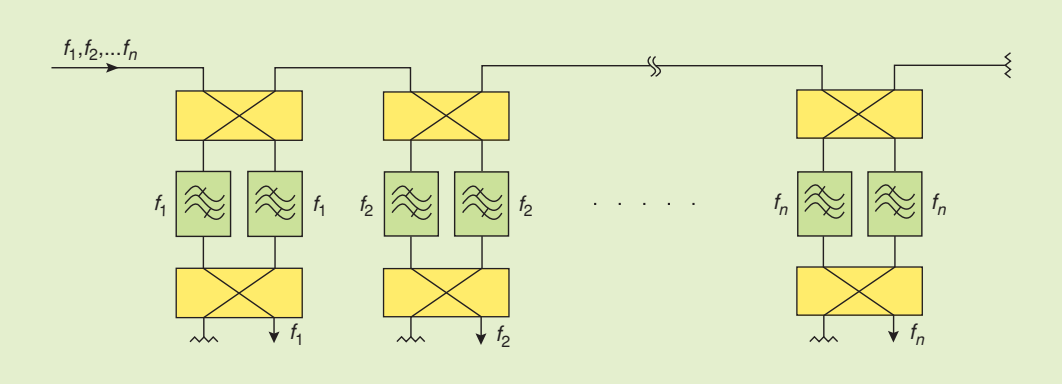

Figure 2. *Layout of a hybrid-coupled multiplexer.*

Hybrid-Coupled Approach

Figure 2 shows a layout of a hybrid-coupled multiplexer. Each channel consists of two identical filters and two identical 90° hybrids. The main advantage of the hybrid-coupled approach is its directional property, which minimizes the interaction between the channel filters. As a consequence, it is amenable to a modular concept, allowing the integration of additional channels at a later date without disrupting the existing multiplexer design, a requirement in some systems. Another key advantage of this approach is that only half of the input power goes through each filter. Thus, the filter design can be relaxed when using this type of multiplexer in high-power applications. On the other hand, it has the disadvantage of larger size since two filters and two hybrids per channel are required. Another design consideration of such multiplexers is the phase deviation between the two filter paths that the two signals undergo before they add constructively at the channel output. The structure, therefore, must be fabricated with tight tolerances to minimize the phase deviation.

Circulator-Coupled Approach

Each channel in this case consists of a channel-dropping circulator and one filter, as shown in Figure 3. The unidirectional property of the circulator provides the same advantages as the hybrid-coupled approach in terms of amenability to modular integration and ease of design and assembly. The insertion loss of the first channel is the sum of the insertion loss of the channel filter and the insertion loss of the circulator. The subsequent channels exhibit a relatively higher loss due to the insertion loss incurred during each trip through the channel-dropping circulators. This is the most common realization for input multiplexers.

Directional Filter Approach

Figure 4 illustrates a layout of a multiplexer realized by connecting directional filters in series. A directional filter is a four-port device in which one port is terminated in a load. The other three ports of the directional filter essentially act as a circulator connected to a bandpass filter. Power incident at one port emerges at the second port with a bandpass frequency response while the reflected power from the filter emerges at the third port.

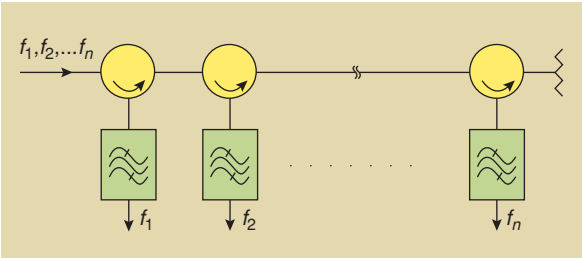

Figure 3. *A circulator-coupled multiplexer.*

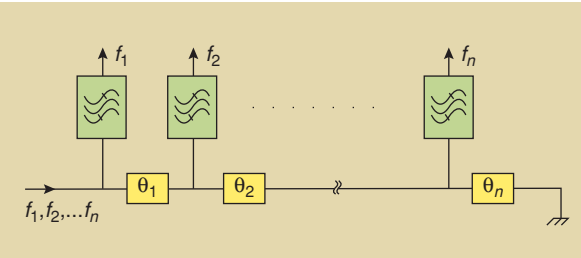

Figure 5. *A manifold-coupled multiplexer.*

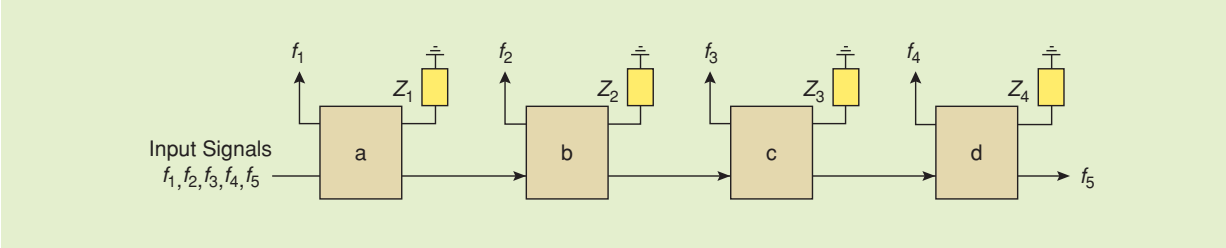

Figure 4. *A directional filter multiplexer.*

Directional filters, however, do not require the use of ferrite circulators. The waveguide version of a directional filter is typically realized by coupling rectangular waveguides operating in TE_{10} modes to a circular waveguide filter operating in TE_{11} modes. The microstrip version consists of one-wavelength ring resonators coupled to one another and to two transmission lines. This multiplexing approach has the same advantages as the hybrid-coupled and circulator-coupled approaches. It is, however, limited to narrow-band applications.

Manifold-Coupled Approach

The manifold-coupled approach shown in Figure 5 is viewed as the optimum choice as far as miniaturization and absolute insertion loss are concerned. This type of multiplexer requires the presence of all the channel filters at the same time so that the effect of channel interactions can be compensated in the design process. It implies that a manifold-coupled multiplexer is not amenable to a flexible frequency plan; any change in the allocation of channels will require a new multiplexer design. Moreover, as the number of channels increases, this approach becomes more difficult to implement. The manifold-coupled multiplexer shown in Figure 5 acts as a channelizer, but the same configuration can be used as a combiner. Figure 6 shows a 19-channel multiplexer employing a waveguide manifold. The manifold-coupled concept can be implemented as well in planar circuits as shown in Figure 7, where three high-temperature superconductivity (HTS) microstrip filters are integrated with a microstrip manifold [17]. In this particular case, one of the channels is connected directly to the manifold. Figure 8 show a three-channel L-band multiplexer using coaxial manifold and combline channel filters. The manifold-coupled multiplexer is widely used for most OMUX applications today, and its design technique is the focus of this article.

Three common manifold multiplexer configurations are shown in Figure 9, with all channel filters connected to one side of the manifold (comb), to both sides (herringbone), and end-fed (applicable to either of the first two).

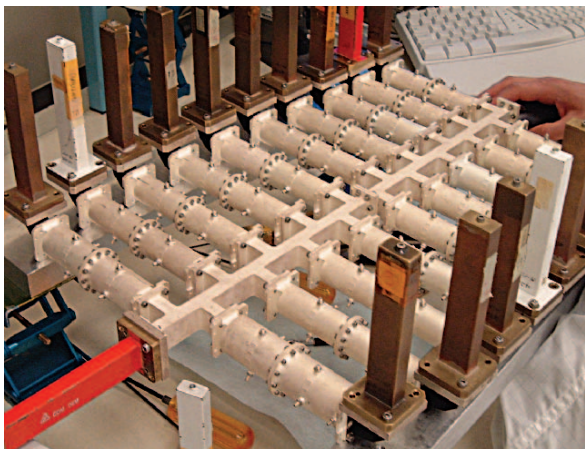

Figure 6. *A 19-channel Ku-band waveguide multiplexer [21].*

The technique is readily applicable to manifold multiplexers incorporating an arbitrary number of channels, regardless of their bandwidths and channel separations.

The design techniques for manifold multiplexers underwent rapid development in the 1970s and 1980s when it was realized that they were ideal for communication satellite payloads [4]–[7]. On the electrical side, design techniques have advanced to the point where it is possible to combine an arbitrary number of channels, regardless of their bandwidths and channel separations. There are no restrictions on the design and implementation of channel filters onto the manifold. The manifold itself is a transmission line, be it a coaxial line or a rectangular waveguide or some other low-loss structure. It is possible to achieve channel performance in the multiplexer configuration close to that of a channel filter by itself. No other multiplexer configuration can match this performance.

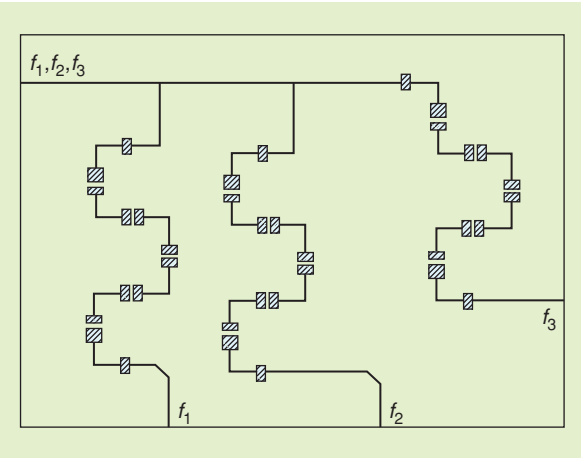

Figure 7. *A three-channel planar HTS multiplexer [17].*

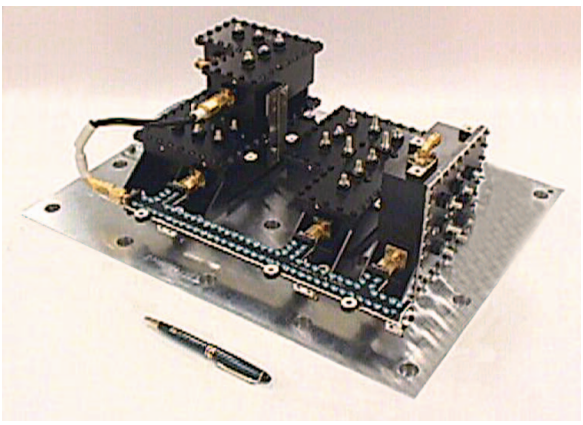

Figure 8. *A three-channel L-band multiplexer using coaxial manifold and combline channel filters [20].*

On the mechanical side, the entire structure may be made to be very lightweight and compact, while rugged enough to withstand the vibrations and other rigors of a launch into space. By using special materials, the whole structure may be made to be electrically stable in the presence of large environmental temperature fluctuations and be able to conduct dissipated RF thermal energy efficiently to a cooling baseplate [20].

Over the past three decades, there have been many advances in the design and implementation of multiplexing networks.

Design of the Manifold-Coupled Multiplexer

Design Methodology

Since there are no directional or isolating elements in the manifold multiplexer (circulators, hybrids), all channel filters are electrically connected to each other through the near lossless manifold and the design of the manifold multiplexer has to be considered as a whole, not as individual channels. In the early days, a number of ingenious techniques were invented [2]–[5], [8], [9] to design the individual filters such that they would properly interact with the other filters on the same manifold and function virtually as if they were operating into a matched termination. However, with the dramatic increase in computer power that has become available in recent years, practical multiplexer design procedure has tended to utilize optimization methods to achieve the final design, in preference to the more limited analytic techniques.

Analysis of Common-Port Return Loss and Channel Transfer Characteristics

At the heart of any circuit optimizer is an efficient analysis routine, for the optimization will call the analysis routine many thousands of times at different frequencies as it progresses with the task of optimizing the various parameters [11]. In general, the two parameters from which the overall cost function is built up are the multiplexer common-port return loss (CPRL) and the individual channel transfer characteristics.

During the optimization process, the subroutines to calculate CPRL channel transfer characteristics at each frequency sampling point will be called many times. Although it would be possible to construct an admittance matrix for the whole multiplexer circuit and analyze it at each frequency point to obtain the desired transfer and reflection data, this matrix will be quite large for the multiplexer with a large number of channel filters and will take a significant amount of CPU time to invert it even though it will be relatively sparse. Moreover, a lot of data will be obtained that is not used for the optimization.

Later on in this section a piecewise optimization strategy, which has been found to be quite efficient in terms of computer CPU time, will be described [13], [14]. Part of the strategy involves optimizing the channel filters one after the other in a repeated cycle. As the optimization parameters of each filter in turn are being optimized, it is only necessary to calculate the transfer

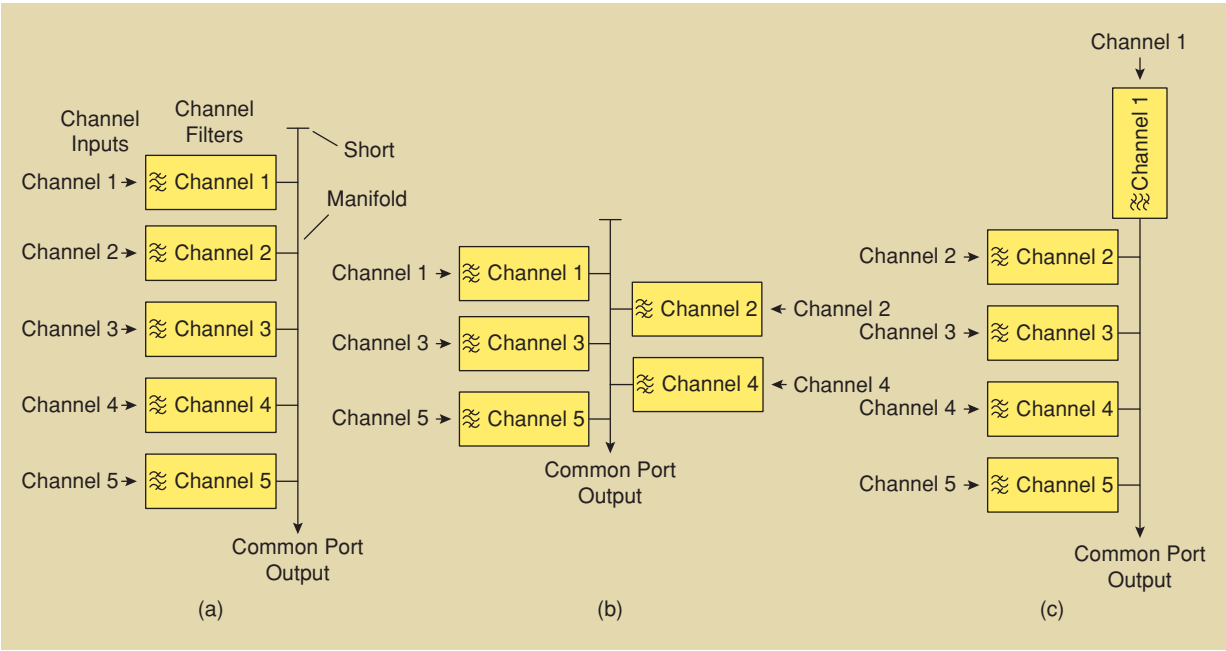

Figure 9. *Common configurations for manifold multiplexers: (a) comb, (b) herringbone, and (c) one filter feeding directly into the manifold.*

characteristic of this filter alone; the others will be relatively unaffected by the changes (assumed small) being made to the filter that is the object of the optimizer's attentions at this stage in the cycle.

To speed up the overall optimization, it becomes more efficient to analyze each filter's input-to-common-port transfer characteristic individually, in addition to the CPRL. The manifold of the multiplexer may be most conveniently represented as an open-wire circuit, with a short circuit at one end and three-port junctions spaced along its length. The channel filters are located at the third port of each junction and are separated from the junction by short lengths of transmission lines (stubs) as shown in Figure 10.

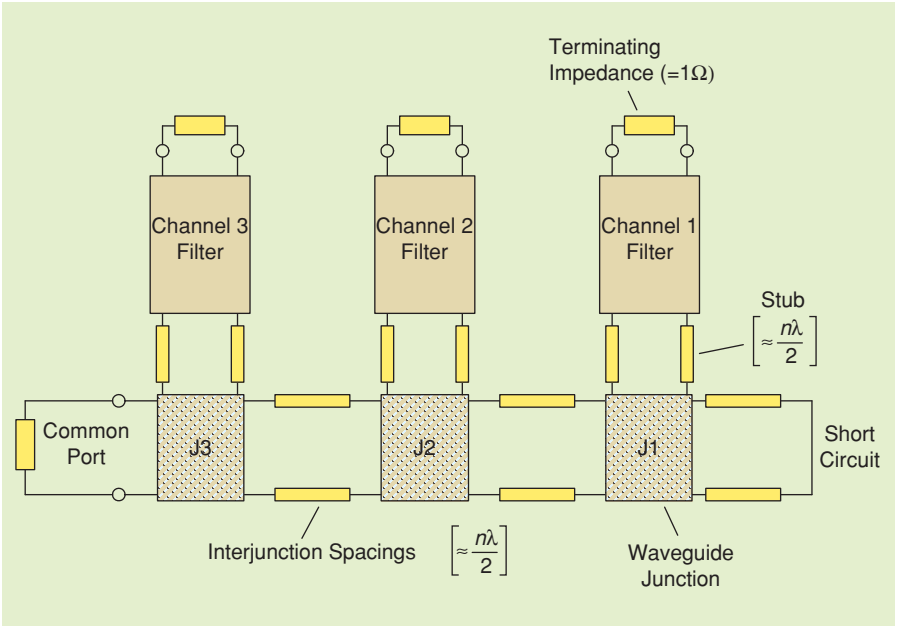

Figure 10. *Open-wire model of waveguide manifold multiplexer (three-channel).*

If the manifold is waveguide, the junctions may be *E*-plane or *H*-plane, and since their intrinsic parameters do not change during the optimization, they are best characterized with three-port *S*-parameters precalculated by a mode-matching routine and stored over a range of frequencies covering the bandwidths of all the channel filters, or specifically at the frequencies of the sampling points. Coaxial junctions are a special case of waveguide junction (*H*-plane). Typically, the junctions are symmetric about ports 1 and 2, leaving the possibility for port 3 to be a different size as described in Figure 11.

Because of reciprocity and the symmetry of the junctions about the vertical axis in Figure 11, $S_{22} = S_{11}$ and $S_{32} = S_{31}$ (*H*-plane) and $S_{32} = -S_{31}$ (*E*-plane). This means that only four parameters—S_{11}, S_{21}, S_{31}, and S_{33}—are needed to completely characterize the electrical performance of the junctions. The *S*-parameter matrices are calculated assuming a matched termination at each port, but if the termination at one port is arbitrary, the two-port *S*-parameters between the other two ports may be defined as follows.

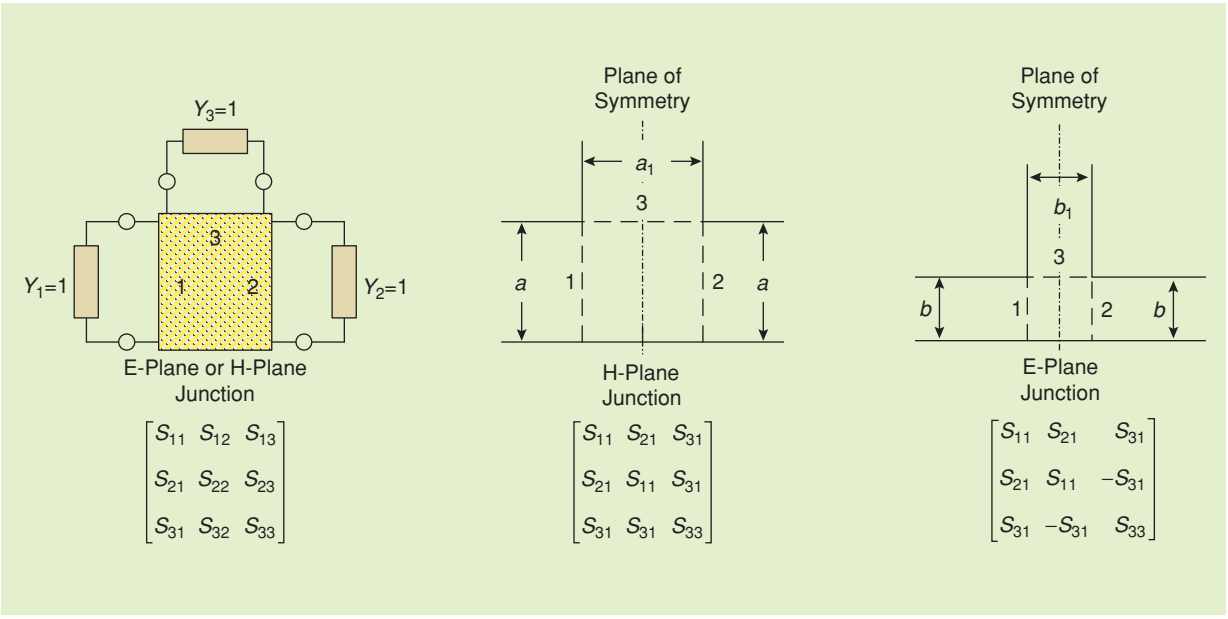

Figure 11. *E-plane and H-plane waveguide junctions and S-parameter matrix representation.*

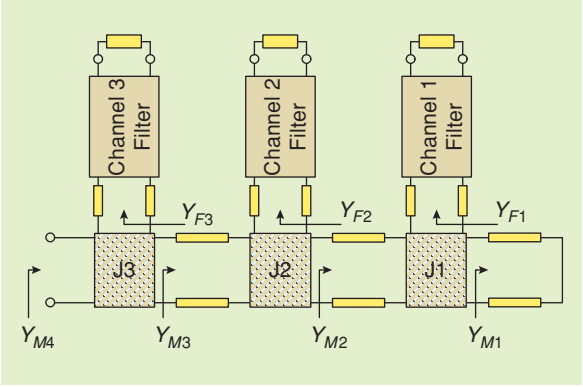

Figure 12. *CPRL computation.*

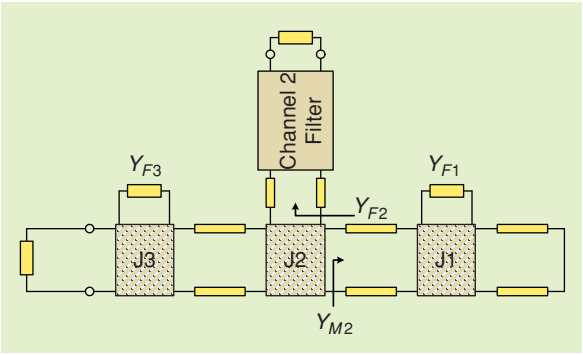

Figure 13. *Channel 2 transfer function calculation.*

1) Admittance $Y_{L2}(\neq 1)$ at port 2:

$$\begin{bmatrix} S'_{11} & S'_{13} \\ S'_{31} & S'_{33} \end{bmatrix} = \begin{bmatrix} S_{11} & S_{13} \\ S_{31} & S_{33} \end{bmatrix} + \frac{\Gamma_2}{1-\Gamma_2 S_{11}} \begin{bmatrix} S_{21}^2 & kS_{21}S_{31} \\ kS_{21}S_{31} & S_{31}^2 \end{bmatrix}, \quad (1)$$

where $\Gamma_2 = (1 - Y_{L2})/(1 + Y_{L2})$, Y_{L2} is the admittance at port 2 of the junction, and $k = 1$ for *H*-plane junctions and -1 for *E*-plane junctions. This modified *S*–matrix also applies if an admittance Y_{L1} is terminating port 1. It is only necessary to change the subscripts from 2 to 1 and vice versa.

2) Admittance $Y_{L3}(\neq 1)$ at port 3:

$$\begin{bmatrix} S'_{11} & S'_{12} \\ S'_{21} & S'_{22} \end{bmatrix} = \begin{bmatrix} S_{11} & S_{12} \\ S_{21} & S_{22} \end{bmatrix} + \frac{\Gamma_3 S_{31}^2}{1-\Gamma_3 S_{33}} \begin{bmatrix} 1 & k \\ k & 1 \end{bmatrix}, \quad (2)$$

where $\Gamma_3 = (1 - Y_{L3})/(1 + Y_{L3})$, Y_{L3} is the admittance at port 3 of the junction, and k has the same meaning as before. These junction *S*-parameters may be easily converted to the [*ABCD*] transfer parameters using standard formulas to enable cascading with the channel filters and stub/manifold line lengths.

CPRL

The common port return loss (CPRL) computation at a given frequency point (e.g., at a sample point) proceeds as follows:

1) Determine the channel filter input admittances Y_{F1}, Y_{F2}, and Y_{F3} at the frequency sample point and store (see Figure 12).
2) Now with known admittances at the port 3 of each junction, the transfer and reflection *S*-parameters [S'_{21}, S'_{11}, see (2)] for each junction may be calculated and converted to [*ABCD*] matrices. Now working from the short-circuit end, the manifold phase lengths and the junctions may be cascaded, at each stage calculating and storing the along-manifold admittances Y_{M1}, Y_{M2}, etc. as shown in Figure 12.

$$Y_{Mi} = \frac{1 + S_{11i}}{1 - S_{11i}}, \quad (3)$$

where $i = 1, 2, \ldots n+1$ and n is the number of channels on the manifold.

The final admittance (Y_{M4} in Figure 12) may be used to calculate the CPRL

$$\Gamma_{CP} = \frac{1 + Y_{Mn+1}}{1 - Y_{Mn+1}}$$
$$\mathrm{RL}_{CP} = -20 \log_{10} \Gamma_{CP} \quad \text{(dB)} \quad (4)$$

If only the manifold spacings $\theta_{M1}, \theta_{M2}, \ldots$ are being optimized, then the filter input admittances $Y_{F1}, Y_{F2}, \ldots$ etc. need only be calculated once at each sample frequency and stored for the optimization of CPRL.

Channel Transfer Characteristics

If optimization is now focused on an individual channel filter and the transfer function between its input and the common port is needed (e.g., for a rejection sample point), the following procedure may be used:

Taking channel 2 as an example, as shown in Figure 13,

1) Calculate the new Y_{F2} for channel 2 with its newly updated parameters.
2) The previously stored value of Y_{M2} may be used in conjunction with equation (1) to calculate S_{31} and S_{11} for junction 2 with Y_{M2} at its port 2.
3) The [*ABCD*] matrices for the channel 2 filter and the S_{31} path of *J*2, and then the rest of the manifold towards the common port (the manifold line length between *J*2 and *J*3, then using equation (2) to find the [*ABCD*] parameters of *J*3 terminated with Y_{F3} at its port 3) may then be cascaded to calculate the transfer characteristic for channel 2. The process may be repeated for the other channels.

For both common-port and transfer characteristics, the computations may be made assuming lossless (purely reactive) components for the filter and stub networks. Then noncomplex arithmetic may be used for the matrix multiplications, inversions, and other calculations, and the process is considerably speeded up.

Channel Filter Design

Being purely reactive (i.e., no resistive elements between the channel inputs and the common-port output), the channel filters of the manifold multiplexer will react with each other through the manifold itself. If the channels are widely spaced, the channel interactions are quite low, because over one filter's passband the other filters are well into their reject regions and will be presenting short circuits at their ports nearest to the manifold. The channel filters may be designed as doubly terminated networks separate from the other filters and the manifold and, when integrated onto the manifold, all that is needed are adjustments to the along-manifold spacings and stub lengths and minor adjustments to the first three or four elements of the filter to recover a good CPRL.

However, as the guard bands between channel filters decrease towards contiguity, they begin to interact strongly along the manifold. Now significant adjustments to the filter parameters are needed in addition to the manifold and stub phase lengths to reach an acceptable CPRL. Although it is possible to optimize doubly terminated filters to operate in a contiguous channel environment, a starting point much closer to the final optimal result is obtained if singly terminated filter prototypes are used in these conditions. The design methods for singly terminated filter prototypes are outlined in [2] and [18].

The singly terminated filter network is useful for the design of contiguous channel manifold multiplexers because the contiguous singly terminated channel filters along the manifold tend to interact in a mutually beneficial manner, providing a conjugate match for each other at their launch points. This natural multiplexing effect may be explained by studying the special characteristics of the input admittance of the singly terminated circuit looking in at the port opposite to the terminated port ($Y_{F1}, Y_{F2}, \ldots$ etc. in Figure 12).

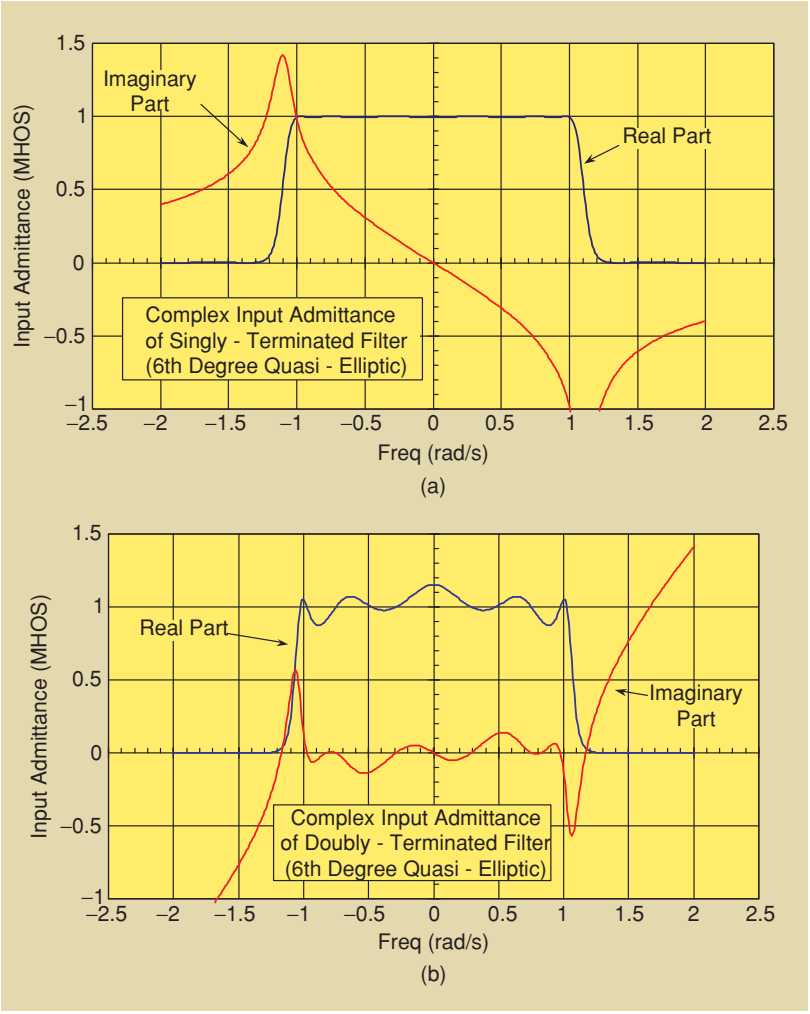

Figure 14. *Characteristics of the real and imaginary parts of prototype input admittance: (a) singly terminated filter and (b) doubly terminated filter.*

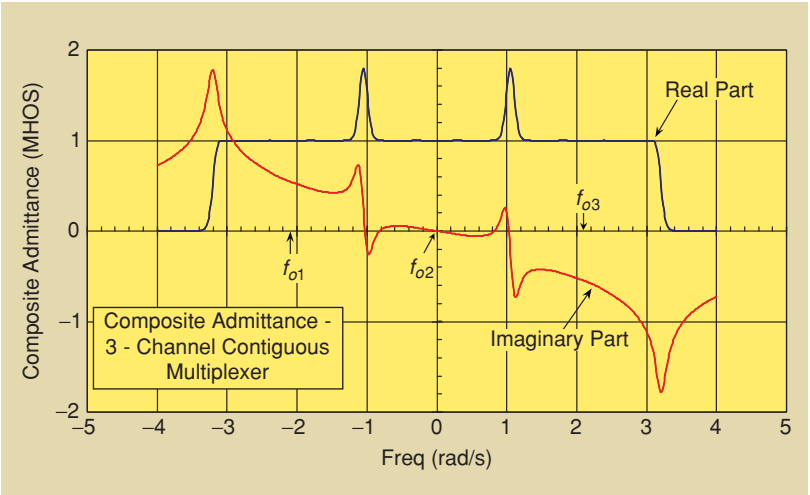

Figure 15. *Singly terminated filter at center frequency f_{02} with two contiguous neighbors f_{01} and f_{03}. Composite admittances as seen from the common port of the manifold.*

The real part of the input admittance has the same characteristic as the filter's own power transfer characteristic. It is close to unity over the filter's passband, dropping to near zero in the out-of-band regions. As frequency increases from minus infinity, the imaginary part

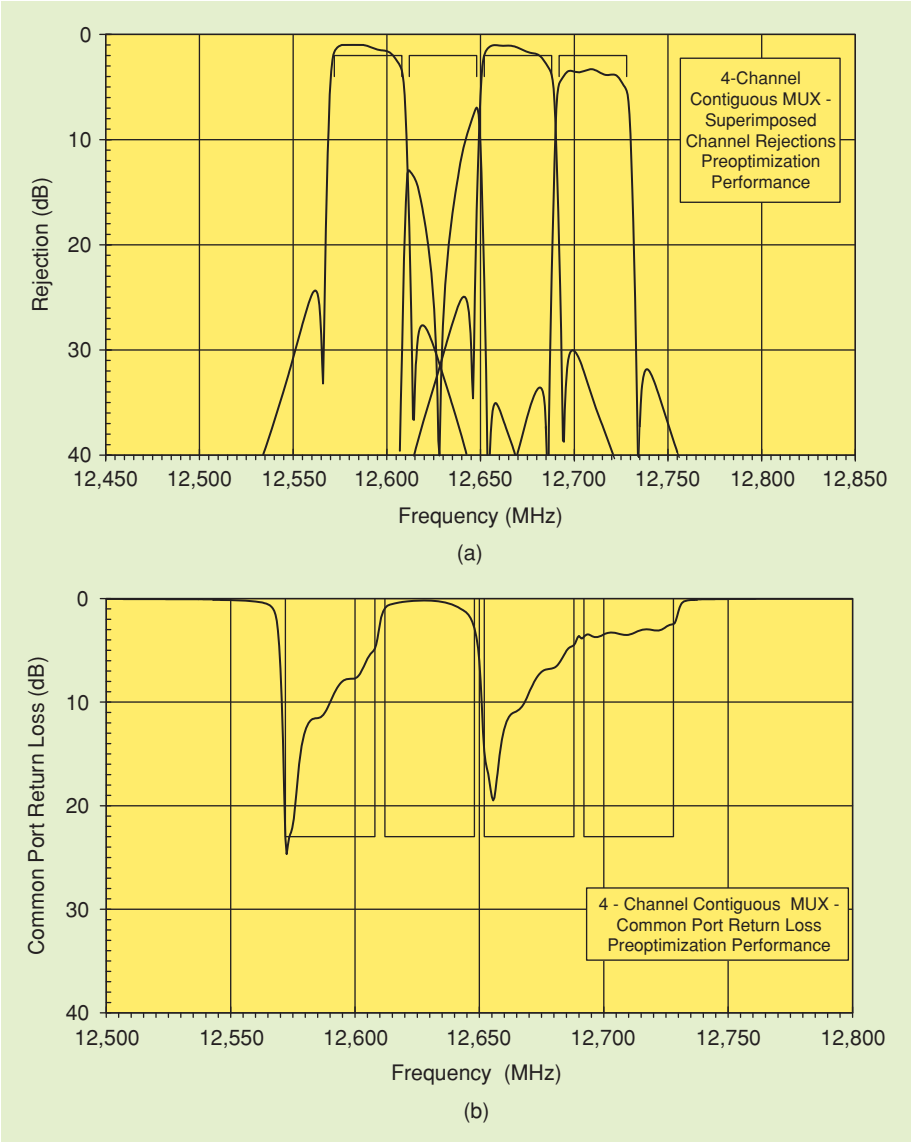

Figure 16. *Four-channel manifold multiplexer—pre-optimization: (a) superimposed channel transfer characteristics and (b) CPRL.*

of the admittance increases from zero towards a positive peak near to the lower passband edge, then traverses the passband with a negative slope towards a negative peak near the upper passband edge. It then slowly returns to zero with a positive slope as frequency continues on towards infinity. Figure 14 illustrates the variations of the real and imaginary parts of the admittance for singly and doubly terminated prototype filters.

If the contiguous-band singly terminated filters are connected to the manifold with the zero impedance termination closest to the manifold junction, then the negative in-band slope of the imaginary part of the admittance will tend to cancel with the positive slopes of the two contiguous neighbors that extend into this filter's passband. The result is illustrated in Figure 15, which shows that the imaginary parts of the source (the singly-terminated filter) and the load (the other filters on the manifold) have partially cancelled, while the unity-valued real part of the source mostly sees the unity load at the common port of the manifold, the impedances at the input ports of the other channel filters being mostly isolated by their own rejection characteristics.

Thus, a conjugate match between the source and the load has been partially achieved for channel filter f_{02}. Although it will not be a perfect conjugate match, it will be better than if doubly terminated filters had been used, and it makes a good point from which to start the optimization process. The channels f_{01} and f_{03} at the edges of the contiguous group on the manifold, having a neighbor on one side only, will tend to have some small in-band and rejection asymmetries after the optimization process.

Optimization Strategy

The networks that model even a moderate-sized waveguide manifold multiplexer tend to be quite complex. An open-wire equivalent circuit of a six-channel manifold multiplexer with sixth-degree quasi-elliptic dual-mode filters has in the order of 90 frequency sampling points and 100 electrical elements of varying sensitivities and different constraints that all need to be correctly valued before the overall multiplexer will operate to specification.

If all these parameters are optimized simultaneously, not only will the amount of CPU time be enormous, but there is little likelihood that the global optimum will be attained, there being a myriad of shallow local optimum solutions. With manifold multiplexers routinely incorporating 20 channels, and perhaps up to 30 in the future, global optimization is clearly unsuitable directly from the start.

For these reasons, most of the major satellite OMUX designers and manufacturers have developed more efficient methods for manifold multiplexer optimization. Among these is the piecewise approach, optimizing parts of the multiplexer separately in repeated cycles while converging upon an optimal solution. The parts or

parameter groups being referred to here might include the first five elements of each channel filter (narrow-band domain), or all the manifold interjunction or stub lengths (wideband domain). It is usual practice to commence the optimization process with the wideband sections first (parameters relating to the manifold and stubs), followed by a shift in emphasis to the narrow-band sections (filter parameters) as the CPRL begins to take shape. A typical design optimization project might proceed as follows:

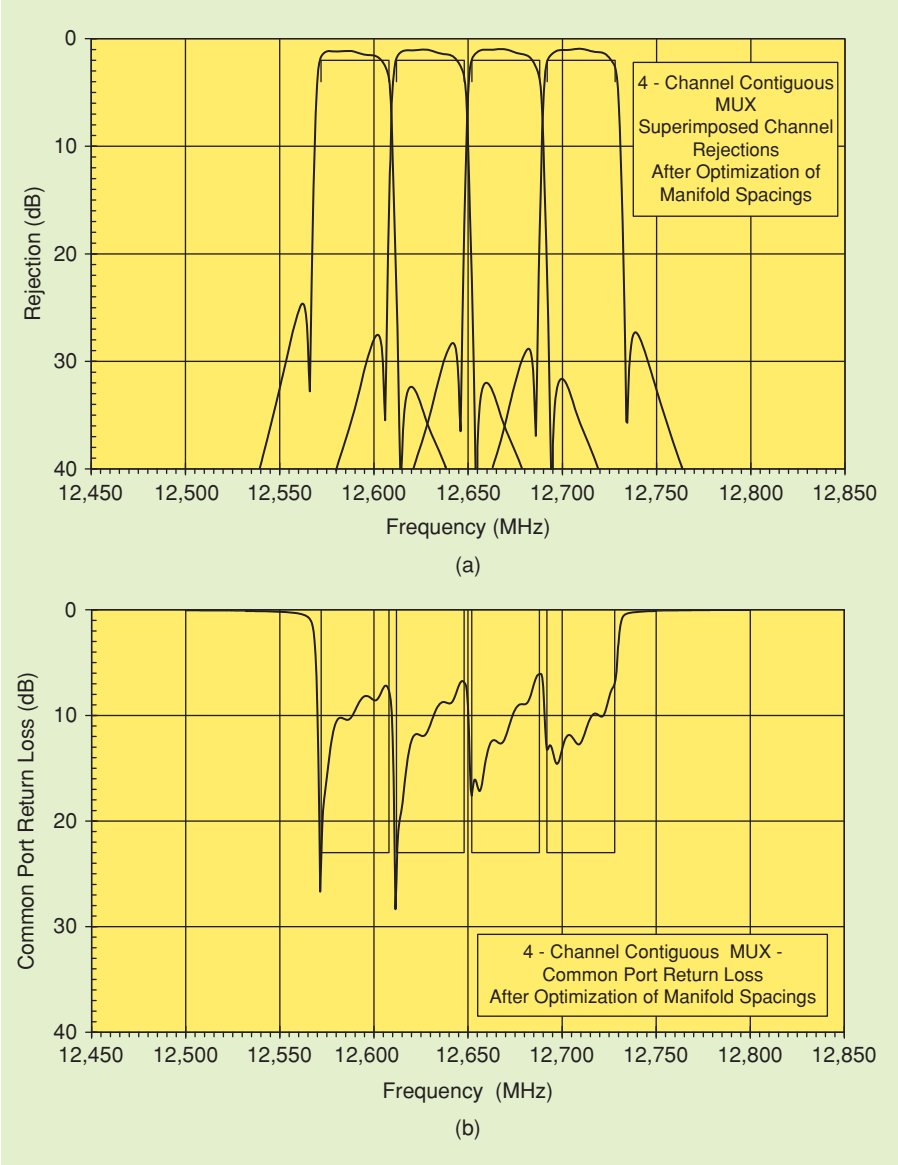

Figure 17. *Four-channel manifold multiplexer after optimization of manifold lengths: (a) superimposed channel transfer characteristics and (b) CPRL.*

• Design

1) Design the channel filter transfer/reflection functions to meet the individual in-band and rejection specifications.
2) Synthesize the corresponding coupling matrices, doubly terminated if the channel filter design bandwidths (DBWs) are separated by guard bands greater than about 25% of the DBWs, singly terminated if otherwise. If singly terminated prototypes are to be used, a more practical design results if the initial prototype is generated with a low return loss to bring the value of the termination at the end opposite to the manifold as close to unity as possible.
3. Set initial manifold spacings between *E*- or *H*-plane junctions at $m\lambda_g/2$, where m is as low as possible for a convenient mechanical layout. Set the initial manifold short/first junction spacing at $\lambda_g/4$ (*H*-plane) or $\lambda_g/2$ (*E*-plane). λ_g is the wavelength in the manifold waveguide at the center frequency of the nearest filter to the length of waveguide in the direction of the common port.
4. Set initial manifold junction-filter stub lengths at $n\lambda_g/2$. Again, n should be as small as possible.

• Optimization

1) Design wideband components. Optimize spacings between the junctions and between the short and first junction and the stub lengths. This often has the most dramatic effect in terms of improvement in CPRL.
2) Optimize stubs and the first three or four parameters of channel filter 1 [M_{S1} (filter manifold coupling), M_{11} (first resonance tuning), and M_{12} (resonance 1 to resonance 2 coupling)].
3) Repeat the cycle for all the channels, possibly omitting the stub length since this does not change much after the first cycle of optimization, until the improvements in the cost function begin to become negligible.

• Refinement

1) Repeat optimization of manifold and stub lengths.
2) Reoptimization with a fine step on all of each channel filter's parameters, most lightly on the elements furthest away from the manifold, and not at all on the final coupling M_{LN} (i.e., the input coupling to the multiplexer filter from the channel high-power amplifier).

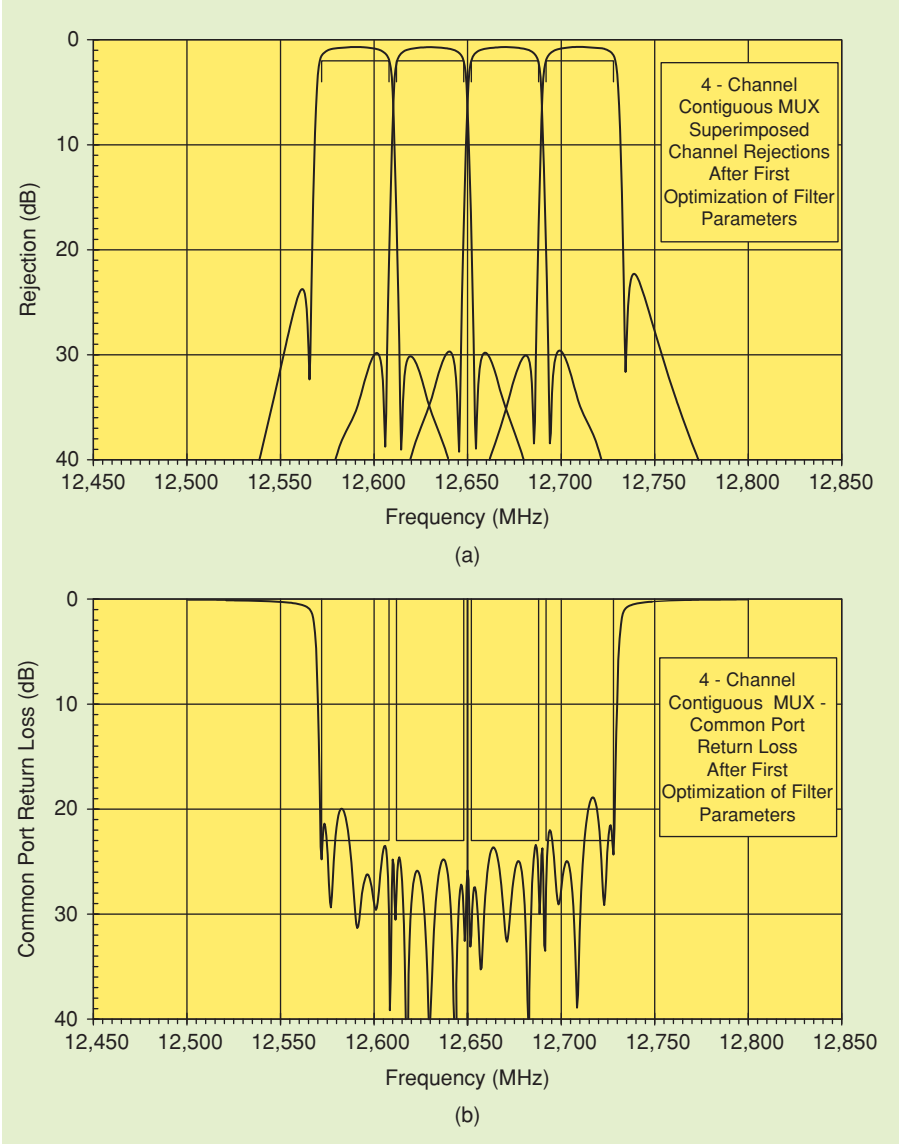

Figure 18. *Four-channel manifold multiplexer after first optimization of filter parameters: (a) superimposed channel transfer characteristics and (b) CPRL.*

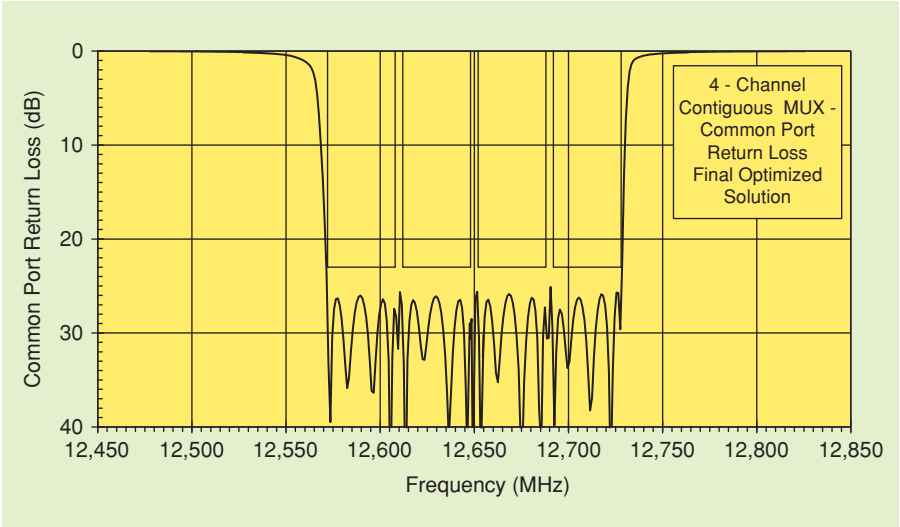

Figure 19. *Four-channel manifold multiplexer: final performance of CPRL.*

Demonstration of the Piecewise Optimization Process

The piecewise optimization process will be demonstrated through the optimization of a four-contigous-channel Ku-band waveguide manifold multiplexer. The channel electrical specifications for this particular case were satisfied with 5-2 quasi-elliptic filters with 30-dB rejection lobe levels and DBWs of 38-MHz and 40-MHz center frequency spacings, which falls within the definition of contiguity.

Designing the filters as singly terminated prototypes and attaching them to the manifold with the initial manifold spacings and stub lengths gives a poor performance, as shown in Figure 16. The CPRL is poor and one of the channels is unrecognizable.

Figure 17 shows the dramatic improvement that results from the optimization of the along-manifold lengths. Now the channel rejection characteristics are close to design, and the average CPRL is on the order of 10 dB.

Further improvement in CPRL is obtained after first optimization of the stub lengths and the first four parameters (first coupling iris M_{S1}, first cavity tuning state M_{11} , second coupling M_{12} , second cavity tuning state M_{22}) of each filter. The computed response following this procedure is described in Figure 18. The inner rejection lobe levels are close to the design of 30 dB, but the outer lobe levels—because there are no neighbors on the outer side of the group—have dropped to about 24 dB. The effect of not having a

contiguous neighbor on one side is evident in the rejection responses of channels 1 and 4—the lobe levels and rejection slopes on the outer sides are not as steep as the sides with a contiguous neighbor. This causes a small amount of asymmetric in-band distortion to group delay and insertion loss as well.

Then the refinement of return loss optimization cycles is carried out, and the final result is shown in Figure 19. Now the CPRL is above 23 dB over all the channel bandwidths. The simulations have all been made assuming a Q_u factor of 12,000, but the optimizations were carried out with a lossless network to speed up the process. Using a moderate-speed PC (700 MHz), the entire optimization process took about 2 min.

This optimization strategy appears to work well even for larger numbers of channels. Figure 20 shows the CPRL and rejection characteristics of a manifold multiplexer with 20 contiguous channels at C-band (fourth-degree filters) [21], which was designed using the piecewise optimization process. This multiplexer has on the order of 300 frequency sampling points and 220 electrical elements of varying sensitivities and different constraints that all need to be correctly valued before the overall multiplexer will operate to specification.

The main advantage of the hybrid-coupled approach is its directional property, which minimizes the interaction between the channel filters.

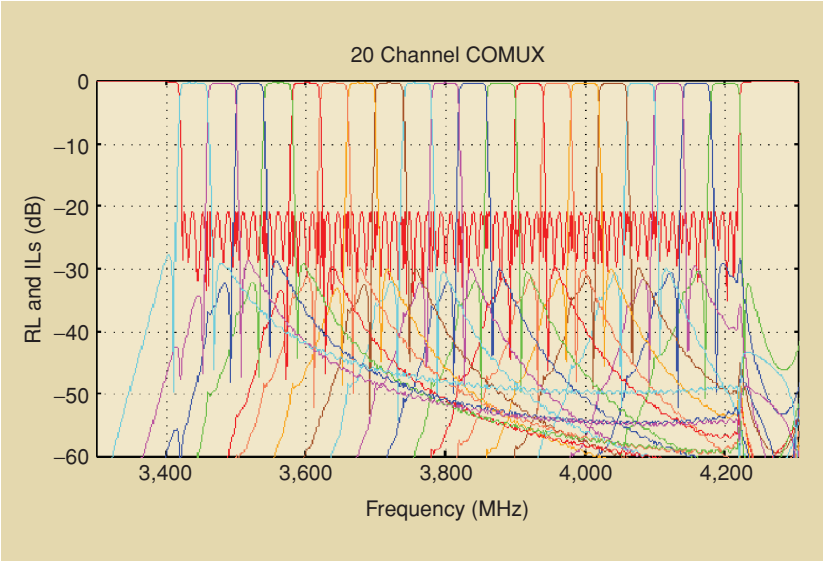

Figure 20. *20-channel manifold multiplexer: superimposed channel transfer characteristics and CPRL.*

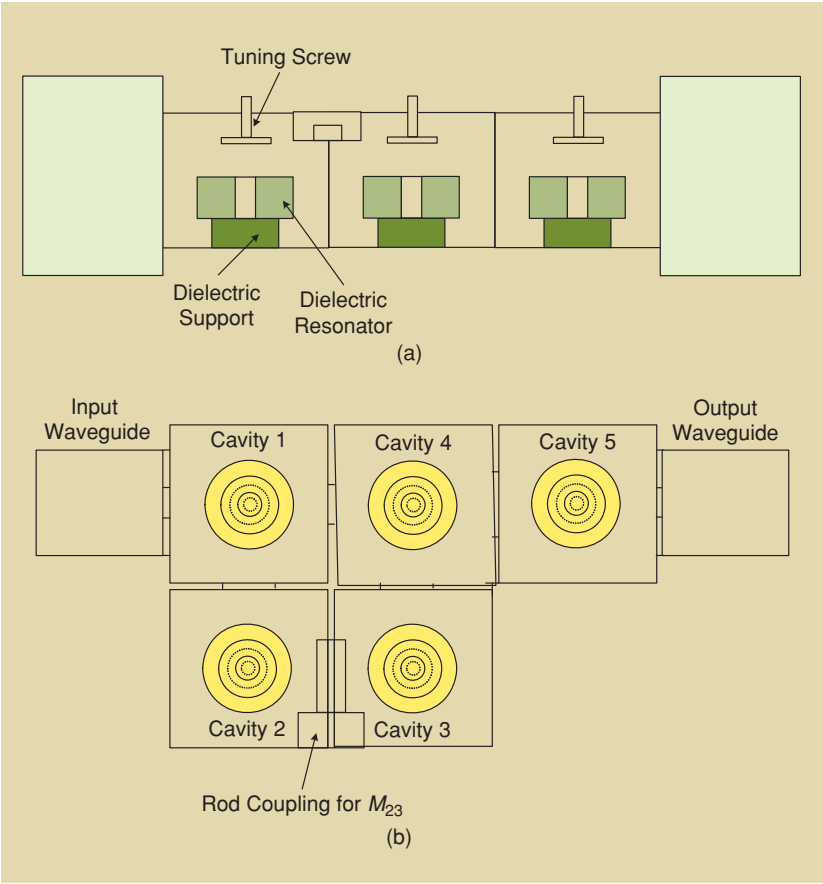

Figure 21. *Fifth-degree DR filter structure: (a) side view and (b) top view.*

Further Optimization Using EM Techniques

Optimization techniques for multiplexer design have been developed to a high degree of sophistication now, and worthy of note here is the space mapping technique [23], which involves optimizing a coarse model [circuit or hybrid circuit model with embedded electromagnetic (EM)-modeled components] and a fine model (e.g., full-wave electromagnetic modeling). Because of the large number of optimization variables, the fine-model EM simulator takes a formidable amount of computer CPU time and has to be used sparingly during the optimization process. On the other hand, the coarse simulator can analyze the circuit very rapidly, especially if the S-parameters of fixed

A direction filter is a four-port device in which one port is terminated in a load.

and noninteracting elements (e.g., the manifold waveguide junctions) are modeled in advance by EM techniques and are available to the main program either as look-up tables or with the call of a rapid specialist routine. It, therefore, provides a means to simulate the manifold multiplexer with a good degree of accuracy and efficiency.

To illustrate the complete multiplexer design procedure including EM optimization, we consider a 10-channel manifold-coupled output multiplexer in the frequency band of 3.5-4.25 GHz. Eight channels have a bandwidth of 1.5%, and the remaining two have a bandwidth of 0.8%. Every channel is a fifth-degree dielectric resonator (DR) filter as shown in Figure 21.

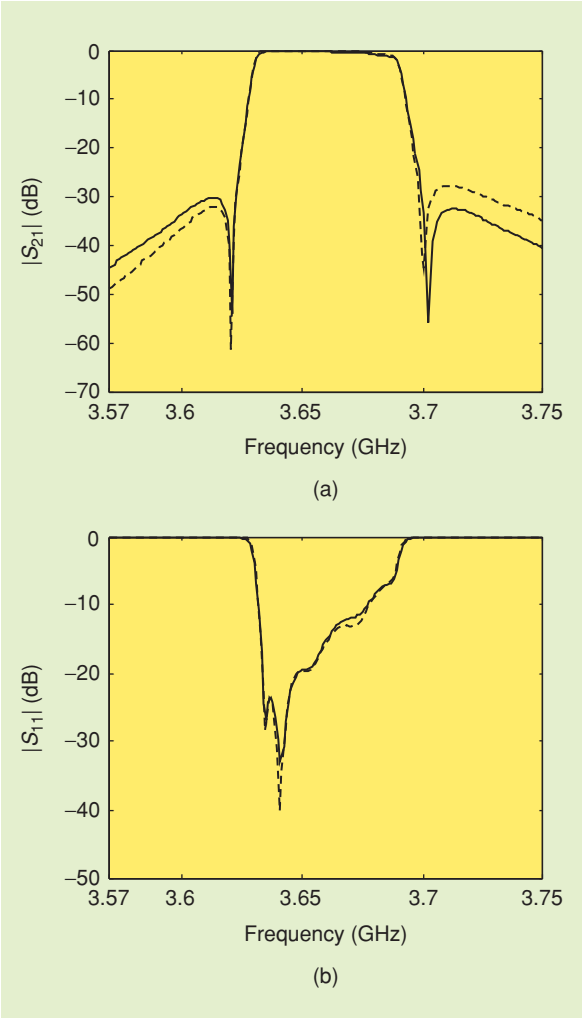

Figure 22. *Responses of the first channel of the 10-channel DR output multiplexer (solid line is the ideal response and dotted line is the EM response at the optimal design parameters); $|S_{21}|$ and $|S_{11}|$ in dB.*

Ansoft HFSS is used as a fine model of every channel and the network model is used as a coarse model.

Ideal channel coupling values are obtained in the first step of the design procedure in the preceding sections. Space-mapping optimization [23] is then applied to each channel to get the optimal channel dimensions. For example, the results of applying space-mapping optimization to the first channel are shown in Figure 22 (seven iterations are required). An accurate multiplexer model is obtained by replacing each channel with the corresponding S-parameter sweep obtained by HFSS at the optimal channel dimensions. As a result, the new multiplexer model includes channel dispersion and spurious modes. Finally, the manifold parameters are reoptimized to meet the required specifications. Figure 23 compares the multiplexer ideal response and the EM response, where every channel is replaced by its simulated *S*-parameters (by Ansoft HFSS). The measured response of the multiplexer is shown in Figure 24. The spurious modes predicted by

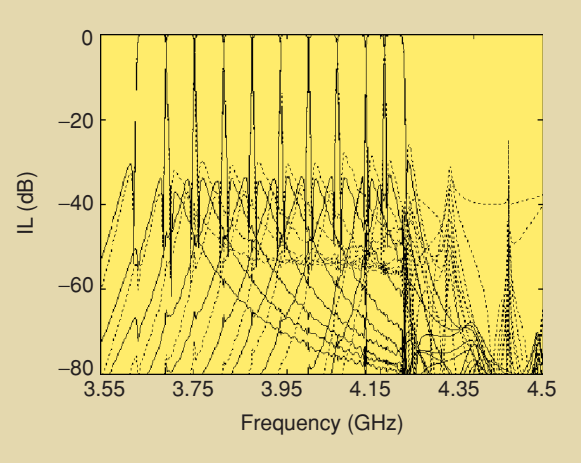

Figure 23. *The ideal response of the 10-channel DR multiplexer prototype (solid line) versus the EM response (dotted line).*

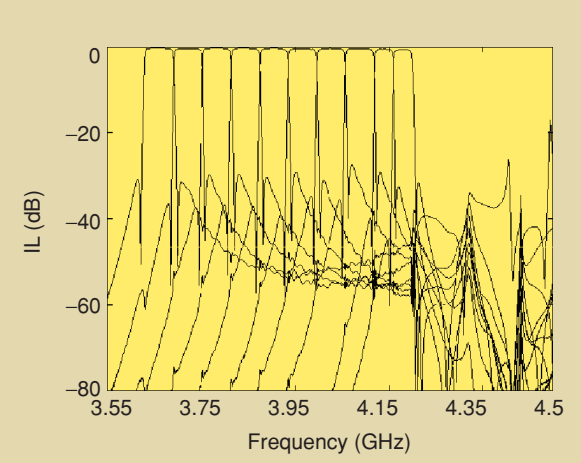

Figure 24. *Measured response of the 10-channel DR multiplexer.*

EM analysis in Figure 23 correlate very well with the measurements in Figure 24. Finally, a fully integrated multiplexer assembly is shown in Figure 25 together with input and output circuitry.

Conclusions

Following a brief review of different types of multiplexer configurations, a systematic design approach has been outlined for the design of manifold-coupled multiplexers. The piecewise approach, optimizing parts of the multiplexer separately in repeated cycles while converging upon an optimal solution, has proved to be very effective for most practical applications. The technique is readily applicable to manifold multiplexers incorporating an arbitrary number of channels, regardless of their bandwidths and channel separations. There are no restrictions on the design and implementation of channel filters onto the manifold; they may be asymmetric, and may incorporate transmission zeros, group delay equalization zeros, or both. The manifold itself is a transmission line, be it a coaxial line or a rectangular waveguide or some other low-loss structure. The costly EM simulation is used economically on manifold junctions and channel filters through the use of space-mapping optimization techniques, where EM-based simulators are used to fine-model each multiplexer channel and coupling matrix representation is used to coarse-model the performance. Fine details such as tuning screws may be included in the design process. This design procedure takes into account the effects of dispersion and spurious modes and, as a result, the overall design and final tuning time can be significantly reduced.

Acknowledgement

The authors would like to thank Prof. Raafat Mansour for providing part of the material in the "Multiplexer Configurations" section.

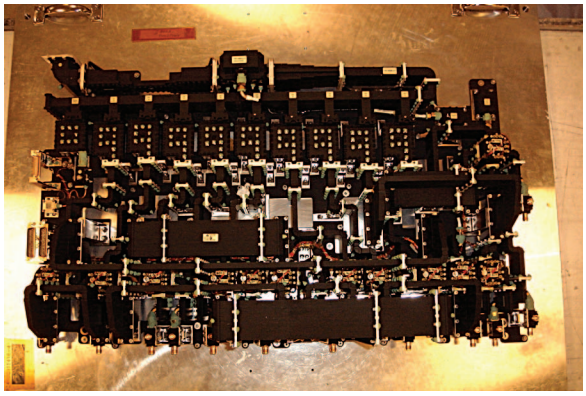

Figure 25. *A fully integrated C-band 10-channel multiplexer assembly with DR filters.*

References

[1] J. Uher, J. Bornemann, and U. Rosenberg, *Waveguide Components for Antenna Feed Systems—Theory and CAD*. Norwood, MA: Artech House, 1993.

[2] G. Matthaei, L. Young, and M.T. Jones, *Microwave Filters, Impedance Matching Networks and Coupling Structures.* Norwood, MA: Artech House, 1985.

[3] E.G. Cristal and G.L. Matthaei, "A technique for the design of multiplexers having contiguous channels," *IEEE Trans. Microwave Theory Tech.*, vol. MTT-10, pp. 88–93, Jan. 1964.

[4] A.E. Atia, "Computer aided design of waveguide multiplexers," *IEEE Trans. Microwave Theory Tech.*, vol. MTT-22, pp. 322–336, Mar. 1974.

[5] M.H. Chen, F. Assal, and C. Mahle, "A contiguous band multiplexer," *Comsat Tech. Rev.*, vol. 6, pp. 285–307, Fall 1976.

[6] C.M. Kudsia, J. Dorey, j. Heierli, K.R. Ainsworth, G.L.P. Lo, "A new type of low loss 14 GHz high power combining network," in *Proc. 9th Eur. Microwave Conf.*, England, Oct. 1979, pp. 386–391.

[7] C.M. Kudsia, K.R. Ainsworth, and M.V. O'Donovan, "Microwave filters and multiplexing networks for communication satellites in the 1980s," in *Proc. AIAA 8th Communications Satellite Systems Conf.*, Apr. 1980.

[8] J.D. Rhodes and R. Levy, "Design of general manifold multiplexers," *IEEE Trans. Microwave Theory Tech.*, vol. 27, no. 2, pp. 111–123, Feb. 1979.

[9] J.D. Rhodes and R. Levy, "A generalized multiplexer theory," *IEEE Trans. Microwave Theory Tech.*, vol. 27, no. 2, pp. 99–111, Feb. 1979.

[10] D. Doust, et al., Satellite multiplexing using dielectric resonator filters," *Microwave J.*, vol. 32, no. 12, pp. 93–166, Dec. 1989.

[11] J. Bandler, S. Daijavad, and Q.-J. Zhang, "Exact simulation and sensitivity analysis of multiplexing networks," *IEEE Trans. Microwave Theory Tech.*, vol. MTT-34, pp. 111–102, Jan. 1986.

[12] D.S. Levinson and R.L. Bennett, "Multiplexing with high performance directional filters," *Microwave J.*, pp. 92–112, Jun. 1989.

[13] D. Rosowsky, "Design of manifold multiplexers," in *Proc. ESA Workshop on Microwave Filters*, Jun. 1990, pp. 145–156 .

[14] U. Rosenberg, D. Wolk, and H. Zeh, "High performance output multiplexers for Ku-band satellites," in *Proc. 13th AIAA International Communication Satellite Conf.*, Los Angeles, Mar. 1990, pp. 747–752.

[15] C. Kudsia, R. Cameron, and W.C. Tang, "Innovation in microwave filters and multiplexing networks for communication satellite systems," *IEEE Trans. Microwave Theory Tech.*, vol. MTT-40, pp. 1133–1149, Jun. 1992.

[16] M. Guglielmi, "Simple CAD procedures for microwave filters and multiplexers," *IEEE Trans. Microwave Theory Tech.*, vol. MTT-42, pp. 1347–1352, Jul. 1994.

[17] R.R. Mansour, S. Ye, V. Dokas, B. Jolley, W.C. Tang, and C. Kudsia, "System integration issues of high power HTS output multiplexers," *IEEE Trans. Microwave Theory Tech.*, vol. MTT-48, pp. 1199–1208, Jul. 2000.

[18] M.H. Chen, "Singly-terminated pseudo-elliptic function filter," *Comsat Technical Rev.*, vol. 7, pp. 527–541, Fall 1977.

[19] S. Lundquist, M. Mississian, M. Yu, and D. Smith, "Application of high power output multiplexers for communications satellites," in *Proc. 19th AIAA Int. Communication Satellite System Conf. and Exhibit*, pp. 12–15, May 2001.

[20] S. Lundquist, M. Yu, D.J. Smith, and W. Fitzpatrick, "KU-band temperature compensated high power multiplexers," in *Proc. 20th AIAA Int. Commun. Satellite Syst. Conf. and Exhibit*, May 12–15, 2002.

[21] M. Yu, "Design of multiplexers with many channels," in *Proc. IEEE International Microwave Symp.*, San Francisco, Jun. 2006.

[22] M. Yu, "EM based `smart' design techniques for filters and multiplexers," in *Proc. IEEE Int. Microwave Symp.*, Fort Worth, Texas, Jun. 6–11, 2004.

[23] M.A. Ismail, D. Smith, A. Panariello, Y. Wang, and M. Yu, "EM based design of large-scale dielectric resonator filters and multiplexers by space mapping," *IEEE Trans. Microwave Theory Tech. (Special Issue on Electromagnetics-Based Optimization of Microwave Components and Circuits)*, vol. 52, no. 1, pp. 386–392, Jan. 2004.

measurements on each device of course still depend upon its own connections.

Once the system with adapter has been calibrated to give corrected measurements of reflection coefficient, it can be used in the usual ways for corrected measurements of transmission coefficient.

Equation (5) has another use as an arbitrary way of dealing with redundant calibration data. Suppose the network analyzer is calibrated at first with three short circuits, to improve the plausibility of the results for highly reflecting devices [1]. If then the matched load is connected, one can pretend that an adapter is involved and apply (5). A new calibration results such that reflection magnitudes are appropriately corrected at high and low values.

Acknowledgment

The author wishes to thank D. R. Craib for discussions of the sliding load problem.

References

[1] J. E. Dalley, "Computer-aided microwave impedance measurements," *IEEE Trans. Microwave Theory Tech. (Special Issue on Computer-Oriented Microwave Projects)*, vol. MTT-17, pp. 572–576, Aug. 1969.
[2] E. L. Ginzton, *Microwave Measurements*. New York: McGraw-Hill, 1957, p. 287.

Computer-Aided Design of Waveguide Multiplexers

A. E. ATIA

***Abstract*—A procedure based on an analysis algorithm and practical rules is described for the design of waveguide multiplexers. Simple rules, which enable the designer to quickly find a near-optimum solution in a small number of iteration steps, are given. An example of a 6-channel communications multiplexer, which utilizes narrow-bandpass elliptic function waveguide filters, is also included.**

Introduction

In a multicarrier communications satellite repeater, an output multiplexer is normally needed to combine the power outputs from the traveling-wave tube amplifiers. Such a multiplexer must have the smallest possible amount of loss consistent with the required flatness in the passbands of each channel and with the selectivity required for the rejection of adjacent channels. The most suitable configuration for this application is a waveguide-manifold-type multiplexer such as that shown in Fig. 1.

Various relatively simple decoupling techniques have been previously described for the design of such multiplexers [1]. However, these techniques were found to be unsuitable for the present application, partly because extra decoupling resonators may be needed, thus increasing the size, weight, and loss of the multiplexer, and partly because the guard bands are not wide enough, although the filters have narrow bandwidths.

This paper describes a method for computer-aided design of the multiplexer. When separately and individually connected to a matched load and driven by a matched source, all filters used have the same low-pass normalized prototype characteristics. Hence, each filter may be separately tuned prior to multiplexer assembly, thus considerably reducing the effort involved in practical alignment of the multiplexer. Harmful interaction between the filters is eliminated by properly spacing them along the waveguide manifold. This approach closely simulates the process which would be followed in practical experimental design of the multiplexer.

Manuscript received July 3, 1973; revised September 4, 1973. This work was supported by the Communications Satellite Corporation.
The author is with COMSAT Laboratories, Clarksburg, Md. 20734.

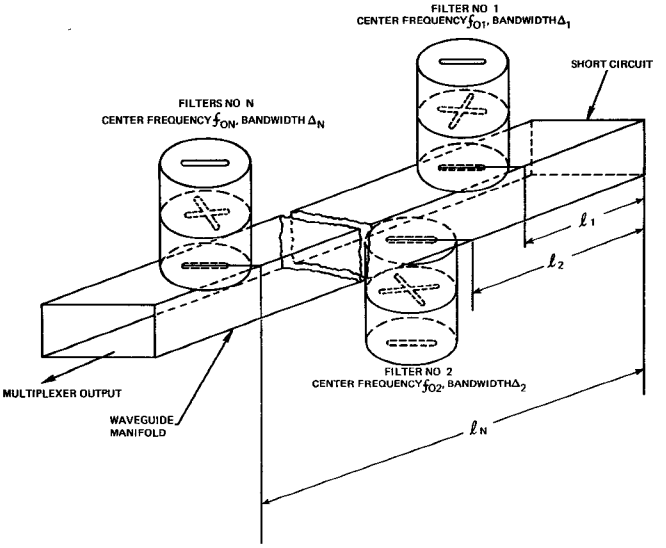

Fig. 1. Waveguide-manifold-type multiplexer.

Multiplexer Configuration and Analysis

The multiplexer to be designed consists of N filters mounted on the wide side of a rectangular waveguide manifold, as shown in Fig. 1. The waveguide is short circuited at one end, while the other end, or output port, is terminated in a matched load. All of the filters are derived from the same normalized prototype equivalent, although they have different center frequencies and bandwidths. The filters are numbered $1,2,\cdots,N$, with filter number 1 nearest to the short circuit and filter N farthest from it. The distance of the centers of the coupling slots of filter number k from the short-circuit end of the waveguide manifold is l_k; its center frequency is f_{0k} and its bandwidth is Δ_k, $k = 1,2,\cdots,N$.

The equivalent circuit of the configuration shown in Fig. 1 can be derived from an equivalent circuit of the filters, such as that shown in Fig. 2 [2], and the equivalent circuit of a T junction of the broad wall of a waveguide. Each of the T junctions may be represented by an E-plane connection [3]. The equivalent circuit parameters B_a and B_b are the same as in [3, p. 365]. Thus the complete equivalent circuit of the multiplexer is as shown in Fig. 3, in which the filters are represented by their lumped element equivalent circuit, the waveguide is represented by dispersive lengths of transmission line, and the junction effects by the susceptances B_a and B_b.

For convenience in the analysis, a set of total voltages and currents and an equivalent set of incident and reflected waves at the junctions of the filter's terminal planes and the waveguide are used in Fig. 3. Furthermore, the analysis is performed for a channel separating multiplexer rather than a summing multiplexer. All impedance levels are normalized to the waveguide characteristic impedance, which is assumed to be unity, and all filters are terminated in equal output loads R_0. Any individual filter can be analyzed to yield its Y parameters when it is considered to be a 2-port network. Only four normalized polynomials, the filter bandwidth, and the center frequency are needed to obtain the Y parameters of any filter [2]. Thus if the kth filter has terminal voltages and currents $[V_1^{(k)},V_2^{(k)}]$ and $[I_1^{(k)},I_2^{(k)}]$, respectively, then the Y matrix of the filter imposes the following constraints:

$$\begin{bmatrix} I_1^{(k)} \\ I_2^{(k)} \end{bmatrix} = \begin{bmatrix} Y_{11}^{(k)} & Y_{12}^{(k)} \\ Y_{12}^{(k)} & Y_{22}^{(k)} \end{bmatrix} \begin{bmatrix} V_1^{(k)} \\ V_2^{(k)} \end{bmatrix}$$

and, at the output terminals,

$$V_2^{(k)} = -I_2^{(k)} R_0. \tag{2}$$

Equations (1) and (2) can be solved to yield

$$I_1^{(k)} = U_k V_1^{(k)} \tag{3}$$

where

$$U_k = Y_{11}^{(k)} - \frac{Y_{12}^{(k)2} R_0}{1 + Y_{22}^{(k)} R_0}. \tag{4}$$

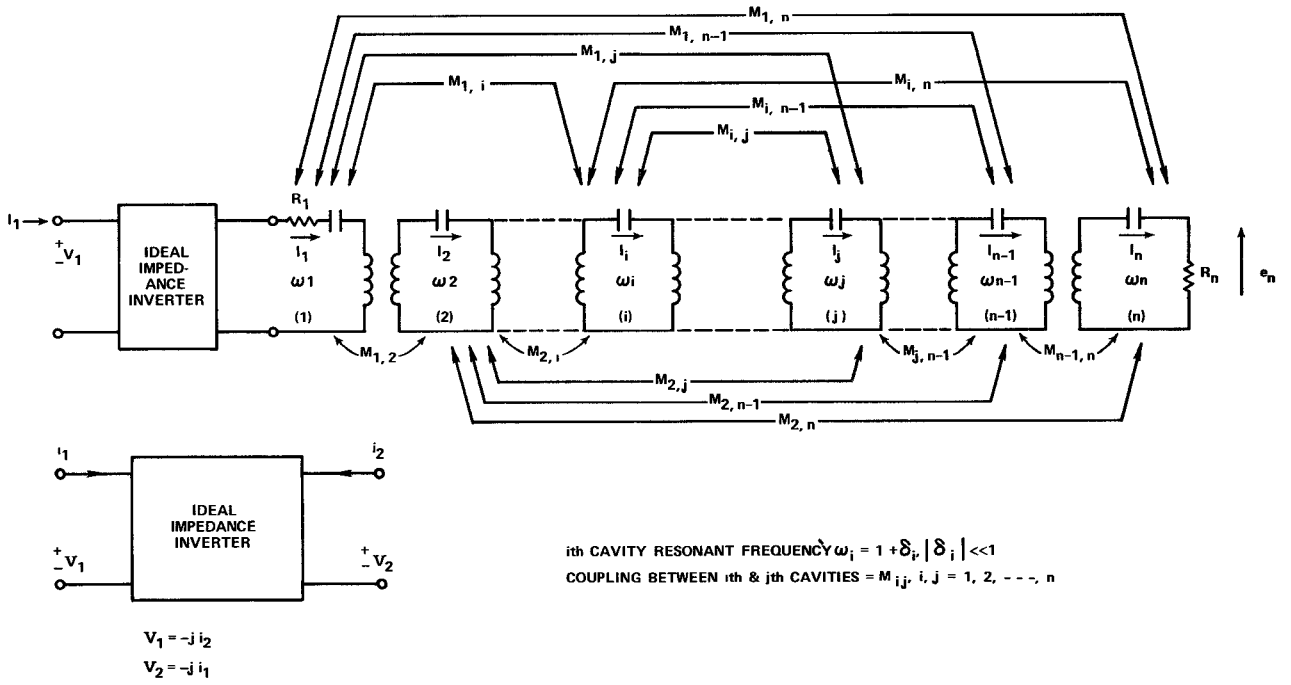

Fig. 2. Equivalent circuit of a multiple coupled cavity waveguide filter.

$$Q_{e_k} = \frac{\pi}{2}\left(\frac{B_{b_k}}{Y_0}\right)^2\left(\frac{\lambda'_g}{\lambda}\right)^2 \qquad k = 1,2,\ldots,N$$

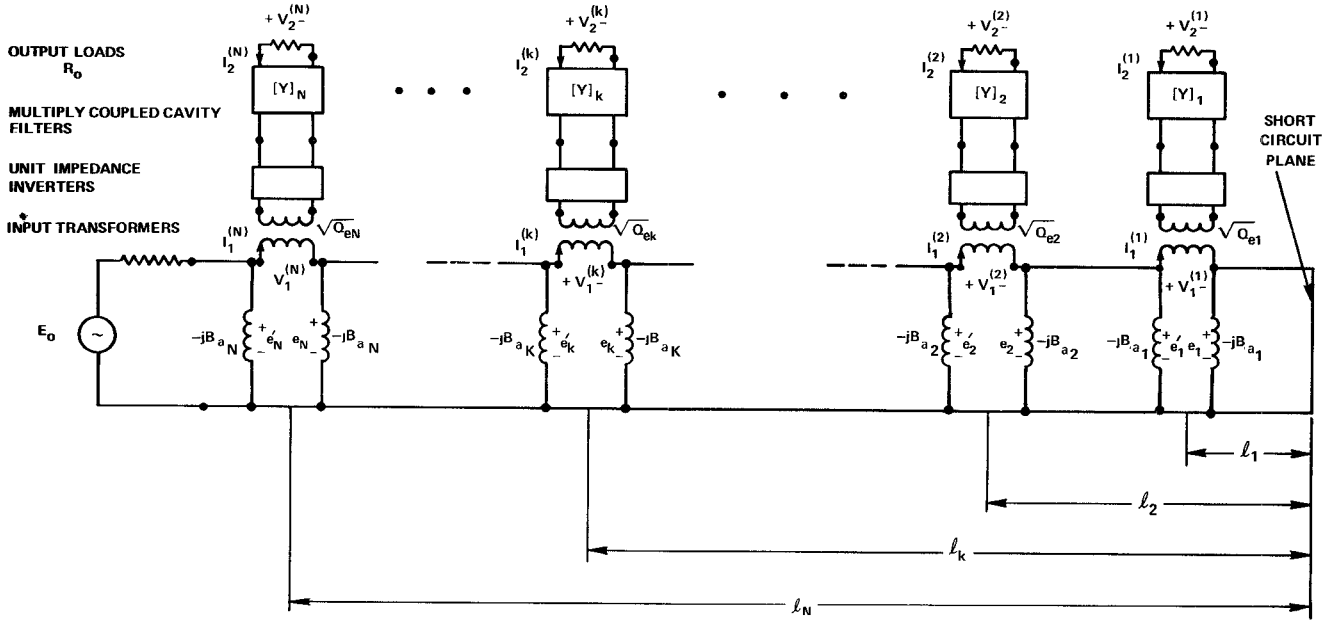

Fig. 3. Equivalent circuit of a series connected waveguide multiplexer.

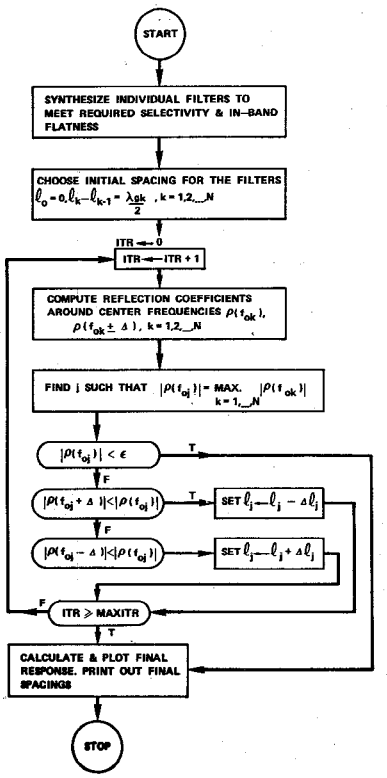

Fig. 4. Design procedure flow chart.

FILTER'S k	POSITION ℓ_k
1	2.203
2	4.319
3	6.353
4	8.314
5	10.213
6	12.051

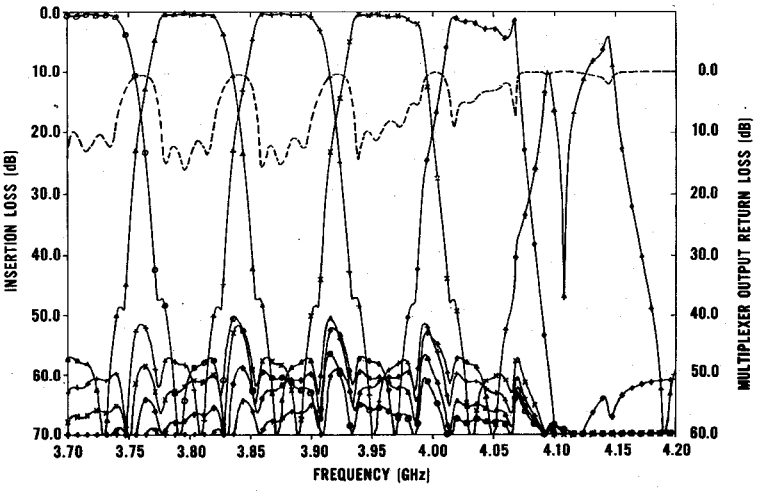

Fig. 5. Multiplexer insertion and return loss with initial spacings.

FILTER'S k	POSITION ℓ_k
1	1.830
2	4.090
3	6.145
4	8.145
5	10.045
6	12.051

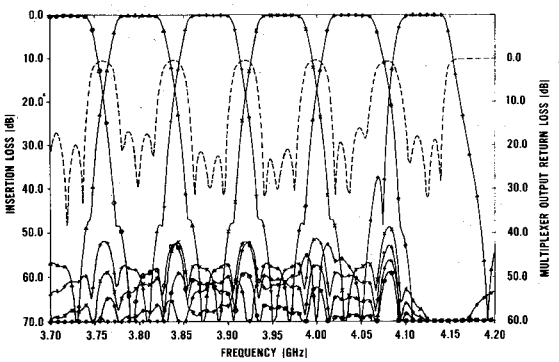

Fig. 6. Multiplexer insertion and return loss with final spacings.

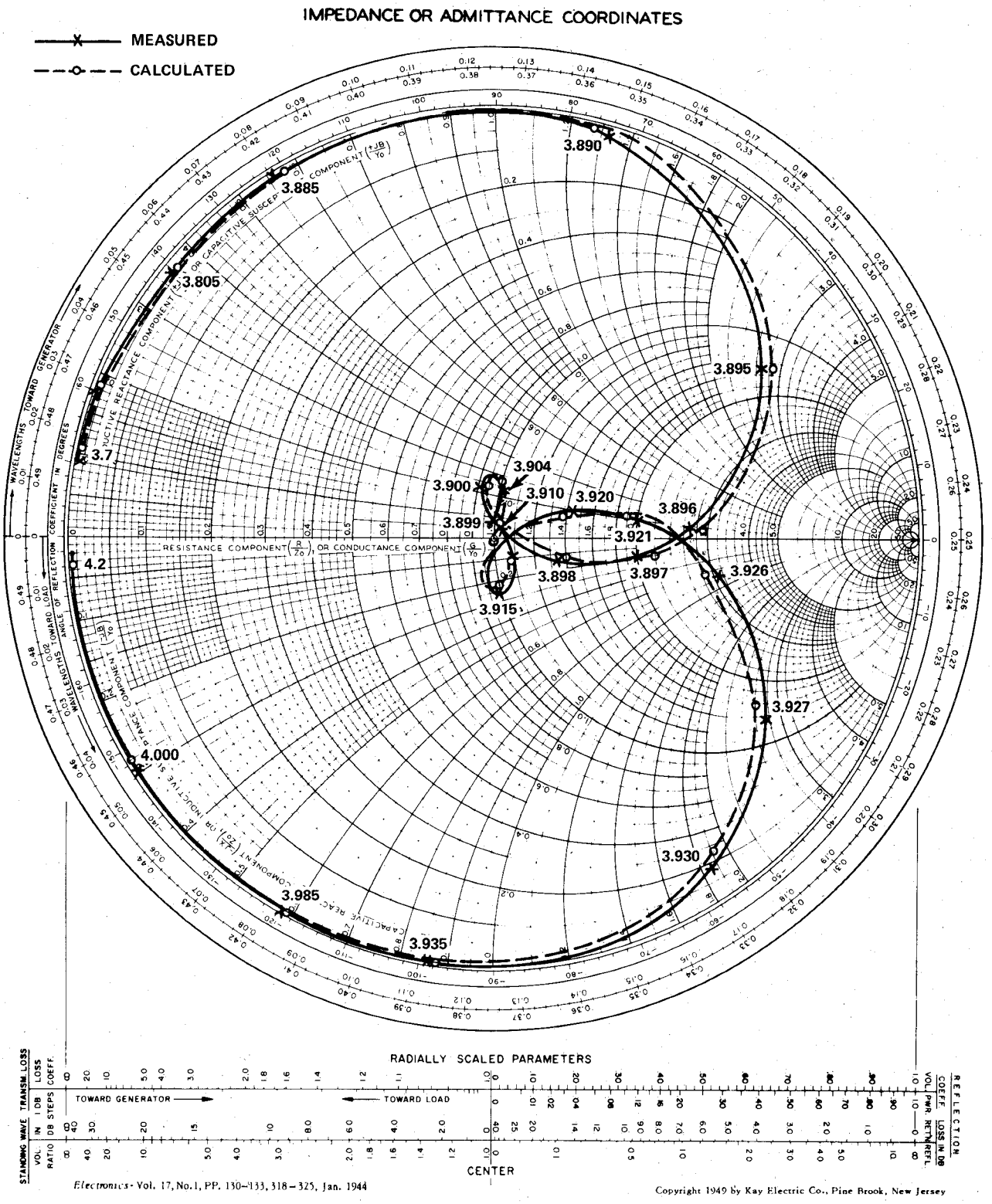

Electronics - Vol. 17, No. 1, PP. 130–133, 318–325, Jan. 1944

Fig. 7. Input reflection coefficient of a typical filter.

Assuming a unit incident voltage wave at the plane of the short circuit in the waveguide, the following algorithm can be used to compute the relevant quantities defined in Fig. 3:

$$V_{\text{inc}}^{(0)\prime} = 1 \tag{5a}$$

$$V_{\text{ref}}^{(0)\prime} = -1 \tag{5b}$$

$$l_0 = 0. \tag{5c}$$

Then,

$$V_{\substack{\text{inc}\\\text{ref}}}^{(k)} = V_{\substack{\text{inc}\\\text{ref}}}^{(k-1)\prime} \exp\left[\frac{\pm j2\pi(l_k - l_{k-1})}{\lambda_g}\right] \tag{6a}$$

$$\begin{matrix} e_k \\ i_k \end{matrix} = V_{\text{inc}}^{(k)} \pm V_{\text{ref}}^{(k)} \tag{6b}$$

$$I_1^{(k)} = i_k - jB_{ak}e_k \tag{6c}$$

$$V_1^{(k)} = \frac{I_1^{(k)}}{U_k} \tag{6d}$$

$$e_k' = V_1^{(k)} + e_k \tag{6e}$$

$$i_k' = I_1^{(k)} - jB_{ak}e_k' \tag{6f}$$

$$V_{\substack{\text{inc}\\\text{ref}}}^{(k)\prime} = \tfrac{1}{2}[e_k' \pm i_k'] \tag{6g}$$

where $k = 1,2,\cdots,N$, and λ_g is the guide wavelength. The generator voltage E_0, the voltage insertion loss ratio t_k of the kth filter, and the input reflection coefficient ρ are given, respectively, by

$$E_0 = I_1^{(N)} + e_N' \tag{7}$$

$$t_k = 2\left(\frac{1}{R_0}\right)^{1/2}\frac{V_2^{(k)}}{E_0} = -2(R_0)^{1/2}\frac{Y_{12}^{(k)}}{1 + R_0Y_{22}^{(k)}}\frac{V_1^{(k)}}{E_0} \tag{8}$$

$$\rho = \frac{e_N' - I_1^{(N)}}{e_N' + I_1^{(N)}}. \tag{9}$$

Design Procedure

The design procedure, summarized by the flow chart of Fig. 4, is described as follows.

1) Synthesize individual bandpass filters to meet the required selectivity and in-band flatness of the multiplexer specifications [2], [4].

2) Choose initial spacings for the filters. These spacings can be either $l_k = k\lambda_{gk}/2$, or according to the rule, $l_0 = 0$, $l_k - l_{k-1} = \lambda_{gk}/2$, $k = 1,2,\cdots,N$, where λ_{gk} is the guide wavelength at the center frequency f_{0k} of filter number k.

3) Compute the frequency response of the multiplexer using the analysis algorithm described in the previous section.

4) Find j so that

$$|\rho(f_{0_j})| = \max_{k=1,2,\cdots,N} |\rho(f_{0k})|. \tag{10}$$

5) If $|\rho(f_{0_j})| < \epsilon$ (a prespecified allowable reflection coefficient), then all reflection coefficients are acceptable. Print out the results and stop; otherwise, continue to step 6).

6) Change the spacing l_j of filter number j according to the following rule.

If $|\rho(f_{0_j} + \Delta)| \lesseqgtr |\rho(f_{0_j})|$, then set the new value of l_j equal to $l_j + \Delta l_j$, where

$$\Delta l_j = \lambda_{g_j}\left[1 - \frac{\lambda_g(f_{0_j} \pm \Delta)}{\lambda_{g_j}}\right] \tag{11}$$

and $\lambda_g(f_{0_j} \pm \Delta)$ is the guide wavelength at frequency $(f_{0_j} \pm \Delta)$.

7) If the allowable number of iterations has been exceeded, stop; otherwise, return to step 3).

The convergence of the iteration procedure to an acceptable solution was fairly rapid in all cases tested. This can be attributed to the fact that, although the initial choice of spacings does not produce the desired response, it is not very far from being optimum. The rule for changing the spacings is similar to the procedure for an empirical design approach. Namely, at each step, the filter having the worst return loss is moved by an amount which will move the position of the best return loss to its center frequency.

Example and Discussion

The above procedure has been used in the design of a 6-channel multiplexer. The filters used are 4-pole elliptic-function-type filters having 0.05-dB ripple and 42-MHz bandwidth. The insertion and return losses with the initial spacings and after the application of the optimization procedure are shown in Figs. 5 and 6, respectively. The final result of Fig. 6 was obtained after moving every filter at least twice (two iteration cycles).

The success of the procedure from a practical point of view depends largely on how closely the equivalent circuit models for the filters of Fig. 2 and the junction of [3] represent the actual behavior of these elements over the entire frequency band of the multiplexer. Fig. 7 compares the calculated and measured input reflection coefficients of a typical filter. Although a complete multiplexer assembly designed according to the procedure has not been made, the close agreement of the measured characteristics of a single filter and the computed response indicates that the present approach should yield a satisfactory practical design.

Conclusion

A procedure for the computer-aided design of waveguide multiplexers has been described. This method is based on an analysis algorithm for the equivalent circuit of the multiplexer. Simple rules for the optimization of the filter spacings allow the optimum design to be obtained in a small number of iteration steps. The filters used in the multiplexer can be either direct-coupled (Chebychev) or multiple-coupled (elliptic function) cavity filters.

An example of a 6-channel waveguide multiplexer for the frequency band of 3.7–4.2 GHz is included.

References

[1] G. L. Matthaei, L. Young, and E. M. T. Jones, *Microwave Filters, Impedance Matching Networks and Coupling Structures*. New York: McGraw-Hill, 1964, ch. 16.
[2] A. E. Atia and A. E. Williams, "Narrow-bandpass waveguide filters," *IEEE Trans. Microwave Theory Tech.*, vol. MTT-20, pp. 258–265, Apr. 1972.
[3] N. Marcuvitz, Ed., *Waveguide Handbook*, (Radiation Laboratory Series, vol. 10). New York: McGraw-Hill, 1947.
[4] J. K. Skwirzynski, *Design Theory and Data for Electrical Filters*. Princeton, N. J.: Van Nostrand, 1965.

Microwave Circuit Optimization Employing Exact Algebraic Partial Derivatives

GEORGE R. BRANNER

***Abstract*—A technique for the optimization and sensitivity analysis of broad classes of electrical networks is illustrated. The method utilizes the exact algebraic partial derivatives of functions with respect to any desired independent variable. This completely automated technique has the obvious advantage that the derivatives of any circuit response function with respect to any desired component parameter may be obtained with no additional analytical effort on the part of the designer. Several examples are given to illustrate the procedure.**

Manuscript received July 5, 1973; revised October 29, 1973.
The author is with the Department of Electrical Engineering, University of California, Davis, Calif., and ESL, Inc., Sunnyvale, Calif.

A Rigorous Three Plane Mode-Matching Technique for Characterizing Waveguide T-Junctions, and its Application in Multiplexer Design

Xiao-Peng Liang, *Student Member*, *IEEE*, Kawthar A. Zaki, *Fellow*, *IEEE*, and Ali E. Atia, *Fellow*, *IEEE*

Abstract—**A rigorous method for modeling rectangular waveguide T-junctions is presented. The method characterizes the waveguide discontinuity three times when the side-arm of the T-junction is terminated in a short circuit with three different lengths, and hence is called the three plane mode-matching technique (TPMMT). Computed and measured data on both *E*-plane and *H*-plane T-junctions are compared, showing excellent agreement for the magnitudes and phases of the scattering matrix elements. Element values of equivalent circuit models proposed by Marcuvitz [6] are computed and approximated by simple polynomials or rational functions, giving excellent accuracy. By using the *S*-parameters obtained from the TPMMT method, a network model of a waveguide manifold multiplexer is formulated. All parameters of the multiplexer, including the manifold dimensions and the filters, are optimized using this network model in terms of the multiplexer specification. The experimental results match the computed optimum results without further adjustment.**

I. Introduction

WAVEGUIDE T-junctions play an important role in designing microwave circuits, such as multiplexers used in modern communication systems [1]–[4], and power dividers [5]. Modeling waveguide T-junctions is an old problem. Initially, equivalent circuits were derived based on electrostatic approximations [6]. These approximations do not give sufficiently accurate results for many applications. In recent years, the finite element method (FEM) and the boundary element method (BEM) have been applied to solve this problem, and gave very good results [7]. However, these methods require considerable computing effort.

Mode-matching techniques have been used in the past for the solution of a wide range of waveguide discontinuity problems. For mode matching to be valid, the geometry of the configuration must have proper boundaries to allow the division of the structure into regions, the expansions of the fields in terms of natural modes in each region, and then the infinite set of mode-matching equations can be truncated to a finite set and solved numerically. If the field representation in any region cannot be expanded in terms of natural modes, mode matching will be invalid [8]. Unfortunately waveguide T-junctions have a region (Region 4 in Fig. 1(a)) where the fields cannot be expanded in terms of natural modes.

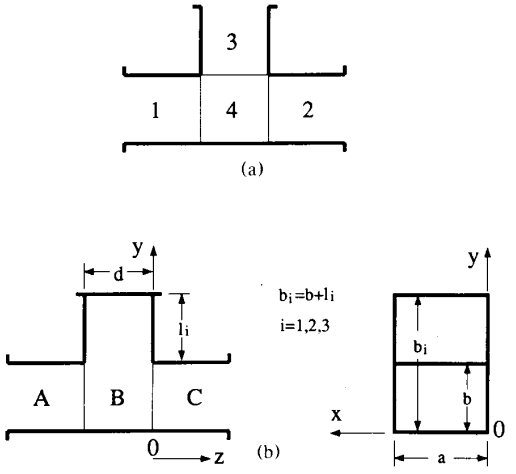

Fig. 1. The cross sections of T-junction and side-arm shorted T-junction.

One approach, introduced in the late 1960's [9], uses equivalent-circuit concepts applied to waveguide modes. This method calculates the admittance matrix of the T-junction by successively placing short circuits exactly at two of the three openings of the T-junction (i.e., at the thin lines in Fig. 1(a)), yielding three one ports consisting of shorted uniform waveguides. The same strategy is used in [4], [5] to compute the scattering matrix of the T-junction.

This paper uses the mode-matching technique directly, by modifying the configuration to avoid the field defective regions. The method modifies the configuration by plac-

Manuscript received March 15, 1991; revised July 6, 1991.

X-P. Liang and K. A. Zaki are with the Electrical Engineering Department, University of Maryland, College Park, MD 20742.

A. E. Atia is with COMSAT Systems Division, 22300 Comsat Drive, Clarksburg, MD 20871.

IEEE Log Number 9102779.

ing a short circuit on the side arm of the T-junction some distance away from the discontinuity. The scattering matrix of the resulting two-port network is then computed rigorously by mode matching. By repeating the same process with three different positions of the short circuit on the side arm, the three-port scattering matrix of the T-junction can be extracted. Since the solution is obtained by using mode matching three times, the method proposed will be called the three plane mode-matching technique (TPMMT).

The computed results using the TPMMT were verified by experimental measurements, and excellent agreement was obtained for both the magnitudes and phases of all the scattering matrix elements of both *E*- and *H*-plane T-junctions.

Accurate circuit models of T-junctions suitable for use in CAD programs are derived. The topologies of the models are the same as those introduced by Marcuvitz [6]; however, the element values are derived as simple polynomials or rational functions of frequency, from the scattering matrix obtained from the TPMMT.

Using the T-junctions model from the TPMMT, a network model of a manifold type multiplexer is developed. The dimensions of the manifold and the coupling parameters of the filters are optimized on this network model in terms of the multiplexer specification. An example 4-channel *S*-band multiplexer is built in accordance with the optimized design. Each of the four filters was built and tuned separately to its optimized response, and the multiplexer was then assembled as a five-port network. The computed and measured results agreed remarkably without further adjustment.

II. Three Plane Mode-Matching Technique (TPMMT)

A. Three Plane Measurement Method

A waveguide T-junction is modeled by a three-port network as shown in Fig. 2(a). We developed a method, called three plane measurement method, to measure the scattering parameters of this three-port network by a network analyzer. The method can be described as follows. 1) Connect three short circuits, (one at a time), with reflection coefficient $e^{j\theta_i}$ $(i=1,2,3)$ to one of the three ports (port 3). 2) Measure the *S*-parameters of each of the resulting two-port networks $[S_{mi}]$, $i=1,2,3$, (port 1 to port 2) by a network analyzer (Fig. 2(b)). Let these two port parameters be

$$[S_{mi}]=\begin{bmatrix} S_{m11i} & S_{m12i} \\ S_{m21i} & S_{m22i} \end{bmatrix}, \qquad i=1,2,3. \tag{1}$$

3) Calculate the *S*-parameters of the three-port network from the three measured two-port network *S*-parameters. Assuming the three-port network *S*-parameters are

$$[S]=\begin{bmatrix} S_{11} & S_{12} & S_{13} \\ S_{21} & S_{22} & S_{23} \\ S_{31} & S_{32} & S_{33} \end{bmatrix}. \tag{2}$$

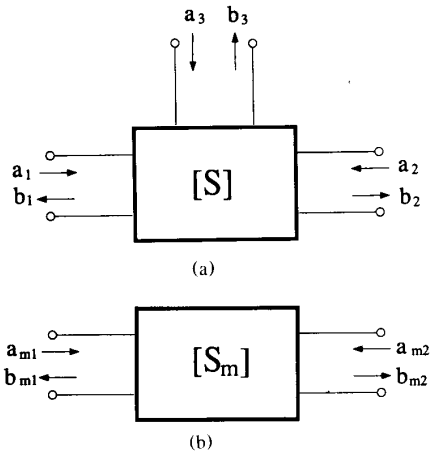

Fig. 2. Three-port and two-port networks.

Then, the relationship between $[S]$ and $[S_{mi}]$ can be easily derived:

$$S_{m11i}=S_{11}+\frac{S_{31}^2 e^{j\theta_i}}{1-S_{33}e^{j\theta_i}}, \qquad i=1,2,3 \tag{3a}$$

$$S_{m21i}+S_{21}=\frac{S_{31}^2 e^{j\theta_i}}{1-S_{33}e^{j\theta_i}}, \qquad i=1,2,3. \tag{3b}$$

Where θ_i is the phase of ith short. The reciprocity and the symmetry properties of the T-junction have been used in eq. (3). These are

$$S_{13}^2=S_{31}^2=S_{23}^2=S_{32}^2 \tag{4a}$$

$$S_{12}=S_{21} \tag{4b}$$

$$S_{11}=S_{22} \tag{4c}$$

and

$$S_{m11i}=S_{m22i} \tag{5a}$$

$$S_{m12i}=S_{m21i}. \tag{5b}$$

Solving (3a), S_{11}, S_{33} and S_{31}^2 can be obtained, and then substituting S_{33} and S_{31}^2 into (3b), S_{21} can be calculated.

B. T-Junction Scattering Parameter Modeling

Inspired by the three plane measurement method, three shorts (with different phases) are used to modify the T-junction configuration. Once the side-arm of the T-junction is shorted and regions 3 and 4 are combined to form region B in Fig. 1(b), this new region is considered a uniform waveguide of cross section $(a\times b_i)$, different from the cross section of regions A and C $(a\times b)$, and length d. The problem is therefore reduced to a waveguide discontinuity problem of three waveguides: two infinite waveguides A and C of cross section $a\times b$, separated by a length d of waveguide B of cross section $a\times b_i$. The same procedure as in the three plane measurement method is used to obtain the *S*-parameters of the T-junction, except that the *S*-parameters of the three two-port

networks are now computed by using mode-matching techniques instead of measurements by the network analyzer.

Consider a TE_{10} mode incident from $z < -d$ on the junction discontinuities at $z = -d$ and 0. Due to the presence of these discontinuities, reflected waves are generated in region A, transmitted and reflected waves in region B, and transmitted waves in region C. Because the discontinuities are in only the y-direction in the x-y plane, the fields in each region will have the same variation in the x-direction. In order to calculate the reflected and transmitted fields for each mode in each region, the total transverse fields in each region are expanded in terms of the appropriate waveguide modes in the region: For region A ($z \leqslant -d$),

$$\bar{E}_t = \hat{e}_{A1} e^{-\gamma_{A1}(z+d)} + \sum_i A_i \hat{e}_{Ai} e^{\gamma_{Ai}(z+d)} \tag{6a}$$

$$\bar{H}_t = \hat{h}_{A1} e^{-\gamma_{A1}(z+d)} - \sum_i A_i \hat{h}_{Ai} e^{\gamma_{Ai}(z+d)} \tag{6b}$$

For region B ($-d \leqslant z \leqslant 0$),

$$\bar{E}_t = \sum_j \hat{e}_{Bj} \left[B_j^+ e^{-\gamma_{Bj} z} + B_j^- e^{\gamma_{Bj} z} \right] \tag{7a}$$

$$\bar{H}_t = \sum_j \hat{h}_{Bj} \left[B_j^+ e^{-\gamma_{Bj} z} - B_j^- e^{\gamma_{Bj} z} \right] \tag{7b}$$

For region C ($z \geqslant 0$),

$$\bar{E}_t = \sum_k C_k \hat{e}_{ck} e^{-\gamma_{ck} z} \tag{8a}$$

$$\bar{H}_t = \sum_k C_k \hat{h}_{ck} e^{-\gamma_{ck} z} \tag{8b}$$

where $\hat{e}_{Ai}, \hat{h}_{Ai}, \gamma_{Ai}; \hat{e}_{Bj}, \hat{h}_{Bj}, \gamma_{Bj}$; and $\hat{e}_{Ck}, \hat{h}_{Ck}, \gamma_{Ck}$ are the transverse electric and magnetic eigen-fields and the propagation constants of the normal waveguide modes in the regions A, B, and C, respectively. By applying the boundary conditions that the tangential electric and magnetic fields be continuous at $z = -d$ and 0 and taking the inner products with orthogonality relations on the eigen-mode fields, the following infinite sets of linear equations in the unknown coefficients B_j^+ and B_j^- are obtained:

$$\sum_m \left[W_{lm} B_m^+ + X_{lm} B_m^- \right] = 2 \langle \hat{e}_{A1}, \hat{h}_{Bl}^* \rangle \tag{9a}$$

$$\sum_m \left[Y_{lm} B_m^+ + Z_{lm} B_m^- \right] = 0 \tag{9b}$$

where

$$W_{lm} = e^{\gamma_{Bm} d} T_{lm} + e^{\gamma_{Bl} d} \langle \hat{e}_{Bl}, \hat{h}_{Bl}^* \rangle \delta_{lm} \tag{10a}$$

$$X_{lm} = -e^{-\gamma_{Bm} d} T_{lm} + e^{-\gamma_{Bl} d} \langle \hat{e}_{Bl}, \hat{h}_{Bl}^* \rangle \delta_{lm} \tag{10b}$$

$$Y_{lm} = T_{lm} - \langle \hat{e}_{Bl}, \hat{h}_{Bl}^* \rangle \delta_{lm} \tag{10c}$$

$$Z_{lm} = -T_{lm} - \langle \hat{e}_{Bl}, \hat{h}_{Bl}^* \rangle \delta_{lm} \tag{10d}$$

$$\langle \hat{e}, \hat{h}^* \rangle = \int_s (\hat{e} \times \hat{h}^*) . \hat{n} dS \tag{10e}$$

and

$$T_{lm} = \sum_i \left[\frac{\langle \hat{e}_{Ai}, \hat{h}_{Bm}^* \rangle}{\langle \hat{e}_{Ai}, \hat{h}_{Ai}^* \rangle} \right]^* \langle \hat{e}_{Ai}, \hat{h}_{Bl}^* \rangle. \tag{10f}$$

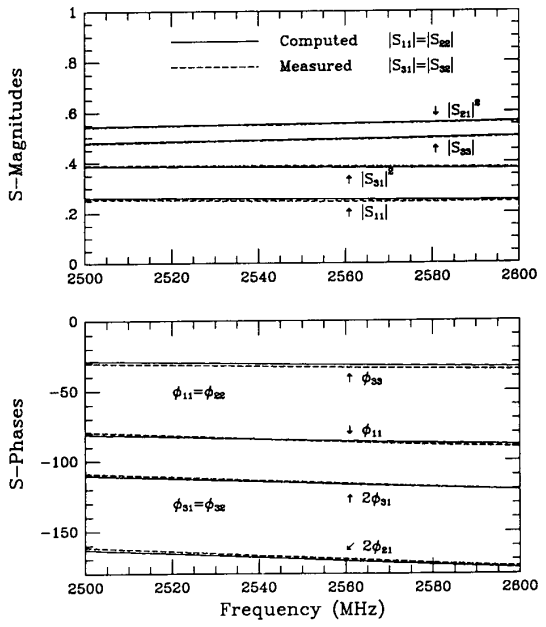

Fig. 3. Scattering parameters for an S-band E-plane T-junction with $a = 2b = 3.4$ inch, $d = b = 1.7$ inch.

The numerical solution of (9) for B_m^+ and B_m^- is achieved by truncating the infinite set to a finite number of equations. The A_i's and C_k's are given by

$$A_i = \delta_{i1} - \frac{\sum_j \left[B_j^+ e^{\gamma_{Bj} d} - B_j^- e^{-\gamma_{Bj} d} \right] \langle \hat{h}_{Bj}, \hat{e}_{Ai}^* \rangle}{\langle \hat{h}_{Ai}, \hat{e}_{Ai}^* \rangle} \tag{11a}$$

$$C_k = \frac{\sum_j \left[B_j^+ - B_j^- \right] \langle \hat{h}_{Bj}, \hat{e}_{Ck}^* \rangle}{\langle \hat{h}_{Ck}, \hat{e}_{Ck}^* \rangle}. \tag{11b}$$

Once the coefficients of the eigen-mode fields in each region are obtained, the incident and scattered waves on the equivalent multiport network (due to multi-modes) of the side-arm shorted T-junction are taken as proportional to the coefficients A_i and C_k, respectively. The proportionality constants are the normalization factors $\langle \hat{e}_{Ai}, \hat{h}_{Ai}^* \rangle$ or $\langle \hat{e}_{Ck}, \hat{h}_{Ck}^* \rangle$. Thus a two-port network shown in Fig. 2(b) can be used to characterize the discontinuity problem. Since regions A and C have the same cross sections the corresponding S-parameters are simply,

$$S_{11} = S_{22} = A_1 \tag{12a}$$

$$S_{21} = S_{12} = C_1. \tag{12b}$$

A computer program was developed to compute the S-parameters of both E-plane and H-plane rectangular waveguide T-junctions. Convergence of the solutions was checked by increasing the number of modes used in the

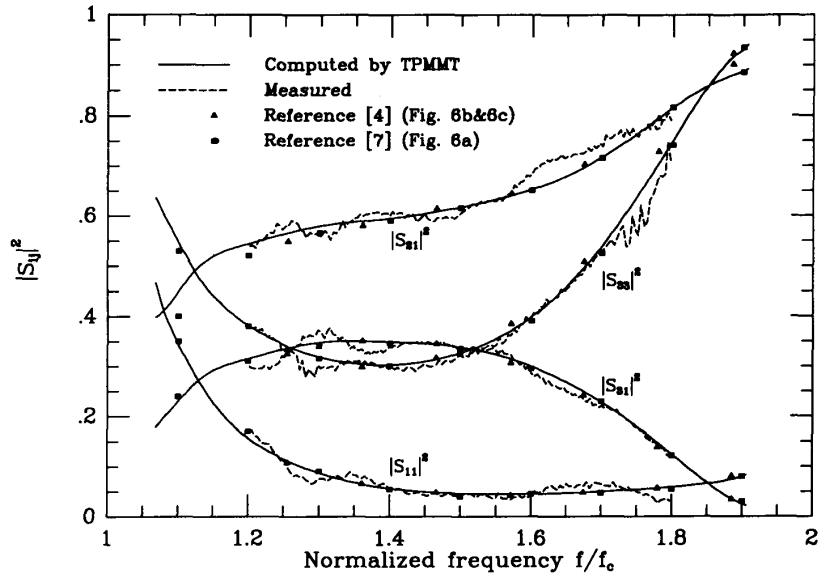

Fig. 4. Scattering parameters for an H-plane T-junction with $d = b = 2a = .9$ inch, $a = 45$ inch.

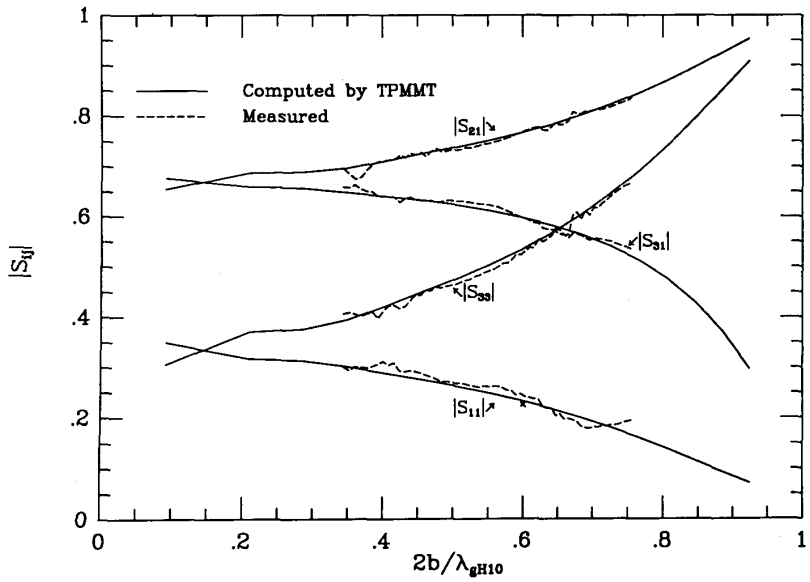

Fig. 5. Scattering parameters for an E-plane T-junction with $a = 2b = 3.4$ inch, $d = b = 1.7$ inch.

mode-matching techniques. Six modes in each region were found to be sufficient for convergence of the S-parameters to within 0.5%.

Using the three plane method, the best choice of lengths for the three shorts is to make the phase difference between each two of the three lengths $\pm 120°$. Considering the higher order modes excited by the T-junction, a certain minimum distance from the mouth of the T to the short is necessary to avoid higher order mode interaction between the short reference plane and the T-junction. On the other hand, the longer the minimum distance is, the more the number of modes in region B is needed. As a compromise, it is found that $(0.6-0.8)\lambda_g$ is the best choice for the minimum short circuit distance.

Fig. 3 shows the computed results by the TPMMT method, and the measured data from an HP8510B network analyzer, showing the magnitudes and the phases of an S-band E-plane T-junction over the frequency band from 2.5 to 2.6 GHz. Agreement between the computed and measured data is remarkable.

Fig. 4 compares the measured S-parameters of an H-plane T-junction with that computed by the TPMMT

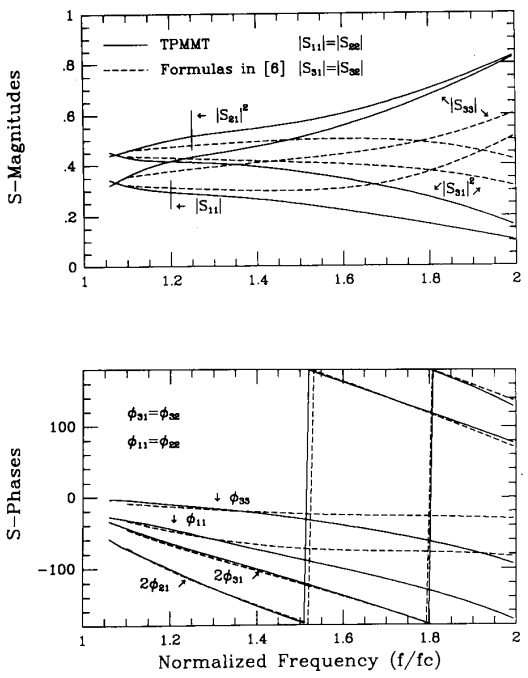

Fig. 6. Comparison between the results of TPMMT and equivalent circuit for E-plane T-junction with $a = 2b$, $d = b$.

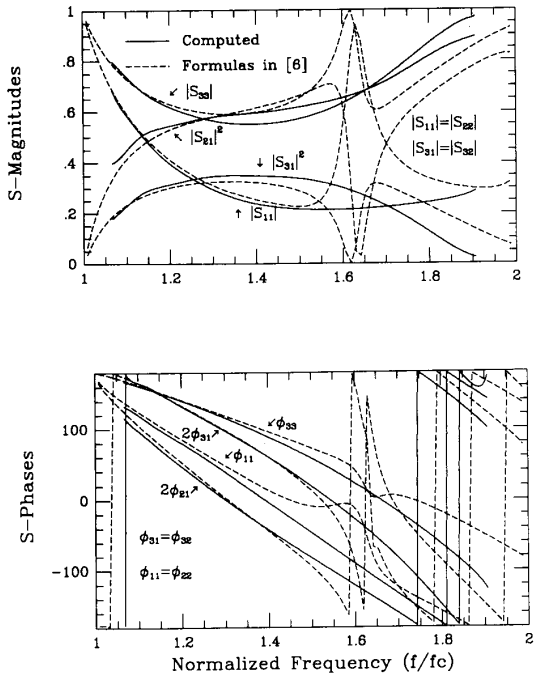

Fig. 7. Comparison between the results of TPMMT and equivalent circuit for H-plane T-junction with $b = 2a$, $d = b$.

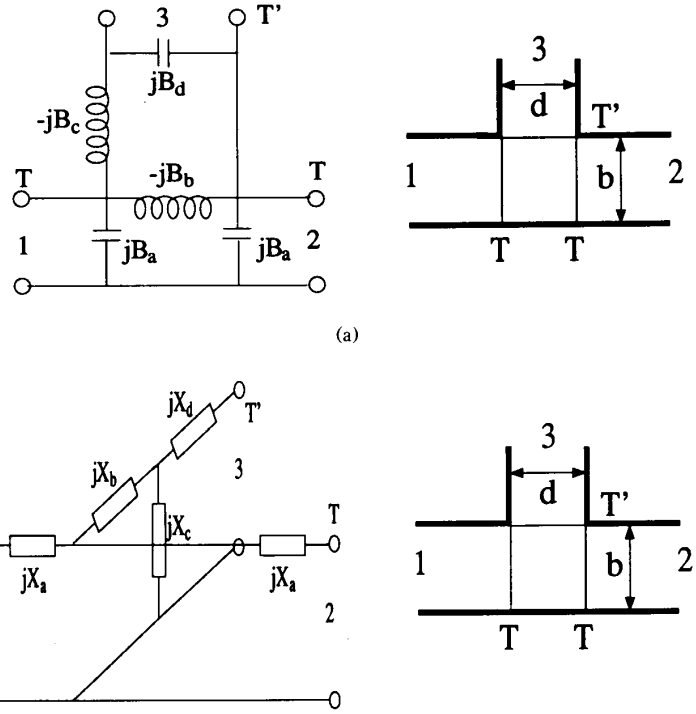

Fig. 8. T-junction equivalent circuits. (a) E-plane. (b) H-plane.

TABLE I
POLYNOMIAL COEFFICIENTS FOR E-PLANE T-JUNCTION WITH DIMENSIONAL PARAMETERS $a = 2b$, $d = b$

$k \backslash b's$	$b_0^{(k)}$	$b_1^{(k)}$	$b_2^{(k)}$	$b_3^{(k)}$	$b_4^{(k)}$	$b_5^{(k)}$	$b_6^{(k)}$
a	114.0511	−506.5494	920.1419	−878.7803	467.6217	−131.7710	15.4160
b	−13.1787	50.4164	−76.5400	57.7981	−21.6393	3.2407	—
c	560.9282	−2154.8618	3457.6345	−2957.0832	1419.8324	−362.6318	38.4726
d	−48.4935	216.9668	−398.1267	383.1617	−203.4954	56.5548	−6.4179

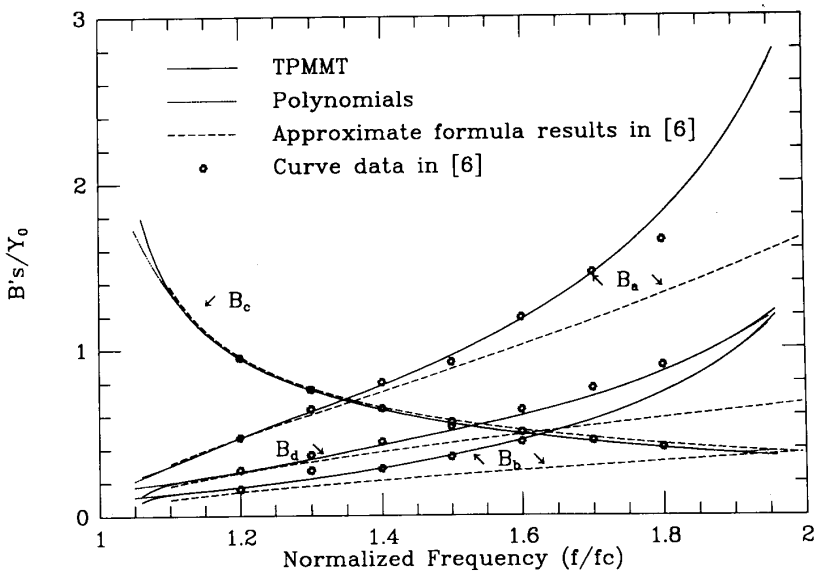

Fig. 9. Equivalent circuit parameters for E-plane T-junction with $a = 2b$, $d = b$.

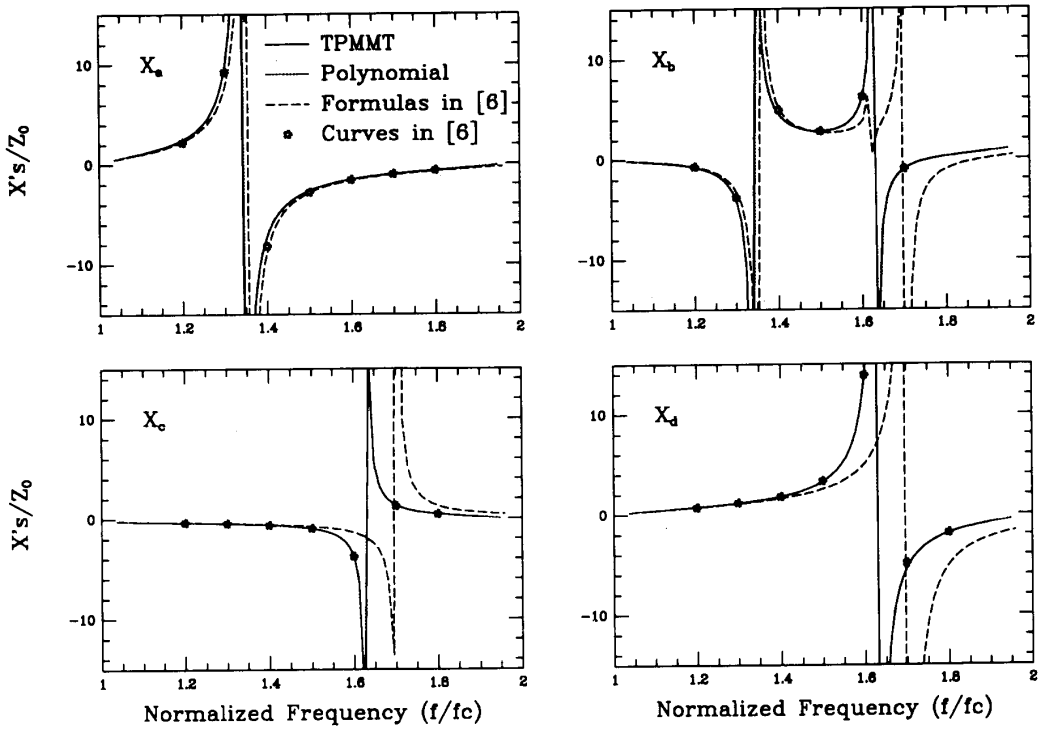

Fig. 10. Equivalent circuit parameters for H-plane T-junction with $b = 2a$, $d = b$.

TABLE II
POLYNOMIAL COEFFICIENTS AND POLES FOR H-PLANE T-JUNCTION WITH DIMENSIONAL PARAMETERS $b = 2a$, $d = b$

$k \setminus x's$	$x_0^{(k)}$	$x_1^{(k)}$	$x_2^{(k)}$	$x_3^{(k)}$	$x_4^{(k)}$	$x_5^{(k)}$	$x_6^{(k)}$	P_1	P_2
a	195.8846	−810.7328	1394.7536	−1276.3331	654.0399	−177.9816	20.0767	1.3417	—
b	−58.5277	249.8083	−442.8782	417.3045	−220.2853	61.7781	−7.1977	1.3417	1.6298
c	−104.2241	424.1251	−715.9226	642.8116	−323.8097	86.7534	−9.6568	1.6298	—
d	7.7803	−20.4710	21.0150	−11.0336	2.8589	−0.2650	—	1.6298	—

and other published methods [4], [7]. The results are in excellent agreement over the total waveguide frequency band.

Fig. 5 gives the performance of an E-plane T-junction over a total waveguide frequency band. The results computed by TPMMT and measurements are in agreement.

C. T-Junction Equivalent Circuit

The methods of waveguide T-junction characterization, including finite element, boundary element [7], Y-parameter [9] and the TPMMT methods solve the boundary value problems to obtain the scattering matrix of the three-port network. All these methods cannot be easily adopted and incorporated in microwave circuit CAD programs.

Although the present analysis is valid for any dimensional parameters, all the data and comparisons presented in this section are for $a = 2b$, $d = b$ for the E-plane and $b = 2a$, $d = b$ for the H-plane cases shown in Fig. 1(b).

Figs. 6 and 7 compare the S-parameters magnitudes and phases, obtained from the TPMMT and from the equivalent circuits [6] for E-plane and H-plane T-junctions, respectively. The curves for the equivalent circuit model were computed using approximate expressions given in [6] (i.e., (1) to (5) of Section 6.1 for the E-plane, and (1) to (4) of Section 6.5 for the H-plane. Note, however, that the parameter B in Section 6.5 has an error, it should be $B = (1/\pi)(1 + x^2)/(1 - x^2) + 0.3246$).

Very accurate circuit model representations of E- and H-plane T-junctions may be derived by using topologies introduced by Marcuvitz [6], but the element values are derived from the TPMMT solutions. The element values are given in terms of simple polynomials or rational functions of the normalized frequency variable $\Omega = (f/f_c)$ where f is the frequency and f_c is the cut-off frequency of the TE_{10} fundamental mode in the waveguide. The circuit models of the E- and H-plane T-junctions introduced by Marcuvitz [6] are shown in Fig. 8(a) and (b), respectively. The scattering matrix elements of each of the T-junctions are computed by TPMMT as a function of the normalized frequency Ω. At each Ω, the element values of the circuit of Fig. 8(a) and (b) are derived from the scattering matrix.

For the E-plane T-junction, the three-port Y-parameters are computed from the scattering matrix $[S]$ using the relation $[Y] = ([I] - [S])([I] + [S])^{-1}$, where $[I]$ is the unit matrix. The element values of the equivalent circuit in Fig. 8(a) are then easily shown to be given by

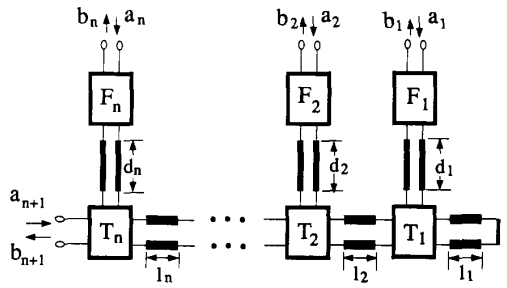

Fig. 11. n-channel multiplexer network.

$$jB_c = y_{31} \tag{13a}$$

$$jB_b = y_{21} - jB_c \tag{13b}$$

$$jB_a = y_{11} + jB_b + jB_c \tag{13c}$$

$$jB_d = y_{33} + jB_c. \tag{13d}$$

Each of the element values B_a, B_b, B_c and B_d of Fig. 8(a) are expressed as a sixth order polynomial in Ω:

$$B_k(\Omega) = \sum_{i=0}^{6} b_i^{(k)} \Omega^i \tag{14}$$

where $k = a, b, c, d$. The coefficient $b_i^{(k)}$ are obtained by fitting the element values obtained from the scattering matrix to expressions (14) with the mean square regression method. Table I gives the polynomial coefficients $b_i^{(k)}$. Fig. 9 compares the circuit element values obtained from the TPMMT, the polynomial approximations (14), the approximate expressions and the curves of reference [6] (Figures 6.1–4 to 6.1–7 in [6]).[1] The data from the curves in [6] are very accurate, it is not clear, however, how the curves were generated.

For the H-plane T-junction a similar procedure is used. The three-port Z-parameters are computed from the scattering matrix using the relation $[Z] = ([I] + [S])([I] - [S])^{-1}$. The element values of the equivalent circuit in Fig. 8(b) are given by

$$jX_c = z_{31}. \tag{15a}$$

$$jX_b = z_{21} - jX_c \tag{15b}$$

$$jX_a = z_{11} - jX_b - jX_c \tag{15c}$$

$$jX_d = z_{33} - jX_c. \tag{15d}$$

[1]Note that there is an error in labeling the parameters of these curves in [6]. The parameter b/λ_g shown in the curves should read $2b/\lambda_g$.

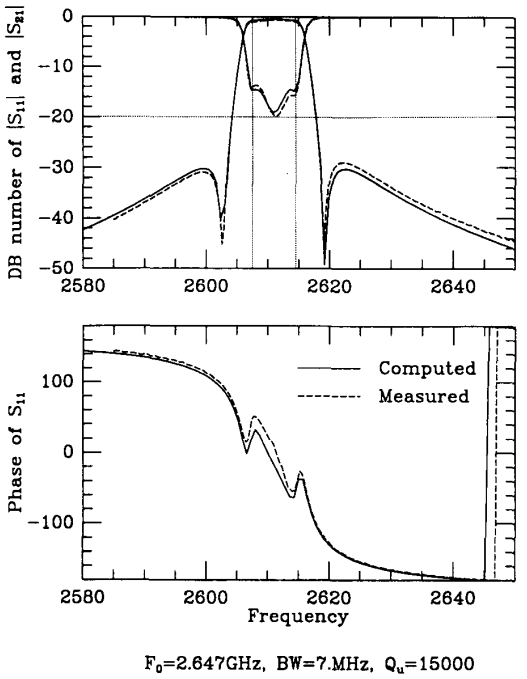

Fig. 12. Individual filter response for a typical channel.

The reactance element values X_a, X_b, X_c and X_d of Fig. 8(b) are expressed as rational functions of the normalized frequency Ω:

$$X_k(\Omega) = \sum_{i=0}^{6} x_i^{(k)} \Omega^i / (\Omega - P_1) \tag{16}$$

where $k = a, c, d$; and

$$X_b(\Omega) = \sum_{i=0}^{6} x_i^{(b)} \Omega^i / [(\Omega - P_1)(P_2 - \Omega)]. \tag{17}$$

Fig. 10 compares the variation of the circuit element values for the H-plane T-junction. Table II gives the polynomial coefficients $x_i^{(k)}$ and the poles P_1 and P_2.

III. Multiplexer Model and Optimization

The n-channel multiplexer shown in Fig. 11 consists of a waveguide manifold and n band-pass filters connected to it through n waveguide T-junctions. Methods for the analysis, optimization and design of such multiplexer are described in [1]–[3]. The practical success of the multiplexer designs are critically dependent on the accuracy of the models used to compute the frequency dependence of the filter and T-junction scattering parameters. Typically measured S-parameters of the T-junctions are used, together with a circuit model of the filters to model the multiplexer response. Computer optimization routines are then employed to find optimum values of the manifold spacings l_k and d_k (shown in Fig. 11), as well as the filter parameters. When a satisfactory computer optimized solution is achieved, it usually takes several experimental steps to practically obtain the same result. We used the T-junction model developed in the previous section, together with a modified circuit model of the filters described in [1] to design a four channel S-band multiplexer. After the computer optimization had been performed, the four filters were designed, built, tuned, and tested individually. The waveguide manifold was also built with the optimized dimensions. The four channel multiplexer was then assembled and tested *without any further tuning*. The result was extremely close to the computer design.

Fig. 12 shows typical computed results superimposed on the measured individual filter characteristics (both magnitude and phase of the reflection coefficient are shown). The filters used initially, before optimization, are doubly terminated four-pole elliptic function filters with .05 dB pass band ripple and 30 dB minimum out of band rejection. Fig. 13 shows the computed optimized multiplexer response, while Fig. 14 shows the measured multiplexer response.

IV. Conclusion

A rigorous method is presented to model rectangular waveguide T-junctions. The method is a combination of mode-matching and a three plane measurement method. The computed and measured results of magnitude and phase of the scattering matrix elements are in excellent agreement for both E-plane and H-plane T-junctions. The equivalent circuit models for both E-plane and H-plane T-junctions are used with their parameters derived from the electromagnetic model. These parameters are represented by polynomials and they provide very good accuracy (less than 1% magnitude error and less than 2° of phase error of the scattering parameters).

The optimization procedure of the multiplexer network model gives very good design of the manifold and the filters of the multiplexer. An experimental multiplexer built in accordance with the optimized design shows remarkable agreement with the theoretical results, without any additional tuning.

The TPMMT may also be used to solve other problems which have field deficiencies in some regions, such as right angle bends in waveguides, T-junction series, etc.

Acknowledgment

The authors wish to acknowledge the extremely thorough, helpful and constructive comments by the reviewers, who suggested numerous improvements. The authors are grateful to Prof. A. Oliner for many valuable suggestions and discussions.

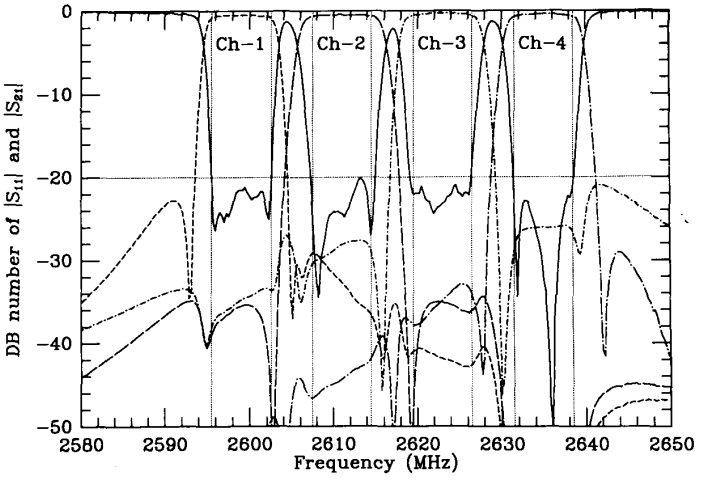

Fig. 13. Computed 4-channel multiplexer response.

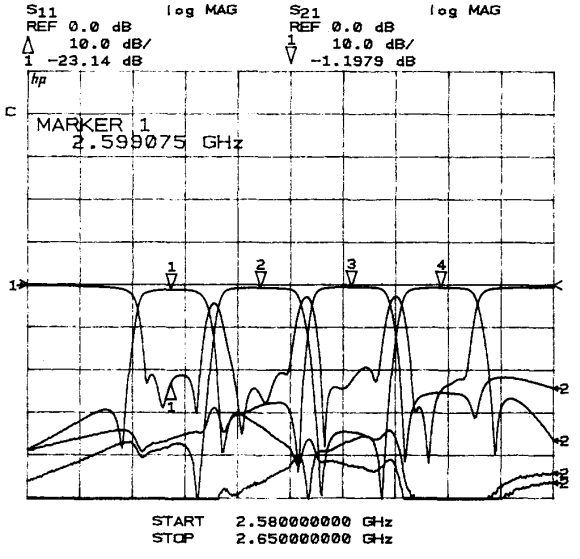

Fig. 14. Measured 4-channel multiplexer response.

References

[1] A. E. Atia, "Computer-aided design of waveguide multiplexers," *IEEE Trans. Microwave Theory Tech.*, vol. MTT-22, pp. 332–336, Mar. 1974.

[2] J. D. Rhodes and R. Levy, "Design of general manifold multiplexers," *IEEE Trans. Microwave Theory and Tech.*, vol. MTT-27, pp. 111–123, Feb. 1979.

[3] R. G. Egri, A. E. Williams, and A. E. Atia, "A contiguous-band multiplexer design," in *IEEE MTT-S Int. Microwave Symp. Dig.*, 1983, pp. 86–88.

[4] J. Dittloff and F. Arndt, "Rigorous field theory design of millimeter-wave *E*-plane integrated circuit multiplexers," *IEEE Trans. Microwave Theory Tech.*, vol. MTT-37, pp. 340–350, Feb. 1989.

[5] F. Arndt *et al.*, "Optimized *E*-plane T-junction series power dividers," *IEEE Trans. Microwave Theory Tech.*, vol. MTT-35, pp. 1052–1059, Nov. 1987.

[6] N. Marcuvitz, *Waveguide Handbook*, Radiation Laboratory Series, vol. 10, New York: McGraw-Hill, 1951.

[7] M. Koshiba and M. Suzuki, "Application of the boundary-element method to waveguide discontinuities," *IEEE Trans. Microwave Theory Tech.*, vol. MTT-34, pp. 301–307, Feb. 1986.

[8] L. Lewin, "On the inadequacy of discrete mode-matching techniques in some waveguide discontinuity problems," *IEEE Trans. Microwave Theory Tech.*, vol. MTT-18, pp. 364–372, July 1970.

[9] E. D. Sharp, "An exact calculation for a T-junction of rectangular waveguides having arbitrary cross sections," *IEEE Trans. Microwave Theory Tech.*, vol. MTT-15, pp. 109–116, Feb. 1967.

Xiao-Peng Liang (S'90) was born in Shanxi, China, in 1960. He received the B.S. and M.S. degrees in Beijing Institute of Technology, Beijing, China, in 1982 and 1984, respectively, both in electrical engineering.

From 1984 to 1987, he worked in Electrical Engineering Department, Beijing Institute of Technology, as a faculty member, where his research dealt mainly with the six-port measurement technique. He is presently a graduate student in the Electrical Engineering Department, University of Maryland at College Park, working towards the Ph.D. degree. His research interests are in the area of modeling microwave and millimeter-wave waveguides, devices and circuits.

Kawthar A. Zaki (SM'85–F'91), for photograph and biography see this issue page 2076.

Ali E. Atia (S'67–M'69–SM'78–F'87) received the B.S. degree from Ain Shams University, Cairo, Egypt, in 1962, and the M.S. and Ph.D. degrees from the University of California, Berkeley, in 1966 and 1969, respectively, all in electrical engineering.

Prior to joining COMSAT in 1969, he held various research and teaching positions at both these universities. As a Senior Scientist in the Microwave Laboratory at COMSAT Laboratories, he has made original contributions to satel-

lite transponder and antenna technologies, most notably the development of the dual-mode microwave filters technology. He has also made significant contributions to several satellite programs, including INTELSAT IV-A, V, V-A, VI, ARABSAT, and AUSSAT. He was responsible for the design, implementation, qualification, and testing of major subsystems in COMSAT's NASA ATS-F propagation experiment and the COMSTAR Ka-band beacon experiment. As Senior Director in COMSAT Systems Division he was responsible for communications systems design, integration, implementation, and testing under contracts with various government and commercial customers. Presently he is Vice President and Chief Engineer for COMSAT Systems Division, Clarksburg, MD.

Dr. Atia is an Associate Fellow of the AIAA and a Member of Sigma Xi.